MODELLING OF CARBON DIOXIDE (CO_2) CAPTURE USING METAL-ORGANIC FRAMEWORKS (MOFs)

BY

BAMIDELE OLUFEMI EYITOPE

A Thesis Presented to the

DEANSHIP OF GRADUATE STUDIES

KING FAHD UNIVERSITY OF PETROLEUM & MINERALS

DHAHRAN, SAUDI ARABIA

In Partial Fulfillment of the
Requirements for the Degree of

MASTER OF SCIENCE

In

MECHANICAL ENGINEERING

MAY 2015

KING FAHD UNIVERSITY OF PETROLEUM & MINERALS

DHAHRAN 31261, SAUDI ARABIA

DEANSHIP OF GRADUATE STUDIES

This thesis, written by Bamidele Olufemi Eyitope under the direction of his thesis advisor and approved by his thesis committee, has been presented to and accepted by the Deanship of Graduate Studies, in partial fulfilment of the requirements for the degree of **MASTER OF SCIENCE in MECHANICAL ENGINEERING**

Thesis Committee

Dr. Rached Ben-Mansour (Advisor)

Dr. Mohammed Antar (Member)

Dr. Tahar Laoui (Member)

Dr. Zuhair Mattoug Gasem

Department Chairman

Dr. Salam A. Zummo

Dean of Graduate Studies

12/4/15

Date

Dedicated to God Almighty, my beloved parents, siblings and fiancé for their prayers, consistent support and encouragement in all I do.

ACKNOWLEDGEMENT

All glory to God Almighty for the strength, courage, wisdom and understanding He granted unto me for the successful completion of this work. Once more in my life, He has shown His awesomeness; I therefore return all glory of the success of this work back unto Him.

My gratitude to King Fahd University of Petroleum and Minerals for the opportunity granted unto me to do my M.S. program in the prestigious institution. I also wish to acknowledge the support I received from King Abdulaziz Centre for Science and Technology (KACST) Carbon Capture and Sequestration Technology Innovation Center (CCS-TIC #32-753) at King Fahd University of Petroleum and Minerals (KFUPM) for funding this work through Project No. CCS10. The support of KFUPM through the Research Institute and the Deanship of Scientific Research is greatly appreciated. Thank you for the good academic environment, lessons and financial support during my study.

My sincere gratitude and appreciation goes to my distinguished advisor, Dr Rached Ben-Mansour for his constant endeavour, guidance and motivation during my study. His insights, advice and suggestions were the building blocks for the successful completion of my work. I am highly grateful! I also thank Dr. Mohammed Antar and Dr. Tahar Laoui for their suggestions, contributions and time during my program. Indeed, I had the best thesis committee of all time!

Finally, I would like to acknowledge all Faculties, staffs and students of Mechanical Engineering department whom I interacted with during my Master program. I thank Mr Lateef Kareem and Mr Meboob Basha of the KFUPM Research Institute for their time, suggestions and guidance. May God bless you.

TABLE OF CONTENT

LIST OF TABLES

LIST OF FIGURES

THESIS ABSTRACT (ENGLISH)

NAME: BAMIDELE OLUFEMI EYITOPE

TITLE: MODELING OF CO_2 CAPTURE USING METAL-ORGANIC FRAMEWORKS (MOFS)

MAJOR: MECHANICAL ENGINEERING

DATE: MAY 2015

The challenges of global warming and carbon dioxide emissions cannot be overemphasized. The use of CO_2 emitting facilities and equipment is increasing by day. Some popular CO_2 emitters include: industrial processes, automobiles, ships, aircrafts amongst others. Reportedly, between 1991 – 2006, the European Aviation Industry *alone* recorded about 87% increments in greenhouse gases emissions; this indeed is a great source of concern. Carbon Capture has been suggested to be a viable solution to abate the challenges of earth warming and climatic changes caused by these emissions. This thesis work is a computational study of adsorption-separation of CO_2 from an N_2/CO_2 gas. A detailed one-dimensional, transient mathematical model has been formulated to include the heat and mass transfer, the pressure drop and multi-component mass diffusion. The model has been implemented on a MATLAB program using second order discretization. Validation of the model was performed using a complete experimental data set for carbon dioxide separation using activated carbon and zeolite 13X. Simulation of the adsorption breakthrough experiment, adsorptive storage and pressure swing adsorption on fixed bed have been carried out to evaluate the capacities of Mg-MOF-74, MOF-5 and MOF-177 for CO_2 capture with varying feed gas temperature and pressure. A novel method for PSA with heat regeneration system is also presented here in. Feed temperature ranges from 28^{o}C to 150^{o}C while feed pressure ranges from 1 bar to 50 bar. The results show the superiority of MOF adsorbent in comparison to activated carbon and zeolites.

MASTER OF SCIENCE DEGREE

KING FAHD UNIVERSITY OF PETROLEUM & MINERALS

Dhahran, Saudi Arabia

THESIS ABSTRACT (ARABIC)

الاسم : بامديلى اوليفيمى ايتوبى

العنوان: نمذجة احتجاز CO_2 باستخدام (MOFS)

التخصص: قسم الهندسة ميكانيكية

التاريخ: مايو/ 2015

بين عام 1991- 2006, سجلت صناعة الطيران الاوربية لوحدها تقريبا 87% زيادة في الانبعاثات المسببة للاحتباس الحراري وهذا بالطبع مصدر عظيم للاهتمام .

تحديات الاحتباس الحراري وانبعاثات ثاني اكسيد الكربون لا يمكن حصرها. استخدام الادوات التي تبعث ثاني اكسيد الكربون تزداد يوما بعد يوم. بعض باعثات ثاني اكسيد الكربون تتضمن: العمليات الصناعية, المركبات, السفن, الطائرات , الخ.

احتجاز الكربون تم اقتراحه ليكون حل متاح لانحسار تحديات الاحتباس الحراري للارض والتغيرات المناخيه المسببه بهذه الانبعاثات.

هذا البحث عبارة عن دراسة حسابية لفصل CO_2 من غاز ال N_2/ CO_2. تم وضع نموذج رياضي مفصل احادي البعد انتقالي ليتضمن انتقال الحرارة والكتله, انخفاض الضغط, انتشار الكتلة متعدد المكونات. النموذج تم تنفيذه عن طريق برنامج MATLAB باستخدام التفريد من الدرجة الثانية. تم التحقق من صحة النموذج باستخدام بيانات تجريبية كاملة لفصل ثاني اكسيد الكربون باستخدام كربون منشط وزيولايت 13X. محاكاة تجربة اختراق الامتزاز, التخزين الامتزازي وضغط التارجح الامتزازي في قطعة ثابتة تم عملها لتقييم سعات MOF-5, Mg-MOF-74 و MOF-177 لاحتجاز CO_2 مع تغيير درجة حرارة وضغط غاز التغذية.طريقة جديدة ل PSA مع نظام اعادة توليد الحرارة ايضا تم تقديمه هنا. حدود درجة حرارة التغذية من 301 الي 423 كلفن وحدود ضغط التغذية من 1 الي 50 بار. اوضحت النتائج اسبقية ال MOFمقارنة مع الكربون المنشط والزيولايت.

CHAPTER 1

INTRODUCTION

1.1 Research Background

Global pursuit of green environment has been the subject of the day in recent years and it cannot be overemphasized. Environmental degradation began the day man began his pursuit for better and easier living. With initial ignorance, over the years, man's activities continuously depleted his environment and atmosphere, leading to accumulated effect over the years, and eventually resulting in great concern and fear for the world at large. Research has found that since 1993, about 100billion tonnes of earth's ice is being lost every year in the Antarctica, this has caused a rise of about 0.2mm in global sea level every year [1]. Reports have been made about remarkable increase in temperature across the Sahara, ice shelves retreat and partial collapse, increase in ice in the ross sea region due to climate change [1] etc. The change in climate has been attributed mainly to greenhouse effect caused by greenhouse gases; that is, global warming of the atmosphere due to these gases [2]. Greenhouse effect results in increase in temperature of the earth's surface beyond the normal, leading to gross discomfort for inhabitants of earth.

1.2 Greenhouse gases and their effects

Greenhouse effect is caused by greenhouse gases such as; Nitrogen oxide, carbon dioxide, methane and water vapour. These gases act like canopy, trapping some of the energy absorbed from the earth in the atmosphere, thereby making the earth warmer. The gases are emitted as a result of man's activities, with greater bulk in flue (exhaust) gases exited after combustion of fuel. They primarily consist of N_2, H_2O and CO_2 in ratio 13:2:2 by weight.

The most predominant of these greenhouse gases is carbon dioxide (CO_2) because it is emitted in large quantity from several recurrent processes [3]. CO_2 is not only produced during burning of fossil fuels such coal, natural gas and petroleum, but also during industrial activities like refining of oil, domestic and industrial cooking, cement production, iron, steel, flue gas from power plants etc. Flue gases from power generating plants are a major source of CO_2 hence, they are of great concern until man finds reliable alternative sources of power. Pictorial representation of some common sources and effects of CO_2 are presented in figures 1.1 – 1.4

Figure 1.1: CO_2 emission from automobile exhaust [3]

Figure 1.2: Flue gas emission from industries [4]

Figure 1.3: Pictured representation of global warming [5]

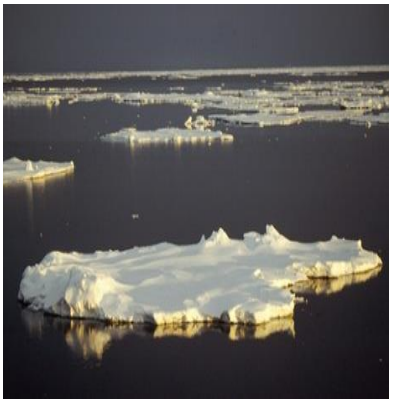

Figure 1.4: Pictured representation of ice shelves around Antarctic Peninsula [1]

There are speculations that in about year 2050, there would be about 257% increase in heat related death rise, hence global call has been made for reduction of CO_2 emitted by any

process into the atmosphere to about 450ppm as this will help avoid dangerous climate changes.

1.3 Reduction of CO_2 from the atmosphere

Several methods have suggested achieving the above goal, some of which include: alternative fuel for combustion, renewable energy fuels, carbon capture and sequestration etc. Based on economic grounds, carbon capture has been suggested to be a viable mean of reduction of CO_2 emission, however to achieve this, efficient technologies need to be researched which include potential carbon capture materials, cost of regeneration etc. [4]. A popular carbon capture technique is Post Combustion Carbon Capture technique, an example of which is adsorption amongst others.

The investigation of carbon capture technologies can be done via experimental procedure, mathematical modelling of experimental works or a combination of both processes. Mathematical modelling however has its advantages over experiments with respect to cost and time savings, flexibility and possibility of parametric studies amongst others. Some of the known experimental procedures for analysing adsorptive carbon capture systems include: breakthrough experiment, timed pressure change experiment for adsorption and desorption processes known as Pressure Swing Adsorption Experiment (PSA), timed temperature change experiment for adsorption and desorption processes known as Temperature Swing Adsorption (TSA) experiment, Vacuum Swing Adsorption (VSA) experiment, Electric Swing Adsorption (ESA) Experiment etc. The breakthrough experiment is used to test the material's capacity for carbon capture while PSA, TSA, VSA and ESA are used to test durability and capacity of the material for repeated cycle of adsorption and desorption processes.

The use of mobile CO_2 emitters is continuously increasing and consequently, the increase in CO_2 emission. It has been reported that between 1991 and 2006, the European aviation industry alone recorded about 87% increments in greenhouse gases emissions [5]. This indeed calls for a great source of concern; however, a good number of existing researches are focused on the above carbon capture technologies with emphasis on stationary CO_2 emitters e.g. industrial and home wastes. The task of carbon capture becomes more challenging considering cases of mobile CO_2 emitters e.g. automobiles, ships, aircrafts etc. as this would involve carbon capture and storage pending the time of arrival of the carrier vessel at cylinder offloading stations. Hence, one of the objectives of this thesis work is to studies numerically, adsorptive of CO_2 in MOF beds.

1.4 Post carbon capture processing

After carbon capture, the captured CO_2 is regenerated in order to make the carbon capture material re-usable. The regenerated CO_2 is then stored for industrial applications such as: food and beverages manufacturing, green house growing, oil well stimulation, freezing and chilling, chemical synthesis, CO_2 snowing etc. The adsorbent materials can also be used to build CO_2 capture systems that can be mounted in exhaust systems of automobiles, ships, power plants to reduce CO_2 emission into the atmosphere. This research studies a potential post combustion carbon capture process known as adsorption with the view of modelling carbon capture process using Metal-Organic Frameworks (MOFs) as carbon capture material.

1.5 Problem Statement

This thesis work shall simulate mathematical models for adsorption and desorption processes for the removal of carbon dioxide (CO_2) from flue gas, assuming dry flue gas containing 15%

of CO_2 and 85% of N_2. Simulations of adsorption experiments shall be carried out on MATLAB commercial code and the simulated experiments shall be employed to test carbon capture potentials of Metal-Organic Frameworks' (MOFs).

1.6 Significance of study

In a drive towards greener environment, an efficient simulation of the process of carbon capture is vital. The simulation can be used to comprehend and predict the behaviour of the carbon capture processes, materials and systems for better optimization of the technique. At the end of this work:

- ✓ The simulated mathematical model would be able to satisfactorily predict the behaviour of CO_2 capture systems that work on adsorption principle.
- ✓ A demonstration of the potentials of MOFs (e.g. Mg-MOF-74 and Mg-MOF-5) in Carbon Capture shall be established.
- ✓ An algorithm for parametric study of any potential adsorption carbon capture materials shall be available.
- ✓ Contribution to research and development in the area of Carbon Capture which shall serve as building block for further study on the use of adsorption separation of gaseous mixtures shall be achieved.

In addition to these, this work shall lead to:

i. **Enhanced environmental safety**: Reduction in environmental pollution and degradation caused by CO_2 from flue gas emitting equipment and machineries.

ii. **Enhanced equipment reliability:** The ability to maintain service continuity with minimum CO_2 emission during abnormal system conditions shall be enhanced.

iii. **Enhanced carbon capture material predictability:** With the use of the algorithm that is to the written, quick parametric studies can be carried out on potential CO_2 adsorbents to determine their feasibility and efficiencies in carbon capture.

iv. **Enhanced maintainability:** The carbon capture system can be maintained with minimum interruption to service during machine operation.

v. **Enhanced Flexibility:** Ability to modify numerical code to suite any particular engineering system or geometry in use.

vi. **Enhanced Simplicity:** The CO_2 capture algorithm is easy to understand and operate.

vii. **Enhanced Transparency:** The data generated from the CO2 capture algorithm can be easily acquired, interpreted and modified for various adsorption systems and materials.

1.7 Research objectives

The main objective of this thesis work is to develop a mathematical model capable of simulating the adsorption process for the separation of CO_2/N_2 gas mixture needed for carbon capture. The specific objectives of the work are to:

1. Develop a one-dimensional (1-D), transient, mathematical model to investigate numerically the adsorption and desorption processes under different operating temperatures and pressures.

2. To carry out numerical simulations of the break through experiment for separation of Carbon dioxide for different adsorbent materials including: activated carbon (AC) and Mg-MOF-74.
3. To carry out numerical simulation of storage of Carbon dioxide in different adsorbent materials including: Metal Organic Framework materials (e.g. MOF-5 & MOF-177) and Activated Carbon material (AC).
4. To carry out numerical simulations of Pressure Swing Adsorption (PSA) experiment for cyclic separation of Carbon dioxide for Mg-MOF-74.

1.8 Thesis outline

This thesis contains eight (8) chapters.

Chapter 1 introduces the context of the research, the eminent problem of carbon dioxide emission, the suggested solution of carbon capture, why carbon capture is the subject of this thesis, the significance of this work and its scope. Possible solutions to carbon capture are mentioned, a highlight of post carbon capture processes and possible uses of captured CO_2 are provided.

Chapter 2 reviews some existing literatures on post combustion carbon capture, adsorption as a good technique for post combustion carbon capture, traditional materials for adsorption carbon capture, the advent of MOFs and their potential use as carbon capture material, prediction of adsorption carbon capture systems, description some experimental works (Breakthrough experiment, Pressure Swing Adsorption (PSA) and Adsorptive storage) for adsorption carbon capture, mathematical models of gas-solid adsorption, description of some experimental and numerical research that have been carried out on adsorption carbon capture.

Chapter 3 describes the methodology adopted for numerical simulation of breakthrough experiment and adsorptive storage while chapter 4 describes the methodology adopted for numerical simulation of Pressure Swing Adsorption Experiment. These chapters also highlight the experimental data employed for validation of the prepared algorithms.

Chapters 5, 6, and 7 present the results of this thesis work. They present validations of the prepared algorithms with experimental results, the results of simulations of breakthrough experiment, adsorptive storage and Pressure Swing Adsorption. All results are discussed in this chapter. Chapter 5 presents the results of simulation of breakthrough experiment of CO_2 on Mg-MOF-74. Chapter 6 presents the results of simulation of adsorptive storage simulations of CO_2 on MOF-5 and MOF-177. Chapter 7 presents the results of simulation of Pressure Swing Adsorption experiment on Mg-MOF-74.

Finally, Chapter 8 closes the thesis work. It concludes the discussed results and makes recommendations for further research in this field.

CHAPTER 2

LITERATURE REVIEW

2.1 REDUCTION OF CO_2 EMISSIONS

H. Herzog et al [6] suggested three methods to reduce CO_2 emissions due to coal combustion;

(i) Reduction of coal burning (ii) Improvement of coal fired plats' efficiencies

(iii). Capture and storage of carbon dioxide i.e. Carbon Capture and Sequestration

Reduction of coal burning is a difficult task to achieve because of popular power generation through coal burning. Reduction of coal burning could therefore require reduction in electricity demand or finding a suitable replacement fuel for coal which may take time and be challenging to enforce. The task may also be difficult because coal is readily available, plenty and cheap for use for the common man. The second method which is the improvement of coal fired plant efficiency can be thought of to have insufficient effect when compared to the target of reducing CO_2 emission to near-zero. The third method, Carbon Capture and Sequestration (CCS), can be a matchless method if well harnessed. It would permit continuous use of coal and reduction of emissions associated with its combustion. It would also buy time for the development of new alternatives to coal. Besides this, following GCEP report, 2005, carbon capture has been suggested to be economically viable to achieve the goal of reducing greenhouse gases emission into the atmosphere [4].

2.2 CARBON CAPTURE

Research in the Carbon Capture and Sequestration (CCS) technologies is fast growing; broad varieties of technologies and materials are being researched and developed by the day [7]. While some technologies are being developed, others have been developed to industrial scale

usage. However, most researched technology for carbon capture need further improvements with respect to efficiency and associated cost of operation. An example is the popular post-combustion carbon capture by absorption of CO_2 in amine solutions. Even though this technology has been in use for quite a long time in the industry, the technology has its own challenges which would be enumerated later on in this work. Several other challenges exist for scientists and engineers alike with respect to commercialization of researched technologies for carbon capture. Some of the challenges have to do with research for further development, understanding and prediction of carbon capture materials, while some have to do with improvement on materials' carbon capture capacity, selectivity, stability [7] etc. These have made sorbents' research the rave of the moment with quite challenging tasks to complete.

Research in carbon capture materials has been described challenging because for instance: For good modification of properties of known sorbents suitable for carbon capture account must be made for size of gas molecules and electronic behaviour of such molecules, however, the very small difference in the kinematic diameters of gas molecules makes separation of CO_2 solely based on gas molecule size difficult to achieve. An example of this is in the synthesis of a perfect material for the purpose of separating a mixture containing: CO_2 (3.30A˚), CH_4 (3.76A˚), and N_2 (3.64A˚). These gas components all have close values of kinematic diameters, hence it would be highly challenging to separate such mixtures [7].

Notwithstanding the challenges faced in carbon capture, electronic properties like quadrupolar-moment and polarization have been of great help as bases of separation, because their significant difference for each gas. The popular techniques for carbon capture are highlighted below.

TECHNIQUES OF CARBON CAPTURE

The following are applied as carbon capture techniques:

a. Oxy-Combustion Carbon Capture
b. Pre-Combustion Carbon Capture
c. Post-Combustion Carbon Capture

Oxy-Combustion Carbon Capture

Oxy-Combustion Carbon Capture is a technique which employs pure Oxygen (≥ 95%) for combustion rather than air. Oxy-fuel combustion has the advantage that it emits about 75% less flue gas compared to air fuelled combustion. In addition, its effluent gas consists mainly H_2O and CO_2 [8]. Some of the challenges of applying Oxy-Combustion technique include:

a. High energy consumption for supply of pure oxygen.
b. It is a developing technology with no experience in commercial scale [7].

Pre-Combustion Carbon Capture

Pre-Combustion Carbon Capture technique implies Carbon expulsion before combustion. This is only possible in plants such as Integrated Coal Gasification Combined Cycle (IGCC) in which gasification of coal is first done to synthesize gas mixtures of carbon monoxide and hydrogen which is called syngas. This method has advantage over the other techniques because it is cheaper however; it has its own challenges. Some of the challenges of using pre-combustion carbon capture technique include:

a. Only few plants use Integrated Coal Gasification Combined Cycle (IGCC) as compared with pulverized Coal power plant (PC) [6].
b. In sufficient technical know-how and poor operability
c. Absence of single concise process for overall operational performance;

d. System requires further research and development for industrial application [7].

Post Combustion capture

Post-Combustion capture (PCC) is the separation and capture of carbon dioxide from flue gas of power plants and other combustion engines after combustion for the purpose of reducing atmospheric pollution and further environmental deterioration due to CO_2 emissions. Post-combustion carbon capture is advantageous because of its ease of integration with existing power plants without need to change the existing plant's configuration; its maintainability is flexible and independent of the plant's operation, it has proven to be more suitable for gas plants than pre-combustion or oxy-combustion combustion techniques [6]. PCC can be used for both coal fired and gas operated power plants, however, for coal fired power plants, there is need for further analysis of cost trade-off between plant's operation optimization and CO_2 capture [2,3]. The following section discusses in details post-combustion carbon capture technologies.

2.3 POST-COMBUSTION CARBON CAPTURE TECHNOLOGIES

Like most other technologies, PCC is a developing technology and it is with challenges such as:

a. Additional compression and energy requirement for storage of captured carbon dioxide.
b. Necessity for treatment of large volumes of flue gas, due to the low partial pressure of CO_2 in flue gas.
c. Huge energy requirement for regeneration of sorbent e.g. amine solution[7].
d. Inefficient materials for carbon capture [11].
e. High flue gas temperature that can lead to sorbent degradation

f. Presence of unfriendly components such as oxygen, SO_x, NO_x, Fly Ash, Soot etc. during carbon capture that can lead to equipment corrosion, erosion, mist generation from sorbents, foaming, scaling, plugging of equipment and sorbent degradation etc. [12].

One of the most challenging aspects of PCC is material challenge because it is directly linked with the other challenges. The efficiency of carbon capture materials determines the volume of flue gas that can treated by the material per carbon capture cycle, which determines the frequency of regeneration required to activated the material after saturation which subsequently determines the number of cycles the materials can undergo before degradation and replacement. The frequency of regeneration of a given material and the nature of bonding between the materials and the captured CO_2 mostly influence the energy requirement for regeneration which is a bulk of the cost of carbon capture and sequestration.

The prominent researched post combustion carbon capture technologies suggested to overcome the challenges of carbon capture include:

i. Absorption CO_2 separation
ii. Membrane CO_2 separation
iii. Cryogenic CO_2 separation
iv. Micro-Algal Bio-fixation
v. Adsorption [13].

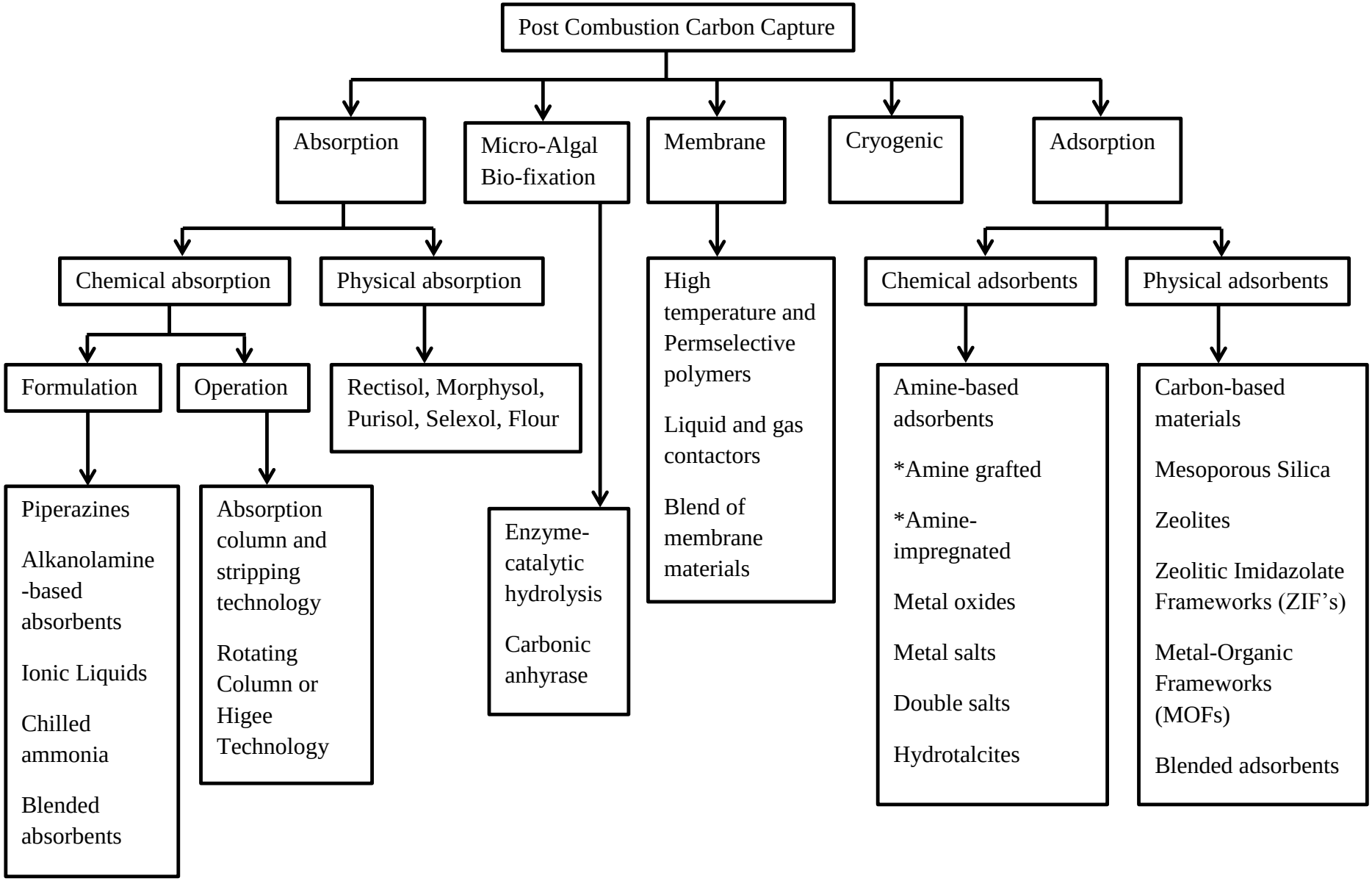

Figure 2.1: Post combustion Carbon Capture Processes

2.3.1 ABSORPTION CARBON CAPTURE

Absorption also known as “wet scrubbing” is a process of imbibing (absorbing) carbon dioxide from flue gas into absorbent solution by chemical action, leaving the effluent gas stream to pass freely through the absorption column. The dilute absorbent is re-concentrated, regenerated or reactivated in a stripper for reuse in CO_2 capture. The popular absorbents are the aqueous amines and ammonia-based solutions. Aqueous amine solutions are more corrosive than the ammonia-based solutions and less efficient at lower temperatures however, they remain popularly used because ammonia-based solutions are toxic bringing about the need for extra care in their use to prevent their escape into the environment [6]. Some of the specific challenges of absorption carbon capture technology include:

i. Huge energy requirement for reactivation of sorbate
ii. High volume of absorber is required
iii. Equipment corrosion is inherent
iv. Low gas-liquid contact surface area
v. Low rate of absorption [14]

Below is a schematic of absorption carbon capture process

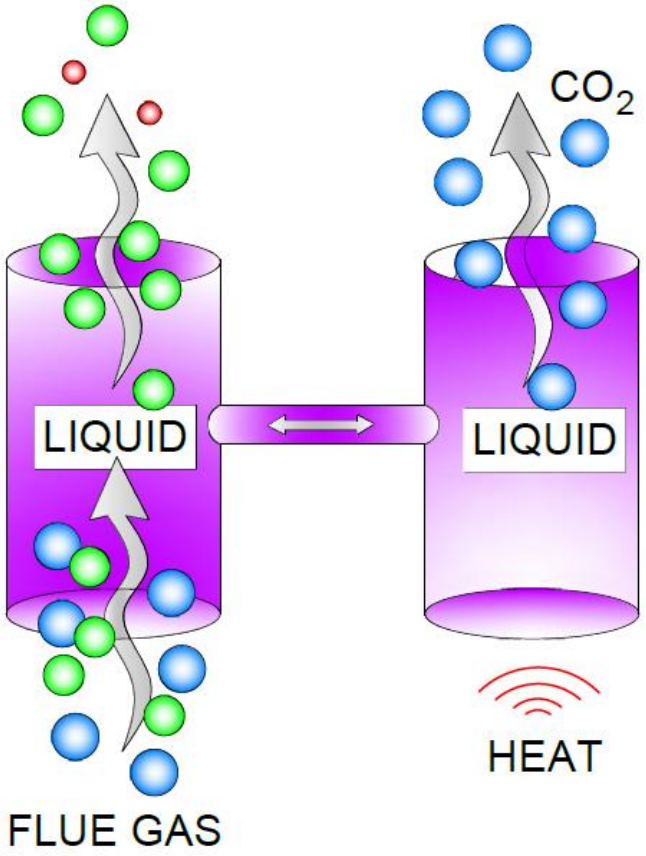

Figure 2.2: Schematics of Absorption carbon capture process

The two main types of absorption include:

i. Physical absorption [15,16]

ii. Chemical absorption [17,18]

Chemical Absorption

Post combustion carbon capture by chemical absorption of involves the absorption of CO_2 in solutions of aqueous alkanolamines. Flue is passed through a vertical absorption column that is packed with absorbent materials, as the gas stream flows through the packed bed, CO_2 is absorbed in the sorbent leaving the effluent gases to flow out through the top of the column. After the sorbent is spent, it is thermally regenerated in a stripper; the regenerated gas is further compressed for storage while the sorbent is returned back to the absorption column

for reuse. Chemical absorption is a matured and commercialized post combustion carbon technology; however, the absorbents used in the process (aqueous alkanolamines) are corrosive. They endanger absorption column walls and linkers'. In addition, the regeneration of spent sorbents is hugely energy demanding and capital intensive. Furthermore, alkanolamines tend to degrade quickly leading to operational, economic and environmental challenges [14,19].

Several alternative sorbents have been suggested to overcome the above challenges, however the challenges persist. A popular group of absorbents; Piperazines (PZ); exhibit good carbon capture properties with high resistance to thermal degradation to a tune of about 150^{o}C however, they have low solubility in water at low temperatures therefore necessitating CO_2 capture with PZ's at high temperatures [20,21]. Another group of adsorbents; aqueous Monoethanolamines (MEA); with one of the fastest rates of chemical reaction degrade when subjected to high temperature [22]. MEA's also degrade in the presence of dissolved oxygen(DO) thereby necessitating frequent replacement of sorbents leading to high incurred cost of carbon capture [22,23]. Ionic Liquids (IL) is a class of absorbents used for both physical and chemical absorption. They are remarkably thermally stabile, non-toxic with minimal vapour pressure. The popular IL's however have high viscosity due to the hydrogen bonds between their anions and cations. Their viscosity increases with CO_2 absorption leading to low absorption capacity [24].

Physical absorption

Unlike chemical absorption, physical absorption is a less corrosive technique with better stability of sorbents. However, more absorbent is required for CO_2 capture at an equivalent rate as chemical absorbents [14]. Most existing physical absorption processes are done under high pressure and low temperature. Some of the popular of physical absorption processes include: Rectisol process, Morphysol process, Purisol process, Flour process and Selexol process amongst others. The interaction between physical absorbents and captured CO_2 is described by Henry's law therefore no chemical reaction exist between the absorbents and the captured CO_2. Desorption of physically absorbed CO_2 is done under low pressure and high temperature condition, leading to lesser energy requirement for regeneration [4]. Physical absorbents can be solid or liquids. Some popularly reported ones include: Selexol, Glycol, Rectisol and Carbonates amongst others [17]. Selexol is commercially being used for CO_2 capture, Glycol is mostly applicable for CO_2 capture at high concentration and it has the disadvantage of quick CO_2 desorption at atmospheric pressure. Glycerol carbonate has high selectivity for CO_2, but low CO_2 absorption capacity [25].

A lot of research are on-going to optimize the properties of known absorbents and develop novel ones, some of the suggested solutions to overcome the challenges of absorption carbon capture include: mixture of physical and chemical sorbents e.g. sulfinol, use of absorbent degradation inhibitors [26], improved stripper operation technology [27], blending of PZ's and alkanolamines [20], blending of IL's and Alkanolamines [28], blending of aqueous amines with organic components [29] amongst others.

Higee Technology

This technology was developed to reduce mass transfer resistance between adsorbate and adsorbent at contact interface in conventional absorption process and to reduce the cost of carbon capture due to large sizes of spray column, packed bed or bubbly column, the Higee technology was developed. The Higee technology enhances CO_2 transfer to absorbent through centrifugal effect in a rotating packed bed (RPB). Under gravity, the centrifugal effect created by the rotating packed bed helps to atomize the liquid absorbent thereby creating larger gas-liquid surface area of contact and lower resistances to mass transfer. RPB's have been categorized based on the flow directions of the fluids within the bed. The two main classes are the cross flow and counter current flow. Higee technology has been applied for absorption, desorption and other functionalities outside carbon capture [30]–[32].

2.3.2 MEMBRANE CARBON CAPTURE

This technology involves the use of membranes to sieve out of CO_2 from flue gas. The configurations of carbon capture membranes are specially designed for CO_2 selectivity and made from materials such as ionic liquid [33], ammonium [34], polymides [35], blend of metal oxides and silica [36], mixed matrix [37] amongst others. Membranes work based on the principle of varying partial pressure of the capture gas across the membrane. A concentration gradient is created between upstream and downstream, due to which CO_2 is trapped in membrane upstream at higher pressure and desorbed downstream at lower pressure [38]. Below is a schematic of membrane carbon capture process:

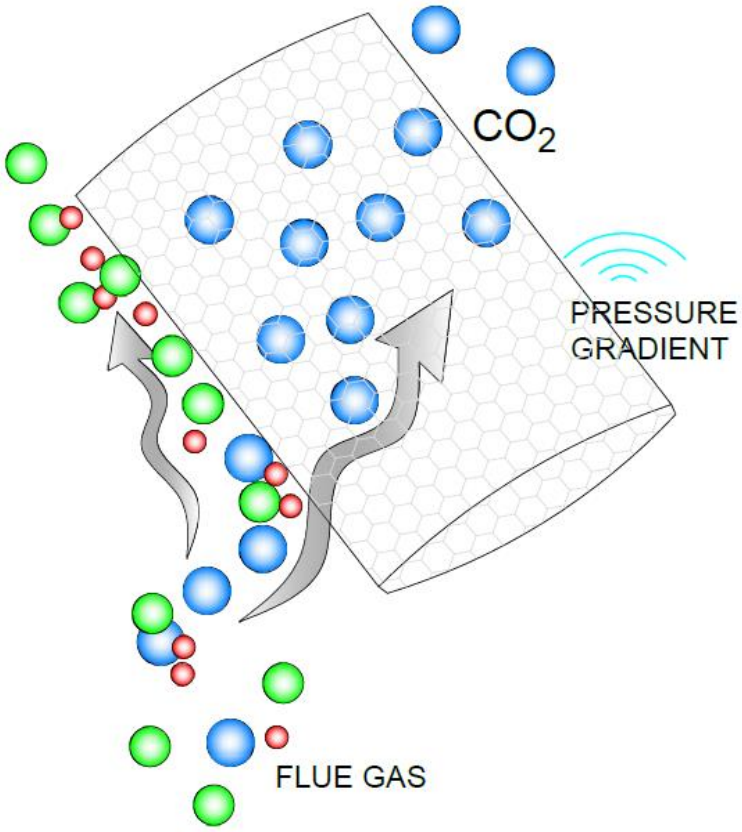

Figure 2.3: Schematics of Membrane carbon capture process

Membranes are the most important component of membrane post combustion carbon capture technology. For suitable and efficient carbon capture, some of the important properties for a potential carbon capture membrane include:

i. High degree of selectivity

ii. High CO_2 permeability

iii. Good chemical and thermal stability

iv. Remarkable durability

v. High resistance to plasticization and ageing

vi. Economical manufacturing process and easy assembling into modules [39].

Even though there are speculations that membrane carbon capture technology could be a potential competition for the commercialized absorption carbon capture process in future if not under estimated [40], to the best of our knowledge; even though membrane carbon capture technology has the advantages of lesser environmental impact and end of pipe applications, most of the researched carbon capture membranes trade-off selectivity for permeability or vice-versa [41]. As compared to absorption carbon capture technology, membrane carbon capture technology is relatively less selective of CO_2, therefore, it is less energy consuming, because of the traded captured CO_2 purity with process energy requirement. Membranes pose peculiar challenges in their use in coal fired plants because of their susceptibility to damage due to accumulated coal particulate deposits on them over time. Furthermore, membrane with large surface areas are required if they are to be used for carbon capture in coal fired plants. Finally, the design and cost of membranes capable of operating efficiently at relatively high temperatures have been a handful challenge for scientists and engineers in general. These and more are some of the major challenges preventing the application of membrane carbon capture technology on an industrial scale [40], [42]–[45].

A popular membrane materials is the polymer group known for their remarkable chemical and thermal stability, high selectivity and mechanical strength for large scale carbon capture purpose [46]. Brunetti et al [43] reviewed some popular polymeric membranes; of the researched polymers, 6-FDA's exhibit remarkable selectivity and CO_2 permeability attributable to their $–CF_3$ components [38]. The Poly(ethylene-Oxides) also known as POE show strong similitude for CO_2 molecules leading to recent research suggestions of multi-block copolymers as possible solution for improvement of POE's carbon capture potentials [47].

Based on upper bound limitation researched by Robeson [48], further research have been carried out to improve intrinsic selectivity and permeability of known polymers. Quite handfuls suggestions have been made about induced chemical reactions using Fixed Site Carrier Membranes (FSCM) as suitable option to overcome the upper bond limit. FSCM present greatly improved selectivity for CO_2. Tested carriers include polymers and micro molecules. A common feature and disadvantage of FSCM's is the need for availability of water on both sides of the membranes for inducing the required chemical reaction. In this feature lies the unanswered question of water evaporation and reaction control under severe carbon capture conditions [45].

Mixed-matrix membranes (MMM) another group of researched membranes formed from inorganic nano or micro particles scattered in continuous phase of polymers have been prepared in two popular forms: flat sheets and hollow fibres. Three and two components mixed-matrix membranes have been successfully prepared. Example of two component MMM are membranes blended with zeolites. For these membranes, increase in CO_2 permeability was recorded however; they are highly sensitive to high temperature especially their thinner samples. In addition to this, to the best of our knowledge no significant improvement in selectivity is recorded in them [49]. Yeny et al [37] prepared a "defect free" three component mixed matrix membrane which incorporated ionic liquid and zeolites. High selectivity and improved interfacial binding between the organic polymer and inorganic zeolite were recorded. However, the recorded selectivity was slightly lower than that of two components MMM [49].

Thermally re-arranged polymers (TR) suggested by Park et al [50]. TR's are polymers whose micro structures have been re-arranged thermally. The reported TR's exhibit good sieving characteristics for CO_2, zero plasticization characteristics, remarkable permeability almost

two orders of magnitude higher than the base polymers and good thermal stability [51], however further research is required for optimization of their permeability and selectivity balance to enable exploration at industrial scale [52].

Other suggested methods to improve the potentials of membrane post combustion carbon capture include: Interfacial polymerization (IP) of polymeric membranes with PDMS interlayer [53] and trimesoyl chloride [54], use of high silica CHA-type zeolite membranes [55], Hybrid Fixed Site Carrier Membranes (FSCM) [56], multi-stage membrane CO_2 capture process [57] and incorporation of poly(ethylene glycol) containing polymeric sub microspheres into polyimide membranes [58] amongst others.

2.3.3 CRYOGENIC CARBON CAPTURE

The cryogenic distillation separation technology uses the principle of liquid state temperature and pressure difference in constituent gases of flue gas for CO_2 capture. In this technique, CO_2 is cooled, condensed and then removed from the flue gas stream. Cryogenic distillation technology has long been in use in the industrial, it is a matured technique most applicable to carbon capture under high CO_2 concentration (greater than about 90% by volume), it is not economical energy-wise and more suitable at low gas temperatures. All these and more make the application of cryogenic CO_2 separation very difficult under real flue gas condition [59]. Below is a schematic of cryogenic carbon capture process:

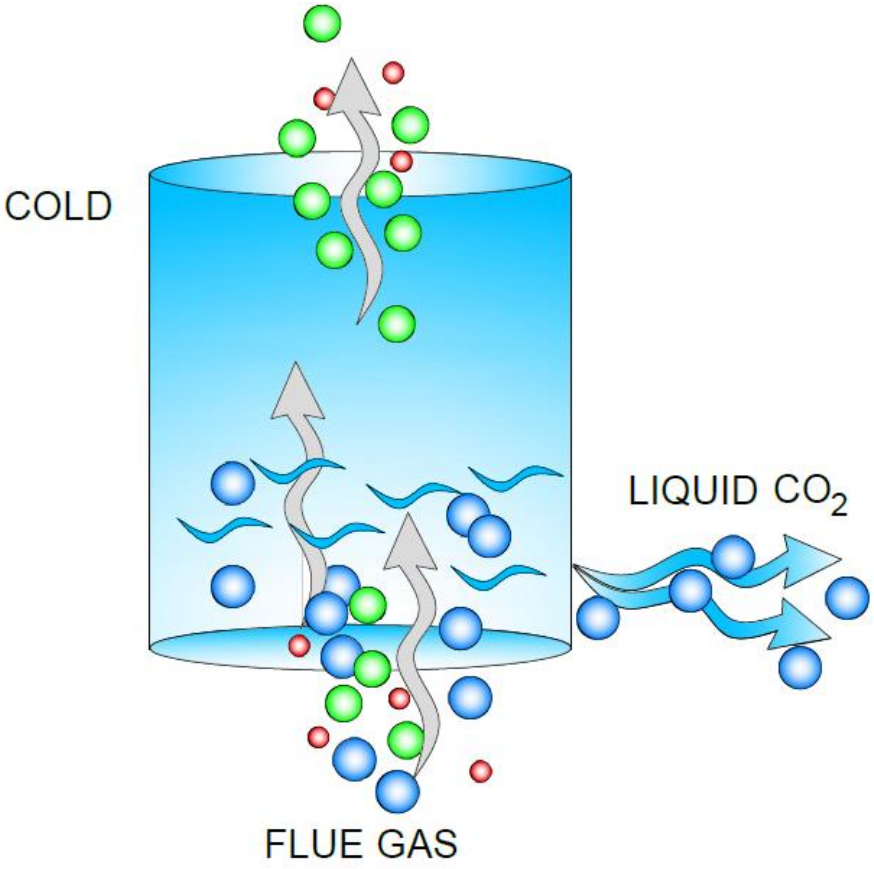

Figure 2.4: Schematics of Cryogenic carbon capture process

2.3.4 MICRO-ALGAL BIO FIXATION

This has long been a potential technique for post combustion carbon capture. This technology entails the use of photosynthetic microalgae for anthropogenic CO_2 capture. Aquatic micro-alga are of greater potential as they have higher carbon fixation rates (about an order greater) than land plants. Micro-algae culturing is quite expensive however, it produces other compounds of economic value for revenue generation. Micro-algae photosynthesis also leads to precipitation of calcium carbonate that can serve as long lasting sink for Carbon [60]. Micro algal bio-fixation is a developing technology that still requires a lot of research. Some of the major challenges in the use of micro algae-bio fixation for post-combustion carbon capture include: the needed source of inorganic nutrient, under developed bioreactor engineering and the high energy requirement for cultivation, harvesting and drying which is

mostly sourced from fossil fuel combustion therefore, defeating the essence of the technology due to further emission of CO_2 [61,62]. Some of the suggestions that have been made to positively balance the CO_2 emitted and captured through micro-algal bio-fixation include: use of industrial flue gas to grow micro-algae, combining unit processes of lipid extraction with hexane, coagulation, catalytic transesterification and raceway pond [61,63] amongst others.

2.3.5 ADSORPTION CARBON CAPTURE

The word Adsorption was coined by German physicist; Heinrich Kayser [8]. Adsorptive separation is a mixture separating process which works on the principle of differences in adsorption/desorption properties of the constituent mixture [64]. *It is defined as an exothermic process that involves adhesion of ions, atoms or molecules from a liquid, gas or dissolved solid to a surface*. The adhered ions, atoms or molecules form film on the surface of the materials to which they are attached and are called *adsorbate* while the material on which they are attached is called the *adsorbent. Adsorption occurs on the surface while absorption entails the whole material volume.* In adsorption, superficial atoms of the adsorbents are not completely encompassed by the remaining adsorbent atoms, this makes them "entice" adsorbates. Adsorption is as a result of surface energy due to the filling of the bonding requirements of the adsorbent by the adsorbate atoms [8]. The particular type of bonding involved is a function of the species involved. Adsorption may take place on physical adsorbents, in which case will involve weak van der Waals forces this is known as physiorption or on chemical materials, involving covalent bonding (chemisorption) and it may occur due to electrostatic attraction. Below is a schematic of adsorption carbon capture process:

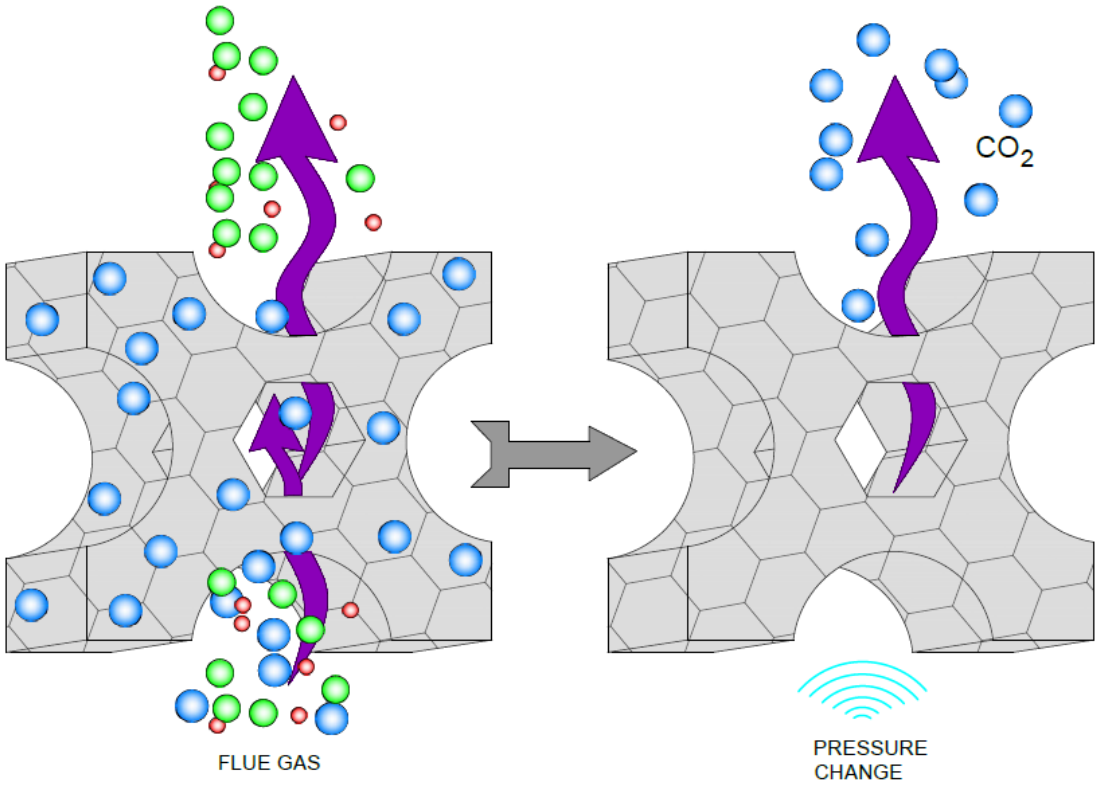

Figure 2.5: Schematics of Adsorption carbon capture process

Adsorption is reportedly said to have a major advantage of easy of adsorbent regeneration by thermal or pressure modulation and it is relatively cheaper [13]. The ease of adsorbent regeneration reduces the energy requirement, hence the cost of carbon capture. Some merits and challenges of adsorption post combustion carbon capture technology include:

Merits of adsorption carbon capture technology

i. Ease of regeneration of adsorbed CO_2

ii. Durability of adsorbent.

iii. Remarkable selectivity of CO2 by adsorbents

iv. Remarkable adsorption capacity of adsorbents

v. High diffusion rate between adsorbate and adsorbents

vi. Good stability of adsorbent after several adsorption/desorption cycle[13]

Challenges of adsorption carbon capture

i. Cost of adsorbent and adsorption processs.

ii. Relatively low rate of adsorption

iii. Low adsorption capacity at low pressure

iv. Poor thermal stability [14]

v. Reduced adsorption capacity in the presence of water vapour

M. Songolzadeh et al [13] identified two classes of sorbents:

a. Chemical adsorbents and

b. Physical adsorbents.

Chemical Adsorbents

Chemical adsorbents capture CO_2 from gaseous mixture by selective adsorption of CO_2 from gas stream through formation of covalent bond. They are amine-based materials gotten from chemical modifications on the surface of solid adsorbents possessing high surface area. During a typical chemical adsorption process, CO_2 molecules interact with the adsorbent surface to form covalent bonds with the adsorbent leading to separation of CO_2 from the gas stream. This reaction can be reversed to regenerate CO_2 which can be harvested for storage. Compared to absorption which uses aqueous amine solutions, amine-based adsorbents require lesser heat for regeneration. They however have low adsorption capacity and are pretty expensive. The popular groups of amine-based adsorbents are the amine impregnated adsorbents and the amine grafted adsorbents [14]. Other groups that have been researched and tried out in recent times include: Metal Oxides and Metal Salts [65], double salts, hydrotalcites [66], Nano materials [67] etc. Further research is required in metal oxides with respect to their carbon capture capacity, rate of regeneration, cost effectiveness, kinetics of carbonation and their ability to withstand multiple adsorption-desorption cycles [65].

Comparison of some classes of chemical sorbents

Out of traditional reported chemical adsorbents mentioned above, calcium oxide is of special interest to researches because it is cheap and it has high adsorption capacity for CO_2 compared to Lithium salts which are more expensive especially in production. On the other hand, reported hydrotalcites have disadvantage of high loss in adsorption capacity after cycles of operation. Double salts could easily be regenerated because of their low energy requirement but their stability is yet to be fully investigated. This situation is the same for the reported alkali metal-based sorbents. Generally, amines are costly and their researched species have low CO_2 adsorption capacity therefore difficult to commercialize [14].

The reported nano-materials have improved stability and maintain good CO_2 capturing capacity for longer adsorption/desorption cycles. However, they have disadvantage of high cost and complicated process of synthesis. Generally, to the best of our knowledge, the reported chemical adsorbents are difficult to regenerate [67].

Physical sorbents

Physical adsorption involves the selective adsorption of CO_2 from gas stream through formation of weak Vanda Waals forces. During this process, there is no chemical reaction between the adsorbent and the adsorbate (CO_2) and no new compounds are formed. Physical adsorption can be easily reversed by heating or reducing the pressure of the saturated adsorbent. Physical adsorbent materials with micro pores (pore size < 2nm) have better adsorption selectivity for CO_2 from gas mixture, however, only few of the reported materials meet this criteria. Examples of traditional physical adsorbents include: activated carbon, zeolite, Zeolitic Imidazolate Frameworks (ZIF's), carbon nanotubes (CNTs), meso-porous silica, coal and more recently Metal Organic Frameworks (MOFs).

Several comparisons have been made between physical adsorbents and chemical adsorbents and it has been shown that, physical adsorbents consume lesser energy in adsorption carbon capture because of their ease of regeneration [3]. If the challenge of selectivity in physical sorbents is successfully overcome, their use for carbon capture could be potential energy saving alternative in place of the dominant amine-based absorption systems in industries today [7]. Notwithstanding the advantages of physical adsorbents, each of the reported physical adsorbents have their peculiar limitations, these limitations are enumerated below.

Comparison of some classes of traditional physical adsorbents

To the best of our knowledge, the reported mesoporous silica materials have the advantages of high volume, surface area and tuneable pore size, thermal and mechanical stability, however, their adsorption capacity is not sufficient especially at atmospheric pressure [67]. Activated carbon are obviously carbonaceous materials and they have the advantages of high adsorption capacity for CO_2, high hydrophobicity, low cost, enormous availability, little regeneration energy requirement and they are insensitive to moisture. Activated carbon however has the disadvantage of application to only high pressure gases. In addition to this, at high temperature they have high sensitivity and low selectivity [67].

Zeolites on the other hand have better selectivity for CO_2/N_2 than most of the reported carbonaceous materials; they possess highly crystalline structures, high surface area, tunable composition structure and ratio. To the best of our knowledge, the reported zeolites have relatively low selectivity and they are hydrophilic i.e. their CO_2 adsorption capacity drops with the presence of moisture in gas [67].

ZIF's are formed when transition metals replace tetrahedron atoms in zeolites. They have high chemical stability, high and tunable porosity, electron withdrawing groups that enhance their interaction with the oxygen group in CO_2 and remarkable CO_2 capture capacity incredibly higher than most reported MOFs e.g. ZIF-69 reportedly has about eight times the adsorption capacity of MOF-177 [68]. ZIF's have modifiable links which can be tuned to develop specific functional group of materials. ZIFs have promising CO_2 capture properties; however, further research is required on them to optimize their potentials [68].

Ultimately, there is need for evolution of a contemporary class of potent, comparatively cheap, and industrially applicable materials for carbon capture applications in order to minimize the uncontrolled emissions of carbon dioxide into the atmosphere. This is necessary on a national and international scale. The major prerequisite for these potential new materials would be that they must validly show:

(a) Stability in air and water
(b) Good thermal stability
(c) Distinct selectivity
(d) Resistance to corrosion
(e) High adsorption capacity for CO_2
(f) Sufficient mechanical strength to endure repeated operations which involve exposure to stream of gases at high pressure.

After continues search, about two decades ago, a new class of materials was discovered, they are simply called MOFs and they are termed so because they are made of Metal-Organic Frameworks [64]. MOFs are organic-inorganic hybrid, porous, solid materials whose research has developed greatly since their inception. Out of all known materials till date,

MOFs have been said to have the highest potentials because: they have the highest surface area per gram and they have flexible design-ability in terms of structure and function [64]. MOFs are very promising; however, most reported MOFs have the disadvantages of reduction in adsorption capacity on exposure to gas mixture. Various researches are being carried out on MOFs to improve their adsorption properties some of which include:

Blending of alkylamines with MOFs; this resulted in high stability, selectivity, recyclability of the developed material, however, an increase in heat of adsorption was recorded which is of great disadvantage in adsorption carbon capture [58].

Recently, a slurry type material was reported [69], the material combines some properties of MOFs, ionic liquids, membranes and amines. It was synthesized by suspending ZIF-8 in glycol-2-methylimidazole solution. It reportedly has low sorption enthalpy, high adsorption capacity at pressure of 1bar, high CO_2 selectivity in binary gas mixture, however further research is required for optimization of the material and for better insights into the material's behaviour under real flue condition. The following sections shall discuss the fast rising group of materials known as Metal-Organic Frameworks (MOFs).

2.4 METAL ORGANIC FRAMEWORKS (MOFs)

Metal-Organic Frameworks, also known as coordination polymers, date back to 1989. They were idealized and first synthesized by Hoskins and Robson [70]. MOFs are porous hybrid Nano-cubes that harness bi-properties; they establish properties of organic and inorganic porous materials. They are porous crystalline materials formulated from metal-containing nodes that bond to organic linking ligands [7,64]. MOFs are constructed by joining cluster containing polyatomic metals (with an assumption of controllable formations throughout

synthesis) serving as Secondary Building Units (SBUs), by rigid organic units by well-built covalent bonds [64].

Different metals have been used to form different MOF geometries e.g. Fe, Rh, Mo, Al, Cr, Mn, Sc, Co, Be all in different combinations. The molecular shapes of MOFs depend on the desired metal combination. Sizes of MOFs can be expanded or reduced by adding, replacing or removing some of their metal composition; this is also applicable to their functionalities. Since their emergence, MOFs have been potential material for Carbon capture, and a lot of research have been and are being carried out on them to improve their potential usage in carbon capture amongst other fields. Figure 2.6 shows the molecular structure of a typical MOF (Mg-MOF-74).

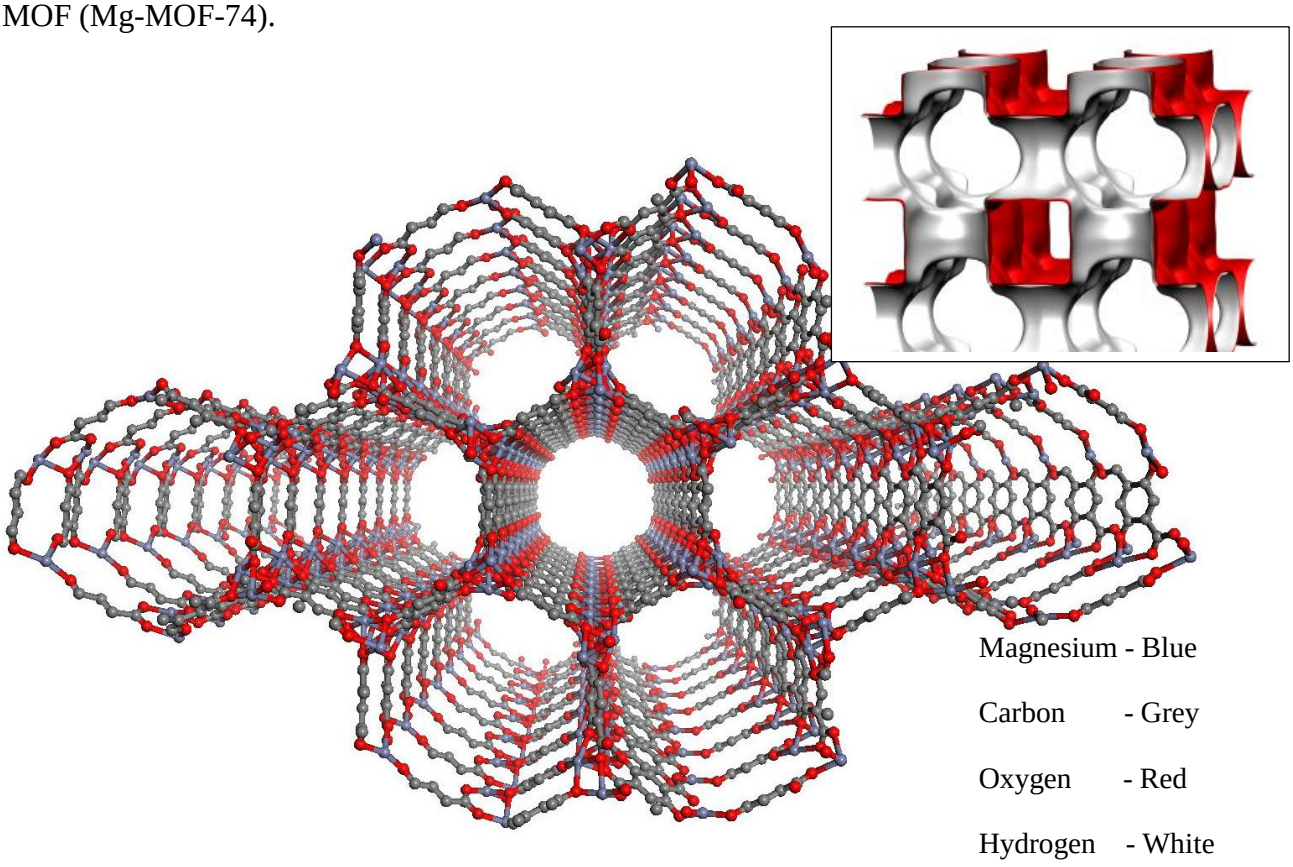

Figure 2.6: Typical molecular structure of Mg-MOF-74

2.4.1 Synthesis of MOFs:

A large number of them have been synthesized by different groups of researchers with the aim of arriving at a suitable formulation with the right properties for efficient carbon capture and other specialized functionalities. As at August 2012, a total of about 37,241 MOF structures were available in the Cambridge Structure Data base [71]. Typically, MOFs are synthesized in a servo-thermal reaction which involves combination of organic ligands and metal salts at comparatively low temperatures usually below 300 ℃. The ligand properties such as ligand length, bulkiness, bond angles, chirality etc. act as major factors to determine the frame work of the resultant MOF [72]. Besides the servo-thermal reaction method, some other methods have been described by researchers for the synthesis of MOFs. These include: The mixture of non-miscible solvents [73], spray drying technic [74], electrochemical approach [75,76], a high-throughput approach [77,78] and microwave irradiation [79,80]. The latter option; Micro wave irradiation; enables access to increased range of temperatures, and it can be used to reduce crystallization time and for controlling distribution of particle size and face morphology. Microwave irradiation however has a disadvantage of small crystal size formation, therefore, poor structural data for the synthesized MOF.

After synthesis, names are given to MOFs merely to reflect the nature of their framework, and the researchers who worked on them [72], after which their properties are tested. Properties such as hydrothermal stability are estimated by subjecting synthesized MOFs to steam at temperature and concentration more than anticipated in practical operating condition with the use of a throughput apparatus. The behaviour of the MOFs during this test is used to determine their potential operating behaviour during adsorption in the presence steam. After the hydrothermal stability test, sample materials could be exposed to X-ray diffraction (XRD) examination to ascertain their structural stability [81]. Reported MOFs have shown good

structural stability and comparatively high hydrothermal stability. Below are some properties of MOFs that affect their adsorption capacity for CO_2.

2.4.2 Some properties of MOFs that affect their adsorption capacity

Carbon capture in MOFs depends on properties such as: pore size or volume, nature of pore surface, rigidity and flexibility of MOFs etc. [7]. The volume and nature of pore to great extent determine the shape of adsorption isotherms, this is due to interaction between molecules of CO_2 leading to large condensation. Reported MOFs have higher adsorption capacity than reported zeolites and activated Carbon because they have more surface area and larger pore sizes. Below is an overview of some important characteristics of MOFs.

Rigidity and flexibility in MOFs:

MOFs could be rigid or flexible, depending on whether or not they show relative movement within their frameworks before or during adsorption. This property to a great extent determines the nature of the adsorption isotherm [7], [82]–[85].

Rigid MOFs have diverse shapes of adsorption isotherms, the most common being the I-shaped isotherms. Some MOFs are with ultrahigh pores which make them exhibit sigmoidal isotherms at temperature close to room temperature and at high pressure, example of this is MOF-177. Reports have also been made of rigid MOFs that exhibit bi-porous structures with channels and cages existing together within them, making them to have stepwise adsorption isotherms [86].

On the other hand, flexible MOFs display stepwise or hysteretic desorption for CO_2 and other gases [7]. Such MOFs are said to 'breath' during adsorption/desorption e.g. M(OH)(bdc)(MIL-53) series, $Sc_2(bdc)_3$ etc. Flexible MOFs e.g. Mg-MOF-74 show great potential for selectivity and they have advantage of smooth increment in volume with

increase in CO_2 loading. The flexibility of MOFs can be improved by post addition of group Alkyl chain length. A popular phenomenon in flexible MOFs is called "gate" phenomenon: Such MOFs exhibit abrupt rise in adsorption isotherm at relatively low pressure, termed "gate" opening pressure, while their saturation occur at a different pressure. The desorption isotherms of these MOFs do not follow reverse trace of their adsorption isotherms; they rather show sudden drop at another pressure (third pressure). Gate phenomenon has been reported by Kitagawa et al [31] and Rosseinsky et al [32] amongst others. An example of such MOFs is Cu (pyrdc) (bpp).

Effect of Heat of adsorption on MOFs:

Another property of gas adsorption that affects CO_2 uptake capacity of MOFs, is heat of adsorption [7]. Heat of adsorption can be estimated with the use of adsorption isotherms of CO_2 capture processes, which can be obtained at various temperatures. Heat of adsorption is an important property in desorption; high heat of adsorption brings about high energy requirement for regeneration/desorption. Heat of adsorption reduces with increase in loading.

Effect of pore morphology on MOFs:

The tenability of pores in MOFs is one of the important properties that distinguish them from other porous materials. Often, the length of organic linkers is the major determinant of the pores size in MOFs [89]. An analysis of the sorbate-framework interactions by T. Duren [70] showed that one dimensional pores with sharp edges are better for gas separation and gas storage at low pressure. However, this is less feasible at higher pressure because of the small volume of these preferred energetic corner regions at such pressures. At lower pressure and smaller pore volume, better selectivity and adsorption rate per unit volume can be achieved; however, this can lead to quicker saturation due to smaller pore volume for accumulation of adsorbate. Some suggested ways by which CO_2 uptake of MOFs has been improved include;

i. Introduction of metal ions to improve MOF capacity of MOFs at high pressure.

ii. After-synthesis-exchange of extra framework cations inside anions MOFs.

iii. Introduction CNTs into MOFs, which could be ameliorated by addition of lithium [81,90].

2.4.3 Other prospective applications of MOFs

MOFs are versatile materials that have been found useful in different fields for many purposes besides carbon capture; however, research is still on going to perfect some of the desired properties of MOFs. Based on existing reports, MOFs have been described useful in: detoxification of industrial waste and air purification [91], microelectronics, lighting and sensing applications, water Purification [91], fuel cell membrane [92,93], chemical sensors [72,94], gas/fuel storage [70,72,95], separation of gas/vapour mixed via adsorption [72,91], [95], selective shape/size catalysis (i.e. Lewis acid catalysis) [72,96], selective catalysis [96], drug storage and delivery [97], medical Imaging [98], templates in the preparation of low dimensional materials [72] etc.

2.4.4 Future research in MOFs

Some of the suggested future research that can be carried out on MOFs includes: development of a description of the dynamic evolution of CO_2 adsorption modelling, long term structural stability in MOFs, Cheap organic linkers, MOFs with higher selectivity in CO_2/N_2 at low pressure, MOFs stability in the presence of ambient moisture for selective adsorption, Synthesis of semiconductor MOFs, comparison of MOFs with popular heterogeneous industrial catalysts, better understanding of molecular level gas-sorbent synergy e.g. design of molecular baskets for CO_2, formulated MOFs with average particles size greater than 1mm (that permit scaling up) for industrial scale usage etc.

In recent past, significant breakthrough has been recorded in MOF research, some of the MOF species that have shown remarkable potentials for carbon capture include: Mg-MOF-74, MOF-5 and MOF-177.

2.4.5 Mg-MOF-74

Mg-MOF-74 also known as Mg_2 (dobdc) is a MOF specie that has been suggested to have great potentials for CO_2 adsorption. This may be due to the fierce synergy initiated between free pair of oxygen atoms revolving in the outer shell of CO_2 structure and free cations from the metals [99]. Few research work have been carried out by scientist and engineers alike to test the capability of Mg-MOF-74 in the removal of cyanogen chloride, ammonia and sulphur dioxide from air [100]. Under similar operating conditions, in the presence of methane (CH_4), Mg-MOF-74 reportedly possesses higher adsorption capacity for CO_2 than zeolite 13X which is currently considered to be the adsorbent with the highest potentials for carbon capture [101]. In addition to this, wet Mg-MOF-74 has six times the performance of BPL activated carbon for adsorption of ammonia [100]. Mg-MOF-74 has great selectivity for CO_2 in bi-gas mixtures of 20% CO_2 and it exhibits easy CO_2 regeneration at low temperature range [102]. Finally, Mg-MOF-74 shows no deterioration in adsorption capacity for up to ten adsorption cycles [103].

This work further test the potentials of the material for CO_2 removal from flue gas (15% CO_2, 80% N_2) and its possible exploration in carbon capture. For this purpose, a numerical study of adsorption separation of CO_2 from flue gas is presented in this study. A simulation of adsorption model of breakthrough experiment on a fixed bed has been carried out to evaluate the capacity of Mg-MOF-74 for CO_2 capture with varying feed gas temperature of 28^{o}C, 50^{o}C, 100^{o}C and 150^{o}C.

2.4.6 MOF-5

MOF-5 reportedly has high porosity and adsorption capacity for CO_2 and other harmful gases at ambient temperature [104]–[106]. To the best of the authors knowledge, of the reported porous materials; next to MOF-177; MOF-5 has the second largest adsorption capacity for CO_2 [107]. The behaviour of MOF-5 isotherms under pressure has been described to be like bulk fluid showing gradual sigmoidal (step) increment with CO_2 loading [106], this behaviour is more pronounced below room temperature. Reports have also shown that MOF-5 has higher adsorption capacity than coal and Activated Carbon at pressures below 1atm with adsorption capacity comparable to zeolite 13X at such pressures [107]. MOF-5 also shows higher adsorption capacity for CO_2 than zeolite 5A at elevated pressure [108], it has good strength to withstand pressures up to the range of 0-225bar without losing its structural integrity. Notwithstanding these advantages, it is important to mention that MOF-5 has been identified to degrade quickly on exposure to moisture [109], and it undergoes thermal degradation at high temperature i.e. above 400^{o}C [79].

2.4.7 MOF-177

MOF-177 reportedly has ultrahigh porosity with high adsorption capacity for CO_2 and other harmful gases at ambient temperature [110]–[112]. To the best of our knowledge, of the reported porous materials, MOF-177 has the largest adsorption capacity for CO_2 with Langmuir surface area of about 4500m^2/g [106,113,114]. Reports have also shown that MOF-177 has higher adsorption capacity than coal and Activated Carbon at pressures below 1atm with adsorption capacity higher than zeolite 13X and NaX at such pressures, it has good strength to withstand high pressure without losing its structural integrity [111].

Notwithstanding these advantages, it is important to mention that MOF-177 has been identified to degrade on exposure to moisture [109], and it low gas selectivity [79].

2.5 MODELING OF ADSORPTION

2.5.1 IMPORTANCE OF ADSORPTION MODELING

It has been reported that if adsorption carbon capture technique is thoroughly researched, optimized and explored in place of absorption carbon capture technique which is dominant in industries today, the cost incurred in CO_2 capture would be cut down by a great deal [115]. Since one of the current challenges in adsorption carbon capture technology is the inadequacy of potent materials for the process, research into better understanding and prediction of the behaviour of adsorption carbon capture materials cannot be over emphasized.

In adsorption carbon capture process, material selection precedes process design. To select good materials (adsorbents) for carbon capture, properties such as: adsorbent selectivity, adsorption capacity, ease of and energy required in desorption are of great importance. After adsorbent selection, before bulk synthesizing of desired materials, there is need for appropriate models to describe the dynamics of the adsorption material, system and process as a whole in order *to save precious time and cost* and *to achieve suitable and effective design of the process* [116,117]. Experimental data could be used for this purpose, however, experimental processes are quite costly and time consuming [118].

Mathematical models for adsorption are experimentally verified and their simulations enable *good estimation of breakthrough behaviour and temperature profiling of constituent gases at different time and point within the adsorption column*. In addition, varieties of materials could be quickly and easily tested for their adsorption potentials using mathematical models. Furthermore, due to variations in composition (in time and space) and temperatures of

adsorption systems and their effects on overall performance of the systems, efficient mathematical model for description and prediction of such transient systems will be appropriate [119].

2.5.2 ADSORPTIVE CARBON CAPTURE EXPERIMENTS

Several technologies have been reported for testing adsorption behaviour of potential materials for gas separation processes. These technologies are established as experiments and employed to verify adsorption properties of desired materials. Some of the technologies work by principle of variation of adsorption related parameters such as: pressure (total or partial), temperature, velocity and concentration of gas species etc. Some reported technologies include: Pressure Swing Adsorption (PSA) [120], Thermal (Temperature) Swing Adsorption (TSA) [121], Vacuum Swing Adsorption (VSA) [122], Electrical Swing Adsorption (ESA) [123] and the popular Breakthrough experiment (BET) [124] etc. This work shall examine the mathematical modelling of the breakthrough experiment, Pressure Swing Adsorption and carbon dioxide storage in Metal Organic Frameworks (MOFs).

Breakthrough Experiment

Breakthrough experiment is carried out to determine the equilibrium time also known as breakthrough time for any given adsorbent material. The adsorption column is packed with pellets of adsorbents which are usually pre-treated (purged) with an inert gas (more often Helium), and the require gas mixture to be separated is passed through the bed at a given flow rate, pressure and temperature. The inlet temperature of the gas stream is termed the temperature at which breakthrough curve is obtained. The total gas flow rate at the inlet is measure by a bubble meter and usually held constant. At the outlet of the adsorption chamber, the time at which the adsorbent can no longer adsorb the gas flowing through it; such that the concentration of the desired component in the gas stream at the inlet is equal to its concentration of the stream at the outlet is called the break through time. The

concentration of the gas at the bed exit is periodically analysed using gas analysers. Breakthrough experiment is used to test the adsorption capacity of materials. The schematics of a gas-solid adsorption system to separate CO_2 from flue gas assuming dry flue gas with composition of 15% CO_2 and 85% N_2 is described in figure 2.7

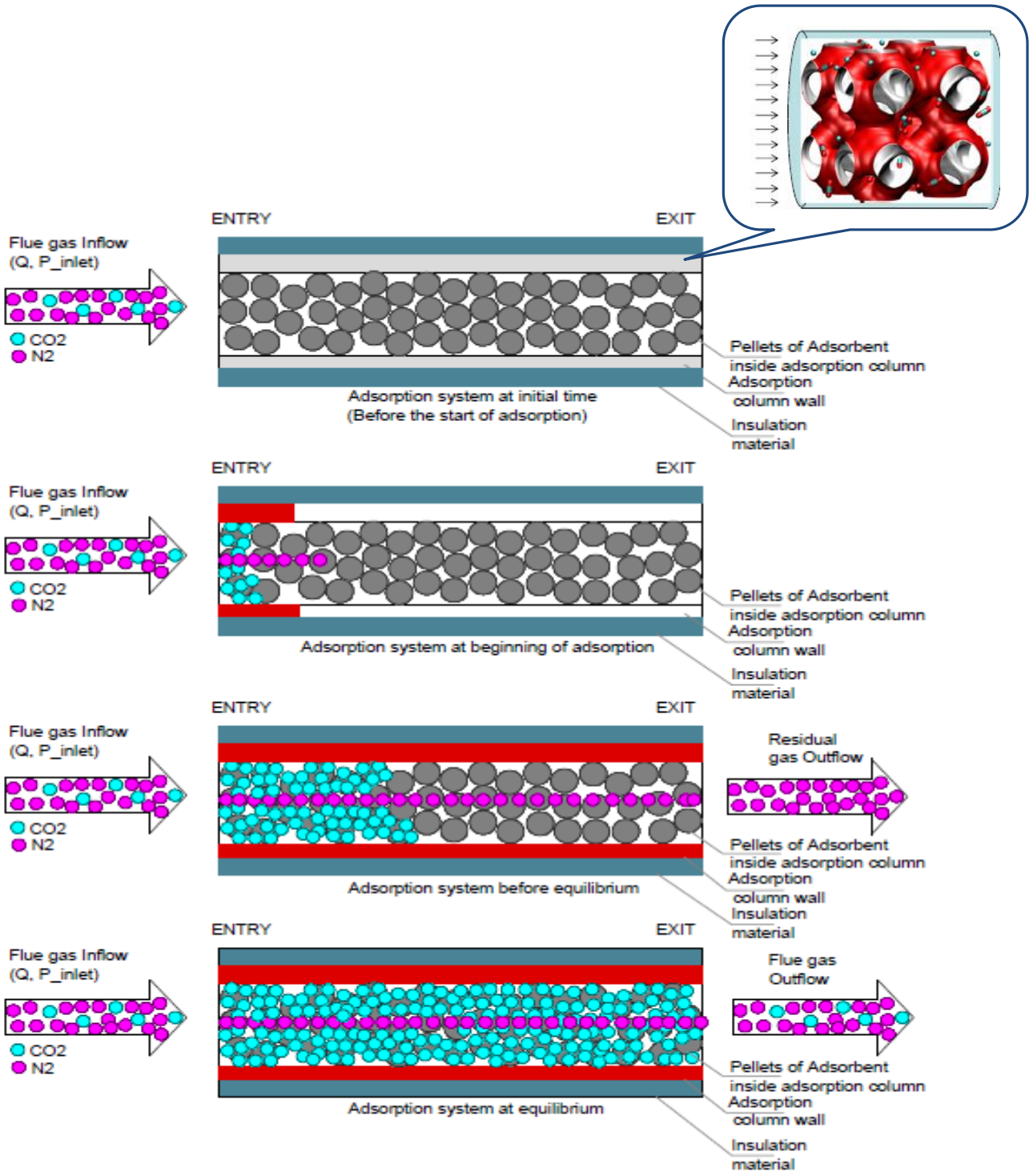

Figure 2.7: Schematics of CO_2 adsorption for breakthrough experiment [125]

Adsorptive CO_2 Storage

Adsorptive gas storage experiment is carried out to determine the behaviour of adsorbent materials during gas filling process. It is very similar to the breakthrough experiment; however, pure component gas is feed into the fixed bed rather than gas mixture. The bed exit remains closed and filling is done at various pressures. The adsorption column is packed with pellets of adsorbents which are usually pre-treated (purged) with an inert gas (more often Helium), and the required pure gas to be stored is passed through the bed at a given flow rate, pressure and temperature. The feed gas temperature and pressure are termed the charging temperature and pressure. The total gas flow rate at the inlet is measure by a bubble meter and may vary. The time at which the adsorbent can no longer adsorb the gas flowing through it; such that the concentration of the gas in the solid phase at the end of the bed is equal to the concentration of the gas in the solid phase at the inlet of the bed is called the filling time. CO_2 storage experiment is used to evaluate gas storage behaviour of adsorbent materials under pressure.

Pressure Swing Adsorption (PSA)

The PSA is an adsorption gas separation process by pressure variation i.e. a pressurization-depressurization system. PSA has been suggested to be preferable over most of the other existing separation technologies when the concentration of the gas to be separated is of importance (i.e. relatively high) because it enhances quick and easy change of gas pressure thereby reducing the time interval required between cycles of adsorption and desorption processes [126]. The PSA process, initially described as the "heatless" process was invented after TSA process by Charles Skarstrom in 1960 for the purpose of oxygen enrichment. However, over the years, PSA technology has been widely applied for several separation processes including: air and hydrogen purification, carbon dioxide capture, gas upgrading etc.

A typical Skarstrom cycle consists of a 2-bed, four step process including: (i) pressurization (ii) feed (iii) blow down and (iv) purge steps [127].

Purging step involves the removal of ambient gases in the adsorbent bed by passing an inert gas (e.g. helium) through the bed. Purging prepares the bed for new adsorption cycles. After purging is the pressurization step. Pressurization of the bed involves subjecting the bed to relatively high pressure by closing the valves at the exit of the bed in order to allow continuous gas inflow with no outflow. The pressurization step helps to increase the gas dispersion rate in the column and breakthrough time during adsorption [128],[129]. The third step is the feed step; 'feeding' involves passing gaseous mixture that is to be separated into the bed i.e. feeding the system with the gaseous mixture (e.g. CO_2/N_2 mixture), this is continued until the adsorbent is saturated. During feeding, un-adsorbed gases are allowed to freely flow out from bed exit as effluent gases. After saturation, the pressure at the bed exit is decreased by some means e.g. vacuum pump or by connection to an unsaturated bed etc. to desorb the adsorbed gases. This process is called counter current blow down (desorption). The adsorbed gases gradually desorb due to pressure gradient until the pressure within the bed and at bed exit are equal. Pressure Swing Adsorption (PSA) is used to test durability of materials to withstand repeated cycles of adsorption and desorption processed without degradation. PSA has advantage over Temperature Swing Adsorption because it does not require additional time for heat exchange (heating and cooling) for adsorption and desorption processes [130]. Figure 2.8 and Table 2.1 show a schematic of PSA and valve sequencing for different steps in the cycle respectively.

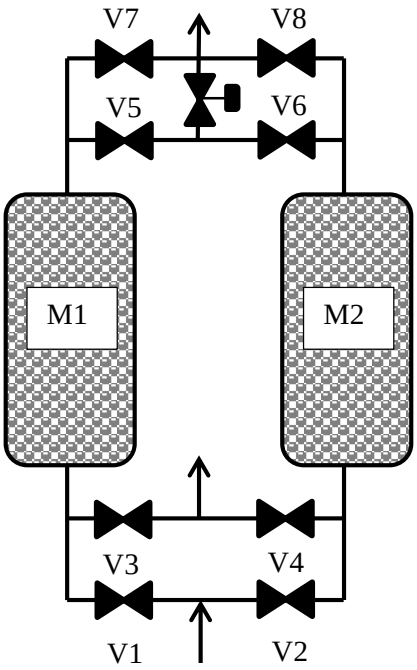

Figure 2.8: Schematics design of two-column PSA unit

Table 2.1: Valve sequencing for different steps in PSA cycle

M1	Feed	Blow down	Purge	Pressurization
	V1, V7	V3	V5, V3	V1
M1	Purge	Pressurization	Feed	Blow down
	V6, V4	V2	V2, V8	V4

In the PSA set up (figure 2.8), the first column (M1) is fed with flue gas at a pressure above atmospheric pressure, the packed bed selectively remove CO_2 from the gas stream leaving nitrogen rich effluent to flow out from valve 7(V7). After a set time e.g. breakthrough, the adsorbent packed in M1 is saturated hence, it no longer adsorbs CO_2. The feed is then directed to the second column (M2). In order to regenerate the saturated bed (M1), valve

3(V3) is opened to initiate pressure drop within the bed. The induced pressure causes desorption of the adsorbed CO_2 making the gas exiting V3 rich in CO_2. A purge step is then initiated to facilitate additional removal of CO_2 from the column. After purging, the bed pressure is restored by pressurizing with the less adsorbed gas. These are the four steps that make up a typical PSA cycle. At the end of a complete cycle additional cycles can be conducted to ensure further purity of the desorbed stream [126].

Several modifications have evolved over the years to improve on the Skarstrom cycle. Modifications including: varying of step times [131], addition of novel steps e.g. pressure equalization step [132], rinse step [133], co-current depressurization [134], use of multiple beds [135], addition of heat and vacuum [136], use of vacuum for regeneration (VPSA) [137] etc.

Cheng-Tung and Wen-Chun [138] Proposed simulated four bed PSA process for oxygen purification on zeolite 5A the steps include: (i) pressurization (ii) feed pressurization (iii) production (iv) blow down (v) purge (vi) pressure equalization. It was suggested that when breakthrough does not occur during the de-pressurizing pressure equalization step, a minimum purge rate gives high recovery for producing a product of high purity. A. Agarwal et al. [139] developed a Reduce Order Model (ROM) for simulation of 2-bed four step PSA process for the separation of methane and hydrogen mixture. A modification of the various steps of the Skarstrom cycle was carried for process optimization. It was suggested that ROM could present a more cost effective approach for gas sequestration. P. Biswas et al. [140] researched 4-bed, eight steps pressure swing adsorption system for separation of hydrogen from gaseous mixture using mathematical modelling. Zeolites and activated carbon were employed as separation media. The steps proposed for the cycle include: (i) co-current feed (i) two subsequent steps of pressure equalization while depressurizing (iii) counter-current blow down (iv) counter-current purge (v) two subsequent steps pressure equalization while

pressurizing (vi) counter-current pressurization. Masoud and Ehsan [141] proposed a 2-bed, six step PSA process for purification of oxygen using zeolite 5A and 13X as adsorbent medium. The PSA steps are as follows: (i) Co-current pressurization (ii) high pressure feed (iii) counter current depressurization (iv) counter-current blow down (v) counter-current purge (vi) co-current pressurization. S. Nilchan and C. Pantelides [142] simulated 2-bed, four step PSA with a view of optimizing the process of oxygen purification. Zeolite 5A was employed as the separation medium and the typical Skarstrom cycle was simulated. Similarly, Harsh Khajuria [143] comprehensively described the designing, modelling, operation and control of PSA systems. Design and control optimization was carried out for 4-bed, nine-step PSA system for hydrogen purification on activated carbon. The simulated steps include: (i) feed (ii) three concurrent steps of co-current depressurization (iii) counter-current blow down (iv) counter-current purge (v) pressure equalization (vi) counter-current re-pressurization. Daeho et al [144] researched PSA and Fractional Vacuum PSA (FVPSA) processes for CO_2 sequestration from flue gas using zeolite 13X as adsorbent. It was suggested that high temperature is better for higher purity of CO_2 than ambient temperature. In like manner, Carlos A. Grande et al. [133] performed experimental and numerical analysis of a 1-bed four step PSA to evaluate the behaviour of zeolite 13X in carbon dioxide sequestration from flue gas. The steps considered include: (i) counter-current pressurization (ii) feed (iii) counter-current blow down (iv) purge. The model was adopted for analysis of an existing power plant while a "Rinse" step was included to make up 5-step PSA process for the analysis. Dantas et al [131] also simulated one-bed, four step PSA process for CO_2 separation from flue gas. The steps employed by Dantas et al. were the typical steps of Skarstrom cycle while the separation medium was activated carbon.

This thesis work further tests the behaviour of a group of potential carbon capture materials popular known as Metal Organic Frameworks (MOFs) for CO_2 removal from flue gas (15%

CO_2 wt N_2) for possible exploration in carbon capture and mitigation of the challenges of global warming. One of the objectives of this thesis is to carry out numerical study of Pressure Swing Adsorption separation of CO_2 from flue gas. A simulation of adsorption model of this experiment on a fixed bed has been carried out to evaluate the capacity of Mg-MOF-74 for CO_2 capture with varying feed gas temperature of 301K and 423K, varying pressurization and purge duration. We also present a novel technique of heat regeneration to enhance the PSA process for CO_2 sequestration.

2.6 MATHEMATICAL MODELS OF ADSORPTION

The dynamic behaviour of adsorption systems can be categorized based on the nature of interaction between the constituent gas species and the solid at equilibrium and the complexity of the mathematical model needed for describing the adsorption mass transfer process [145]. The relationship between the constituent gas species and the solid at equilibrium can be estimated from the performance of a material as evaluated by its adsorption isotherm. Adsorption isotherms are curves describing the behaviour of the gas stream (adsorbate) when it interacts with the solid material (adsorbent) during adsorption. Isotherms basically predict the adsorption equilibrium of a given system. The equilibrium of an adsorption system is reached when the adsorbent can no longer adsorb the adsorbate i.e. when the specie concentration in the flowing stream no longer changes. In view of this, in testing of ideal adsorbent for carbon capture, it is paramount to establish equilibrium correlations for the adsorption systems; hence, proper understanding of isotherms is important for prediction and optimization of adsorption systems [146].

Divers equilibrium isotherm models exist some of these include: Freundlich, Langmuir, Toth, Khan, Henry, Sips, Florg-Huggins, Temkin, Dubinin-Radushkevisc isotherms and so on

[119]. However, more often than not, a combination of these models has been used [146]. Of all the models, the most popularly used are the Freundlich, Langmuir and Toth isotherm models.

With exception of the adsorption isotherms, the mathematical models to predict the dynamics of adsorption systems for the different material are similar with the basic differences in the assumptions made for the type of flow, mass transfer, momentum or energy equation depending on the system being described and the experience of the individual carrying of the modelling. The complexity of the mathematical models therefore depends on the level of concentration and the choice of rate equations and flow models [145].

Adsorption models are made of coupled partial differential equations and algebraic equations representing the flow field and energy transfer within the field [117]. The adsorption flow field is a fixed bed on which adsorption takes place with suitable boundary conditions. Simultaneous solutions are required for the system of PDE's which makes the adsorption system tasking and error prone. Hence, the need for simplified models and assumptions for easier computation and optimization of adsorption processes.

Based on the work of Farooq and Ruthven [147], 1-dimensional mathematical model is adequate for a simple estimate and description of the dynamic behaviour of an adsorption system. In addition to this, according to Ahn and Brandani [124] in order save computational time, 1-D model can be adopted to give a good approximation of the behaviour of an adsorption system. For this reason, most of the models that have been worked on and the one that will be discussed in this thesis shall be 1-Dimensional mathematical model. Regardless of the assumptions made in several existing works, the basic mathematical models are as stated below.

The concentration and mole fraction of components/species 'j' in gas stream is expressed as:

$$C_j = y_j P/(RT_g) \quad (2.1)$$

Where: P and T_g are the total pressure and temperature of the gas stream, respectively [117]. The dependence of adsorption equilibrium on temperature of gas stream can be expressed with Van't Hoff's equation which is given by:

$$K_{eq,j} = K_{0,j}\, e^{(-\Delta H_j/RTg)} \quad (2.2)$$

Where: $K_{eq,j}$ is the equilibrium adsorption constant, ΔH_j is the isosteric enthalpy of adsorption of component 'j', $K_{0,j}$ is the adsorption constant at infinite dilution and R is the universal gas constant. At times $K_{eq,j}$ could be replaced by b_j and $K_{0,j}$ replaced by $b_{0,j}$ (which shares the same meaning as $K_{0,j}$) in Langmuir parameter equations which mean the same thing as above definitions [117].

The amount of component adsorbed at equilibrium $q_j{}^*$ is expressed by the isotherm equation which could be either of the isotherms listed earlier in this write up. This quantity is expressed as a function of the concentration of each gas component and temperature of the bulk gas stream i.e. $q_j{}^* = f(Cj, Tg)$.

Equations 2.3 – 2.5 represent Toth, Langmuir extended and Henry's isotherms respectively and the adsorption equilibrium for individual component would be expressed as:

$$q_j{}^* = q_{m,j} K_{eq,j} P_j/[1 + (K_{eq,j} P_j)^n]^{1/n} \quad (2.3)$$

$$q_j{}^* = q_{m,j} b_j P_j/[1 + \textstyle\sum_1^n bP] \quad (2.4)$$

$$q_j{}^* = K_p P_j \quad (2.5)$$

Where: $q_j{}^*$ is the amount adsorbed at equilibrium, $q_{m,j}$ is the maximum adsorb-able concentration which is also referred to as the monolayer capacity, K_p is Henry's adsorption constant, P_j is the partial pressure of the components in the gas stream and 'n' is the

heterogeneity parameter of the solid for each gas species [117].

Mass Balance

Rate of mass transfer:

Several mas transfer models have been suggested to describe the mass deposition process during adsorption. Some of these include: Linear Driving Force Approximation (LDF), Double LDF, modified LDF with concentration dependent diffusivity, LDF with lumped mass transfer coefficient etc. The type of mass transfer rate model assumed determines the mass transfer rate model/equation to be employed. LDF is most popularly used because it is physically consistent and analytically simpler than the other mass transfer models.

Assuming Linear Driving Force Model like in the case of this study, the mass transfer rate to the adsorbent for individual component can be written as:

$$\frac{\partial \bar{q}_j}{\partial t} = K_{L,j}(q_j^* - \bar{q}_j) \tag{2.6}$$

Where: $K_{L,j}$ is the overall mass transfer coefficient for component 'j', $\bar{q}_j$ is the average mass of component 'j' transferred to the adsorbent particles [117].

The global mass transfer coefficient has the advantage that it takes into account all possible resistances to mass transfer with respect to resistances within and outside the adsorbent particles. The Mass transfer coefficient can be expressed in form of intra and extra particle resistances [117]:

$$\frac{1}{K_L} = \frac{r_p q_o}{3k_p C_o} + \frac{r_p^2 q_o}{15\varepsilon_p D_e C_o} + \frac{r_c^2 q_o}{15D_c} \tag{2.7}$$

The first, second and third terms on the right of the equation are the film, macro-pore and micro-pore mass transfer resistances respectively. K_L is external mass transfer coefficient, r_c radius of adsorbent crystal, r_p radius of adsorbent particle,C_o is the concentration of specie in the feed at feed gas temperature T_{gfeed} ε_p is the particle porosity, q_o is the value of mass adsorbed at equilibrium, D_c is the micro-pore diffusivity. It has been shown that molecular

diffusivity is dominant for macro-pore resistances [119][148]. Assuming dominant inter-crystalline diffusion resistances, the modified mass transfer coefficient can be expressed as:

$$\frac{1}{K_L} = \frac{r_c^2 q_o}{15 D_c} \tag{2.8}$$

Where $\frac{D_c}{r_c^2}$ is the diffusion time constant. Even though this assumption reduces the adsorption capacity of the material concerned, it gives reasonable prediction of the material behaviour under the described condition [148].

Conservation of mass

Equations 2.9 and 2.10 are the transport equations for the gas phase.

i. Mass balance for components/specie equation:

$$\varepsilon \frac{\partial C_j}{\partial t} + \left(\frac{\partial u C_j}{\partial X} + \frac{\partial v C_j}{\partial Y} + \frac{\partial w C_j}{\partial Z} \right) = \varepsilon D_{ax} \left(\frac{\partial^2 C_j}{\partial^2 X} + \frac{\partial^2 C_j}{\partial^2 Y} + \frac{\partial^2 C_j}{\partial^2 Z} \right) - (1 - \varepsilon) \rho_p \frac{\partial \bar{q}_j}{\partial t} \tag{2.9}$$

ii. Bulk gas mass balance:

$$\varepsilon \frac{\partial C_T}{\partial t} + \left(\frac{\partial u C_T}{\partial X} + \frac{\partial v C_T}{\partial Y} + \frac{\partial w C_T}{\partial Z} \right) = \varepsilon D_{ax} \left(\frac{\partial^2 C_T}{\partial^2 X} + \frac{\partial^2 C_T}{\partial^2 Y} + \frac{\partial^2 C_T}{\partial^2 Z} \right) - \sum_j \left(\frac{(1-\varepsilon)}{\varepsilon} \rho_p \frac{\partial \bar{q}_j}{\partial t} \right) \tag{2.10}$$

Where: D_{ax} is the axial mass dispersion coefficient, ε is the void fraction of the material, u, v and w are the x, y, and z components of the superficial velocity. ρ_p is the adsorbent particle density, C_j is the specie concentration and C_T is the bulk gas concentration. The first and last term on the left are the unsteady and the convective terms respectively, while the first term and last terms on the right are the diffusion term and accumulation terms respectively [117].

iii. Global mass balance:

Several mass transfer models have been suggested to describe the mass deposition process during adsorption. Some of these include: plug flow, axial dispersed plug flow, Non-Darcian flow etc. The type of mass transfer flow assumed determines the mass transfer

model/equation to be employed. Assuming an axial dispersed plug flow like in the case of this study, the *continuity equation* for the flow can be expressed as:

$$\varepsilon \frac{\partial C_T}{\partial t} + \left(\frac{\partial u C_T}{\partial X} + \frac{\partial v C_T}{\partial Y} + \frac{\partial w C_T}{\partial Z} \right) = -\sum_j \left(\frac{(1-\varepsilon)}{\varepsilon} \rho_p \frac{\partial \bar{q}_j}{\partial t} \right) \quad (2.11)$$

Where: C_T and u are the total concentration and superficial velocity of the gas stream. ε and ρ_p are the void fraction and particle density of the adsorbent respectively [117].

Pressure drop

iv. The pressure drop within the adsorption column is can be expressed by Ergun's formula. This formula also gives the relationship between the superficial velocity and the total pressure at any point in the column. This equation is expressed as:

$$-\frac{\partial P}{\partial Z} = 150 \frac{\mu_g (1-\varepsilon)^2}{\varepsilon^3 d_p^2} u + 1.75 \frac{(1-\varepsilon)}{\varepsilon^3 d_p} \rho_g \, u^2 \quad (2.12)$$

Where: The first term accounts for the viscous pressure drop and the last term accounts for turbulence in the system [117].

Energy equations:

v. Energy balance for gas stream:

$$\varepsilon \, \rho_g C_{v,g} \frac{\partial T_g}{\partial t} + \rho_g C_{p,g} \left(\frac{\partial u T_g}{\partial X} + \frac{\partial v T_g}{\partial Y} + \frac{\partial w T_g}{\partial Z} \right) = \varepsilon \lambda_L \left(\frac{\partial^2 T_g}{\partial X^2} + \frac{\partial^2 T_g}{\partial Y^2} + \frac{\partial^2 T_g}{\partial Z^2} \right) -$$

$$C_s (1-\varepsilon) \rho_p \frac{\partial T_s}{\partial t} + (1-\varepsilon) \rho_p \sum_j \left(-\Delta H_j \frac{\partial \bar{q}_j}{\partial t} \right) - \frac{4 h_w}{d_{int}} (T_g - T_w) \quad (2.13)$$

Where: $C_{v,g}$ and $C_{p,g}$ are the specific heat capacities of the gas at constant volume and pressure respectively. λ_L is the axial heat dispersion coefficient. C_s is the specific heat capacity of the adsorbent material, T_s is the temperature of the solid adsorbent, h_w is the coefficient for internal convective heat transfer, and d_{int} is the internal diameter of the bed. The second to the last and the last terms on the right hand side are the accumulation term and

the convective heat transfer from the gas to the adsorption column wall respectively [117].

vi. Energy balance for adsorbent (solid phase):

$$\rho_p C_s \frac{\partial T_s}{\partial t} = \rho_p \sum_j \left(-\Delta H_j \frac{\partial \bar{q}_j}{\partial t}\right) + \frac{6h_f}{d_p}(T_g - T_s) \quad (2.14)$$

Where: h_f is the film heat transfer coefficient and d_p is the adsorbent particle diameter. The second term on the right hand side represents the convective heat transfer from the gas to the solid adsorbent [117].

vii. Energy balance for adsorption column wall:

$$\rho_w C_{p,w} \frac{\partial T_w}{\partial t} = \alpha_w h_w\left(T_g - T_w\right) + \alpha_{wl} U\left(T_g - T_\infty\right) \quad (2.15)$$

Where: ρ_w and $C_{p,w}$ are the density and specific heat capacity of the wall respectively. α_w and α_{wl} are the ratio of the internal surface area of the wall to its volume and the ratio of the logarithmic mean surface area of the column shell to the volume of the column respectively. The first term on the right hand side accounts for the heat transfer from the gas to the column, while the second term on the right hand side represents the heat transferred from the gas to the ambient. This will be neglected if the system is operating under adiabatic condition [117].

$$\alpha_w = d_{int}/l(d_{int} + l) \quad (2.16)$$

$$\alpha_{wl} = d_{int}/\{(d_{int} + l)\ \ln[(d_{int} + l)\ /\ d_{int}]\} \quad (2.17)$$

Where: $'l'$ is the column wall thickness.

Boundary Conditions (B.C's):

The popular Dackwarts boundary conditions are applied in adsorption-desorption processes. Boundary conditions for bed inlet and exit depend on the experiment being simulated. All boundary conditions employed are stated in chapters 3&4.

Initial conditions:

The initial conditions for bed depend on the experiment being simulated. All boundary conditions employed are stated in chapters 3&4.

Dimensionless numbers and correlations [117]***:***

Reynolds Number

$$Re = \frac{(\rho_g * U_{inlet} * d_p)}{\mu_g} \quad (2.18)$$

Prandtl Number

$$Pr = \frac{(C_{p,g} * \mu_g)}{k_g} \quad (2.19)$$

Nusselt Number

$$Nu = 2.0 + 1.1 * \left(Re^{0.6} * Pr^{1/3}\right) \quad (2.20)$$

Pecklet Number

$$Pe = \frac{0.508 * \left(Re^{0.020} * L\right)}{d_d} \quad (2.21)$$

Heat and mass transfer coefficients and correlations for system [117]***:***

Effective axial thermal conductivity of gas mixture in axial direction

$$\lambda_L = k_g * (10 + 0.5 * Pr * Re) \quad (2.22)$$

Internal convective heat transfer coefficient between gas and solid wall

$$h_w = k_g * (12.5 + 0.048 * Re) \quad (2.23)$$

Film heat transfer coefficient between gas and solid adsorbent

$$h_{f,j} = Nu * k_g / d_p \quad (2.24)$$

Axial dispersion coefficient

$$D_{ax} = \frac{U_{inlet} * L}{Pe} \quad (2.25)$$

2.7 REVIEW OF EXPERIMENTAL AND NUMERICAL RESEARCH WORKS ON ADSORPTION CARBON CAPTURE

The tables below summarize some experimental and numerical research works that have been carried out on post combustion carbon capture by adsorption:

Table 2.2: Review of Experimental Works on Post-Combustion Carbon Capture by Adsorption.

S/N	YEAR	AUTHORS' NAMES	APPLICATION TYPE		MATERIAL TYPE
			EXPERIMENTAL METHOD	MATHEMATICAL SOLUTION	
1	1974	Carter and Husain [149]	Breakthrough experiment	Fortran	Molecular sieve
2	1989	R. Kumar [150].	……	Finite difference method with the use of IBM 370/165	Zeolite 5A and BPL carbon
3	1994	Hwang and Lee [151].	Breakthrough experiment.	DGEAR commercial code.	Activated carbon
4	1995	K. T. Chue et al	PSA	…….	Zeolite 13X and activated carbon
5.	1995	K. S. Hwang et al [152]	Breakthrough experiment.	DIVPAG and DNEQNF commercial codes.	Activated carbon.
6	1996	Diangne et al [153]	PSA	Euler's method	Zeolite(5A, 13X and 4A)
8	2000	Ding and Alpay [154]	PSA	gPROMS commercial code	Hydrotalcite

9	2001	Takamura et al [155].	……	Discretisation of coupled PDEA equations in space and time. Final solution of ODE with variable time step.	Zeolites (Na-X and Na-A)
10	2003	Choi et al [156].	Break through experiment and PSA operation	MATLAB function.	Zeolite 13X
11	2004	Chou and Chen [122]	Vacuum Swing Adsorption (VSA)	Upwind difference and cubic spline method. Integration by integration with the use of LSODE from ODEPACK commercial code.	Zeolite 13X
12	2004	S. Cavenati et al [157]	Breakthrough experiment.	MATLAB commercial code.	Zeolite 13X
13	2005	S. Cavenati et al [158]	PSA	gPROMS commercial code.	Carbon molecular sieve 3K
14	2005	Ahn and Brandani [124].	Break through experiment.	gPROMS commercial code.	Carbon Monoliths
15	2006	S. Cavenati et al [159].	Layered Pressure Swing Adsorption (LPS)	gPROMS	Zeolite 13X
16	2006	Moreira et al [160].	……	PDECOL in FORTRAN commercial code.	Hydrotalcite (Al-Mg).
17	2006, 2007	Delgado et al [161][162].	Breakthrough experiment	PDECOL in FORTRAN commercial code.	Silicalite pellets, sepiolite, and resin.

18	2009, 2010 and 2011	Dantas et al [116][117][163]	Break through experiment and PSA	gPROMS commercial code.	Zeolites 13X and activated carbon
20	2010	A. Agarwal [164].	PSA	NPL solver	
21	2011	Krishna and Baten	PSA and Breakthrough experiment.	Molecular simulation with the use of Configuration-Bias Monte Carlo (CBMS).	Zeolites (MFI, JBW, AFX, NaX) and MOFs (MgMOF-74, MOF-177, CuBTTri-mmen)
22	2012	N. Casas et al [165].	Break through experiment.	Gear's with IMSL DIVPAG commercial package	Activated carbon
23	2012	Mulgundmath et al [166].	Breakthrough experiment.	……	Ceca 13X by
24	2013	N. Cases et al [167]	PSA and break through experiment.	Via Gear's method with IMSL DIVPAG (Fortran) commercial code.	MOF and UiO-67/MCM-41
25	2013	R. Sabouni [168].	Breakthrough experiment.	COMSOL	CPM-5
26	2013	RPPL Riberro et al [123].	Electrical Swing Adsorption (ESA).	gPROMS commercial code	Activated carbon honeycomb monolith and Zeolite 13X
27	2014	S. Krishnamurthy et al [169].	Break through experiment and VSA	MATLAB commercial code.	Zeochem zeolite 13X

Table 2.3: Review of Numerical Works on Post-Combustion Carbon Capture by Adsorption

S/N	Year	Authors' names	Application type	Model Dimens-ion	Mass transfer model	Isotherm Type	Energy Model	Pressure and Velocity model	Solution Type
1	1974	Carter and Husain [149]	Modelling of adsorption of Carbon dioxide and water vapour on molecular sieve	1-D, transient.	From experimental data.	Langmuir isotherm	Isothermal.	Negligible pressure drop.	Numerical solution on Fortran.
2	1989	R. Kumar [150].	Modelling of blow down of adsorption of CO2 from gaseous mixture of; CO_2/H_2 CO_2/CH_4 CO_2/N_2 on Zeolite 5A and BPL carbon by PSA.	1-D, transient.	Local equilibrium model	Langmuir isotherm	Non-Isothermal. Adiabatic system Negligible radial temperature gradient.	Negligible pressure gradient across adsorption bed. Flow behaviour: Plug flow	Numerical solution. Finite difference method with the use of IBM 370/165

S/N	Year	Authors' names	Application type	Model Dimens-ion	Mass transfer model	Isotherm Type	Energy Model	Pressure and Velocity model	Solution Type
3	1994	Hwang and Lee [151].	Modelling of adsorption and desorption of gaseous mixture of CO_2 and CO on activated carbon by breakthrough experiment	1-D, transient.	LDF approximation model	Langmuir isotherm	Isothermal. Temperature of column wall, adsorbent and gas were all accounted for.	Negligible pressure gradient across adsorption bed. Flow behaviour: Axial dispersed plug flow	Numerical solution with the use of DGEAR commercial code.
4	1995	K. T. Chue et al	Modelling of the adsorption of CO_2 from CO_2/N_2 mixture on Zeolite 13X and activated carbon by PSA	1-D, transient.	Adsorbed concentration by IAS model	Langmuir isotherm	Non-isothermal. Adiabatic. Thermal equilibrium between gas and solid phase.	Negligible pressure drop in bed. Flow behaviour: Axial dispersed plug flow	…….

S/N	Year	Authors' names	Application type	Model Dimens-ion	Mass transfer model	Isotherm Type	Energy Model	Pressure and Velocity model	Solution Type
5.	1995	K. S. Hwang et al [152]	Modelling of adsorption of gaseous mixture of CO_2 and CO on activated carbon by breakthrough experiment.	1-D, transient.	LDF approximation model. Lumped mass transfer coefficient.	Extended Langmuir isotherm	Isothermal. Non-adiabatic and adiabatic systems. Temperature of column wall, adsorbent and gas were all accounted for. Negligible radial temperature gradient.	Negligible pressure gradient across adsorption bed. Flow behaviour: Plug flow. Negligible radial velocity	Numerical solution. Linear algebras were solved using DIVPAG commercial code while non-linear algebra equations were solved using DNEQNF commercial code.
6	1996	Diangne et al [153]	Modelling of adsorption of CO_2 from air by PSA on Zeolite (5A, 13X and 4A)	1-D, transient.	LDF approximation model	Langmuir isotherm	Isothermal	Negligible pressure drop. Flow behaviour: Ideal plug flow.	Euler's method
7	2000	Ding and Alpay [154]	Modelling of adsorption and desorption of CO_2 on hydrotalcite at high temperature	1-D, transient.	LDF model based on pore diffusion	Langmuir isotherm	Non-isothermal. Negligible radial temperature gradient. Thermal equilibrium between fluid and particles	Pressure distribution by Ergun's equation. Flow behaviour: Axial dispersed plug flow.	Numerical solution with the use of gPROMS commercial code

S/N	Year	Authors' names	Application type	Model Dimens-ion	Mass transfer model	Isotherm Type	Energy Model	Pressure and Velocity model	Solution Type
8	2001	Takamura et al [155].	Modelling of CO_2 adsorption from gaseous mixture of CO_2 and N_2 on Zeolites (Na-X and Na-A)	1-D, transient.	LDF approximation model	Langmuir isotherm	Isothermal	Negligible pressure drop. Flow behaviour: Plug flow. Flow behaviour: Plug flow.	Discretisation of coupled PDEA equations in space and time. Final solution of ODE with variable time step.
9	2003	Choi et al [156].	Modelling of CO_2 adsorption from flue gas mixture containing $13\%\ CO_2$, $83\%\ N_2$ and $4\%\ O_2$ on zeolite 13X by break through experiment and PSA operation	1-D, transient.	LDF approximation model	Extended Langmuir isotherm	Non-isothermal. Adiabatic system Negligible temperature gradient in radial direction	Negligible pressure drop in radial direction. Flow behaviour: Plug flow. Gas flow rate in bed is mainly affected by bed height	Numerical solution with the use of MATLAB function

S/N	Year	Authors' names	Application type	Model Dimens-ion	Mass transfer model	Isotherm Type	Energy Model	Pressure and Velocity model	Solution Type
10	2004	Chou and Chen [122]	Modelling of CO_2 adsorption from flue gas mixture containing 20% CO_2, 80% N_2 and on zeolite 13X by VSA.	1-D, transient.	Local equilibrium model	Extended Langmuir isotherm	Non-isothermal. Negligible radial temperature gradient. Thermal equilibrium between fluid and particles	Negligible pressure gradient Flow behaviour: Axial dispersed plug flow.	Analytical + numerical solution. Solution of spatial derivatives by upwind difference. Solution of flow rates by cubic spline. Solution of temperature, concentration and adsorbed mass by integration with the use of LSODE from ODEPACK commercial code.
11	2004	S. Cavenati et al [157]	Modelling of fixed bed adsorption of CO_2, CH_4 and N_2 on Zeolite 13X at high pressure by breakthrough experiment.	…….	Experimental measurement	Toth Isotherm and Multisite Langmuir isotherm	Isothermal	Experimental measurement	Numerical solution to solve for mass deposited in adsorbent using MATLAB commercial code.

S/N	Year	Authors' names	Application type	Model Dimens-ion	Mass transfer model	Isotherm Type	Energy Model	Pressure and Velocity model	Solution Type
12	2005	S. Cavenati et al [158]	Modelling of fixed bed adsorption of CO_2 from a gaseous mixture of 45% CO_2 and 55% CH_4 on carbon molecular sieve 3K by PSA	1-D, transient.	A double LDF approximation model.	Multisite Langmuir isotherm	Non-isothermal. Negligible radial temperature gradient.	Pressure distribution by Ergun's equation. Flow behaviour: Axial dispersed plug flow.	Numerical solution with the use of gPROMS commercial code.
13	2005	Ahn and Brandani [124].	Modelling of fixed bed adsorption and desorption of CO_2 on Carbon Monoliths by break through experiment.	1-D, transient.	LDF approximation model	Langmuir isotherm	Isothermal	Relationship between average velocity and average pressure drop was estimated with the use of equation by Cornish 1928. Flow behaviour: Axial dispersed plug flow.	Numerical solution with the use of gPROMS commercial code.

S/N	Year	Authors' names	Application type	Model Dimens-ion	Mass transfer model	Isotherm Type	Energy Model	Pressure and Velocity model	Solution Type
14	2006	S. Cavenati et al [159].	Modelling of fixed bed adsorption of CO_2 from a gaseous mixture of $20\%\ CO_2/$ $60\%\ CH_4/$ and $20\%\ N_2$ on zeolite 13X by Layered Pressure Swing Adsorption (LPS)	1-D, transient.	Bi-LDF model	Multicomp-onent extension of multisite Langmuir	Non - Isothermal. Temperature of column wall, adsorbent and gas were all accounted for. Negligible radial temperature gradient.	Pressure distribution by Ergun's equation. Flow behaviour: Axial dispersed plug flow.	Numerical solution with the use of gPROMS
15	2006	Moreira et al [160].	Modelling of fixed bed adsorption of Helium diluted CO_2 on hydrotalcite (Al-Mg).	1-D transient.	LDF approximation model. Calculation of mass transfer coefficient by theoretical correlations.	Langmuir isotherm	Isothermal	Negligible pressure drop. Flow behaviour: Axial dispersed plug flow.	Numerical with the use of PDECOL in FORTRAN commercial code.

S/N	Year	Authors' names	Application type	Model Dimens-ion	Mass transfer model	Isotherm Type	Energy Model	Pressure and Velocity model	Solution Type
16	2006, 2007	Delgado et al [161][162] .	Modelling of fixed bed adsorption of CO2 from gaseous mixture of; CO_2/He CO_2/CH_4 CO_2/N_2 on Silicalite pellets, sepiolite, and resin using break through experiment	1-D transient.	LDF approximation model. Lumped mass transfer coefficient.	Extended Langmuir isotherm	Non-isothermal. Negligible radial temperature gradient.	Pressure distribution by Ergun's equation. Pressure variation in time and space. Flow behaviour: Axial dispersed plug flow.	Numerical solution by PDECOL commercial code.
17	2009, 2010 and 2011	Dantas et al [116] [117] [163]	Fixed bed adsorption of gaseous mixture of; CO_2/N_2 and CO_2/He on zeolites 13X and activated carbon by break through experiment and PSA	1-D, transient.	LDF approximation model. Lumped mass transfer coefficient.	Toth Isotherm	Non-Isothermal. Adiabatic and non-adiabatic system. Model accounted for Heat transfer in gas, solid and wall.	Pressure distribution by Ergun's equation. Axial dispersed plug flow.	Numerical solution using gPROMS commercial code.

S/N	Year	Authors' names	Application type	Model Dimens-ion	Mass transfer model	Isotherm Type	Energy Model	Pressure and Velocity model	Solution Type
18	2010	P. Biswas et al [170].	Modelling of adsorption separation of gaseous mixture of CO, CH_4, H_2, CO_2 on Zeolite 5A and activated carbon.	1-D, transient.	LDF model. Lumped mass transfer coefficient	Multisite Langmuir model	Isothermal. Assuming temperature of wall, gas phase and adsorbent are equal.	Pressure distribution by Ergun's equation. Flow behaviour: Axial dispersed plug flow	Discretisation by Newton based approach. Algebraic solution.
19	2010	A. Agarwal [164].	Fixed bed adsorption of CO_2 from gaseous mixture of CO_2/N_2 , 45% CO_2/ 55% H_2 by PSA	1-D, transient.	LDF approximation model. Lumped mass transfer coefficient.	Dual site Langmuir isotherm	Temperature equilibrium between gas phase adsorbent. Constant column wall temperature.	Pressure distribution by Ergun's equation. Flow behaviour: Axial dispersed plug flow	Numerical solution with the use of interior point NPL solver.

S/N	Year	Authors' names	Application type	Model Dimens-ion	Mass transfer model	Isotherm Type	Energy Model	Pressure and Velocity model	Solution Type
20	2011	Krishna and Baten	Modelling of PSA performance and break through characteristics of zeolites (MFI, JBW, AFX, NaX) and MOFs (MgMOF-74, MOF-177, CuBTTri-mmen) for gaseous mixture of CO_2/N_2	1-D, transient.	……..	…….	Isotherm	Negligible pressure drop. Assumed flow behaviour: Plug flow	Molecular simulation with the use of Configuration-Bias Monte Carlo (CBMS).
21	2012	N. Casas et al [165].	Fixed bed adsorption of CO_2 from gaseous mixture of CO_2/H_2 on activated carbon by break through experiment.	1-D, transient.	LDF model. Lumped mass transfer coefficient	Langmuir and Sip isotherms.	Thermal equilibrium between gas stream and adsorbent. Column wall temperature is accounted for separately.	Pressure distribution by Ergun's equation. Flow behaviour: Plug flow.	Finite volume method and time integration on IMSL DIVPAG commercial package using Gear's method.

S/N	Year	Authors' names	Application type	Model Dimens-ion	Mass transfer model	Isotherm Type	Energy Model	Pressure and Velocity model	Solution Type
22	2012	Mulgund math et al [166].	Fixed bed adsorption of CO_2 from gaseous mixture of 10% CO_2/ 90% N_2 on Ceca 13X by break through experiment.	1-D, transient.	LDF approximation model for external fluid film mass transfer	Langmuir isotherm	Non-Isothermal. Temperature of column wall, adsorbent and gas were all accounted for.	Negligible pressure drop. Flow behaviour: Axial dispersed plug flow.	……..
23	2013	N. Cases et al [167]	Mathematical modelling of CO_2 adsorption from CO_2/H_2 mixture in MOF and UiO-67/MCM-41 by PSA and break through experiment.	1-D, transient.	Mass transfer coefficient determined by fitting of experimental data measured in the range of interest.	Langmuir isotherm	Non-Isothermal. Adiabatic. Model accounted for Heat transfer in gas, solid and wall. Isosteric heat of adsorption and heat capacities of the fluid and the solid phase	Pressure distribution by Ergun's equation.	Integration via Gear's method with the use of IMSL DIVPAG (Fortran) commercial code.

S/N	Year	Authors' names	Application type	Model Dimens-ion	Mass transfer model	Isotherm Type	Energy Model	Pressure and Velocity model	Solution Type
24	2013	R. Sabouni [168].	Modelling of adsorption of CO_2 From in CPM-5 by breakthrough experiment.	1-D, transient.	Mass transfer coefficient determined by fitting of experimental data	Langmuir-Freundlich isotherm	Isothermal	Negligible pressure drop through column. Constant gas velocity through column	Numerical solution with the use of COMSOL
25	2013	RPPL Riberro et al [123].	Modelling of CO2 adsorption from flue gas by a mixture of Activated carbon honeycomb monolith and Zeolite 13X hybrid system by Electrical Swing Adsorption (ESA).	1-D, transient.	Two different LDF models; one for micro pores and the other for macro pores. Lumped mass transfer parameter for meso pores and micro pores; obtained from Bosanquet equation	Multisite Langmuir model	Temperature equilibrium between the solid phases. Negligible temperature gradient in adsorbent.	Pressure distribution by Ergun's equation. Assumed flow behaviour: Axial plug flow	Numerical solution with the use of gPROMS commercial code

S/N	Year	Authors' names	Application type	Model Dimens-ion	Mass transfer model	Isotherm Type	Energy Model	Pressure and Velocity model	Solution Type
26	2014	S. Krishnam urthy et al [169].	Modelling of CO2 adsorption from dry flue gas in Zeochem zeolite 13X by break through experiment and VSA	1-D, transient.	LDF approximation model.	Extended dual site Langmuir model.	Non-Isothermal	Non Isobaric. Pressure distribution by Darcy's equation.	Numerical solution by stiff ODE solver; ode23s in MATLAB commercial code.

CHAPTER 3

RESEARCH METHODOLOGY FOR SIMULATION OF BREAKTHROUGH EXPERIMENT AND ADSORPTIVE STORAGE

3.1 MATHEMATICAL MODEL FOR FIXED BED ADSORPTION

The conservation laws; mass, momentum and energy correspondence; have been used to describe the fixed bed adsorption experiment. Fluid flow behaviour has been characterized with axially dispersed plug flow model and the mass transfer rate has been expressed with Linear Driving Force model (LDF). For the breakthrough experiment, flue gas was passed through the adsorption column with both ends of the column opened. CO_2 is removed from the gas stream as it passes through the bed while the effluent is allowed to escape via the bed exit. Breakthrough was attained when the feed concentration of CO_2 equal the concentration of CO_2 at the bed. For the adsorptive storage simulation, CO_2 was passed through the adsorption bed while the bed exit was shut. The filling time was reached when the concentration of CO_2 adsorbed at the closed bed end equal the concentration of CO_2 adsorbed at the bed inlet.

3.1.1 Model Assumptions:

The following assumptions shall be made:

- Ideal gas behaviour
- Adiabatic process for breakthrough experiment simulation
- Non-adiabatic process for gas storage simulation
- Negligible radial concentration and temperature gradients.

- Constant fluid properties
- Constant bed porosity
- LDF mass transfer model with single lumped mass transfer coefficient.
- Axial dispersed plug flow
- Pressure drop by Ergun's equation
- Toth equilibrium isotherm model for adsorptive behaviour of Activated Carbon, Langmuir equilibrium isotherm model for adsorptive behaviour of Mg-MOF-74, MOF-5 and MOF-177
- Mass transfer resistance is dominated by inter-crystalline diffusion for Mg-MOF-74, MOF-5 and MOF-177

3.1.2 Governing Equations

After the application of the above assumptions to the adsorption equations, the following equations:

➢ The concentration and mole fraction of components/species 'j' in gas stream:

$$C_j = y_j P/(RT_g) \tag{3.1}$$

Where: P and T_g are the total pressure and temperature of the gas stream respectively, C_j and y_j are the concentration and mole fraction of component j.

$$\frac{\partial \bar{q}_j}{\partial t} = K_{L,j}(q_j^* - \bar{q}_j) \tag{3.2}$$

➢ The amount of component adsorbed at equilibrium ${q_j}^*$

Assuming Toth isotherm in the case of Activated Carbon, the adsorption equilibrium for individual component is expressed as:

$${q_j}^* = q_{m,j} K_{eq,j} P_j/[1 + (K_{eq,j} P_j)^n]^{1/n} \tag{3.3}$$

- The dependence of adsorption equilibrium on temperature of gas stream (Van't Hoff's equation):

$$K_{eq,j} = K_{0,j}\, e^{(-\Delta H_j/RTg)} \tag{3.4}$$

Assuming Langmuir isotherm in the case of MOF-5 and MOF-177 the adsorption equilibrium for individual component is expressed as:

$$q_j{}^* = q_{m,j} b_j P_j / [1 + b_j P_j] \tag{3.5}$$

Assuming the extended Langmuir isotherm in the case of Mg-MOF-74, the adsorption equilibrium for individual component is expressed as:

$$q_j{}^* = q_{m,j} b_j P_j / [1 + \sum_1^n bP] \tag{3.6}$$

- The dependence of adsorption equilibrium on temperature of gas stream:

$$b_j = b_{0,j}\, e^{(E_j/RTg)} \tag{3.7}$$

Where: $q_{m,j}$ is the maximum adsorb-able concentration which is also referred to as the monolayer capacity and P_j is the partial pressure of the components in the gas stream. b_j and $K_{eq,j}$ are the parameters in the pure component adsorption isotherm, $-E_j$ and ΔH_j are the enthalpies of adsorption of component 'j', $b_{0,j}$ and $K_{0,j}$ are the adsorption constants at infinite dilution, T_g is the bulk gas temperature and R is the universal gas constant.

- Mass balance for components/specie equation:

$$\varepsilon \frac{\partial C_j}{\partial t} + \left(\frac{\partial u C_j}{\partial Z}\right) = \varepsilon D_{ax} \left(\frac{\partial^2 C_j}{\partial^2 Z}\right) - (1-\varepsilon)\rho_p \frac{\partial \bar{q}_j}{\partial t} \tag{3.8}$$

- Bulk gas mass balance:

$$\varepsilon \frac{\partial C_T}{\partial t} + \left(\frac{\partial u C_T}{\partial Z}\right) = \varepsilon D_{ax} \left(\frac{\partial^2 C_T}{\partial^2 Z}\right) - \sum_j (1-\varepsilon)\rho_p \frac{\partial \bar{q}_j}{\partial t} \tag{3.9}$$

Where: D_{ax} is the axial mass dispersion coefficient, ε is the void fraction of the material, u is the superficial velocity. ρ_p is the adsorbent particle density, ε is the bed viodage, C_j is the specie concentration and C_T is the bulk gas concentration. The first and last term on the left

are the unsteady and the convective terms respectively, while the first term and last terms on the right are the diffusion term and accumulation terms respectively.

- Pressure drop within adsorption column:

$$-\frac{\partial P}{\partial Z} = 150\frac{\mu_g(1-\varepsilon)^2}{\varepsilon^3 d_p^2}u + 1.75\frac{(1-\varepsilon)}{\varepsilon^3 d_p}\rho_g\, u^2 \tag{3.10}$$

Where: d_p is the adsorbent particle diameter, ρ_g is the bulk gas density.

- Energy balance for gas stream:

$$\varepsilon\,\rho_g C_{v,g}\frac{\partial T_g}{\partial t} + \rho_g C_{p,g}\left(\frac{u\,\partial T_g}{\partial Z}\right) = \varepsilon\lambda_L\left(\frac{\partial^2 T_g}{\partial Z^2}\right) - C_s(1-\varepsilon)\rho_p\frac{\partial T_s}{\partial t} +$$

$$(1-\varepsilon)\rho_p\sum_j\left(-\Delta H_j\frac{\partial\bar{q}_j}{\partial t}\right) - \frac{4h_w}{d_{int}}(T_g - T_w) \tag{3.11}$$

Where: $C_{v,g}$ and $C_{p,g}$ are the specific heat capacities of the gas at constant volume and pressure respectively. λ_L is the axial heat dispersion coefficient. C_s is the specific heat capacity of the adsorbent material, T_s is the temperature of the solid adsorbent, h_w is the coefficient for internal convective heat transfer, and d_{int} is the internal diameter of the bed. The second to the last and the last terms on the right hand side are the accumulation term and the convective heat transfer from the gas to the adsorption column wall respectively.

- Energy balance for adsorbent (solid phase):

$$\rho_p C_s\frac{\partial T_s}{\partial t} = \rho_p\sum_j\left(-\Delta H_j\frac{\partial\bar{q}_j}{\partial t}\right) + \frac{6h_f}{d_p}(T_g - T_s) \tag{3.12}$$

Where: h_f is the film heat transfer coefficient and d_p is the adsorbent particle diameter. The second term on the right hand side represents the convective heat transfer from the gas to the solid adsorbent.

- Energy balance for adsorption column wall:

$$\rho_w C_{p,w}\frac{\partial T_w}{\partial t} = \alpha_w\, h_w(T_g - T_w) + \alpha_{wl}\, U(T_g - T_\infty) \tag{3.13}$$

$$\alpha_w = d_{int}/l(d_{int} + l) \tag{3.14}$$

$$\alpha_{wl} = d_{int}/\{(d_{int} + l)\ \ln[(d_{int} + l)\ /\ d_{int}]\} \tag{3.15}$$

Where: l is the column wall thickness, ρ_w and $C_{p,w}$ are the density and specific heat capacity of the wall respectively. α_w is the ratio of the internal surface area of the wall to its volume. α_{wl} is the ratio of logarithm mean surface area of column shell to volume of the column, U is the external overall heat transfer coefficient and T_∞ is the ambient temperature. The first term on the right hand side accounts for the heat transfer from the gas to the column, while the second term on the right hand side represents the heat transferred from the wall to the ambient. This will be neglected if the system is operating under adiabatic condition to give:

$$\rho_w C_{p,w} \frac{\partial T_w}{\partial t} = \alpha_w h_w (T_g - T_w) \tag{3.16}$$

Boundary Conditions (B.C's):

The popular Dackwarts boundary conditions have been applied. They are given as:

$$z = 0: \quad \varepsilon D_{ax} \left(\frac{\partial c_j}{\partial z}\right)\Big|_{z+} = -u(c_j|_{z-} - c_j|_{z+}) \tag{3.17}$$

$$z = L: \quad \left(\frac{\partial c_j}{\partial z}\right)\Big|_{z-} = 0 \tag{3.18}$$

$$z = 0: \quad \varepsilon \lambda_L \left(\frac{\partial T_g}{\partial z}\right)\Big|_{z+} = -ucC_s(T_g|_{z-} - T_g|_{z+}) \tag{3.19}$$

$$z = L: \quad \left(\frac{\partial T_g}{\partial z}\right)\Big|_{z-} = 0 \tag{3.20}$$

$$z = 0: \quad uc_j|_{z-} = uc_j|_{z+} \tag{3.21}$$

Initial conditions:

$$t = 0: \qquad P = P_{inlet};\ T_w = T_g = T_s = T_{g,feed}$$
$$and\ c_j(z,o) = \bar{q}_j(z,o) = 0 \tag{3.22}$$

Some System Properties:

$$\lambda_L = k_g * (10 + 0.5 * Pr * Re) \tag{3.23}$$

$$h_w = k_g * (12.5 + 0.048 * Re) \tag{3.24}$$

$$h_{f,j} = Nu * k_g / d_p \tag{3.25}$$

$$D_{ax} = \frac{U_{inlet} * L}{Pe} \tag{3.26}$$

The Mass transfer coefficient can be expressed as:

$$\frac{1}{K_L} = \frac{r_p q_o}{3k_p C_o} + \frac{r_p^2 q_o}{15\varepsilon_p D_e C_o} + \frac{r_c^2 q_o}{15D_c} \tag{3.27}$$

Assuming dominant inter-crystalline diffusion resistances for Mg-MOF-74, MOF-5 and MOF-177, the modified mass transfer coefficient can be expressed as:

$$\frac{1}{K_L} = \frac{r_c^2 q_o}{15D_c} \tag{3.28}$$

Where $\frac{D_c}{r_c^2}$ is the diffusion time constant. Even though this assumption reduces the adsorption capacity of the material concerned, it gives reasonable prediction of the material behaviour under the described condition [148].

Dimensionless Numbers:

$$Re = \frac{(\rho_g * U_{inlet} * d_p)}{\mu_g} \tag{3.29}$$

$$Pr = \frac{(C_{p,g} * \mu_g)}{k_g} \tag{3.30}$$

$$Nu = 2.0 + \ 1.1 * \left(Re^{0.6} * Pr^{1/3}\right) \tag{3.31}$$

$$Pe = \frac{0.508 * \left(Re^{0.020} * L\right)}{d_d} \tag{3.32}$$

The Partial Differential Algebraic Equations have been linearized using Finite Differential Method; forward differential in time and backward differential in space. This method has been chosen for stability and consistency.

3.2 NUMERICAL SOLUTION

3.2.1 Numerical Solution Method

The governing equations were linearized using Finite Differential Method; forward differential in time and backward differential in space. The adsorption column for the main case study was divided into 100 grid points and the simulation of adsorption model of breakthrough experiment (assuming feed gas of 15% CO_2, 85% N_2), and CO_2 storage experiment (assuming feed gas of 100% CO_2) were carried out using MATLAB commercial code with Mg-MOF-74 as adsorbent for breakthrough experiment, MOF-5 and MOF-177 as adsorbent for CO_2 storage experiment. Similar simulations were also carried out on Activated

Carbon fixed bed. Schematics of the systems under consideration and the associated numerical grids are shown in Figures 3.1 & 3.2

3.2.2 Discretised Governing Equations:

Below are the discretized Partial Differential Algebraic Equations using Finite Differential Method; forward differential in time and backward differential in space.

$$C_{j,(m)}^{n+1} = \frac{y_{j,(m)}^{n+1} * P_{(m)}^{n+1}}{(R * T_{g,(m)}^{n+1})} \tag{3.33}$$

$$K_{eq,j,(m)}^{n+1} = K_{o,j,(m)}^{n+1} e^{(-\Delta H_j / R * T_{g,(m)}^{n+1})} \tag{3.34}$$

$$q_{j,(m)}^{*(n+1)} = \frac{q_{m,j,(m)}^{n+1} * K_{eq,j,(m)}^{n+1} * P_{j,(m)}^{n+1}}{[1+(K_{eq,j,(m)}^{n+1} * P_{(m)}^{n+1})^{nj}]^{1/nj}} \tag{3.35}$$

$$\frac{\bar{q}_{j_{(m)}}^{n+1} - \bar{q}_{j_{(m)}}^{n}}{\Delta t} = K_{L,j}(q_{j,(m)}^{*(n+1)} - \bar{q}_{j_{(m)}}^{n+1}) \tag{3.36}$$

$$\varepsilon \frac{C_{j_{(m)}}^{n+1} - C_{j_{(m)}}^{n}}{\Delta t} + \left(\frac{u_{(m)}^{n+1} * C_{j_{(m)}}^{n+1} - u_{(m-1)}^{n+1} * C_{j_{(m-1)}}^{n+1}}{\Delta Z} \right) = \varepsilon D_{ax} \left(\frac{(C_{j,(m+1)}^{n+1} - C_{j,(m)}^{n+1}) - (C_{j,(m)}^{n+1} - C_{j,(m-1)}^{n+1})}{\Delta Z^2} \right) - (1-\varepsilon)\rho_p \frac{\bar{q}_{j_{(m)}}^{n+1} - \bar{q}_{j_{(m)}}^{n}}{\Delta t} \tag{3.37}$$

$$\varepsilon \frac{C_{T_{(m)}}^{n+1} - C_{T_{(m)}}^{n}}{\Delta t} + \left(\frac{u_{(m)}^{n+1} * C_{T_{(m)}}^{n+1} - u_{(m-1)}^{n+1} * C_{T_{(m-1)}}^{n+1}}{\Delta Z} \right) = \varepsilon D_{ax} \left(\frac{(C_{T,(m+1)}^{n+1} - C_{T,(m)}^{n+1}) - (C_{T,(m)}^{n+1} - C_{T,(m-1)}^{n+1})}{\Delta Z^2} \right) - \sum_j (1-\varepsilon)\rho_p \frac{\bar{q}_{j_{(m)}}^{n+1} - \bar{q}_{j_{(m)}}^{n}}{\Delta t} \tag{3.38}$$

$$-\frac{(P_{(m)}^{n+1} - P_{(m-1)}^{n+1})}{\Delta Z} = 150 \frac{\mu_g (1-\varepsilon)^2}{\varepsilon^3 d_p^2} u_{(m)}^{n+1} + 1.75 \frac{(1-\varepsilon)}{\varepsilon^3 d_p} \rho_g \, (u_{(m)}^{n+1})^2 \tag{3.39}$$

$$\varepsilon\,\rho_g C_{v,g}\,\frac{T_{g(m)}^{n+1}-T_{g(m)}^{n}}{\Delta t}+\rho_g C_{p,g}\left(\frac{u_{(m)}^{n+1}*T_{g(m)}^{n+1}-u_{(m-1)}^{n+1}*T_{g(m-1)}^{n+1}}{\Delta Z}\right)=$$
$$\varepsilon\lambda_L\left(\frac{(T_{g,(m+1)}^{n+1}-T_{g,(m)}^{n+1})-(T_{g,(m)}^{n+1}-T_{g,(m-1)}^{n+1})}{\Delta Z^2}\right)-C_s(1-\varepsilon)\rho_p\,\frac{T_{s(m)}^{n+1}-T_{s(m)}^{n}}{\Delta t}+\ldots$$

$$(1-\varepsilon)\rho_p\sum_j\left(-\Delta H_j\,\frac{\bar{q}_{j(m)}^{n+1}-\bar{q}_{j(m)}^{n}}{\Delta t}\right)-\frac{4h_w}{d_{int}}(T_{g(m)}^{n+1}-T_{w(m)}^{n+1}) \tag{3.40}$$

$$\rho_p C_s\,\frac{T_{s(m)}^{n+1}-T_{s(m)}^{n}}{\Delta t}\;=\;\rho_p\sum_j\left(-\Delta H_j\,\frac{\bar{q}_{j(m)}^{n+1}-\bar{q}_{j(m)}^{n}}{\Delta t}\right)+\frac{6h_f}{d_p}(T_{g(m)}^{n+1}-T_{s(m)}^{n+1}) \tag{3.41}$$

$$\rho_w C_{p,w}\,\frac{T_{w(m)}^{n+1}-T_{w(m)}^{n}}{\Delta t}\;=\;\alpha_w\,h_w\left(T_{g(m)}^{n+1}-T_{w(m)}^{n+1}\right)+\alpha_{wl}\,U\left(T_{g(m)}^{n+1}-T_{\infty}\right) \tag{3.42}$$

Discretized Boundary Conditions:

Discretization of the Dackwarts Boundary Conditions can be written as:

$$z=0:\;\varepsilon D_{ax}\left(\frac{C_{j(m)}^{n+1}-C_{j(m-1)}^{n+1}}{\Delta Z}\right)=\;-(u_{(m-1)}^{n+1}*C_{j(m-1)}^{n+1}-\;u_{(m)}^{n+1}*C_{j(m)}^{n+1}) \tag{3.43}$$

$$z=L:\;\left(\frac{C_{j(m)}^{n+1}-C_{j(m-1)}^{n+1}}{\Delta Z}\right)=\;0 \tag{3.44}$$

$$z=0:\;\varepsilon\lambda_L\left(\frac{T_{g(m)}^{n+1}-T_{g(m-1)}^{n+1}}{\Delta Z}\right)=\;-\rho_g C_s(u_{(m-1)}^{n+1}*T_{g(m-1)}^{n+1}-\;u_{(m)}^{n+1}*T_{g(m)}^{n+1}) \tag{3.45}$$

$$z=L:\;\left(\frac{T_{g(m)}^{n+1}-T_{g(m-1)}^{n+1}}{\Delta Z}\right)=\;0 \tag{3.46}$$

$$z=0:\;u_{(m-1)}^{n+1}*C_{j(m-1)}^{n+1}=\;u_{(m)}^{n+1}*C_{j(m)}^{n+1} \tag{3.47}$$

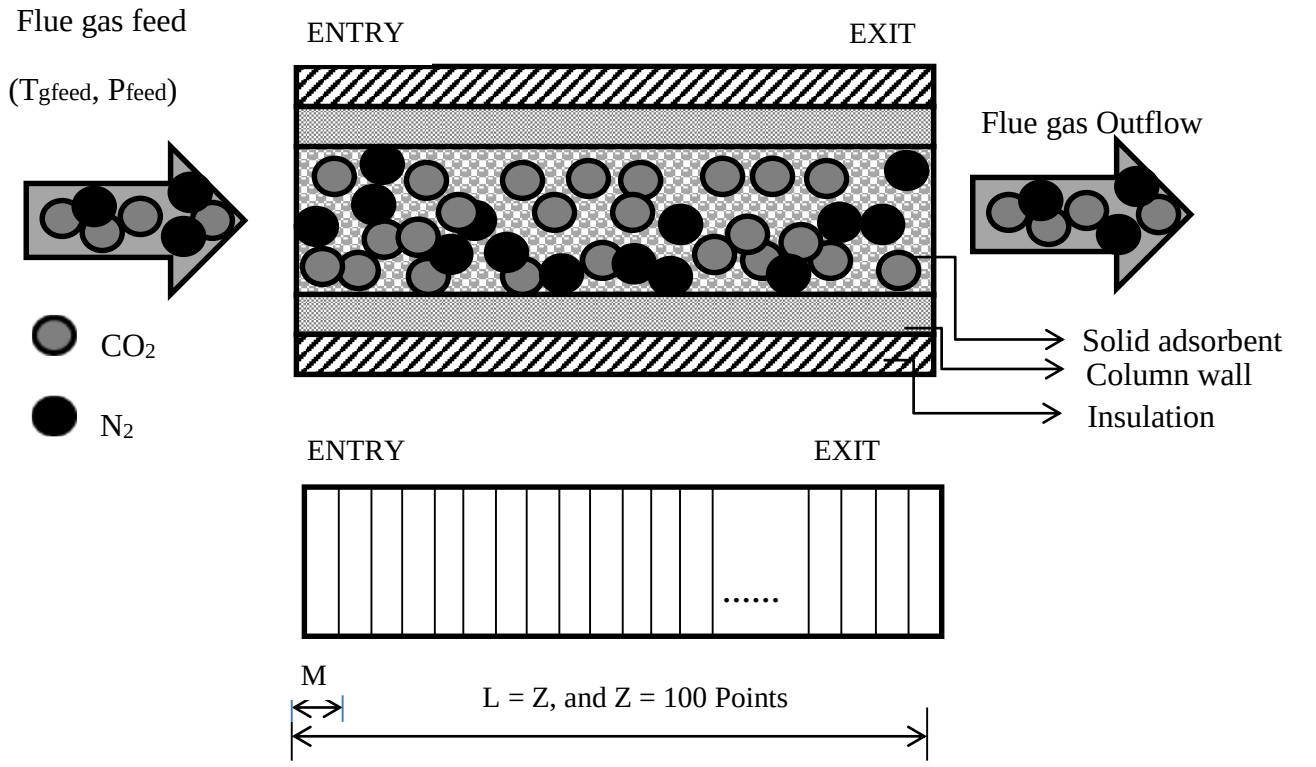

Figure 3.1: Grid for simulation of breakthrough experiment

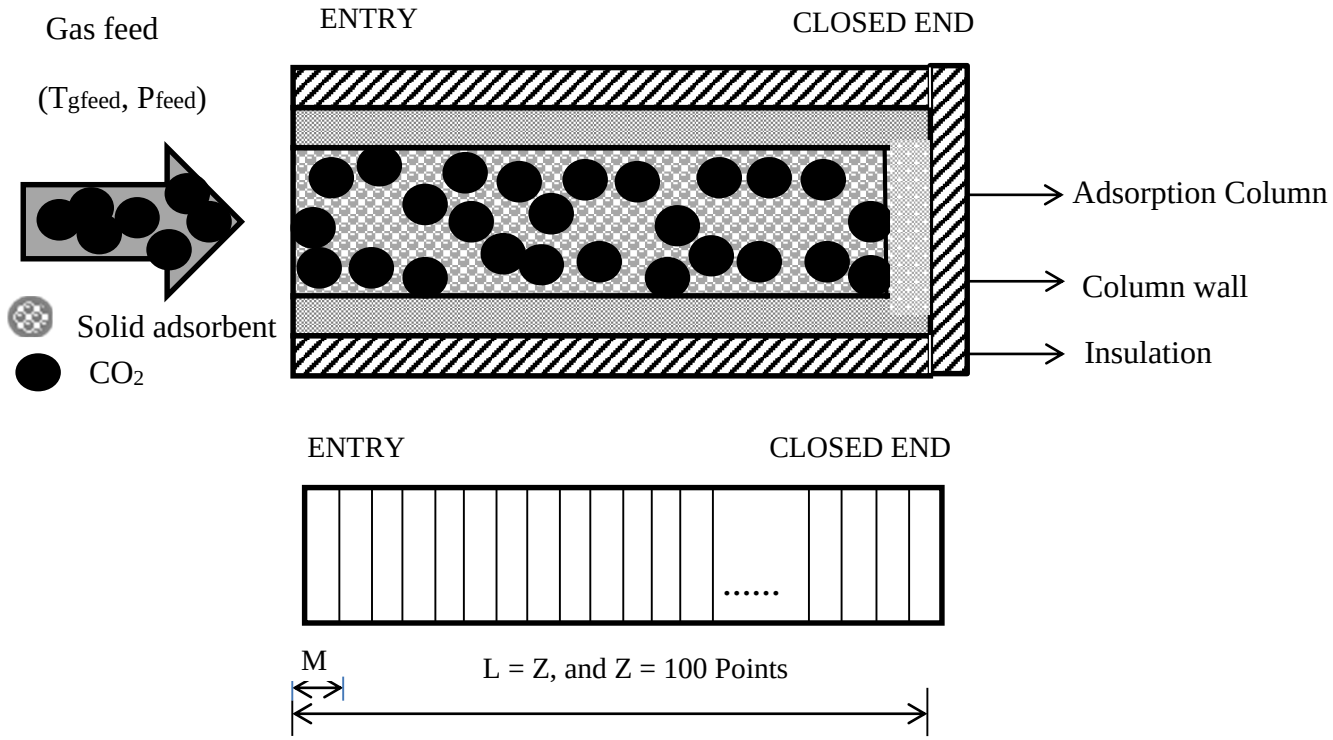

Figure 3.2: Grid for simulation of adsorptive storage

Where: "L" is the Length of adsorption column (0.171m) and "M" is the Size of each division (0.00171m).

An algorithm was written with the discretized coupled ordinary differential equations for adsorptive carbon capture using MATLAB commercial package.

3.3 ADSORPTION SYSTEM PROPERTIES AND EXPERIMENTAL DATA FOR SIMULATION OF BREALTHROUGH EXPERIMENT AND ADSORPTIVE STORAGE

For simulation of breakthrough experiment, the algorithm was validated with the experimental data of Dantas et al [117]. One-Dimensional (1-D) model of break through experiment of adsorption of Carbon dioxide from flue gas (15% CO_2, 85% N_2) on Activated carbon was simulated. For simulation of CO_2 storage experiment, the exit of the bed was made a no-flow region by setting u = 0 at z = L, the modified algorithm was then validated against experimental results of Jinsheng Xiao et al. [171,172] and Hermosilla-Lara et al. [173] for hydrogen adsorption on fixed bed of Activated Carbon. Modified Dubinin-Astakhov (D-A) isotherm model was employed to describe the adsorption equilibrium of the system which is given as:

$$q_j{}^* = q_{m,j} exp[-(\frac{RT_g}{\alpha_{D-A}+\beta_{D-A}} \ln \frac{P_o}{P})^m] \quad (3.48)$$

The system properties used for validation are as described in the tables 3.1-3.5.

3.3.1 Adsorption system properties and experimental data for validation of breakthrough experiment

The following experimental data and system properties were gotten from Dantas et al [117].

Table 3.1: Properties of Adsorption column and bed for CO_2/N_2 Adsorption on fixed bed

Properties	**Value**
Bed Length, L	0.171 m
Bed diameter, dint	0.022 m
Column wall thickness, $\boldsymbol{l}$	0.0015
Column wall specific heat capacity, $\boldsymbol{C_{p,w}}$	440 J/kg-K
Column wall density	7280 kg/m^3

Table 3.2: Properties of Adsorbent (Activated Carbon)

Properties of Activated carbon	**Values**
Particle density, ρ_p	1138 kg/m^2
Particle diameter, d_p	0.0038 m
Bed void fraction, ε	0.52
Solid Specific heat, C_s	800 J/kg-K
BET Surface area	1053 m2/g

Table 3.3: Feed properties of Adsorbate (20% CO_2, 80% N_2)

Properties of binary gas mixture (20% CO_2/N_2)	**Values**
Feed flow rate (Q_{feed})	30 ml/min
Feed pressure (P_{feed})	$102000\ Pa$
Mole fraction of CO_2	0.2
Mole fraction of N_2	0.8

Table 3.4: Thoth Model Parameters for CO_2 & N_2 adsorption on AC

Gas specie	Maximum adsorbed concentration(q_m) mol/kg	Heterogeneity Parameter (n)	Adsorption constant at infinite dilution(K_o), Pa^{-1}	ΔH_j (J/mol)
CO_2	10.05	0.68	7.62e-10	- 21840
N_2	9.74	0.52	6.91e-10	-16310

Table 3.5: LDF Global Mass Transfer Coefficient of CO_2 & N_2 on AC

Run	$T_g\ (K)$	CO_2	N_2
		Global MTC (K_L) s^{-1}	
1	301	0.0025	0.004
2	323	0.0042	0.011
3	373	0.0138	0.042
4	423	0.0323	0.128

At the end of the validation exercise, the simulated results showed that the algorithm closely predicted the experimental results of Dantas et al [117]. The algorithm was further employed to test repeated adsorption of CO_2 on activated carbon. The algorithm was then adopted for evaluation of CO_2 adsorption behaviour of Mg-MOF-74 at gas feed temperatures of 301K, 323K, 373K and 423K. All properties of adsorption system were maintained with the following modifications:

Table 3.6: Properties of Adsorbent (Mg-MOF-74)

Properties of Mg-MOF-74	**Values**				**References**
Particle diameter, d_p	0.0038 m				
Bed void fraction, ε	0.52				
Particle density, ρ	911 kg/m^{25}				[174]
Langmuir specific surface area	1733 m^2/g				[175]
Solid Specific heat, C_s under Helium gas	301K	323K	373K	423K	[110]
	800 J/kg-K	830 J/kg-K	900 J/kg-K	960 J/kg-K	

Table 3.7: Feed properties of Adsorbate (15% CO_2, 85% N_2)

Properties of binary gas mixture (15% CO_2, 85% N_2)	**Values**
Feed flow rate 'Q_{feed}'	30 mL/min
Feed pressure (P_{feed})	102000 Pa
Mole fraction of CO_2	0.15
Mole fraction of N_2	0.85

Table 3.8: Langmuir Isotherm Parameter for Adsorption of CO_2 & N_2 on Mg-MOF-74 Fixed bed

Gas specie	**Max adsorbed conc(q_m) mol/kg**	**Adsorption constant at infinite dilution (b_o), Pa^{-1}**	**ΔH_j (J/mol)**	**References**
CO_2	7.90	1.557 e-11	- 42000	[110]
N_2	14.0	4.96 e-10	-18000	[110]

Table 3.9: Mass Transfer Parameter of CO_2 and N_2 on Mg-MOF-74

Diffusion time constant (s^{-1}) D_c/r_c^2	**CO_2**				**N_2**	**Ref**
	301K	323K	373K	423K	1.97e-2	[110]
	8.11e-3	9.14e-3	11.59e-3	13.24e-3		

As stated on table 3.9, the diffusion time constant of N_2 in the binary gas mixture is assumed constant with temperature. If anything, this will only increase the amount of N_2 adsorbed with no negative effect on the adsorption of CO_2 in the mixture. Results of simulation of breakthrough experiment are presented and discussed in chapter 5.

3.3.2 Adsorption system properties and experimental data for validation of Adsorptive Storage of CO_2

Table 3.10: Properties of Adsorption Column for H_2 Adsorption on Activated Carbon Fixed bed

Properties	**Value**
Bed Length, L	0.255 m
Bed diameter, dint	0.096 m
Column wall thickness, $\boldsymbol{l}$	0.014
Column wall specific heat capacity, $\mathbf{C}_{\boldsymbol{p,w}}$	468 J/kg-K
Column wall density	7830 kg/m3

Table 3.11: Properties of Adsorbent (Activated Carbon) for H_2 Adsorption on AC

Properties of Activated carbon	**Values**
Particle density, ρ	702.4 kg/m^2
Particle diameter, d_p	0.002 m
Bed void fraction, ε	0.66
Solid Specific heat, C_s	825 J/kg-K
Global mass transfer coefficient of H_2 to AC (K_L)	0.15 s^{-1}

Table 3.12: Feed Properties of Adsorbate (H_2)

Properties of feed gas (H_2)	**Values**
Feed velocity 'u'	$5\ e-4\ m/s$
Feed pressure (P_{inlet})	$10\ MPa$
Limit pressure (P_o)	$1470\ MPa$

Table 3.13: Modified Dubinin-Astakhov Model Parameters for Adsorption of H_2 on Activated Carbon fixed bed

Maximum adsorbed concentration (q_m) mol/kg	**Heterogeneity Parameter (m)**	**Enthalpy factor (α_{D-A}), $Jmol^{-1}$**	**Entropy factor (β_{D-A}), $J(molK^{-1})$**	**ΔH_j (J/mol)**
71.6	2	3080	18.9	- 3185

The adsorption system was assumed to be non-adiabatic and readily purged. Feed gas was assumed to be 100% hydrogen and the ambient temperature, initial system temperature and feed gas temperature were set to 295K with the coefficient of heat transfer from column wall to the ambient as 12 W/m^{2}K. Further details of experimental data can be found in Jinsheng Xiao et al [169,170]. The results of the validation exercise showed that the algorithm closely predicted the experimental results. Therefore, further simulations were carried out to examine the effect of feeding CO_2 at higher pressure while setting the initial bed pressure to 1bar compared with feeding CO_2 at higher pressure while setting the initial bed pressure to be the same as the feed pressure. It was found that both cases did not show significant variation in the mass of CO_2 adsorbed, hence, the initial system pressure in this study has been set to be equal to the feed pressure. This was done to prevent system oscillation during simulation caused by the effect of high pressure shock wave due to high feed pressure compared to the

initial pressure within the bed. The algorithm was then adopted for evaluation of CO_2 adsorption behaviour on MOF-5, MOF-177 and activated carbon at a gas feed temperatures of 301K and different feed pressure including 1bar, 2bar, 3bar, 4bar, 5bar, 10bar, 20bar, 30bar, 40bar and 50bar. A parametric study was also carried out to evaluate the effect of bed width and length on the dynamics of adsorption. The three adsorbents were evaluated in this light at gas feed pressure of 1bar and temperature of 301K The properties of adsorption column and activated used are those stated in tables 3.1 & 3.2. Tables (3.14 - 3.19) provide details of the other parameters used for these studies.

Table 3.14: Properties of Adsorbents (MOF-5 and MOF-177)

Properties	**Values**	**References**
Particle diameter, d_p	0.0038 m	
Bed void fraction, ε	0.52	
MOF-5 particle density, ρ	590 kg/m^2	[176]
MOF-5 Langmuir specific surface area	2900 m^2/g	[107]
MOF-5 Specific heat, C_s	750 J/kgK	[177]
MOF-177 particle density, ρ	427 kg/m^2	[176]
MOF-177 Langmuir specific surface area	4500 m^2/g	[114]
MOF-177 Specific heat, C_s	490 J/kgK	[110]

Table 3.15: Feed Properties of Adsorbate (CO_2)

Properties of feed gas	**Values**
Feed flow rate 'Q_{feed}'	30 mL/min
Feed temperature (T_{gfeed})	301K

Table 3.16: Feed Pressure of Adsorbate (CO_2)

Run	$P\ (bar)$	Run	$P\ (bar)$
1	1	6	10
2	2	7	20
3	3	8	30
4	4	9	40
5	5	10	50

Table 3.17: Langmuir isotherm parameter for adsorption of CO_2 on MOF-5 and MOF-177

MOF specie	**Max adsorbed conc(q_m) mol/kg**	**Adsorption constant at infinite dilution (b_o), Pa^{-1}**	**ΔH_j (J/mol)**	**References**
MOF-5	10.258	2.5144 e-12	- 34000	[107]
MOF-177	48	8.06 e-10	-14000	[110]

Table 3.18: Mass transfer parameter of CO_2 & N_2 on MOF-5, MOF-177 and AC

	CO_2 on MOF-5	**CO_2 on AC**	**CO_2 on MOF-177**
Mass transfer parameter K_L (s^{-1})	0.024	0.0027	0.1597
References	[107]	[117]	[108]

To study bed/column size effect, different bed lengths and diameters were varied. To verify the effect if changing the bed length, the bed diameter was held at 0.02m whereas the length was fixed at 0.5 m to study the effect of its diameter. All other bed and column properties were fixed.

Table 3.19: Dimensions of adsorption column for bed size parametric studies

Run	Bed dimension (L x Ø)	
	Varying Bed length	**Varying bed width**
1	0.2m x 0.02m	0.5m x 0.02m
2	0.5m x 0.02m	0.5m x 0.04m
3	1m x 0.02m	0.5m x 0.1m

Results of all simulations of adsorptive storage using the above parameters are described in chapter 6.

CHAPTER 4

RESEARCH METHODOLOGY FOR SIMULATION OF PRESSURE SWING ADSORPTION (PSA) EXPERIMENT

4.1 MATHEMATICAL MODEL FOR FIXED BED PSA

In this work, the conservation laws; mass, momentum and energy; have been employed to describe the fixed bed adsorption experiment. Fluid flow behaviour has been characterized with axial dispersed plug flow model and the mass transfer rate has been expressed with Linear Driving Force model (LDF). The assumptions made in this work include:

4.1.1 Model Assumptions:

The following assumptions have been made:

- Ideal gas behaviour
- Non-adiabatic process
- Negligible radial concentration and temperature gradients
- Constant fluid properties
- Constant bed porosity
- Axial dispersed plug flow
- LDF mass transfer model
- Mass transfer resistance is dominated by inter-crystalline diffusion
- Pressure drop by Ergun's equation
- Extended Langmuir equilibrium adsorption isotherm model
- Heat transfer to heat storage material by conduction and convection processes

4.1.2 Governing Equations

The adsorption step of the PSA is described by equations 3.1 to 3.32. Equation 3.16 is replaced with equation 3.13 in order to cater for the heat exchange between the adsorption system and ambient. For desorption and purge steps, equation 3.2 will now carry a negative sign to model the detachment of the gases from the solid phase. In addition to this, the negative sign in front of the heat of adsorption in the energy balance equations is replaced with a positive sign in order to cater for the endothermic process. The following are the mathematical models for desorption and purge steps of the PSA:

- The concentration and mole fraction of components/species 'j' in gas stream:

$$C_j = y_j P/(RT_g) \tag{4.1}$$

Where: P and T_g are the total pressure and temperature of the gas stream respectively, C_j and y_j are the concentration and mole fraction of component j.

$$\frac{\partial \bar{q}_j}{\partial t} = -K_{L,j}(q_j^* - \bar{q}_j) \tag{4.2}$$

- The amount of component adsorbed at equilibrium $q_j{}^*$

Assuming Toth isotherm in the case of Activated Carbon and zeolite 13X, the adsorption equilibrium for individual component is expressed as:

$$q_j{}^* = q_{m,j} K_{eq,j} P_j/[1 + (K_{eq,j} P_j)^n]^{1/n} \tag{4.3}$$

- The dependence of adsorption equilibrium on temperature of gas stream (Van't Hoff's equation):

$$K_{eq,j} = K_{0,j}\, e^{(\Delta H_j/RTg)} \tag{4.4}$$

Assuming the extended Langmuir isotherm in the case of Mg-MOF-74, the adsorption equilibrium for individual component is expressed as:

$$q_j{}^* = q_{m,j} b_j P_j/[1 + \textstyle\sum_1^n bP] \tag{4.5}$$

- The dependence of adsorption equilibrium on temperature of gas stream:

$$b_j = b_{0,j}\, e^{(-E_j/RTg)} \tag{4.6}$$

Where: $q_{m,j}$ is the maximum adsorb-able concentration which is also referred to as the monolayer capacity and P_j is the partial pressure of the components in the gas stream. b_j and $K_{eq,j}$ are the parameters in the pure component adsorption isotherm, $-E_j$ and ΔH_j are the enthalpies of adsorption of component 'j', $b_{0,j}$ and $K_{0,j}$ are the adsorption constants at infinite dilution, T_g is the bulk gas temperature and R is the universal gas constant.

- Mass balance for components/specie equation:

$$\varepsilon \frac{\partial C_j}{\partial t} + \left(\frac{\partial u C_j}{\partial Z}\right) = \varepsilon D_{ax} \left(\frac{\partial^2 C_j}{\partial^2 Z}\right) - (1-\varepsilon)\rho_p \frac{\partial \bar{q}_j}{\partial t} \tag{4.7}$$

- Bulk gas mass balance:

$$\varepsilon \frac{\partial C_T}{\partial t} + \left(\frac{\partial u C_T}{\partial Z}\right) = \varepsilon D_{ax} \left(\frac{\partial^2 C_T}{\partial^2 Z}\right) - \sum_j (1-\varepsilon)\rho_p \frac{\partial \bar{q}_j}{\partial t} \tag{4.8}$$

Where: D_{ax} is the axial mass dispersion coefficient, ε is the void fraction of the material, u is the superficial velocity. ρ_p is the adsorbent particle density, ε is the bed viodage, C_j is the specie concentration and C_T is the bulk gas concentration. The first and last term on the left are the unsteady and the convective terms respectively, while the first term and last terms on the right are the diffusion term and accumulation terms respectively.

- Pressure drop within adsorption column:

$$-\frac{\partial P}{\partial Z} = 150 \frac{\mu_g (1-\varepsilon)^2}{\varepsilon^3 d_p^2} u + 1.75 \frac{(1-\varepsilon)}{\varepsilon^3 d_p} \rho_g\, u^2 \tag{4.9}$$

Where: d_p is the adsorbent particle diameter, ρ_g is the bulk gas density.

- Energy balance for gas stream:

$$\varepsilon\, \rho_g C_{v,g} \frac{\partial T_g}{\partial t} + \rho_g C_{p,g} \left(\frac{u\, \partial T_g}{\partial Z}\right) = \varepsilon \lambda_L \left(\frac{\partial^2 T_g}{\partial Z^2}\right) - C_s (1-\varepsilon)\rho_p \frac{\partial T_s}{\partial t} +$$

$$(1-\varepsilon)\rho_p \sum_j \left(\Delta H_j \frac{\partial \bar{q}_j}{\partial t}\right) - \frac{4 h_w}{d_{int}} (T_g - T_w) \tag{4.10}$$

Where: $C_{v,g}$ and $C_{p,g}$ are the specific heat capacities of the gas at constant volume and pressure respectively. λ_L is the axial heat dispersion coefficient. C_s is the specific heat capacity of the adsorbent material, T_s is the temperature of the solid adsorbent, h_w is the coefficient for internal convective heat transfer, and d_{int} is the internal diameter of the bed. The second to the last and the last terms on the right hand side are the accumulation term and the convective heat transfer from the gas to the adsorption column wall respectively.

- Energy balance for adsorbent (solid phase):

$$\rho_p C_s \frac{\partial T_s}{\partial t} = \rho_p \sum_j \left(\Delta H_j \frac{\partial \bar{q}_j}{\partial t}\right) + \frac{6h_f}{d_p}(T_g - T_s) \quad (4.11)$$

Where: h_f is the film heat transfer coefficient and d_p is the adsorbent particle diameter. The second term on the right hand side represents the convective heat transfer from the gas to the solid adsorbent.

- Energy balance for adsorption column wall:

$$\rho_w C_{p,w} \frac{\partial T_w}{\partial t} = \alpha_w h_w(T_g - T_w) + \alpha_{wl} U(T_g - T_\infty) \quad (4.12)$$

$$\alpha_w = d_{int}/l(d_{int} + l) \quad (4.13)$$

$$\alpha_{wl} = d_{int}/\{(d_{int} + l) \ln[(d_{int} + l) / d_{int}]\} \quad (4.14)$$

Where: l is the column wall thickness, ρ_w and $C_{p,w}$ are the density and specific heat capacity of the wall respectively. α_w is the ratio of the internal surface area of the wall to its volume. α_{wl} is the ratio of logarithm mean surface area of column shell to volume of the column, U is the external overall heat transfer coefficient and T_∞ is the ambient temperature. The first term on the right hand side accounts for the heat transfer from the gas to the column, while the second term on the right hand side represents the heat transferred from the gas to the ambient.

For simulation of the PSA with heat regenerating system, after incorporation of a packed of storage material, equation 6a was modified to equation 6b as stated below:

$$\rho_w C_{p,w} \frac{\partial T_w}{\partial t} = \alpha_w h_w(T_g - T_w) - \rho_{stor} C_{p,stor} \frac{\partial T_{stor}}{\partial t} \quad (4.15)$$

Where: ρ_{stor} and C_{stor} are the density and specific heat capacity of the heat storage material respectively. The second term on the right hand side represents the heat stored in the heat storage material which in this case is packed sand bed. It is assumed that the packed sand bed is in a refractory material isolate with a layer of fibre glass, with a distance (l_{gap}) of 0.01m from the refractory material to the adsorption column. Hence, there is no heat transfer from sand to ambient.

- Energy balance for energy storage material (packed sand bed):

$$\rho_{stor} C_{p,stor} \frac{\partial T_{stor}}{\partial t} = \alpha_{wl} k_{stor}(1 - \varepsilon_{stor})(T_w - T_{stor}) / l_{gap} + \alpha_{wl} \varepsilon_{stor} U(T_w - T_{stor}) \quad (4.16)$$

Where: k_{stor} and C_{stor} are the thermal conductivity and specific heat capacity of the storage material respectively. ε_{stor} is the porosity of the heat storage packed bed and U becomes the convective heat transfer coefficient between the wall and air in the sand bed.

Boundary Conditions (B.C's):

The popular Dackwarts boundary conditions have been applied. They are given as:

- Counter-current pressurization and co-current feed steps:

$$z = L: \qquad \varepsilon D_{ax} \left(\frac{\partial c_j}{\partial z}\right)\Big|_{z+} = -u(c_j|_{z-} - c_j|_{z+}) \quad (4.17)$$

$$z = 0: \qquad \left(\frac{\partial c_j}{\partial z}\right)\Big|_{z-} = 0 \quad (4.18)$$

$$z = L: \qquad \varepsilon \lambda_L \left(\frac{\partial T_g}{\partial z}\right)\Big|_{z+} = -ucC_s(T_g|_{z-} - T_g|_{z+}) \quad (4.19)$$

$$z = 0: \qquad \left(\frac{\partial T_g}{\partial z}\right)\Big|_{z-} = 0 \tag{4.20}$$

- Counter-current blow down and counter-current purge steps:

  At $z = 0$ and $z = L$

$$\left(\frac{\partial c_j}{\partial z}\right)\Big|_{z-} = 0 \tag{4.21}$$

$$\left(\frac{\partial T_g}{\partial z}\right)\Big|_{z-} = 0 \tag{4.22}$$

- Counter-current Pressurization step:

$$z = L: \qquad P|_{z+} = P|_{feed} \tag{4.23}$$

$$z = 0: \qquad u|_{z-} = 0 \tag{4.24}$$

- Bed inlet for feed and counter-current purge steps:

$$z = L: \qquad u|_{z-} = u|_{z+} \tag{4.25}$$

- Bed outlet for counter-current blow down and counter-current purge steps:

$$z = 0: \qquad P|_{z-} = P|_{purge} \tag{4.26}$$

Initial conditions:

The initial Condition for an unused bed is:

$$t = 0: P = P_{inlet};\ T_w = T_g = T_s = T_{g,inlet}\ \ and\ c_j(z,o) = \bar{q}_j(z,o) = 0 \tag{4.27}$$

The initial condition for subsequent cycles would be the final condition of the previous cycle.

Some System Properties:

Equations 3.23 – 3.28 still hold.

Dimensionless Numbers:

Equations 3.29 – 3.32 still hold.

Performance criteria of the PSA process:

$$\text{Purity of } CO_2 = \frac{\int_{t_{blow\ down}}^{t_{purge}} F_{CO_2} dt}{\sum_{i=1}^{n_{comp}} \int_{t_{blow\ down}}^{t_{purge}} F_j dt} \quad (4.28)$$

$$\text{Recovery of } CO_2 = \frac{\int_{t_{blow\ down}}^{t_{purge}} F_{CO_2} dt}{\int_{0}^{t_{purge}} F_{CO_2} dt} \quad (4.29)$$

$$F_j = uC_jA_b \quad (4.30)$$

Where F_j is the molar flow rate of component "j" at bed exit, C_j is the concentration of component "j", A_b is the bed exit area, $t_{blow\ down}$ and t_{purge} are the time of blow down and purge respectively.

4.2 NUMERICAL SOLUTION

4.2.1 Numerical Solution Method

The governing equations were linearized using Finite Differential Method. For pressurization and feed steps, the Partial Differential Algebraic Equations have been linearized using Finite Differential Method; forward differential in time and backward differential in space. For counter-current blow down and purge steps, the Partial Differential Algebraic Equations have been linearized using forward differential in time and space. These methods have been chosen for stability, consistency and to carter for fluid flow directions in each step. The adsorption column has been divided into 200 grid points and the simulation of PSA experiment (assuming initial feed gas of 15% CO_2, 85% N_2) was carried out using MATLAB commercial code with zeolite 13X and Mg-MOF-74 as adsorbents.

4.2.2 Discretised Governing Equations:

Below are the discretized Partial Differential Algebraic Equations using Finite Differential Method; forward differential in time and space.

$$C_{j,(m)}^{n+1} = \frac{y_{j,(m)}^{n+1} * P_{(m)}^{n+1}}{(R * T_{g,(m)}^{n+1})} \tag{4.31}$$

$$K_{eq,j,(m)}^{n+1} = K_{o,j,(m)}^{n+1} e^{(\Delta H_j / R * T_{g,(m)}^{n+1})} \tag{4.32}$$

$$q_{j,(m)}^{*(n+1)} = \frac{q_{m,j,(m)}^{n+1} * K_{eq,j,(m)}^{n+1} * P_{j,(m)}^{n+1}}{[1+(K_{eq,j,(m)}^{n+1} * P_{(m)}^{n+1})^{nj}]^{1/nj}} \tag{4.33}$$

$$\frac{\bar{q}_{j_{(m)}}^{n+1} - \bar{q}_{j_{(m)}}^{n}}{\Delta t} = -K_{L,j}(q_{j,(m)}^{*(n+1)} - \bar{q}_{j_{(m)}}^{n+1}) \tag{4.34}$$

$$\varepsilon \frac{C_{j_{(m)}}^{n+1} - C_{j_{(m)}}^{n}}{\Delta t} + \left(\frac{u_{(m+1)}^{n+1} * C_{j_{(m+1)}}^{n+1} - u_{(m)}^{n+1} * C_{j_{(m)}}^{n+1}}{\Delta Z} \right) = \varepsilon D_{ax} \left(\frac{(C_{j,(m+1)}^{n+1} - C_{j,(m)}^{n+1}) - (C_{j,(m)}^{n+1} - C_{j,(m-1)}^{n+1})}{\Delta Z^2} \right) - (1-\varepsilon)\rho_p \frac{\bar{q}_{j_{(m)}}^{n+1} - \bar{q}_{j_{(m)}}^{n}}{\Delta t} \tag{4.35}$$

$$\varepsilon \frac{C_{T_{(m)}}^{n+1} - C_{T_{(m)}}^{n}}{\Delta t} + \left(\frac{u_{(m+1)}^{n+1} * C_{T_{(m+1)}}^{n+1} - u_{(m)}^{n+1} * C_{T_{(m)}}^{n+1}}{\Delta Z} \right) = \varepsilon D_{ax} \left(\frac{(C_{T,(m+1)}^{n+1} - C_{T,(m)}^{n+1}) - (C_{T,(m)}^{n+1} - C_{T,(m-1)}^{n+1})}{\Delta Z^2} \right) - \sum_j (1-\varepsilon)\rho_p \frac{\bar{q}_{j_{(m)}}^{n+1} - \bar{q}_{j_{(m)}}^{n}}{\Delta t} \tag{4.36}$$

$$-\frac{(P_{(m+1)}^{n+1} - P_{(m)}^{n+1})}{\Delta Z} = 150 \frac{\mu_g (1-\varepsilon)^2}{\varepsilon^3 d_p^2} u_{(m)}^{n+1} + 1.75 \frac{(1-\varepsilon)}{\varepsilon^3 d_p} \rho_g \, (u_{(m)}^{n+1})^2 \tag{4.37}$$

$$\varepsilon \, \rho_g C_{v,g} \frac{T_{g_{(m)}}^{n+1} - T_{g_{(m)}}^{n}}{\Delta t} + \rho_g C_{p,g} \left(\frac{u_{(m+1)}^{n+1} * T_{g_{(m+1)}}^{n+1} - u_{(m)}^{n+1} * T_{g_{(m)}}^{n+1}}{\Delta Z} \right) = \varepsilon \lambda_L \left(\frac{(T_{g,(m+1)}^{n+1} - T_{g,(m)}^{n+1}) - (T_{g,(m)}^{n+1} - T_{g,(m-1)}^{n+1})}{\Delta Z^2} \right) - C_s (1-\varepsilon)\rho_p \frac{T_{s_{(m)}}^{n+1} - T_{s_{(m)}}^{n}}{\Delta t} + \ldots$$

$$(1-\varepsilon)\rho_p \sum_j \left(\Delta H_j \frac{\bar{q}_{j_{(m)}}^{n+1} - \bar{q}_{j_{(m)}}^{n}}{\Delta t} \right) - \frac{4 h_w}{d_{int}} (T_{g_{(m)}}^{n+1} - T_{w_{(m)}}^{n+1}) \tag{4.38}$$

$$\rho_p C_s \frac{T_{s_{(m)}}^{n+1} - T_{s_{(m)}}^{n}}{\Delta t} = \rho_p \sum_j \left(\Delta H_j \frac{\bar{q}_{j_{(m)}}^{n+1} - \bar{q}_{j_{(m)}}^{n}}{\Delta t} \right) + \frac{6 h_f}{d_p} (T_{g_{(m)}}^{n+1} - T_{s_{(m)}}^{n+1}) \tag{4.39}$$

$$\rho_w C_{p,w} \frac{T_{w(m)}^{n+1} - T_{w(m)}^{n}}{\Delta t} = \alpha_w h_w \left(T_{g(m)}^{n+1} - T_{w(m)}^{n+1}\right) + \alpha_{wl} U \left(T_{g(m)}^{n+1} - T_\infty\right) \quad (4.40)$$

Discretized Boundary Conditions:

Discretization of the Dackwarts Boundary Conditions can be written as:

- Counter-current pressurization step:

$$z = L: \ \varepsilon D_{ax} \left(\frac{C_{j(m+1)}^{n+1} - C_{j(m)}^{n+1}}{\Delta Z}\right) = -(u_{(m)}^{n+1} * C_{j(m)}^{n+1} - u_{(m+1)}^{n+1} * C_{j(m+1)}^{n+1}) \quad (4.41)$$

$$z = 0: \ \left(\frac{C_{j(m+1)}^{n+1} - C_{j(m)}^{n+1}}{\Delta Z}\right) = 0 \quad (4.42)$$

$$z = L: \ \varepsilon \lambda_L \left(\frac{T_{g(m+1)}^{n+1} - T_{g(m)}^{n+1}}{\Delta Z}\right) = -\rho_g C_s (u_{(m)}^{n+1} * T_{g(m)}^{n+1} - u_{(m+1)}^{n+1} * T_{g(m+1)}^{n+1}) \quad (4.43)$$

$$z = L: \ \left(\frac{T_{g(m+1)}^{n+1} - T_{g(m)}^{n+1}}{\Delta Z}\right) = 0 \quad (4.44)$$

$$z = 0: \ u_{(m)}^{n+1} * C_{j(m)}^{n+1} = u_{(m+1)}^{n+1} * C_{j(m+1)}^{n+1} \quad (4.45)$$

- Boundary Conditions for feed:

$$z = 0: \ \varepsilon D_{ax} \left(\frac{C_{j(m)}^{n+1} - C_{j(m-1)}^{n+1}}{\Delta Z}\right) = -(u_{(m-1)}^{n+1} * C_{j(m-1)}^{n+1} - u_{(m)}^{n+1} * C_{j(m)}^{n+1}) \quad (4.46)$$

$$z = L: \ \left(\frac{C_{j(m)}^{n+1} - C_{j(m-1)}^{n+1}}{\Delta Z}\right) = 0 \quad (4.47)$$

$$z = 0: \ \varepsilon \lambda_L \left(\frac{T_{g(m)}^{n+1} - T_{g(m-1)}^{n+1}}{\Delta Z}\right) = -\rho_g C_s (u_{(m-1)}^{n+1} * T_{g(m-1)}^{n+1} - u_{(m)}^{n+1} * T_{g(m)}^{n+1}) \quad (4.48)$$

$$z = L : \left(\frac{T_{g_{(m)}}^{n+1} - T_{g_{(m-1)}}^{n+1}}{\Delta Z}\right) = 0 \quad (4.50)$$

$$z = 0 : u_{(m-1)}^{n+1} * C_{j_{(m-1)}}^{n+1} = u_{(m)}^{n+1} * C_{j_{(m)}}^{n+1} \quad (4.51)$$

- Counter-current blow down and counter-current purge steps:

  At $z = 0$ and $z = L$

$$\left(\frac{C_{j_{(m+1)}}^{n+1} - C_{j_{(m)}}^{n+1}}{\Delta Z}\right) = 0 \quad (4.52)$$

$$\left(\frac{T_{g_{(m+1)}}^{n+1} - T_{g_{(m)}}^{n+1}}{\Delta Z}\right) = 0 \quad (4.53)$$

- Counter-current Pressurization step:

$$z = L : P_{(m+1)}^{n+1} = P|_{feed} \quad (4.54)$$

$$z = 0 : u_{(m-1)}^{n+1} = 0 \quad (4.55)$$

- Bed inlet for feed and counter-current purge steps:

$$z = L : u_{(m)}^{n+1} = u_{(m+1)}^{n+1} \quad (4.56)$$

- Bed outlet for counter-current blow down and counter-current purge steps:

$$z = 0 : P_{(m+1)}^{n+1} = P|_{purge} \quad (4.57)$$

An adsorption-desorption algorithm has been written on MATLAB commercial package with the discretized coupled ordinary differential equations. The algorithm was validated with Carlos A Grande et al's experiment [133]. One-Dimensional (1-D) model of PSA experiment for separation of Carbon dioxide from flue gas (15% CO_2, 85% N_2) on zeolite 13X was simulated. An unused adsorbent bed, readily purged with Helium gas was pressurized counter-currently from 0.1bar to 1.3bar by passing pure nitrogen gas through it at a flow rate of 3l/min for 20s. After this, dry flue gas of component 15% CO_2 and 85% N_2 was feed co-currently into the pressurized system at a constant pressure (1.3bar) for the purpose of separating CO_2 from the gas mixture. After a stipulated feed time (100s), the adsorption

system was regenerated for 70s by subjecting it's outlet to a pressure of 0.1bar after which the system was further purged by passing pure nitrogen gas through the regenerated bed at a flow rate of 0.5l/min for about 120s while the bed outlet was still subjected to pressure of 0.1bar. The system properties used were gotten from Carlos A. Grande et al [133] and T. L. P. Dantas et al [178] as stated in Tables 4.1-4.5. Table 4.1 provides the properties of Adsorption column and fixed bed for CO_2/N_2 Adsorption on fixed bed while Table 4.2 states the properties of Adsorbent (zeolite 13X). Tables 4.3-4.5 present the feed properties of adsorbate (15% CO_2 wt N_2), Thoth Model Parameters and the LDF global mass transfer coefficient respectively.

4.3 ADSORPTION SYSTEM PROPERTIES AND EXPERIMENTAL DATA FOR SIMULATION OF PSA EXPERIMENT

The system properties used for simulation of the PSA are as described in the tables below.

Table 4.1: Properties of Adsorption column and bed for CO_2/N_2 Separation with zeolite 13X

Properties	**Value**	**Reference**
Bed Length, L	0.83 m	[133]
Bed diameter, dint	0.021 m	
Column wall thickness, $\boldsymbol{l}$	0.0015	
Column wall specific heat capacity, $\mathbf{C}_{\boldsymbol{p,w}}$	440 J/kg-K	
Column wall density	721 kg/m3	

Table 4.2: Properties of Adsorbent (Zeolite 13X)

Properties of Zeolite 13X	**Values**	**Reference**
Particle density, ρ	1228.5kg/m^2	[178]
Particle diameter, d_p	0.0001 m	[133]
Bed void fraction, ε	0.33	
Solid Specific heat, C_s	900 J/kg-K	

Table 4.3: Feed properties of adsorbate (15% CO_2, 85% N_2)

Properties of binary gas mixture (15% CO_2/N_2)	**Values**
Feed flow rate (Q_{feed})	3 l/min
Purge flow rate (Q_{purge})	0.5 l/min
Mole fraction of CO_2	0.15
Mole fraction of N_2	0.85
Feed temperature (T_{gfeed})	$363K$
Feed pressure (P_{feed})	$130000\ Pa$
Blow down and purge pressure (P_{purge})	$10000\ Pa$

Table 4.4: Thoth Model Parameters for CO_2 & N_2 adsorption on Zeolite 13X

Gas specie	**Maximum adsorbed concentration(q_m) mol/kg**	**Heterogeneity Parameter (n)**	**Adsorption constant at infinite dilution(K_o), Pa^{-1}**	**ΔH_j (J/mol)**	**Ref**
CO_2	5.09	0.429	4.31e-9	- 29380	[178]
N_2	3.08	0.869	8.81e-10	-17190	

Table 4.5: LDF Global Mass Transfer Coefficient of CO_2 & N_2 on Zeolite 13X

T_g (K)	CO_2	N_2
	Global MTC (K_L) s^{-1}	
363	0.11	0.5

At the end of the validation exercise, the simulated results showed that the algorithm closely predicted the experimental results of Carlos A. Grande et al [133]. The algorithm was then adopted for evaluation of CO_2 adsorption-desorption behaviour of Mg-MOF-74 in four-step PSA with gas feed temperature of 301K and 373K. A single bed was adopted to simulate four steps of the Charles Skarstrom cycle which includes counter-current pressurization, co-current feed, counter-current blow down and counter-current purge [133]. An unused adsorbent bed, readily purged with Helium gas was pressurized counter-currently from 0.1bar to 1.3bar by passing pure nitrogen gas through it at a flow rate of 3l/min. After this, dry flue gas of component 15% CO_2 and 85% N_2 was feed into the pressurized system at a constant pressure (1.3bar) for the purpose of separating CO_2 from the gas mixture. After a stipulated feed time, the adsorption system was regenerated by subjecting its outlet to a pressure of 0.1bar after which the system was further purged by passing pure nitrogen gas through the regenerated bed at a flow rate of 0.5l/min while the bed outlet was still subjected to pressure of 0.1bar. 50 seconds of feed and 25 seconds of depressurization were employed for simulation while the durations of pressurization and purge were varied. Four runs were made to evaluate the effects of the duration of pressurization and purge steps. Three (3) cycles of PSA were simulated to evaluate the capacity of the Mg-MOF-74 for CO_2 capture and sequestration. Subsequent cycles were fed with the effluent from the blow down stage of the previous cycle. After this, twenty-five (25) cycles of runs 1 & 2 were simulated, this time around; the feed gas concentrations of all cycles were the same as the first cycle. Schematic of the PSA and systems are as shown in figures 4.1&4.2, the properties of adsorption column,

adsorbent and heat regeneration material are given in tables 4.6–4.11. The operating pressure and flow rates are remain the same as stated in table 4.3, while the feed temperature, pressurization and purge time for each run are as stated in table 10. Results of all simulation exercise are discussed in chapter 6.

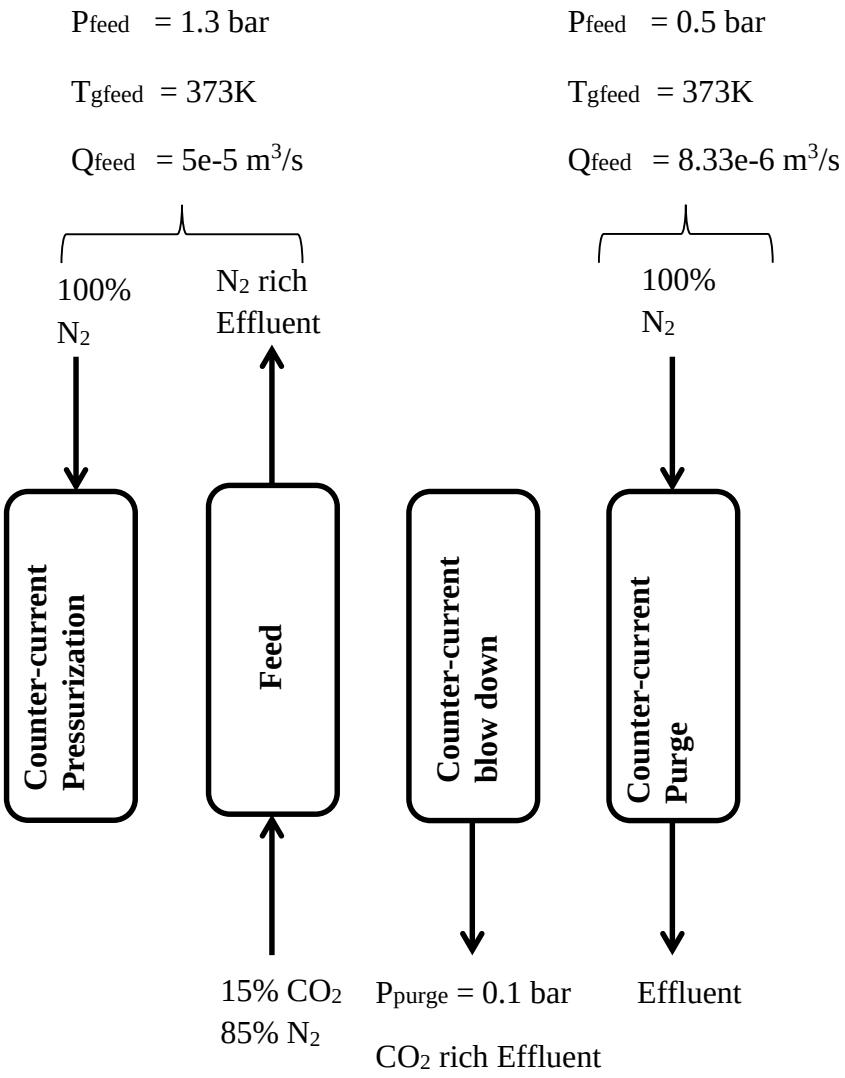

Figure 4.1: Schematics of 4-step PSA process for separation of CO_2 from flue gas

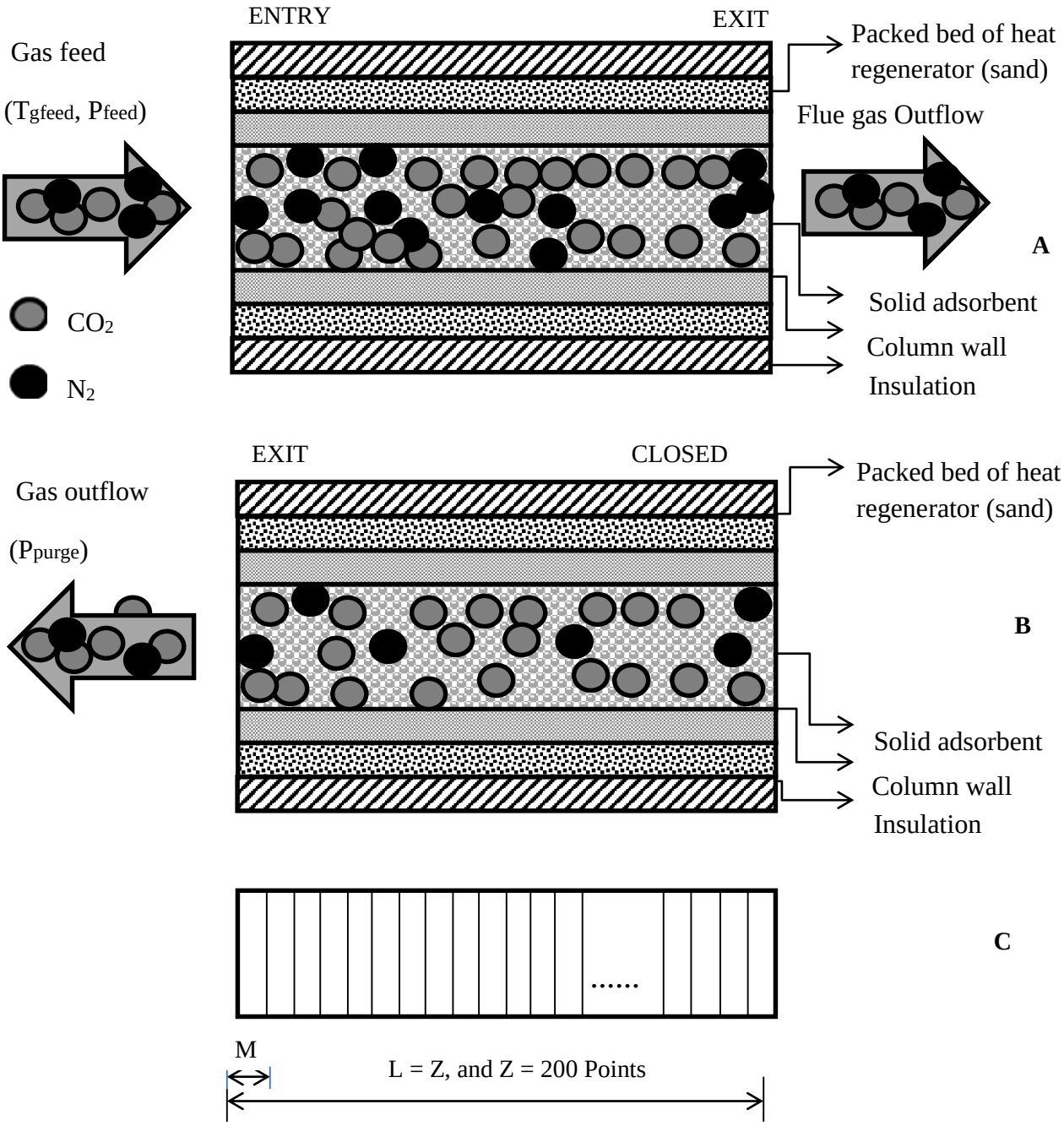

L - Length of adsorption column (0.2m), M - Size of each division (0.001m)

Figure 4.2: Schematics of adsorption (a) and desorption (b) columns with heat regeneration systems and grid points (c) for PSA

Table 4.6: Properties of Adsorption column and bed for CO_2/N_2 separation with Mg-MOF-74

Properties	**Value**	**Properties**	**Value**
Bed Length, L	0.2 m	Column wall specific heat capacity, $\mathbf{C}_{p,w}$	500 J/kg-K
Bed internal diameter, dint	0.02 m	Column wall density	7280 kg/m^3
Bed external diameter, dext	0.0282 m	Column wall thermal conductivity	13.4 W/m-K
Column wall thickness, $\boldsymbol{l}$	0.0041	Thickness of sand bed	0.01 m

Table 4.7: Properties of Adsorbent (Mg-MOF-74)

Properties of Mg-MOF-74	**Values**	**References**
Particle diameter, d_p	0.0038 m	
Bed void fraction, ε	0.52	
Particle density, ρ	911 kg/m^2	[174]
Langmuir specific surface area	1733 m^2/g	[175]
Solid Specific heat, C_s under Helium gas	900 J/kg-K	[110]

Table 4.8: Langmuir isotherm parameter for CO_2 and N_2 on Mg-MOF-74

Gas specie	**Max adsorbed conc(q_m) mol/kg**	**Adsorption constant at infinite dilution (b_o), Pa^{-1}**	**ΔH_j (J/mol)**	**References**
CO_2	7.90	1.557 e-11	- 42000	[110]
N_2	14.0	4.96 e-10	-18000	

Table 4.9: LDF Mass transfer parameter of CO_2 and N_2 on Mg-MOF-74

Mass transfer parameter (s^{-1})	CO_2	N_2	Ref
	0.174	0.2855	[110]

Table 4.10: Simulated PSA experimental conditions

Run	Pressurization time (s)	Purge time (s)	Temperature (K)
1	10	25	373
2	10	50	373
3	20	25	373
4	10	50	301

Table 4.11: Properties of heat regeneration material (sand: quartz)

Properties of sand (quartz)	Value
Thermal Conductivity (k_{stor})	0.2 W/m-K
Specific heat capacity (C_{stor})	880 J/kg-K
Density (ρ_{stor})	1201 kg/m^3
Porosity of packed sand bed (ε_{stor})	0.1

CHAPTER 5

RESULTS OF BREAKTHROUGH EXPERIMENT SIMULATIONS

5.1 Validation of Simulated Adsorption Code with Breakthrough Experiment Results

For reliability of information presented in this work, the written MATLAB code was first validated using the experimental work of Dantas et al [117]. Breakthrough experiment of Dantas et al was simulated for the adsorption separation of CO_2 from flue gas (20% CO_2, wt N_2) using activated carbon as adsorbent. The results obtained from the validation showed closeness between experimental data and simulated results.

A comparison of Breakthrough simulation results using Linear Driving Force Model (LDF) with Breakthrough experimental result.

The work of Dantas et al [117] presents breakthrough experiments for a temperature range of 28-150^{o}C (301 K to 423K). The data provides variation of CO_2 and N_2 concentrations with time at the exit section. Figures 3-6 show a comparison of experimental data and LDF model simulation for the break through curves for the adsorption of CO_2 from binary gas mixture of 20% CO_2wt N_2. These figures show the ratio of species concentrations at bed exit to the feed concentration. The total feed gas flow rate in each case is 30mL/min. The roll-up behaviour of N_2 remains as explained before i.e. the concentration of N_2 at the outlet becomes greater than the feed concentration [179], which is a common behaviour in multi component gaseous mixture adsorption. The quick breakthrough of the LDF model compared to the experimental model may be due the some differences in binary mixture properties used, constant fluid properties (e.g. density, viscosity etc.) and the ideal gas law assumption.

As shown from figures 5.1-5.4, the present model captures the changes in CO_2 and N_2 concentrations with time quite well from the qualitative point of view. The peak in the nitrogen concentration is well captured by the model. The model shows under-prediction of the saturation time. The figures also indicate that the model provides better agreement as the temperature becomes high. The breakthrough time gets shorter as the temperature increases. This is attributed to the fact that nitrogen has higher diffusion at higher temperatures, thus, nitrogen adsorption becomes faster.

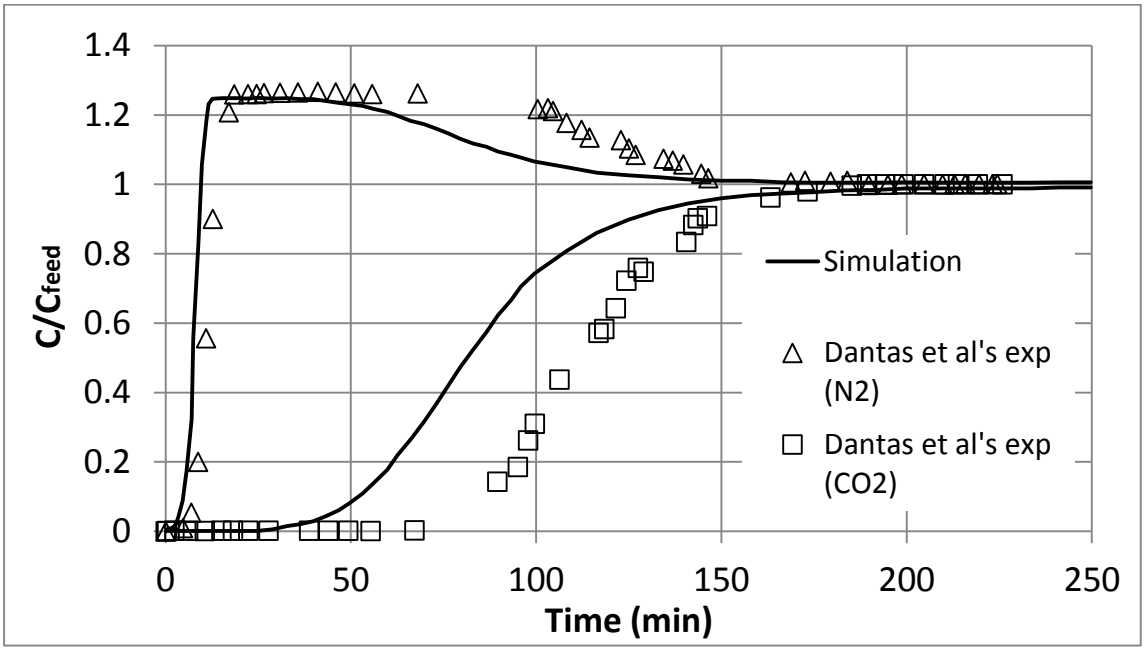

Figure 5.1: Validation breakthrough curve for CO_2 & N_2 on Activated Carbon for T_{gfeed} = 301K. Experimental data [117]

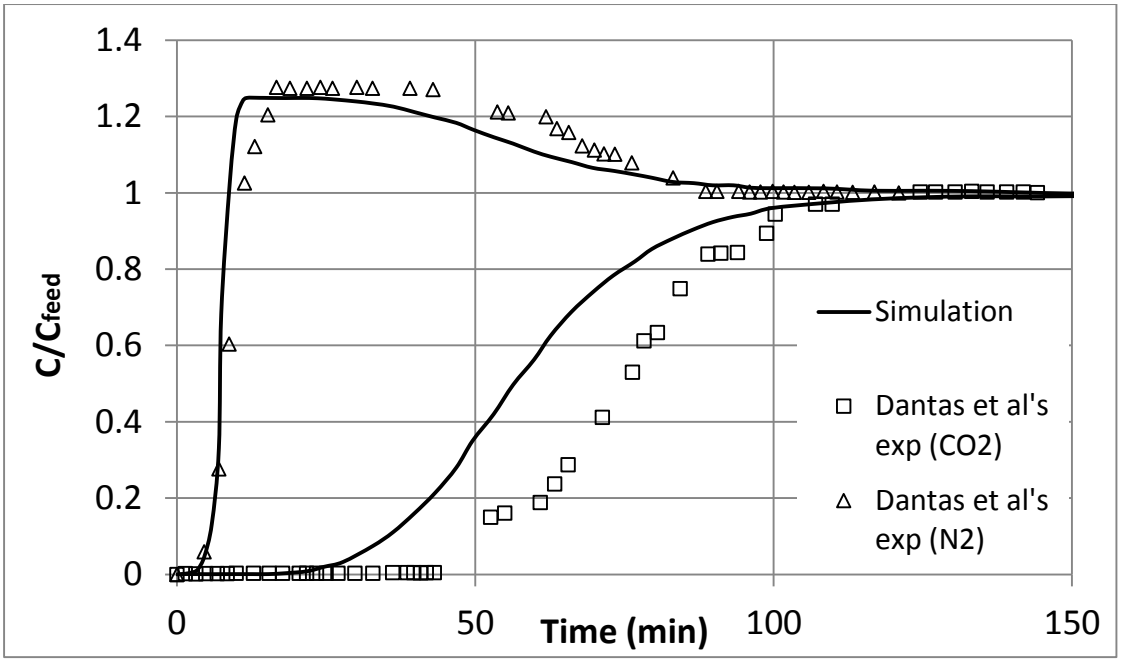

Figure 5.2: Validation breakthrough curve for CO_2 & N_2 on Activated Carbon for T_{gfeed} = 323K. Experimental data [117]

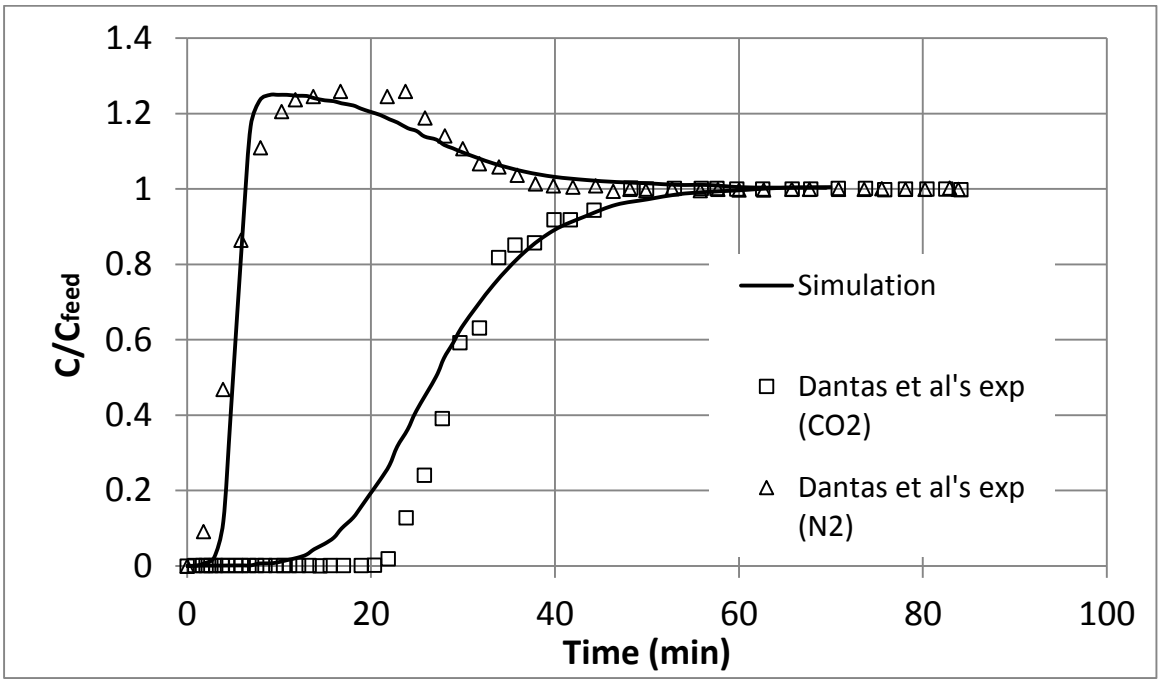

Figure 5.3: Validation breakthrough curve for CO_2 & N_2 on Activated Carbon for T_{gfeed} = 373K. Experimental data [117]

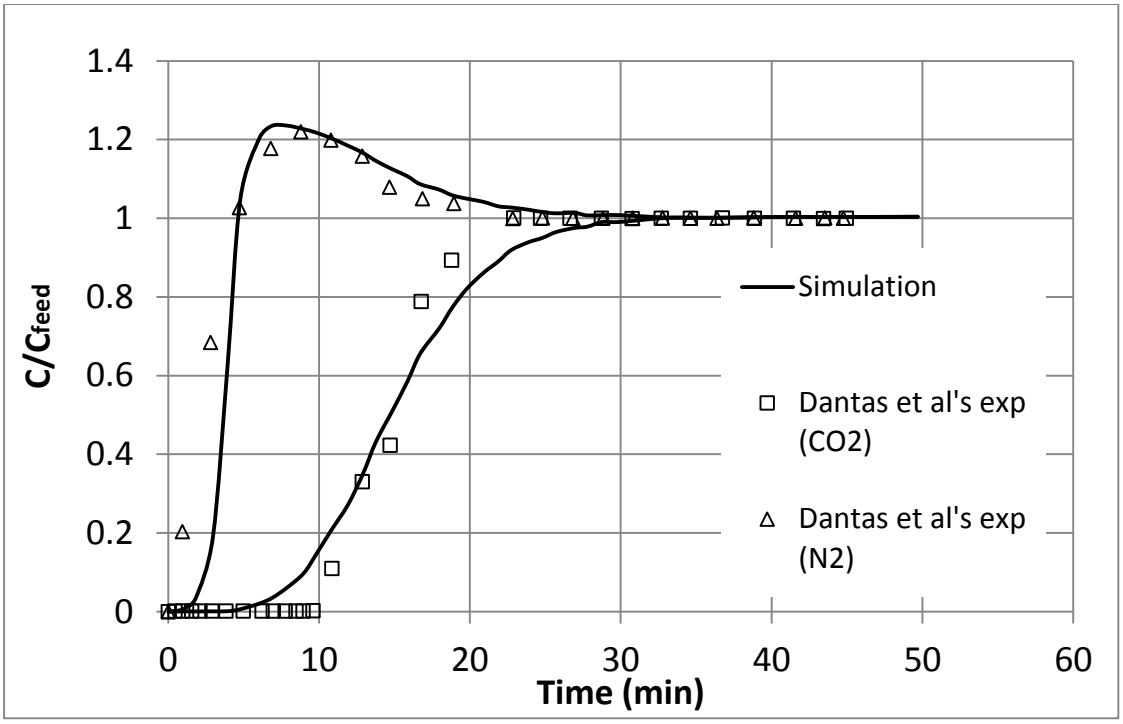

Figure 5.4: Validation breakthrough curve for CO_2 & N_2 on Activated Carbon for T_{gfeed} = 423K. Experimental data [117]

Comparison of results of experimental and simulated mass of CO_2 adsorbed in activated carbon

The amount of component adsorbed at equilibrium q_j^* is expressed by the isotherm equation which could be either of the isotherms listed earlier in this write up. This quantity can be expressed a function of the concentration of each of the gas components and temperature of the gas stream i.e. $q_j^* = f(Cj, Tg)$. Assuming Toth isotherm in the case of this study, the adsorption equilibrium for individual component would be expressed as:

$$q_j^* = q_{m,j} K_{eq,j} P_j / [1 + (K_{eq,j} P_j)^n]^{1/n} \quad (5.1)$$

Where: q_j^* is the amount adsorbed at equilibrium, $q_{m,j}$ is the maximum adsorb-able concentration which is also referred to as the monolayer capacity, $K_{eq,j}$ is the equilibrium adsorption constant, P_j is the partial pressure of the components in the gas stream and 'n' is

the heterogeneity parameter of the solid for each gas species. The dependence of adsorption equilibrium on temperature of gas stream can be expressed with Van't Hoff's equation which is given by:

$$K_{eq,j} = K_{0,j}\, e^{(-\Delta H_j/RTg)} \qquad (5.2)$$

$K_{0,j}$ is the adsorption constant at infinite dilution.

From figure 5.5, comparing the experimental values and the Toth model simulated values for the adsorbed concentration of CO_2 in activated carbon, both data are quite close which suggests that the Toth model satisfactorily predicts the experimental process of CO_2 capture in activated carbon. The next part provides the results for the breakthrough behaviour of Mg-MOF-74.

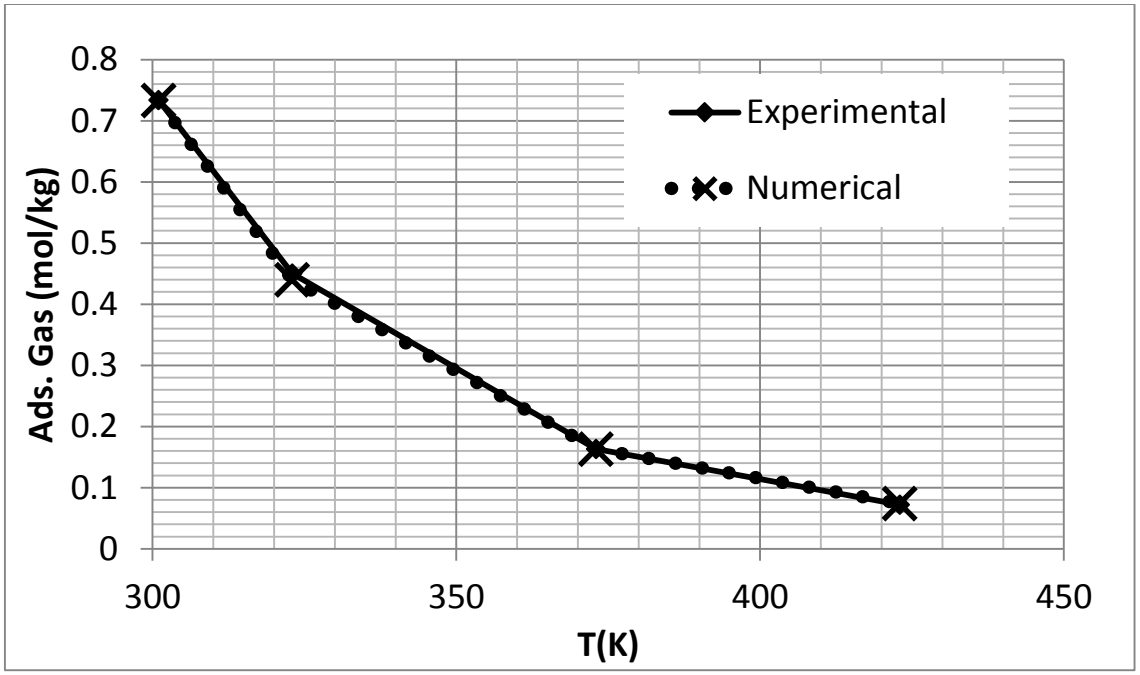

Figure 5.5: Comparison of Simulated and Experimental Result for Adsorbed Amount of CO_2 on Activated Carbon at various temperatures. Experimental data [117]

5.2 Parametric Studies of Breakthrough Behaviour of CO_2 on Mg-MOF-74

The adsorption breakthrough curves CO_2 and N_2 on Mg-MOF-74 for the separation of CO_2 from a binary gas mixture of 15% CO_2 wt N_2 which is as shown in Figures 5.6(a-c) portray that Mg-MOF-74 has very high selectivity for CO_2 which conforms to existing reports. The plots also show that the break through time for CO_2 in the described mixture decreased with temperature. At a feed gas temperature of 301K, CO_2 adsorption took well above 500 minutes before breakthrough which conforms quite closely to existing reports for similar conditions [175,180] This breakthrough time decreases as the feed gas temperature increases, which may be due to reduction in the value of the Langmuir adsorption equilibrium parameter (from extended Langmuir equation 1e) with temperature, which turn decreases the retention time and leads to longer breakthrough. The continuous adsorption of some quantity of CO_2 at bed exit after breakthrough might be due to the flexible nature of Mg-MOF-74 which enables it to expand (breath) before saturation during adsorption [88]. It may also be due to existing suggestion that the single component single site Langmuir model inadequately predicts CO_2 adsorption in Mg-MOF-74 even at loading below 8mol/kg [110]. The roll-up exhibited by Nitrogen in all four cases conforms to existing reports for multicomponent adsorption [179]. This phenomenon is due to the displacement effect of CO_2 on Nitrogen which happens during initial continuous adsorption of CO_2 by the material which leads to a steep rise in the concentration of Nitrogen at bed exit.

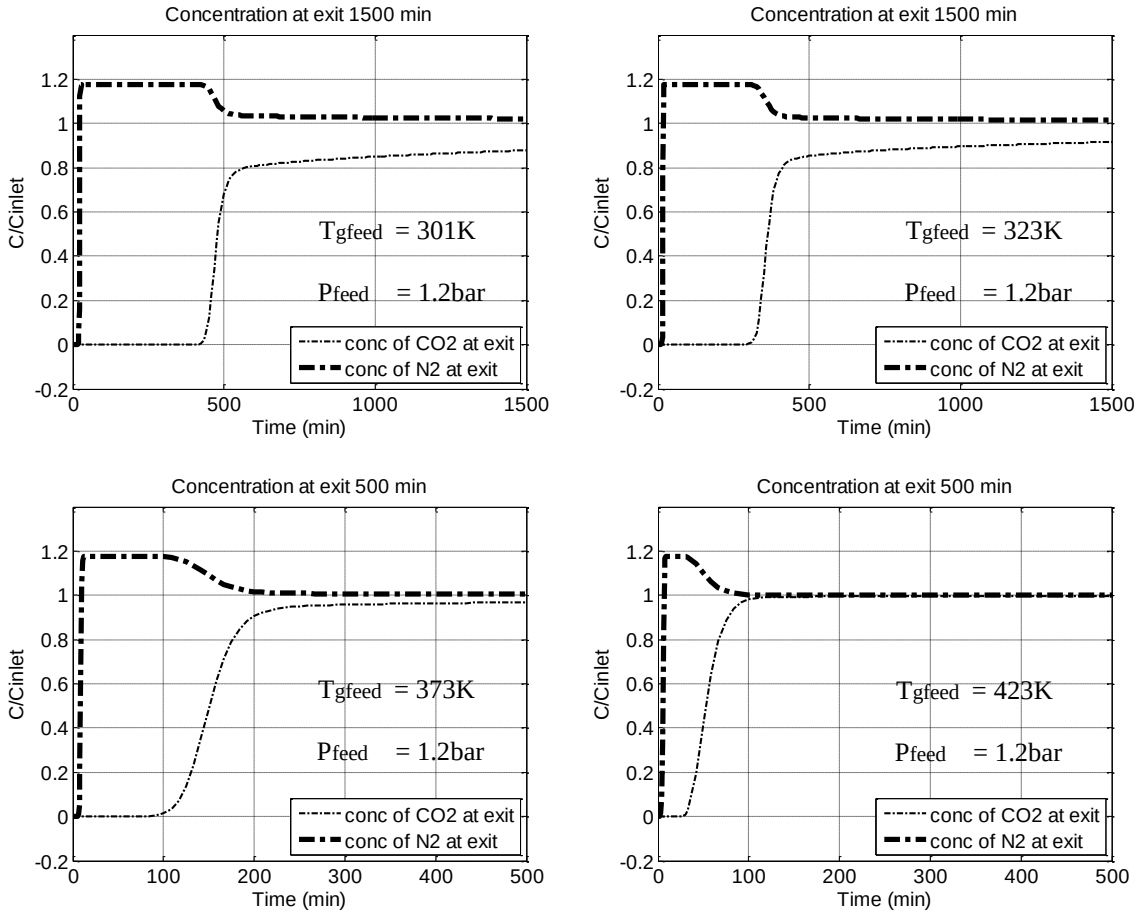

Figures 5.6: Breakthrough curves for CO_2 & N_2 adsorption on Mg-MOF-74 at various feed temperatures

The average amount of CO_2 and N_2 adsorbed per kilogram of Mg-MOF-74 at bed exit as shown in figures 5.7(a-d) shows that the average amount of CO_2 and N_2 adsorbed per kg of Mg-MOF-74 in the mixture reduced with increase in temperature. At a feed gas temperature of 301K, the average amount of CO_2 adsorbed is about 0.585mol/kg, while amount of Nitrogen adsorbed is about 0.3mole per kilogram of adsorbent. The reduction in average mass adsorbed with increase in feed gas temperature may be due to increase in the value of the equilibrium adsorption constant (from Vant' Hoff's equation 3.4 & 3.7) with temperature, which, due to exothermic behaviour, in turn reduces in the retention time and leads to faster breakthrough. At a feed gas temperature of 301K, the average amount of CO_2 adsorbed is about 6.43mol/kg, while mass of Nitrogen adsorbed is about 0.7557mol/kg. This is about

10times the capacity of the activated carbon in Dantas et al's experiment [117]. It also took well above 500 minutes before breakthrough which conforms very closely to existing experimental values for similar conditions. The average mass of N_2 adsorbed decreases as the feed gas temperature increases, which may be due to decrease in the value of the Langmuir equilibrium adsorption parameter (from equation 3.6) with temperature, which in turn reduces in the retention time due to exothermic behaviour leading to longer breakthrough time. The factors responsible for the roll-up exhibited by Nitrogen remain the same as explained for concentration above. The results shown conform with existing reports of mass of gas adsorbed in solid under similar conditions [163]. Table 5.2 shows the average mass of components adsorbed for the runs.

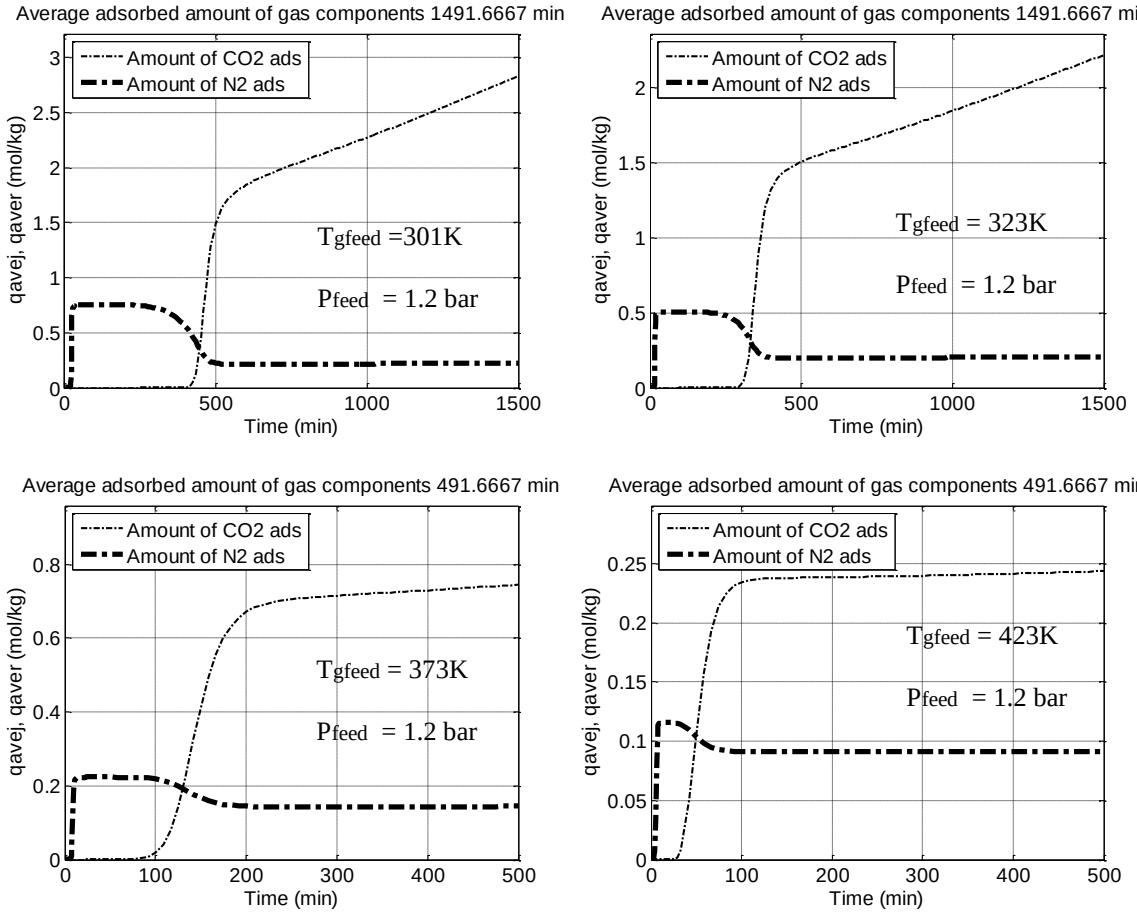

Figure 5.7: Simulated amount of CO_2 & N_2 adsorbed on Mg-MOF-74 at bed exit at various feed temperatures

Table 5.1: Simulated Results for Adsorbed Amount of CO_2 & N_2 per Kilogram of Mg-MOF-74

Temperature (K)	Average amount Adsorbed in Mg-MOF-74 (mol/kg)	
	CO_2	N_2
301	6.4309	0.7557
323	4.7106	0.5045
373	1.1982	0.2235
423	0.2769	0.1156

The bulk gas temperature profiles at bed entry, midpoint and at bed exit, for feed gas temperature of 301K, 323K, 373K and 423K respectively as shown in figure 5.8 show that the temperature of gas at any time at the inlet remains almost constant; this is due to the continuous feed of gas at the given temperatures into the system. Gas temperatures at the middle at exit of the system increased significantly. Gradual increase to peak temperatures is observed after which the temperatures drops back to temperatures close to the feed gas temperature. The peak temperatures are highest at bed exit and they increase with increase in feed gas temperature due to exothermic reaction. The change in temperature decreases with increase in feed gas temperature. At a feed gas temperature of 28^{o}C (301K), the rise in temperature of gas stream at mid-point and exit of the adsorption column are about 45K and 55K respectively. Temperature profile at the middle and exit of the column form a phenomenon termed as "dual-shock wave" which is due huge heat effect by non-linear adsorption equilibrium [181].

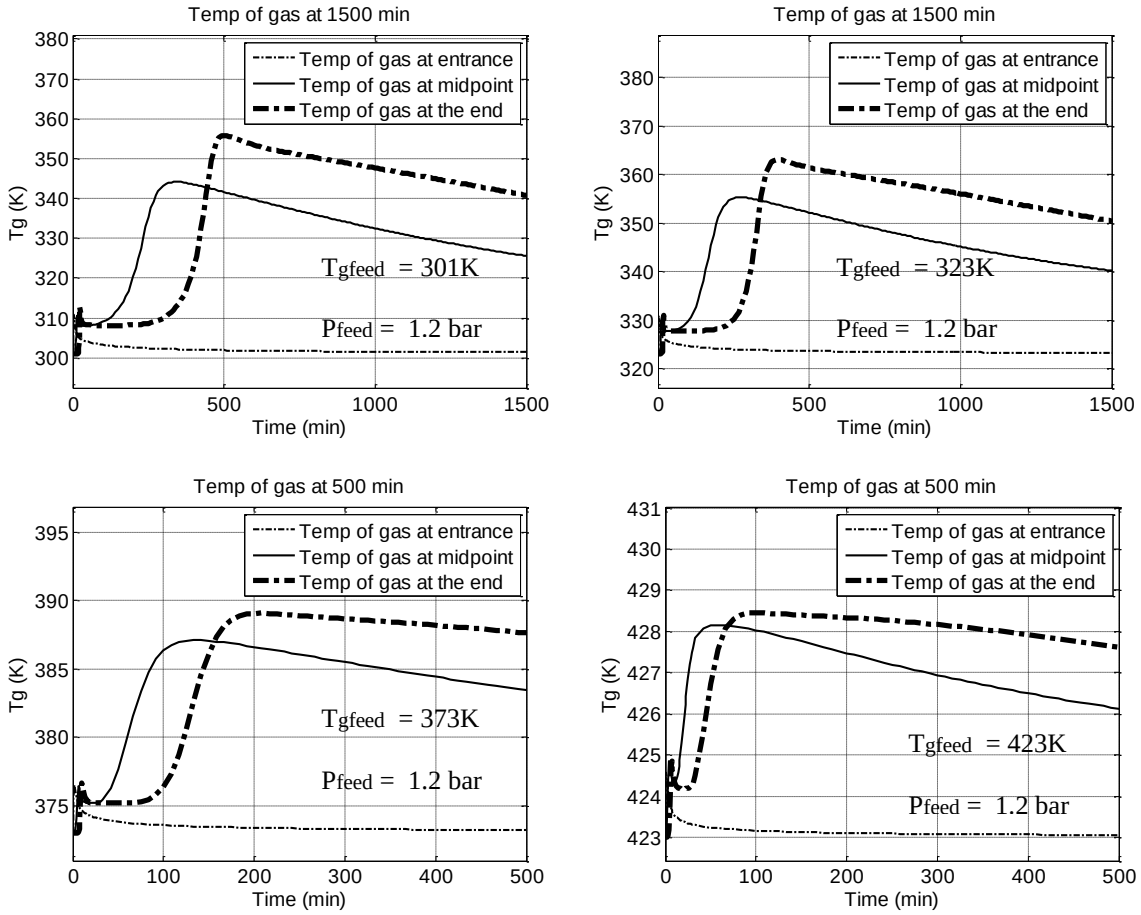

Figure 5.8: Simulated temperature profiles of bulk gas for various feed temperatures during adsorption of CO_2 & N_2 on Mg-MOF-74 bed

The bulk gas temperature distribution over bed length at the begining of adsorption, at various time during adsorption as shown in figure 5.9 shows that for all feed gas temperatures, bulk gas temperature at any time at bed inlet remains almost constant; this is due to the continuous feed of gas at the given temperatures into the system. As adsorption time increased to about 28minute, the gas temperature increased to its peak which occurs in the second half of the bed. This temperature eventually drops back to a temperature just above the feed gas temperature. For times after this, gas temperature increased steadily to peak points at the exit. The highest bulk gas temperature is attained before breakthrough due to large heat exchange during the exothermic reaction. This temperature is attained in the

second half of the column. After breakthrough, no further adsorption takes place, hence reduction in temperature.

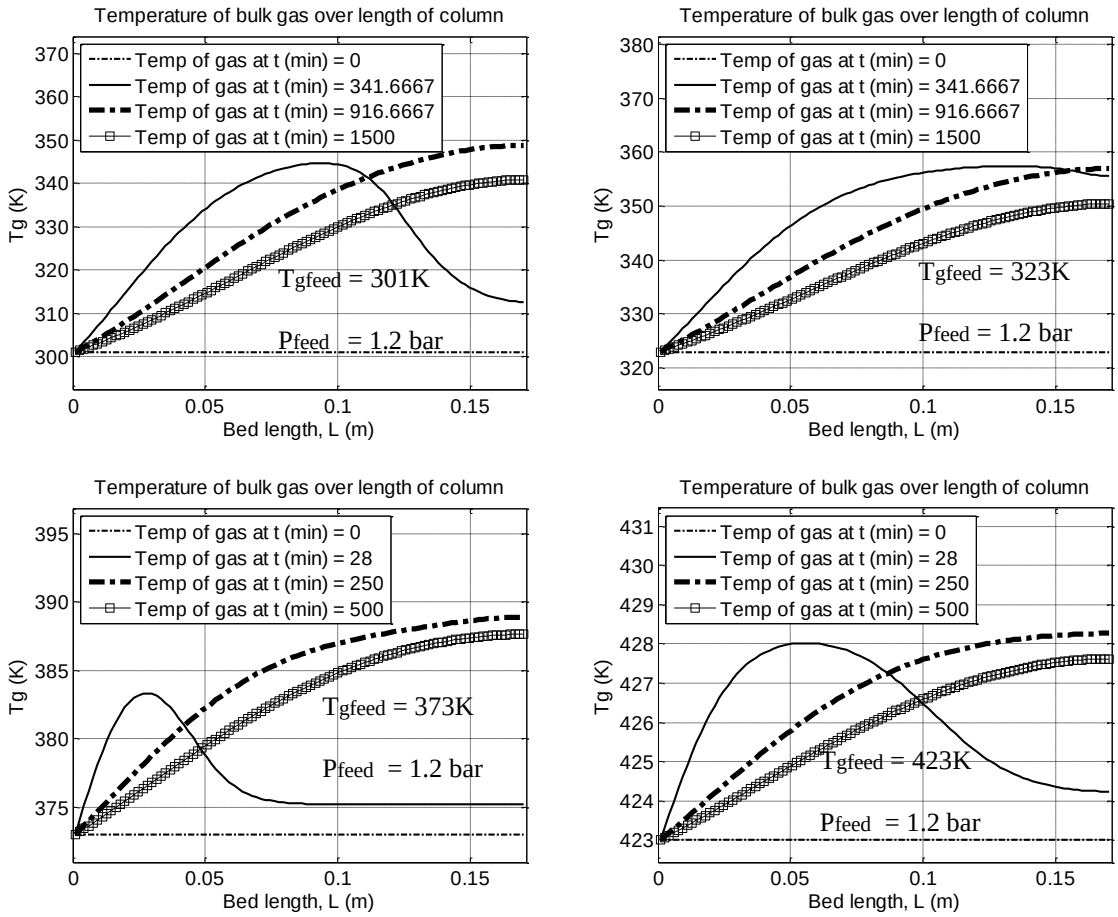

Figures 5.9: Simulated bulk gas temperature distribution along bed length at various times during adsorption of CO_2 & N_2 on Mg-MOF-74

The solid adsorbent temperature profile during adsorption as shown in figure 5.10 shows similar behaviour as that of the bulk gas. It can be seen that temperature of Mg-MOF-74 at any time at the inlet remains almost constant; this is due to the continuous feed of gas at the given temperatures into the system. Gradual increase to peak temperatures is observed after which the temperatures drops back to temperatures close to the feed gas temperature. The peak temperature is highest at the bed exit and it increases with increase in feed gas

temperature. The change in temperature decreases with increase in feed gas temperature. At a feed gas temperature of 28^{o}C (301K), the rise in temperature of gas stream at mid-point and exit of the adsorption column are about 45K and 55K respectively. Temperature profile at the middle and exit of the column form a phenomenon termed as "dual-shock wave" which is due huge heat effect by non-linear adsorption equilibrium [181].

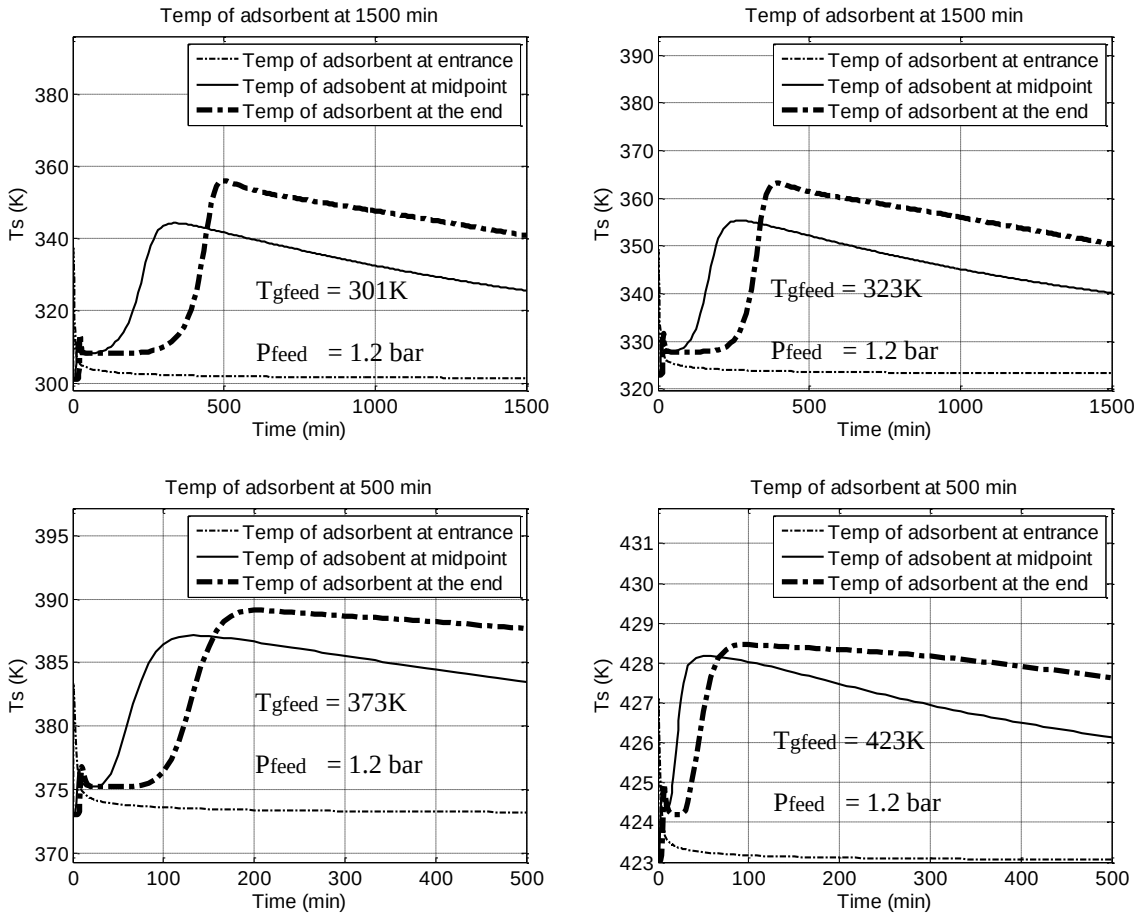

Figures 5.10: Simulated temperature profiles of adsorbent for various feed temperatures during adsorption of CO_2 & N_2 on Mg-MOF-74

The adsorbent temperature distribution over bed length at various tiem during adsorption as shown in figure 5.11 shows that for all feed gas temperatures, adsorbent temperature at any time at bed inlet remains almost constant; this is due to the continuous feed of gas at the

given temperatures into the system. As adsorption time increased to about 28minute, the adsorbent temperature increased to its peak which occurs in the second half of the bed. This temperature eventually drops back to a temperature just above the feed gas temperature. For times after this, adsorbent temperature increased steadily to peak points at the exit. The highest adsorbent temperature is attained before breakthrough due to large heat exchange during the exothermic reaction. This temperature is attained in the second half of the column. After breakthrough, no further adsorption takes place, hence reduction in temperature.

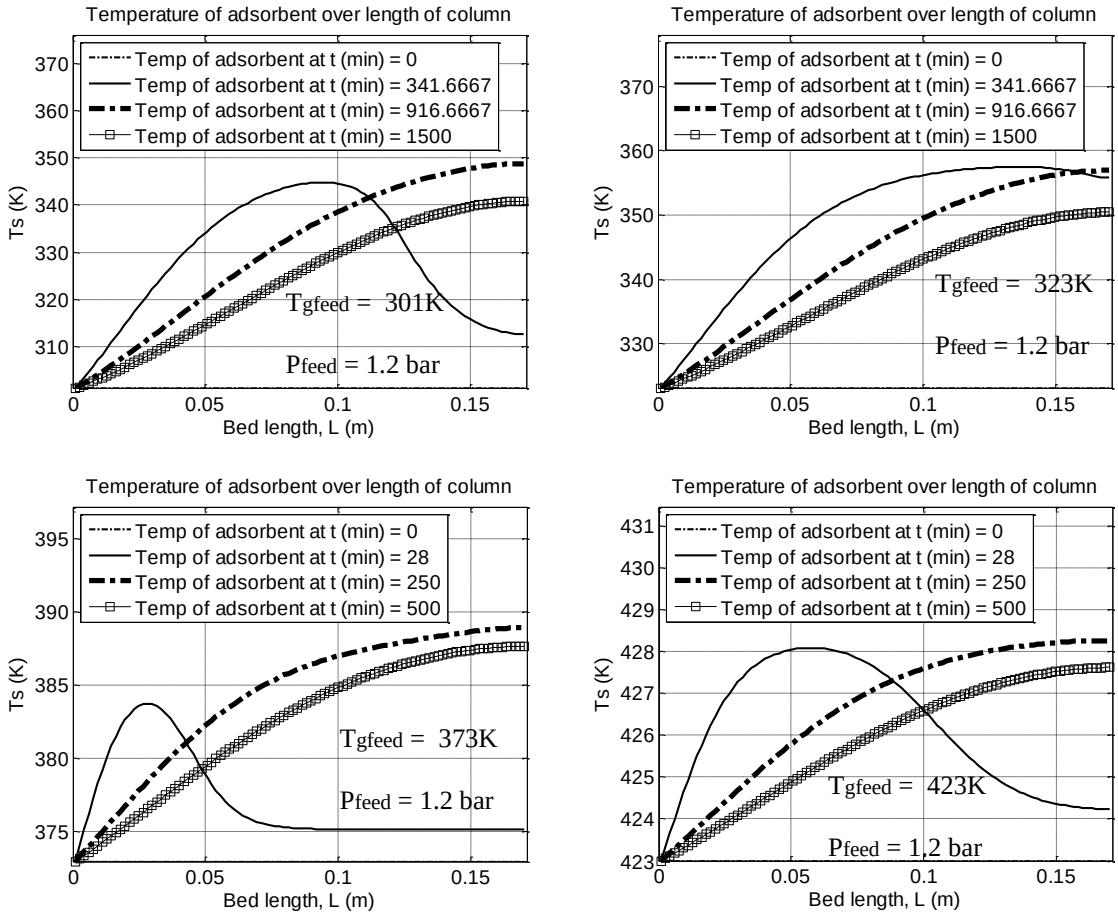

Figures 5.11: Simulated adsorbent temperature distribution along bed length of bed at various times during adsorption of CO_2 & N_2 on Mg-MOF-74

The adsorption column wall temperature profile as shown in figure 5.12 shows that the column wall temperature exhibits similar behaviour as those of the bulk gas and the adsorbent. It can be seen that temperature of the column at any time at the inlet remains

almost constant; this is due to the continuous feed of gas at the given temperatures into the system. Gas temperatures at the middle at exit of the system increased significantly to peak values a little lower than corresponding temperatures of the solid. Gradual increase to peak temperatures is observed after which the temperatures drops back to temperatures close to the feed gas temperature. The peak temperature is highest at the bed exit and it increases with increase in feed gas temperature. The change in temperature decreases with increase in feed gas temperature. At a feed gas temperature of 28^{o}C (301K), the rise in temperature of gas stream at mid-point and exit of the adsorption column are about 45K and 55K respectively. Temperature profile at the middle and exit of the column form a phenomenon termed as "dual-shock wave" which is due huge heat effect by non-linear adsorption equilibrium [181].

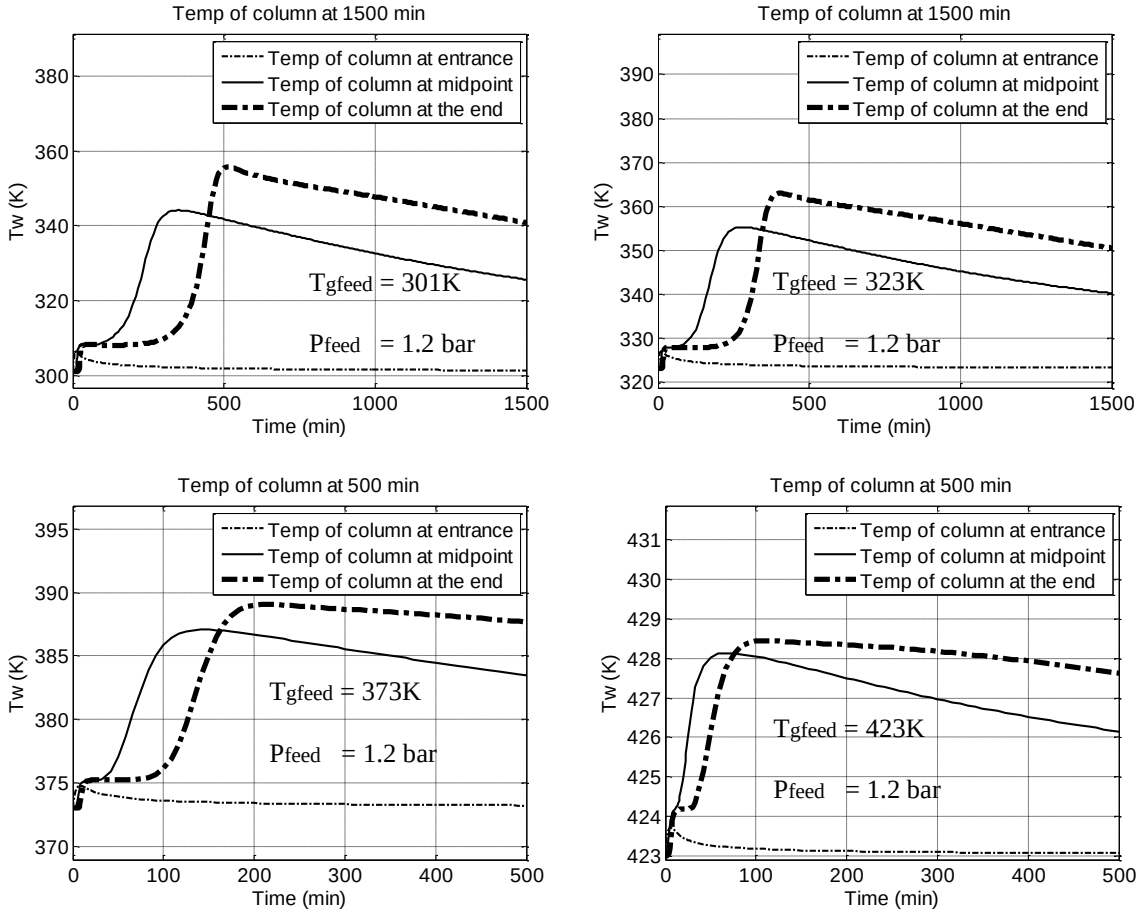

Figures 5.12: Simulated temperature profiles of column wall for various feed temperatures during adsorption of CO_2 & N_2 on Mg-MOF-74

The adsorption column wall temperature distribution at various time as shown in figure 5.13 shows that for all feed gas temperatures, the column wall temperature at any time at bed inlet remains almost constant; this is due to the continuous feed of gas at the given temperatures into the system. As adsorption time increased to about 28minute, the column wall temperature increased to its peak which occurs in the second half of the bed. This temperature eventually drops back to a temperature just above the feed gas temperature. For times after this, column wall temperature increased steadily to peak points at the exit. The highest column wall temperature is attained before breakthrough due to large heat transfer during the exothermic reaction. This temperature is attained in the second half of the column. After breakthrough, no further adsorption takes place, hence reduction in temperature.

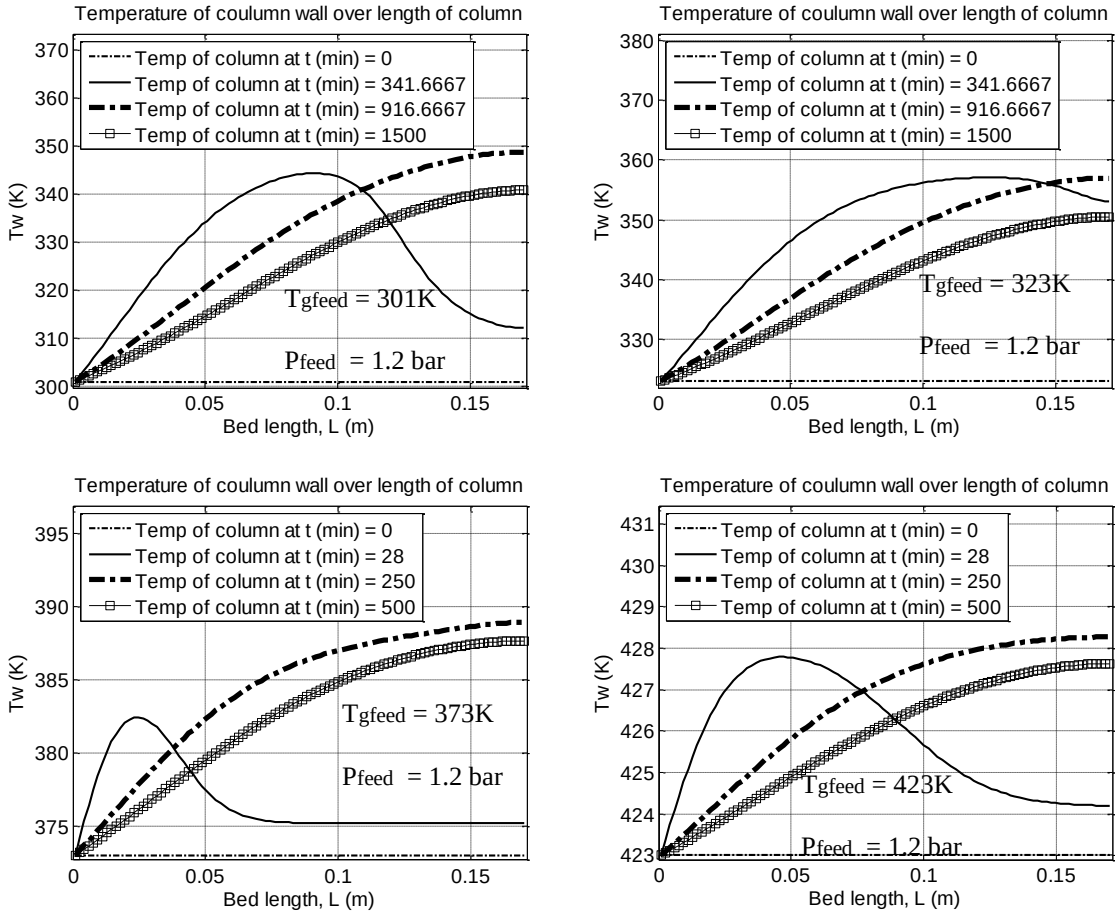

Figures 5.13: Simulated column wall temperature distribution along bed length for various feed times during adsorption of CO_2 & N_2 on Mg-MOF-74

The pressure distribution inside adsorption column as shown in figure 5.14 shows a behaviour similar to adsorption column pressure drop behaviour in existing literatures. This shows that the pressure drop inside adsorption column is negligible which may be due to the mico-scale flow. Hence the reason some researchers assume constant pressure within adsorption column.

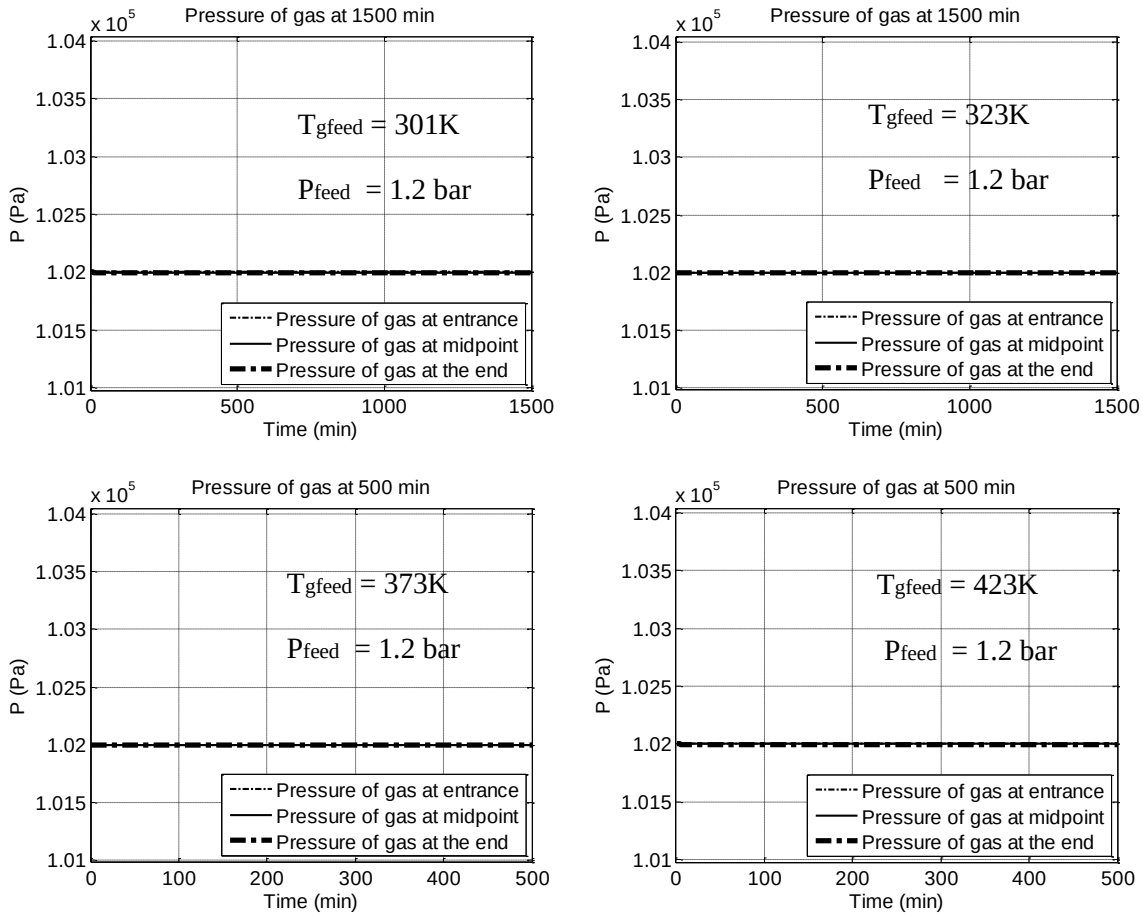

Figure 5.14: Simulated pressure distribution in fixed adsorption bed of Mg-MOF-74

The Simulated Langmuir parameter during adsorption which is as shown in figure 5.15 for CO_2 and figure 5.16 for N_2 shows that for both CO_2 and N_2, that the Langmuir parameter decreases with temperature. At any time at the inlet, Langmuir parameter remains almost constant; this is due to the continuous feed of gas at the given temperatures into the system.

Values of the parameters at the middle and exit of the system exhibit gradual decrease up to the peak temperature after which the parameters increase to values close to the feed parameter values. The parameter is lowest at bed exit due to the temperature at this point.

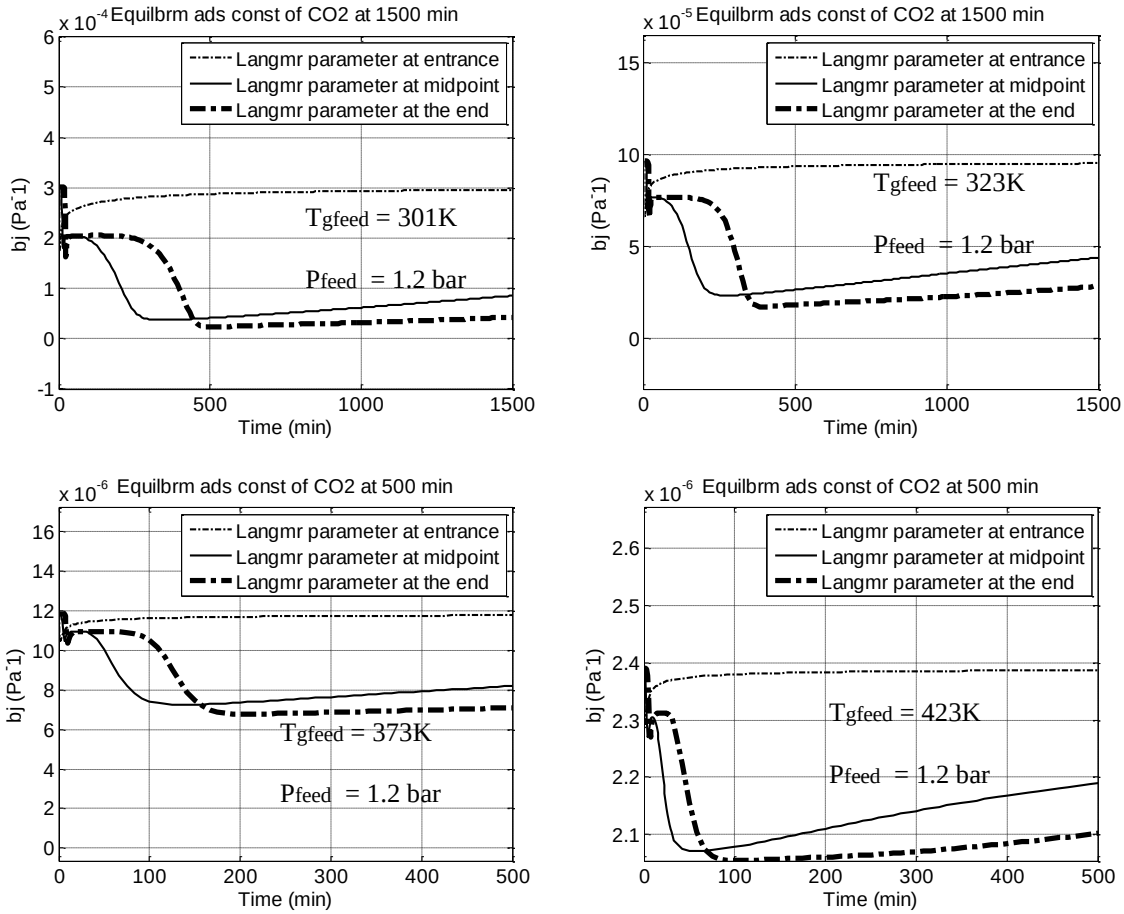

Figures 5.15: Simulated Langmuir Parameter for adsorption of CO_2 on Mg-MOF-74

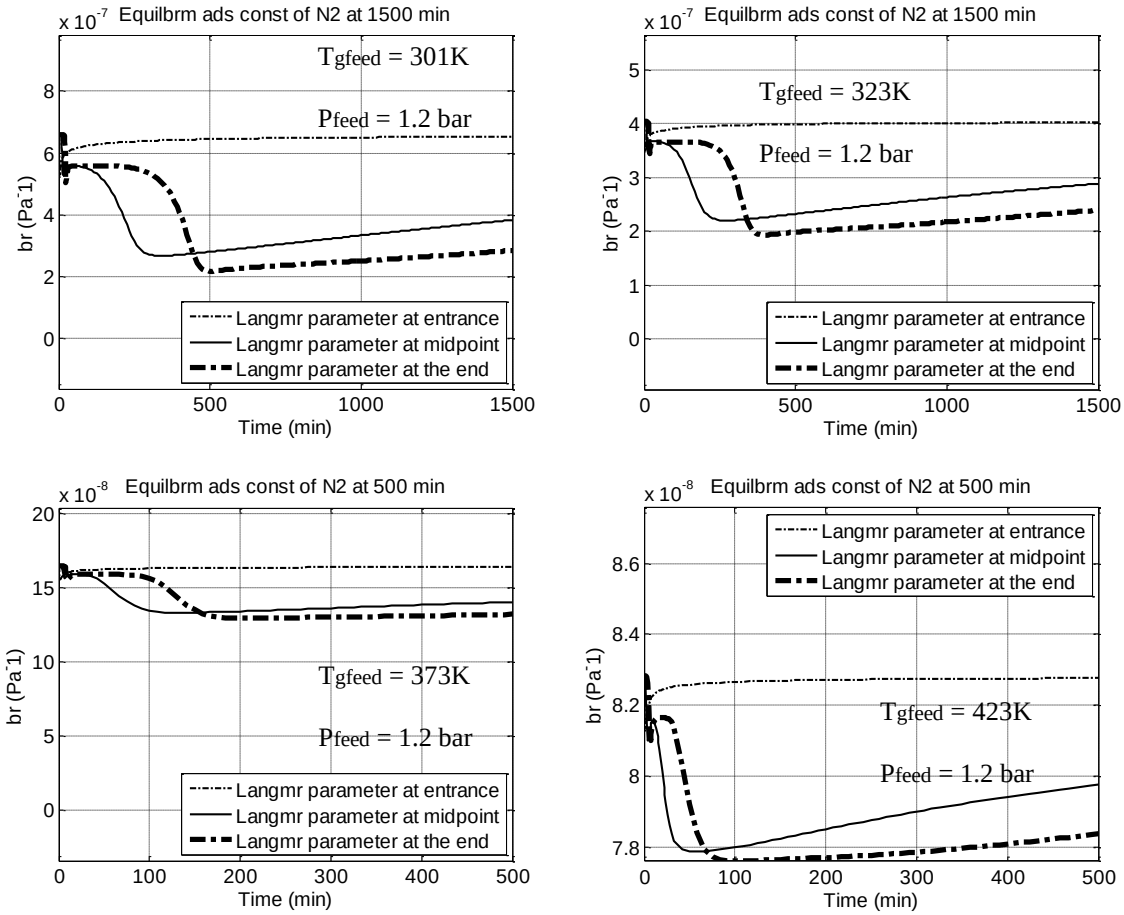

Figures 5.16: Simulated Langmuir Parameter for adsorption of N_2 on Mg-MOF-74

CHAPTER 6

RESULTS OF ADSORPTIVE STORAGE SIMULATIONS

6.1 Validation of simulated Adsorptive Storage Code with Experimental Results

Results generated in this work were compared with experimental data of Jinsheng Xiao et al [171,172] and G. Hermosilla-Lara et al [173] for hydrogen adsorption on Activated Carbon bed. A Close agreement was observed as shown in Fig. 6.2 for pressure variation with time for H_2 adsorption in an activated carbon bed [172].

The pressure fit curve for valve opening process during charging (figure 6.1) shows linear rise in bed pressure until steady state is reached. This signifies gradual opening of the feed gas control valve to allow a controlled pressure rise within the column in order to prevent system damage due to pressure surge. At the end of valve opening stage, the desired feed pressure (10Mpa) is attained; this pressure is maintained throughout the charging process. The total feed gas velocity is 5×10^{-4} m/s and the simulated gas density was acquired using ideal gas law. From the simulated results, it was found that the pressure across fixed bed length was equal at any point in time.

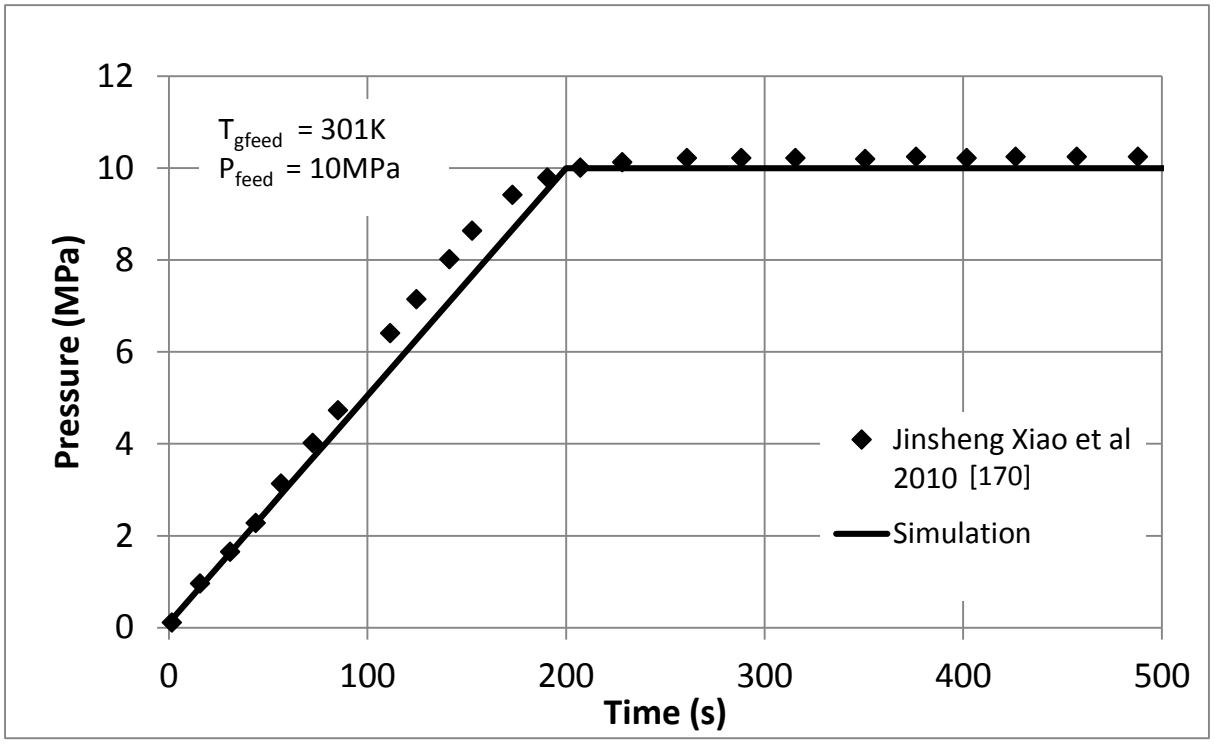

Figure 6.1: Feed pressure curve fit for adsorption of H_2 in Activated Carbon.

A comparison of adsorbed amount of H_2 (in mole) per kilogram of activated carbon at at bed mid-span as predicted by modified Dubinin-Astakhov (D-A) model [172] in comparison with experimental values is as depicted in Fig. 6.2. The adsorbed mass profile shows close agreement with experimental data especially at the end of the charging stage. The deviation experienced during the peak of climb which may be due to higher experimental gas feed pressure at about this time compared to the simulated gas feed pressure. This higher pressure may be due to the manual valve opening process as compared to the simulated process. At the end of the 600 minutes of charging, the amount of Hydrogen stored for both experimental and simulated processes are about 9.14mol/kg and 9.15mol/kg respectively which suggests that the modified Dubinin-Astakhov model satisfactorily predicts the experimental storage process of H_2 in activated carbon.

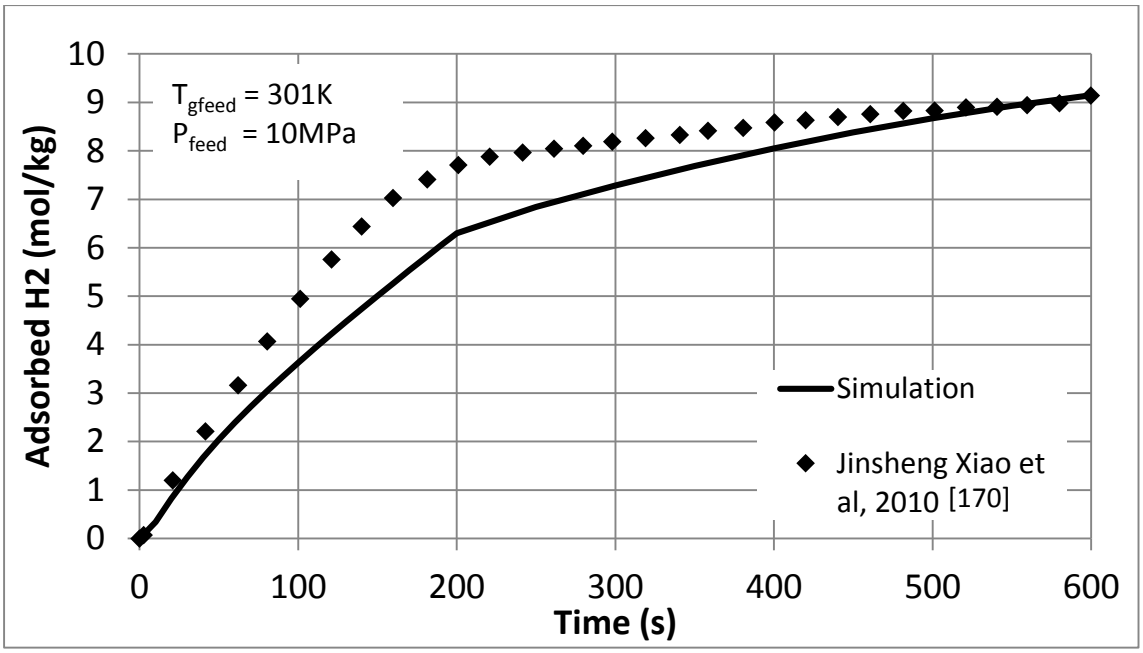

Figure 6.2: Adsorbed amount of H_2 on Activated Carbon at bed mid-span

An evaluation was made for the effect of feeding CO_2 at higher pressure while setting the initial Activated Carbon bed pressure to 1bar compared with feeding CO_2 at higher pressure while setting the initial bed pressure to be the same as the feed pressure (figure 6.3) on the amount of CO_2 adsorbed at mid span of Activated Carbon bed of size 0.171m x 0.022m for 83 minutes (about 5000 seconds) of simulation. It can be seen that both cases do not show significant variation in the mass of CO_2 adsorbed. Hence, the initial system pressure in this study has been set to be equal to the feed pressure. This has been done to prevent system oscillation during simulation caused by the effect of high pressure shock wave due to high feed pressure compared to the initial pressure within the bed.

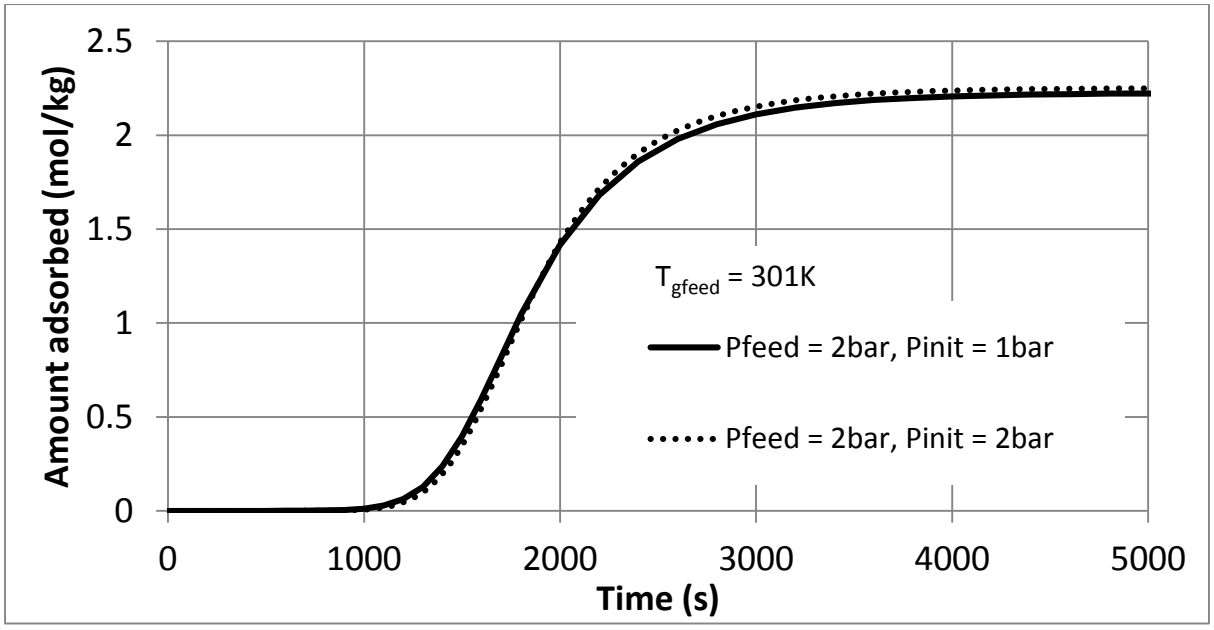

Figure 6.3: Adsorbed amount of CO_2 on Activated Carbon at bed mid-span for 83min

Subsequently, the validated adsorptive storage code was employed for evaluation of the adsorptive storage behaviours on MOF-5 and MOF-177. Below are the simulated results for CO_2 storage behaviour of MOF-5, MOF-177 and Activated Carbon.

6.2 Parametric Studies of Adsorptive Storage of CO_2

6.2.1 Parametric Studies of CO_2 storage on MOF-5

Simulation of the adsorbed mass of CO_2 on MOF-5 shows an increase in the amount of CO_2 adsorbed on MOF-5 with the increase in gas feed pressure which is as shown in Fig 5.4 for pressure values of 1, 2, 5, 10, 30 and 50 bar, respectively. As the pressure increases, CO_2 molecules are pressed against the surface of the solid. This increases the available surface area for CO_2 adsorption within existing adsorption sites. The increase in the available surface area for adsorption in turn leads to an increase in the maximum possible adsorption of CO_2, hence, the amount of adsorbed CO_2 increases. The highest adsorbed amount for MOF-5 after 50 minutes of adsorption is achieved with 50 bar feed pressure which is about 7.4g. This matched with the work of Zhenxia et al [107].

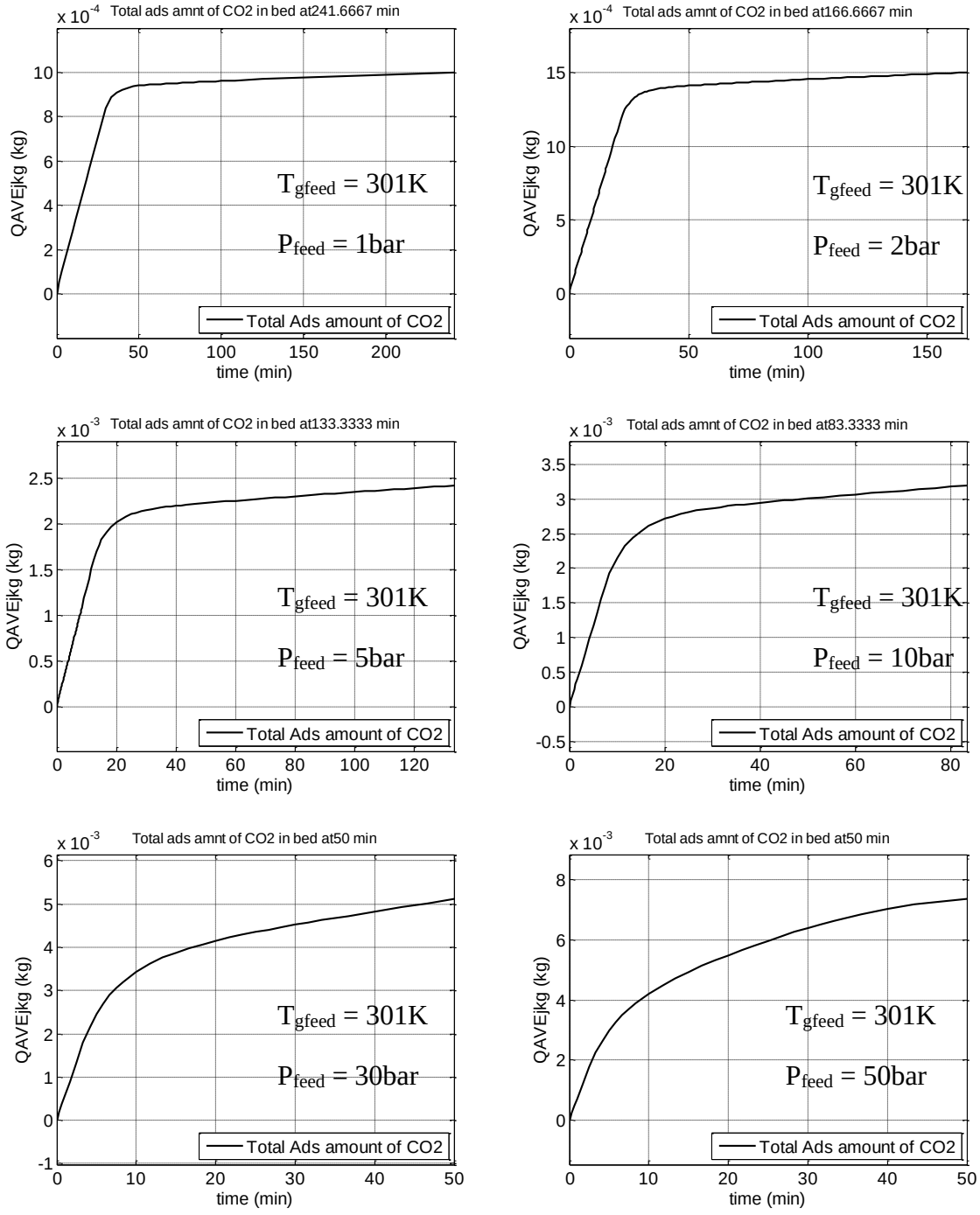

Figure 6.4: Profile of amount of CO_2 stored on MOF-5 for various feed pressures

The same information is re-plottd in Figure 6.5 where the data shown are limited to 50 minutes to see the time profile of the amount absorbed at different pressures. The effect of pressure on the CO_2 absorbed is clear.

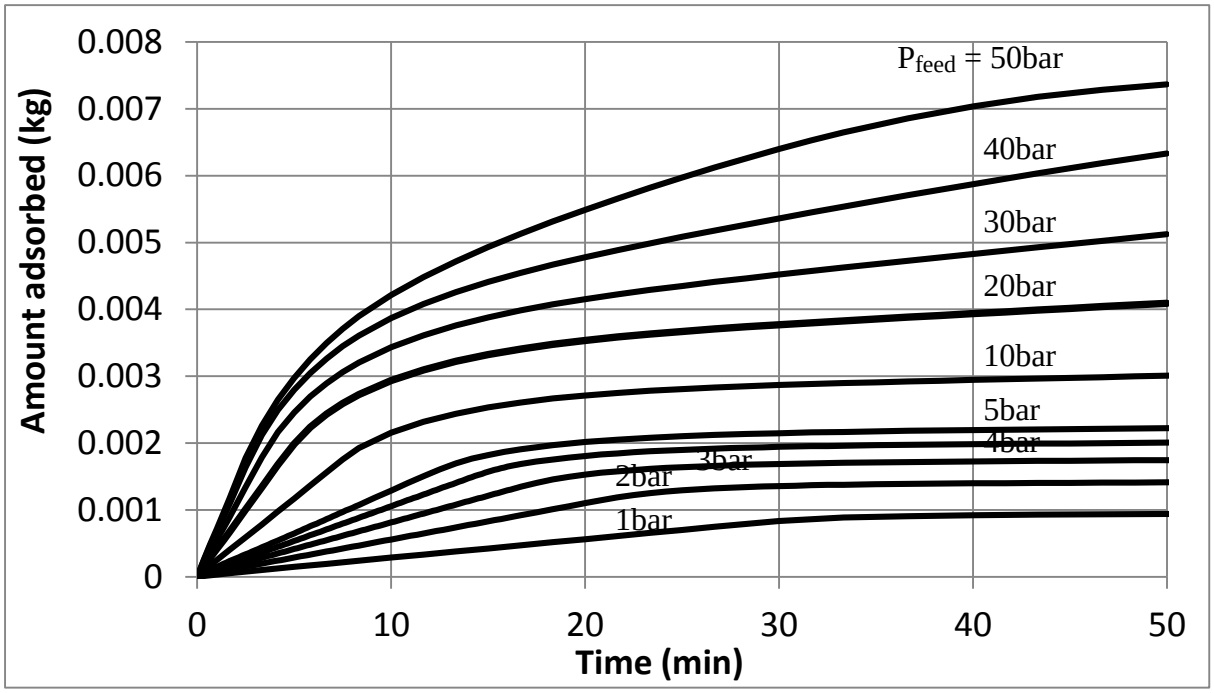

Figure 6.5: Profile of amount of CO_2 stored on MOF-5 for 50min for various feed pressures

Simulation results for bulk gas and column wall temperature profiles during adsorption of CO_2 on MOF-5 are show in Figures 6.6 and 6.7. The figures show an increase in the maximum bulk gas temperature (Fig. 6.6) and column wall temperature (Fig. 6.7) with the increase in feed pressure. This effect is due to the increase in the amount of gas adsorbed within bed with increase in pressure which in turn leads to higher heat generation from the exothermic reaction hence, higher bulk gas temperature and more heat transfer to the walls. The initial fast climb in adsorption leads to roll-up effect in temperature at different points in the bed leading to an increase in temperature especially in the bulk gas at those points to peak values; the highest of these is found at the end of the bed. The roll-up effect may be due to the high amount of heat generated due to initial fast and continuous adsorption of CO_2 at these points. As the bed gets saturated, the rate of adsorption slows down and the peak temperatures drop down to a steady temperature which is maintained through the filling

process. Based on further simulation results, the adsorbent showed similar behaviour as the bulk gas. It assumes similar temperatures in space and time as the bulk gas with negligible difference in values.

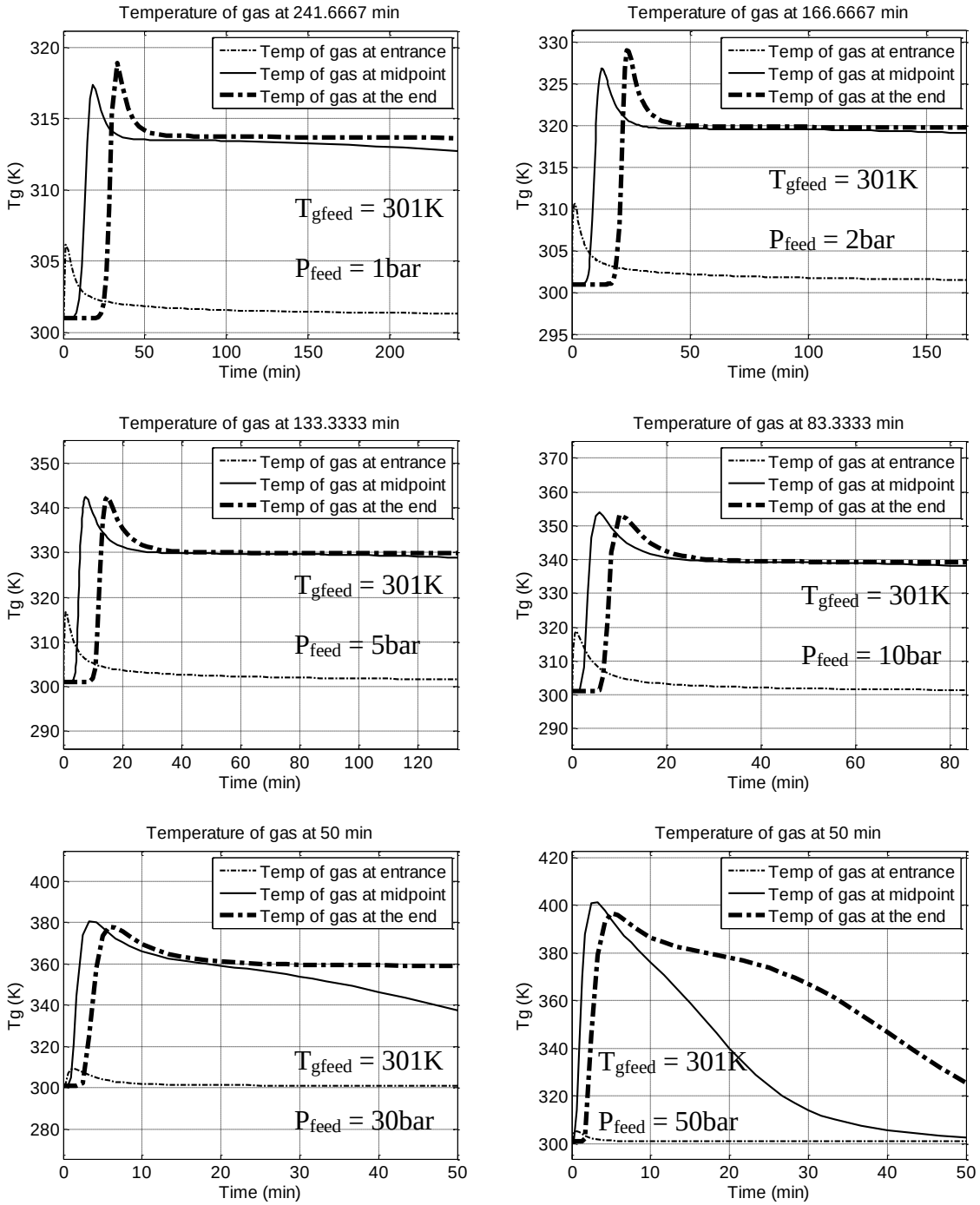

Figure 6.6: Temperature profile of bulk gas for storage of CO_2 on MOF-5 for various feed pressures

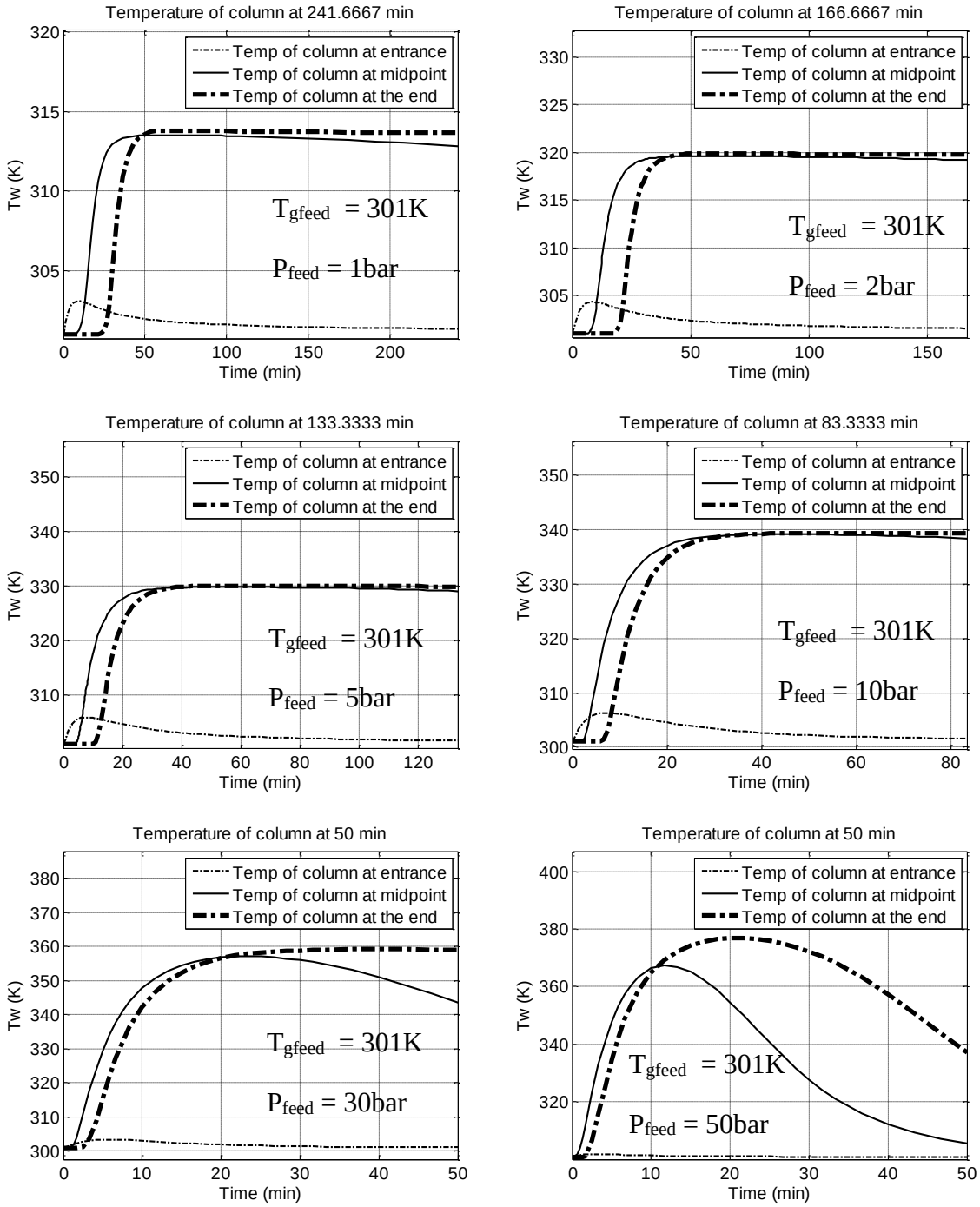

Figure 6.7: Temperature profile of adsorption column wall during adsorption of CO_2 on MOF-5 for various feed pressure

The behaviour of equilibrium adsorption constant from Van't Hoff's equation (equation 3.4) with varying temperature and pressure during adsorption of CO_2 on MOF-5 is depicted in Figure 6.8 that shows a decrease in the minimum adsorption constant with the increase in feed pressure and temperature. This is because the increase in pressure within the bed leads to

a longer time for the bed to get saturated with CO_2, this in turn leads to better adsorption and hence, better gas storage capacity. Values of the parameters at the middle and exit of the system exhibit gradual decrease up to the peak temperature after which the parameters increase back to values close to the feed parameter values. The parameter is lowest at bed exit due to the high temperature at this point.

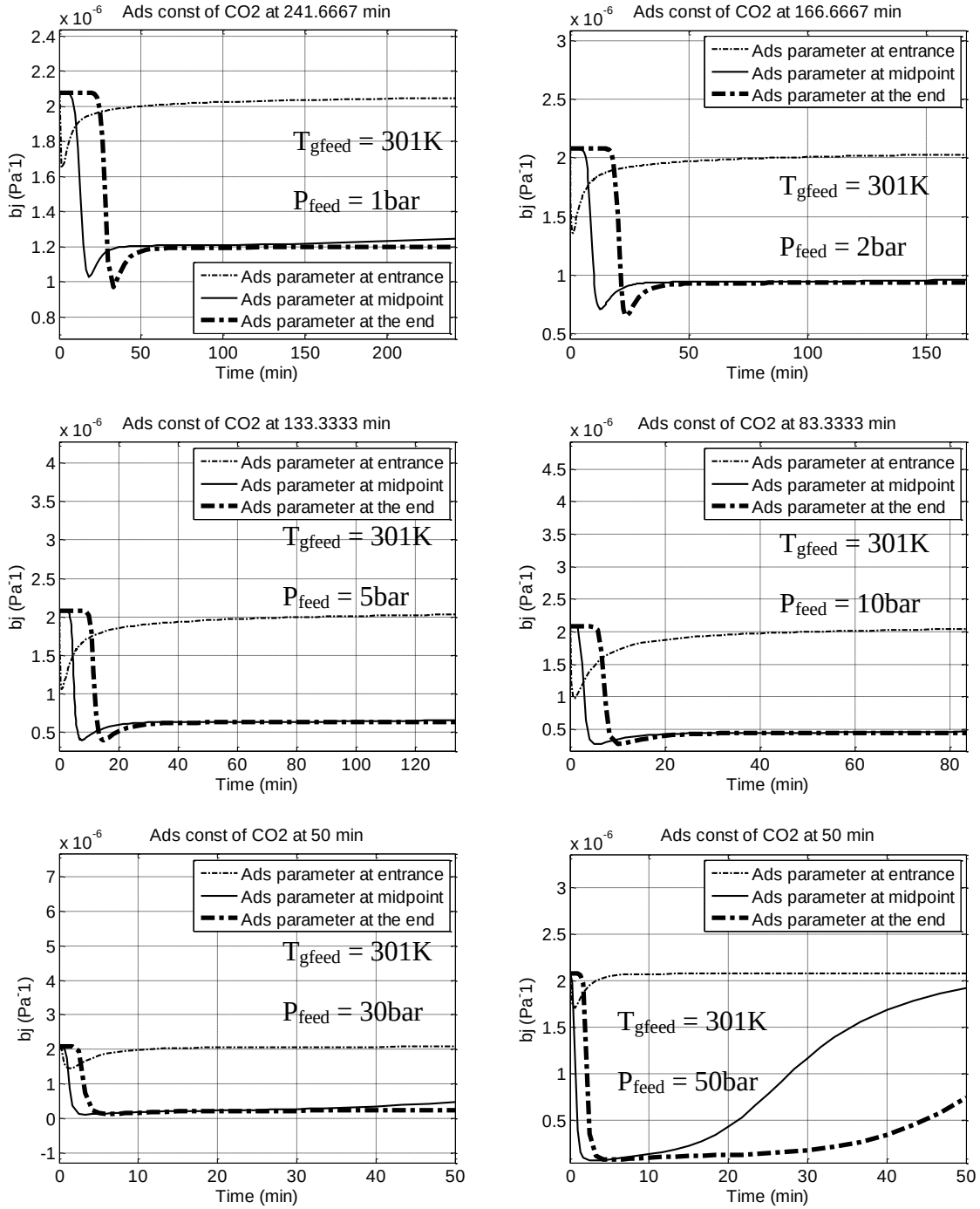

Figure 6.8: Profile of equilibrium adsorption constant for CO_2 adsorption on MOF-5 for various feed pressure

The effects of bed length and diameter on the amount of CO_2 stored on MOF-5 and Activated Carbon are shown in Figures 6.9 and 6.10. The figures show that at any given simulation time, the amount of CO_2 adsorbed on MOF-5 and Activated Carbon beds increases with increase in bed length (Fig. 6.9) or diameter (Fig. 6.10). However, the effect of increase in bed diameter on storeage of CO_2 is much more than the effect of bed length. This may be due to higher increase in column volume per unit increase in bed diameter compared to corresponding increase in column length. Besides, column diameter creates larger surface area of heat exchange between the bed, the wall and ambient hence, lower temperature and better adsorption are achieved within the bed. This effect is further explained by equations 3.14 & 3.15 and by the behaviour of the bulk gas temperature with column size. Finally, the fast climb in adsorption for each bed length and diameter may also increase due to increase in surface area of adsorption within the bed which cause a prolonged time for initial adsorption.

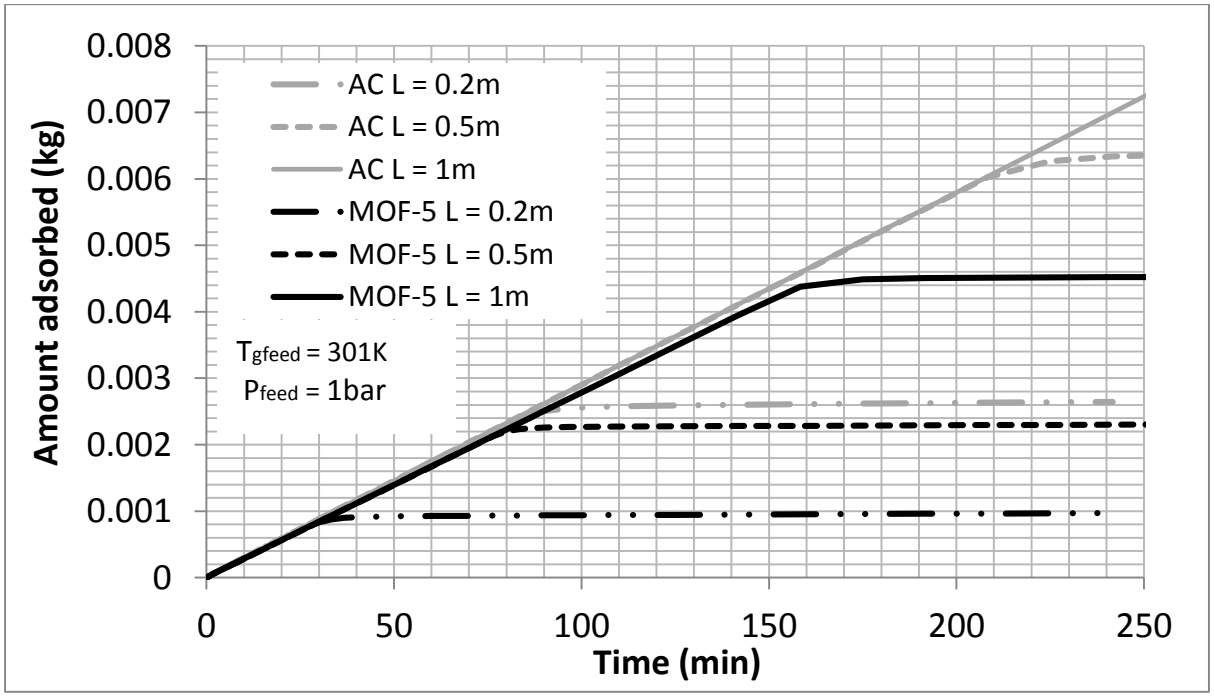

Figure 6.9: Effect of bed length on total amount of CO_2 stored on MOF-5 and Activated Carbon for 250min

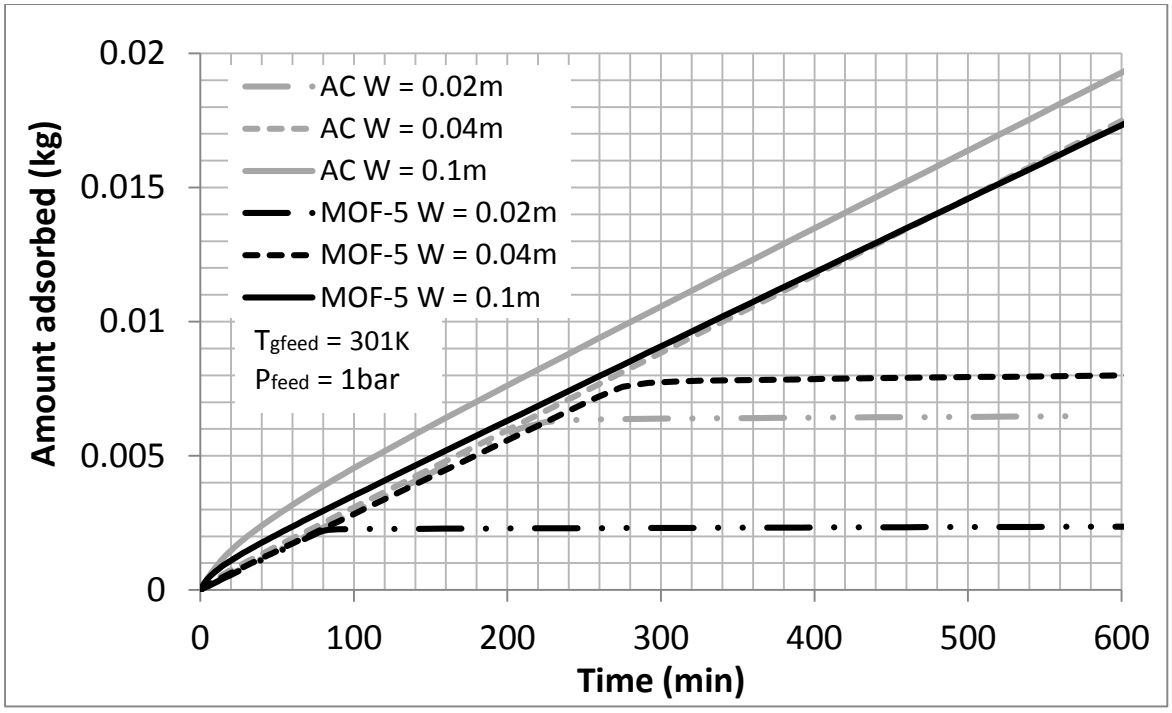

Figure 6.10: Effect of bed diameter on total amount of CO_2 stored on MOF-5 and Activated Carbon for 600min

6.2.2 Parametric Studies of Adsorptive Storage of CO_2 storage on MOF-177

Simulation of the adsorbed mass of CO_2 on MOF-177 shows an increase in the amount of CO_2 adsorbed on MOF-177 with the increase in gas feed pressure which is as shown in fig 6.11 for pressure values of 1, 2, 5, 10, 30 and 50 bar, respectively. As the pressure increases, CO_2 molecules are pressed against the surface of the solid. This increases the available surface area for CO_2 adsorption within existing adsorption sites. The increase in the available surface area for adsorption in turn leads to an increase in the maximum possible adsorption of CO_2, hence, the amount of adsorbed CO_2 increases. The highest adsorbed amount for MOF-177 after 30 minutes of adsorption is achieved with 50 bar feed pressure which is about 11.3g. This matched with the work of Saha D. et al [108].

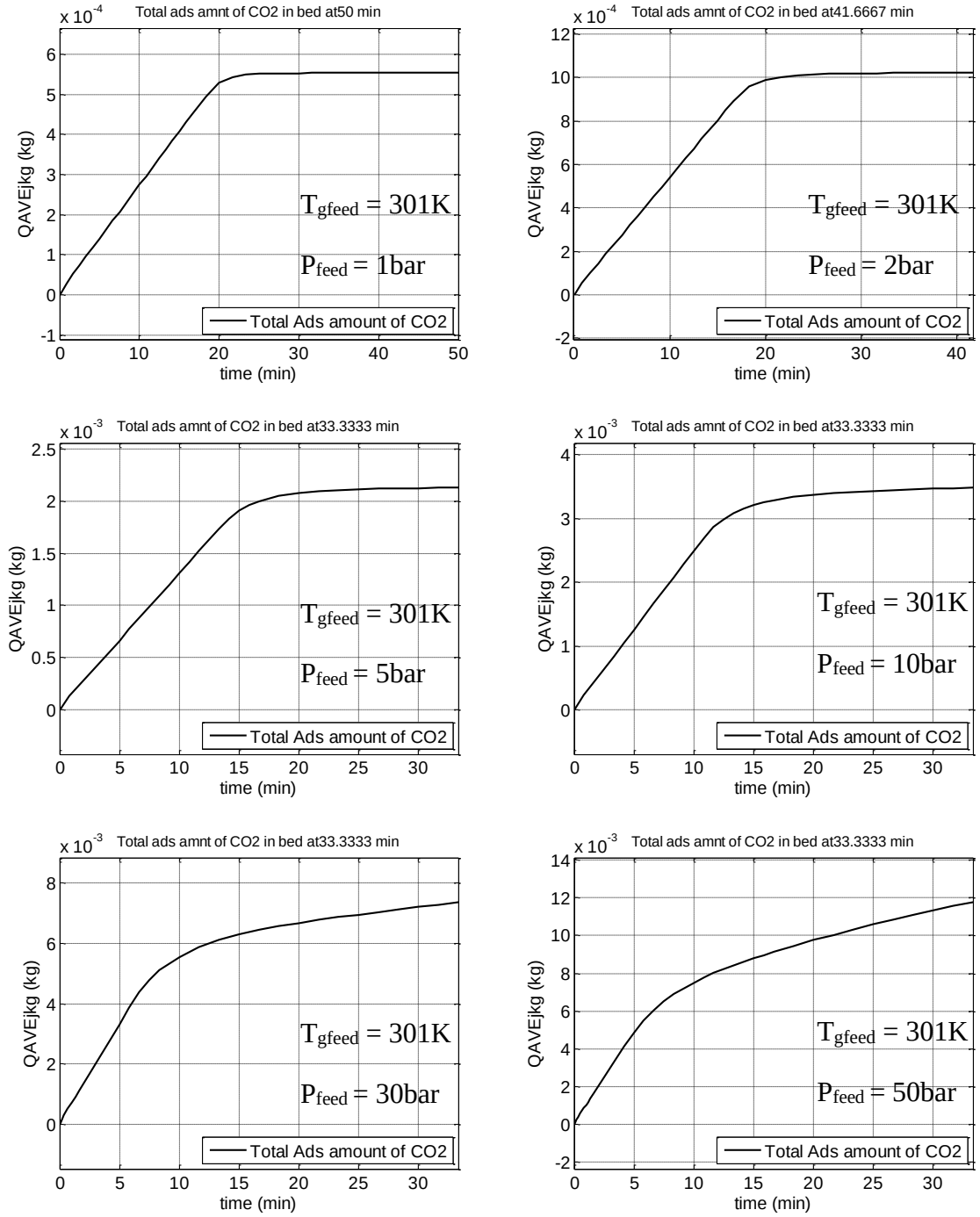

Figure 6.11: Profile of amount of CO_2 stored on MOF-177 for various feed pressures

The same information is re-plottd in Figure 6.12 where the data shown are limited to 30 minutes to see the time profile of the amount absorbed at different pressures. The effect of pressure on the CO_2 absorbed is clear.

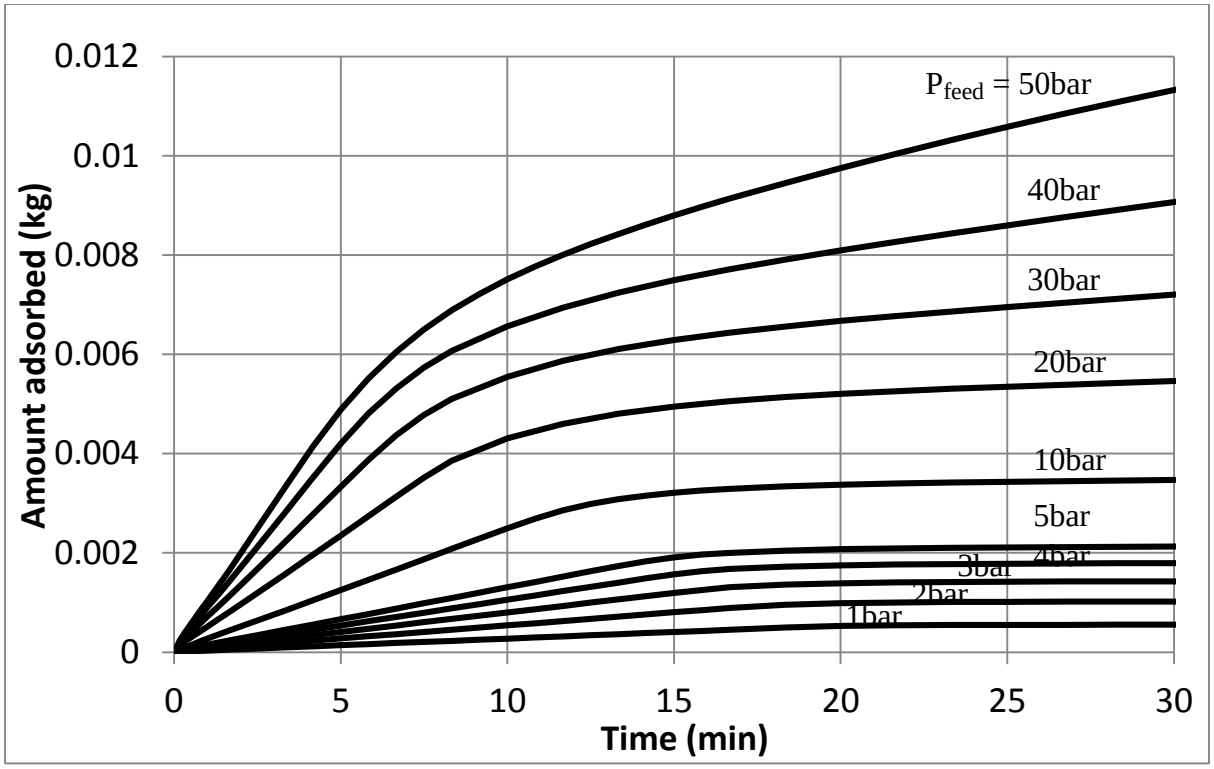

Figure 6.12: Profile of amount of CO_2 stored on MOF-177 for 30min for varying feed pressures

Simulation results for bulk gas and column wall temperature profiles during adsorption of CO_2 on MOF-177 are shown in Figures 6.13 and 6.14. The figures show an increase in the maximum bulk gas temperature (Fig. 6.13) and column wall temperature (Fig. 6.14) with increase in feed pressure. This effect is due to increase in the amount of gas adsorbed within bed with increase in pressure which in turn leads to higher heat generation from the exothermic reaction hence, higher bulk gas temperature and more heat transfer to the walls. The initial fast climb in adsorption leads to roll-up effect in temperature at different points in the bed leading to an increase in temperature especially in the bulk gas at those points to peak values; the highest of these is found at the end of the bed. The roll-up effect may be due to the high amount of heat generated due to initial fast and continuous adsorption of CO_2 at these points. As the bed gets saturated, the rate of adsorption slows down and the peak

temperatures drop down a steady temperature which is maintained through the filling process. Based on further simulation results, the adsorbent showed similar behaviour as the bulk gas. It assumes similar temperatures in space and time as the bulk gas with negligible difference in values.

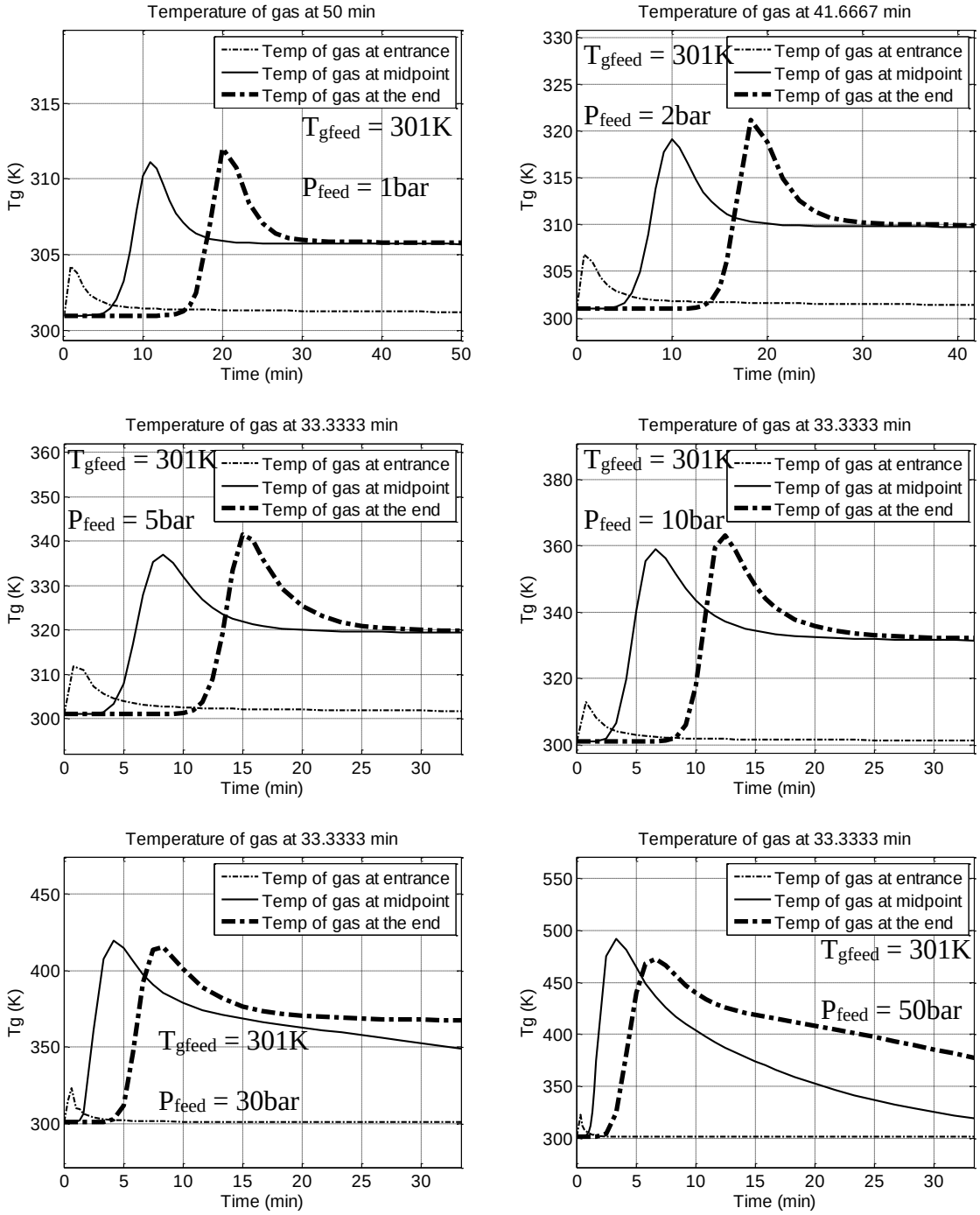

Figure 6.13: Temperature profile of bulk gas for storage of CO_2 on MOF-177 for various feed pressures

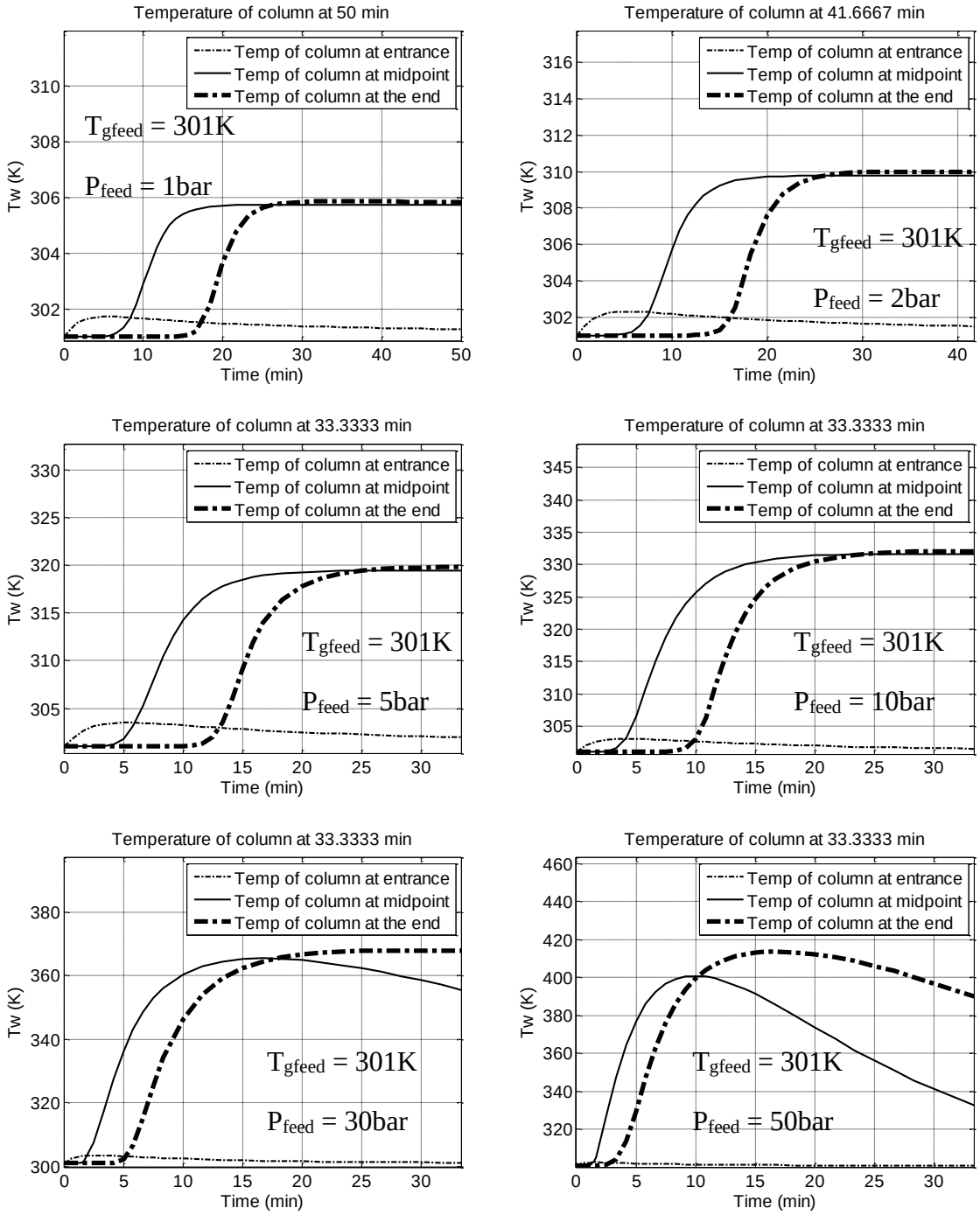

Figure 6.14: Temperature profile of adsorption column wall during adsorption of CO_2 on MOF-177 for various feed pressure

The behaviour of equilibrium adsorption constant from Van't Hoff's equation (equation 3.4) with varying temperature and pressure during adsorption of CO_2 on MOF-177 is depicted in Figure 6.15 that shows a decrease in the minimum adsorption constant with the increase in feed pressure and temperature. This is because the increase in pressure within the bed leads to a longer time for the bed to get saturated with CO_2, this in turn leads to better adsorption and

hence, better gas storage capacity. Values of the parameters at the middle and exit of the system exhibit gradual decrease up to the peak temperature after which the parameters increase back to values close to the feed parameter values. The parameter is lowest at bed exit due to the high temperature at this point.

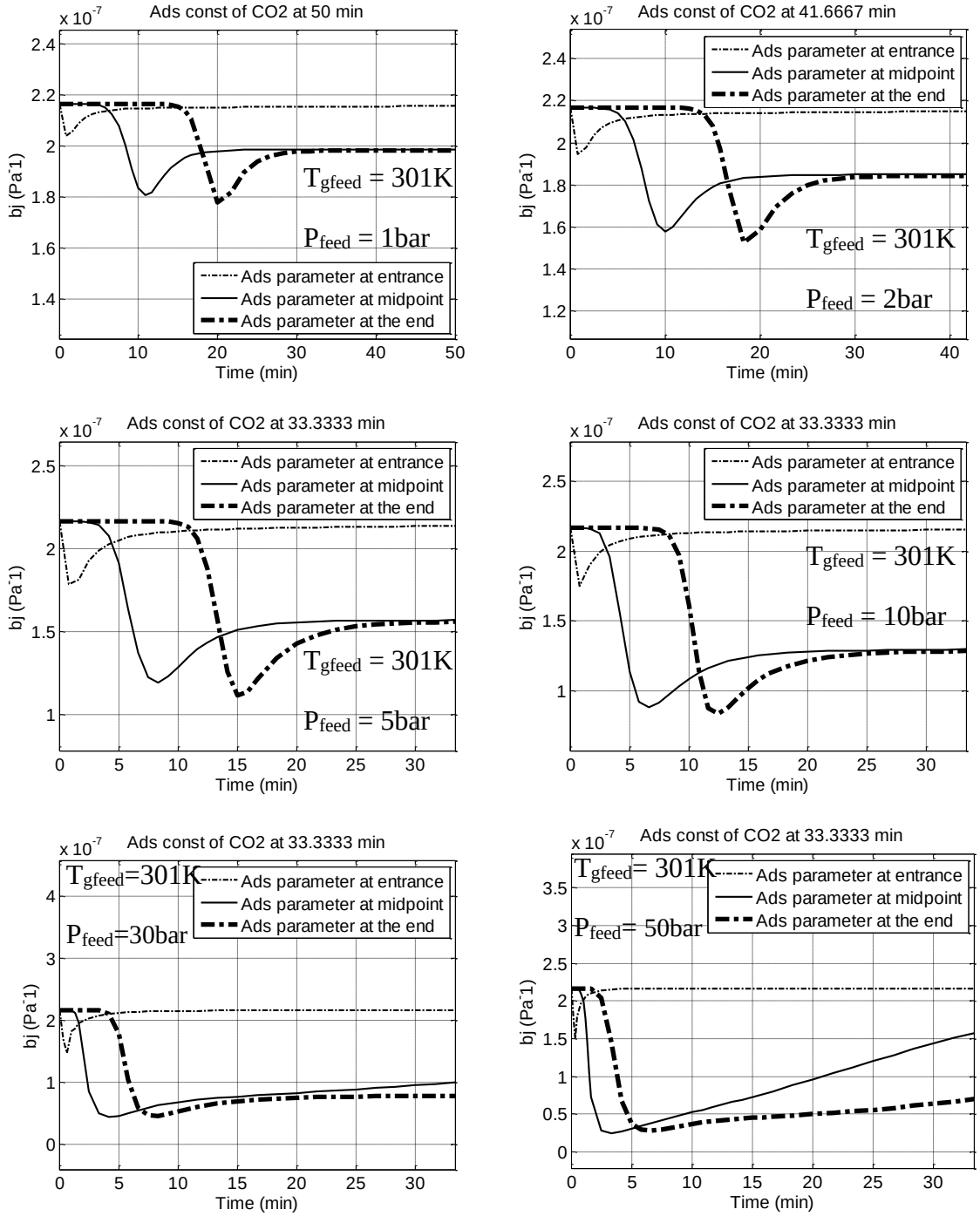

Figure 6.15: Profile of equilibrium adsorption constant for CO_2 adsorption on MOF-177 for various feed pressure

The effects of bed length and diameter on the amount of CO_2 stored on MOF-177 and Activated Carbon are shown in Figures 6.16 and 6.17. The figures show that at any given simulation time, the amount of CO_2 adsorbed on MOF-177 and Activated Carbon beds increases with increase in bed length (Fig. 6.16) or diameter (Fig 6.17). However, the effect of increase in bed diameter on storeage of CO_2 is much more than the effect of bed length. This may be due to higher increase in column volume per unit increase in bed diameter compared to corresponding increase in column length. Besides, column diameter creates larger surface area of heat exchange between the bed, the wall and ambient hence, lower temperature and better adsorption are achieved within the bed. This effect is further explained by equations 3.14 & 3.15 and by the behaviour of the bulk gas temperature with column size. Finally, the fast climb in adsorption for each bed length and diameter may also increase due to increase in surface area of adsorption within the bed which cause a prolonged time for initial adsorption

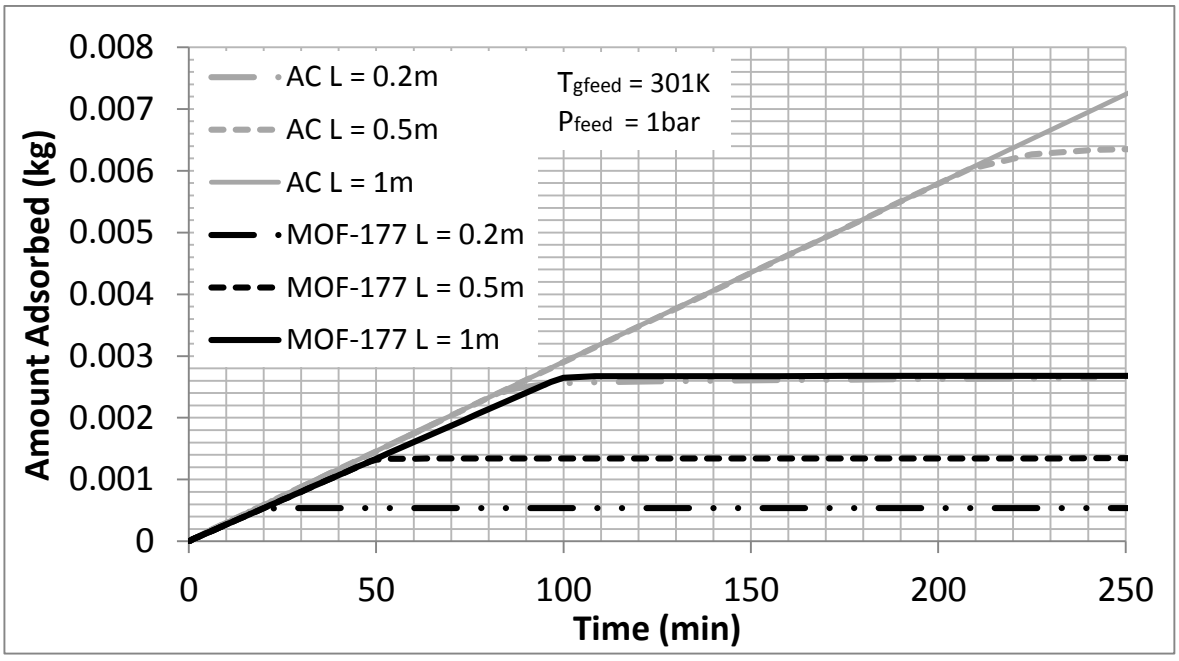

Figure 6.16: Effect of bed length on total amount of CO_2 stored on MOF-177 and Activated Carbon for 250min

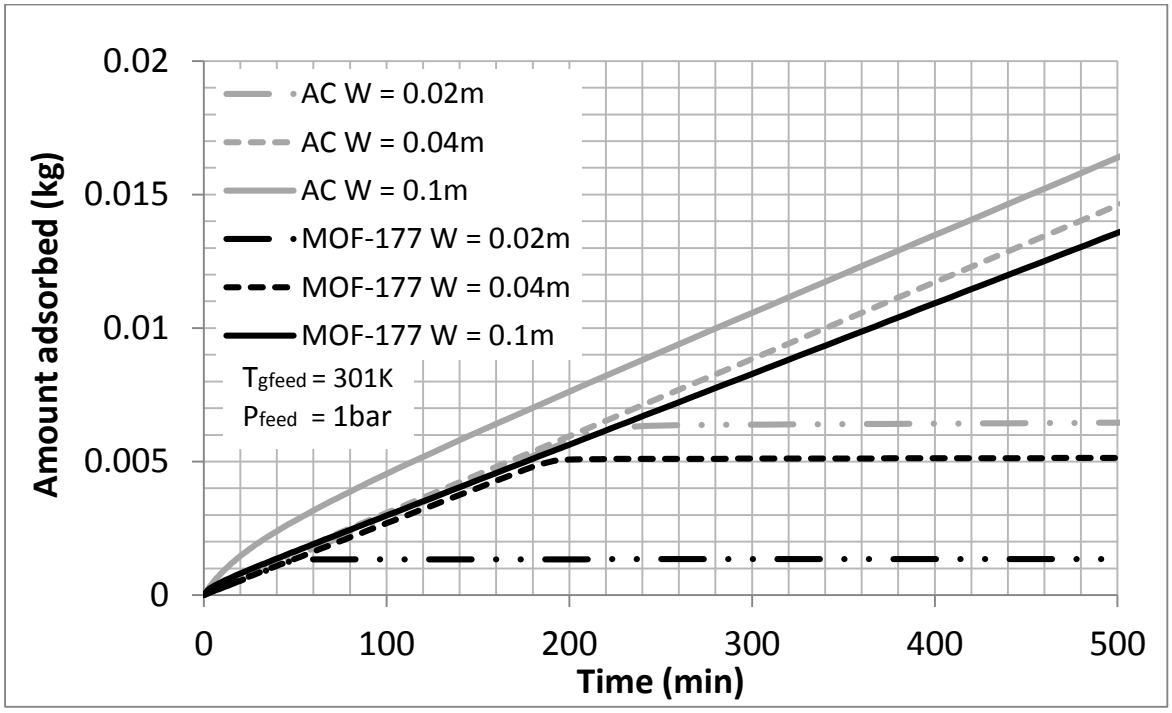

Figure 6.17: Effect of bed diameter on total amount of CO_2 stored on MOF-177 and Activated Carbon for 500min

6.2.3 Simulated Results for Adsorptive Storage of CO_2 storage on Activated Carbon

The simulated results of the amount of CO_2 stored on Activated Carbon with feed gas temperature of 301K at various feed pressures in Figures 6.18 & 6.19 show similar behaviour as MOF-177 and MOF-5 in that the amount of CO_2 stored on AC increases with pressure. For the simulations carried out, the highest amount of CO_2 stored in AC after 50 minutes of feeding is gotten with 50bar feed pressure and it has a value of about 13g as shown in Fig 6.18. This high value compared to MOF-177 may be due to the remakable properties of the particular sample of AC used in this simulation as acknowleged by Dantas et al 2011 [117].

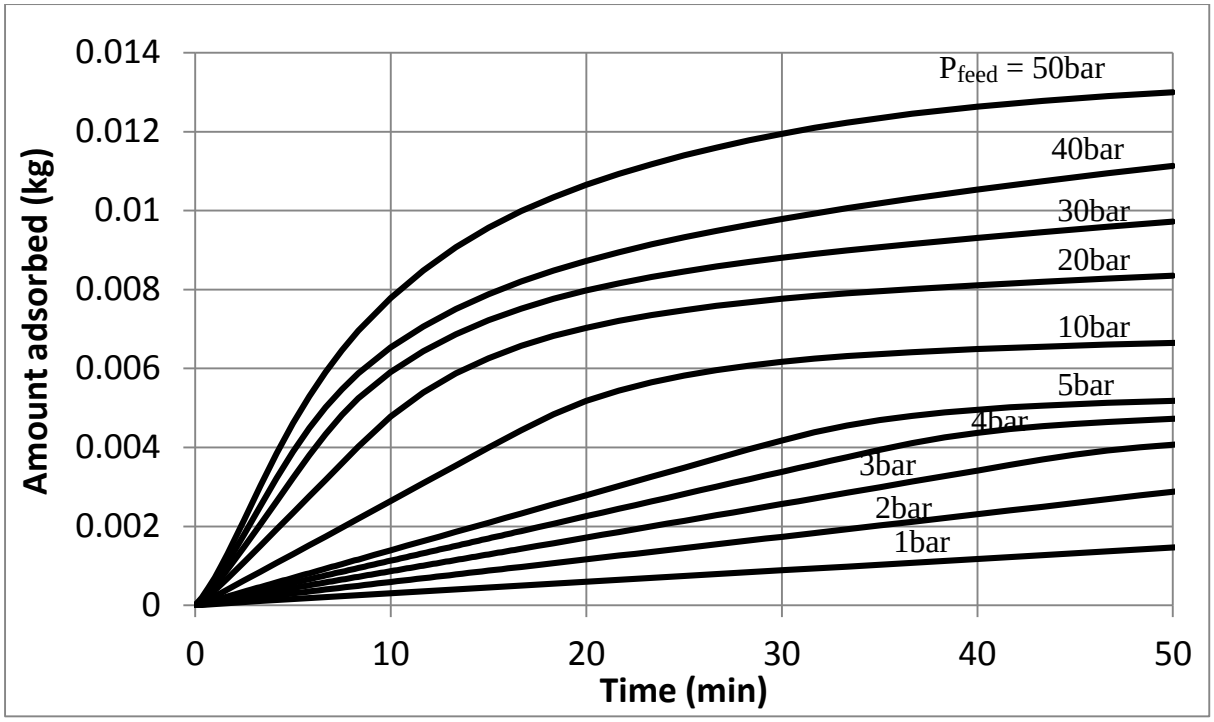

Figures 6.18: Profile of amount of CO_2 stored on Activated Carbon for 50min for varying feed pressures

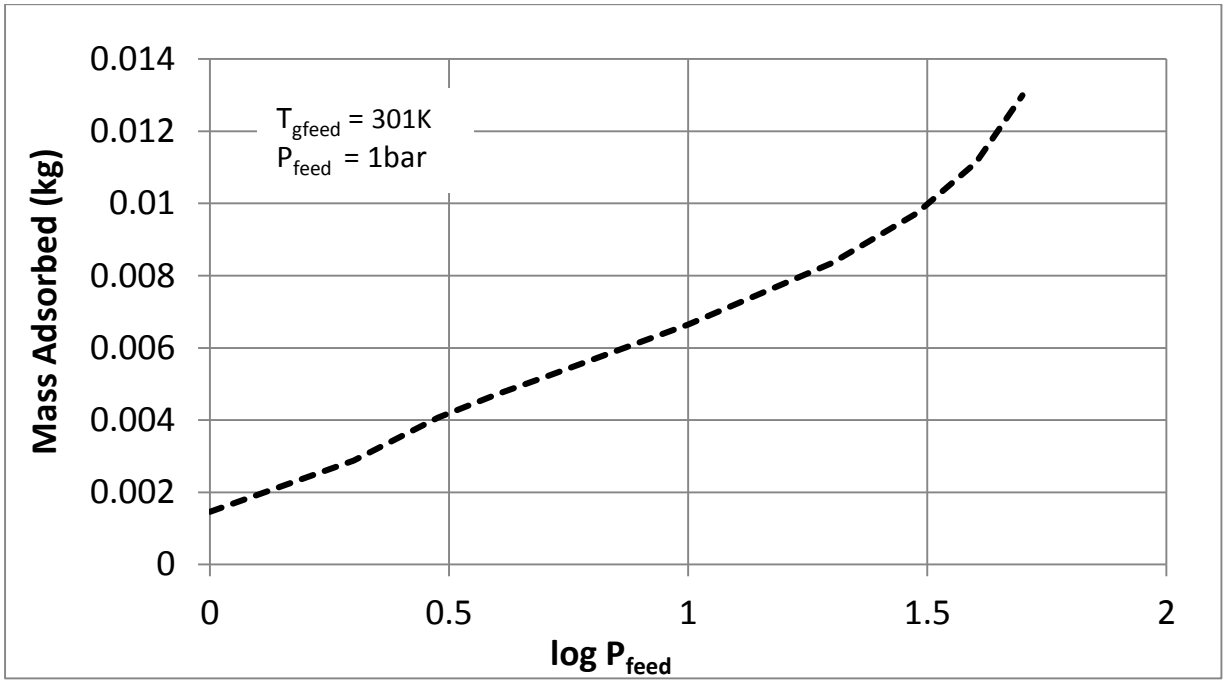

Figure 6.19: Effect of feed pressure on stored amount of CO_2 on Activated Carbon bed for 50min feeding duration

CHAPTER 7

RESULTS OF PRESSURE SWING ADSORPTION EXPERIMENT SIMULATIONS

For reliability of information presented in this work, the written MATLAB code was first used to validate the experimental work of Carlos A. Grande et al [133]. Pressure Swing Adsorption experiment of Carlos A. Grande et al was simulated for the adsorption separation of CO_2 from flue gas (15% CO_2, wt N_2) using zeolite 13X as adsorbent. The results gotten from the validation showed closeness between experimental and simulated data.

7.1 Validation of Simulated Adsorption Code with Pressure Swing Adsorption Experiment Results

The work of Carlos A. Grande [133] presents Pressure Swing Adsorption experiments for a pressure range of 0.1 bar to 1.3 bar, with feed gas temperature of 363K. The data provides variation of CO_2 and N_2 molar flow rate with time at the exit section. Figures 7.1&7.2 show a comparison of experimental data and LDF model simulation for the cycle curves for the adsorption of CO_2 from binary gas mixture of 15% CO_2 wt N_2. These figures show the molar flow rate of species at bed exit during the four steps of the PSA process. The total feed gas flow rate is 3l/min and the purge flow rate is 0.5l/min. The feed pressure is 1.3 bar and the purge pressure is 0.1 bar. The roll-up behaviour of CO_2 is due to the initial increase in concentration of CO_2 during the desorption step caused by the addition of the desorbed gases to the gaseous stream. The roll up behaviour is pronounced in CO2 because of the high selectivity of zeolite 13X for CO_2. As shown from figures 7.1&7.1, the present model captures the changes in CO_2 and N_2 concentrations with time quite well from the qualitative point of view. The peak in the carbon dioxide concentration is well captured by the model.

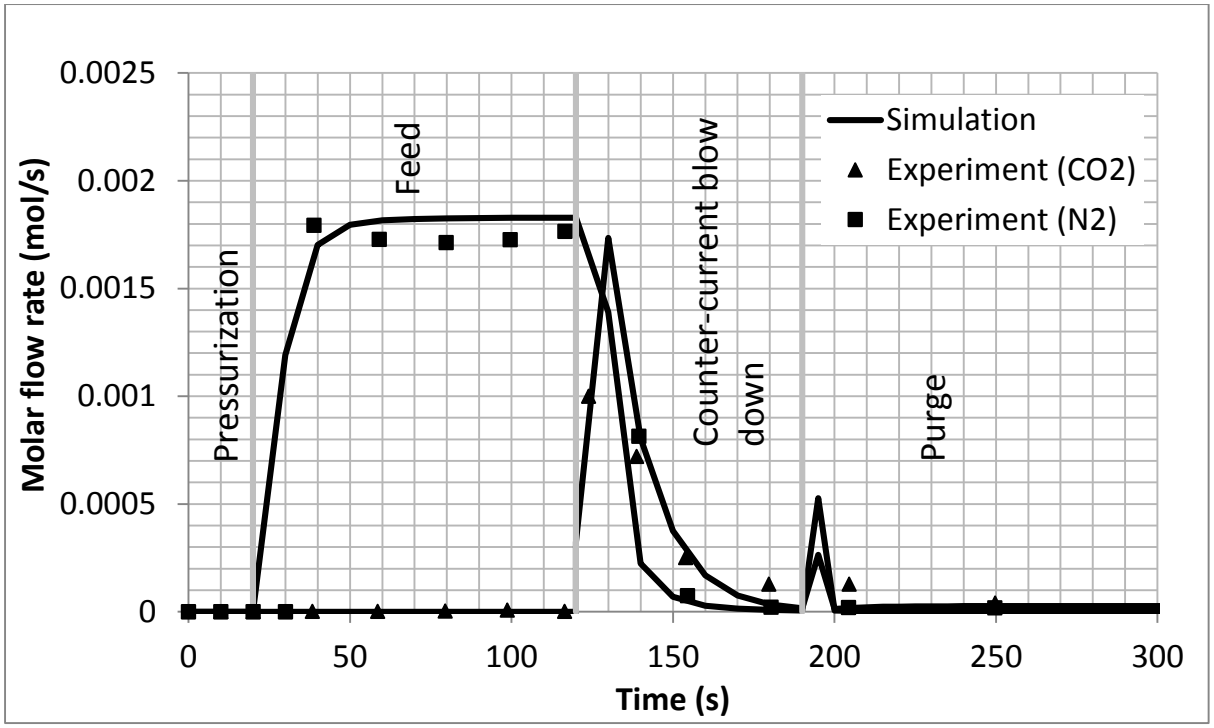

Figure 7.1: Validation of molar flow rate curve of PSA on zeolite 13X for T_{gfeed} = 90°C (363K), Experimental data Carlos A. Grande et al [133]

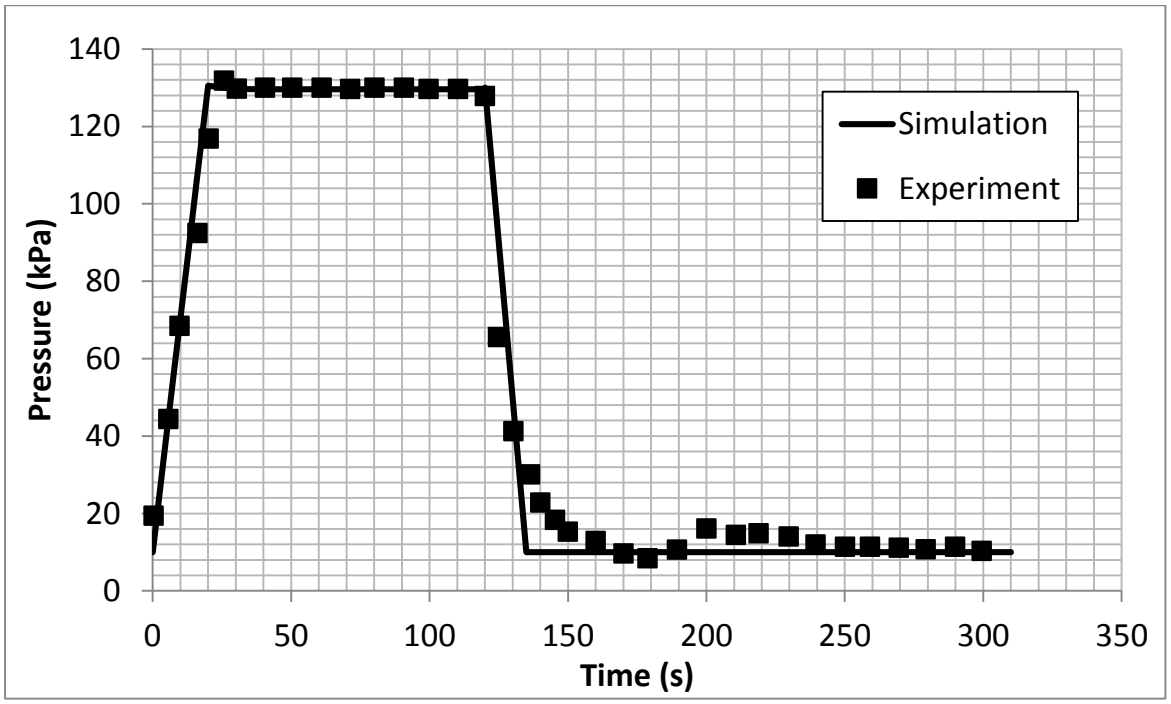

Figure 7.2: Validation of pressure swing curve of PSA on zeolite 13X for Tgfeed = 90°C(363K), Experimental data Carlos A. Grande et al [133]

7.2 The Simulated PSA behaviour of Mg-MOF-74

Three sets of PSA simulations were carried out for CO_2 sequestration using Mg-MOF-74. In the first and the second sets of simulations, the feed for each new cycle was the effluent recovered from the blow down step of the previous cycle. The first one is a PSA system that exchanges heat directly with ambient air, while the other is a PSA system with an incorporated heat regeneration system (HR-PSA) made of packed sand bed. For this PSA process, the adsorption system exchanges heat with the packed bed of regenerator rather than the ambient. Sections 7.2.1 and 7.2.2 present the results of these two cases. For the third set of simulations (section 7.2.3) the feed for all cycles remained the same i.e. 15% CO_2 and 85% N_2 and experimental conditions of runs 1&2 were employed to simulate twenty-five (25) PSA cycles.

7.2.1 PSA behaviour of Mg-MOF-74 without heat regenerator

The first sets of simulations (figures 7.3-7.6) were carried out for PSA process with heat exchange with the ambient. The figures show the curve for molar flow rates at bed exit for a 1-bed, four step PSA for binary gas mixture on Mg-MOF-74; for the removal of CO_2 from a standard gas mixture of 15% CO_2 wt N_2. These figures show four different PSA runs for the flow conditions described in tables 3&10. Each figure portrays the number of cycles simulated in each run for during the process of CO_2 sequestration. The total feed gas flow rate in each case is 3l/min and the purge gas flow rate is 0.5l/min. The column is pressurized from 0.1 bar to 1.3 bar, it is feed at a pressure of 1.3 bar, blown down at a pressure of 0.1 bar and purged at the same pressure. From the plots, it can be deduced that Mg-MOF-74 has very high selectivity and adsorption capacity for CO_2 which conforms to existing reports [182].

The plots also show that it takes three or less cycles for Mg-MOF-74 to capture at least 99% of carbon dioxide from the feed stream. The break through time for CO_2 in the described mixture decreased with increase in temperature and increase in number of cycles. At feed gas temperature of 301K, Mg-MOF-74 exhibited lesser selectivity and required more number cycles for CO_2 separation from flue gas. The roll-up behaviour of CO_2 is due to the initial increase in concentration of CO_2 during the desorption step caused by the addition of the desorbed gases to the gaseous stream.

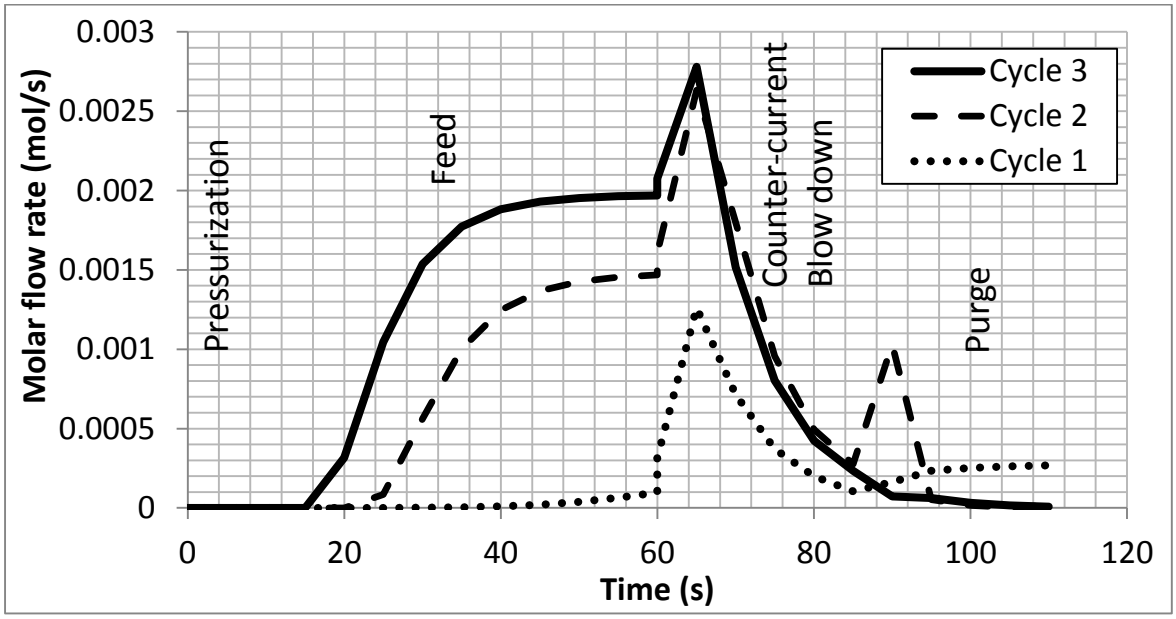

Figure 7.3: Molar flow rate curve of PSA on Mg-MOF-74 for run 1

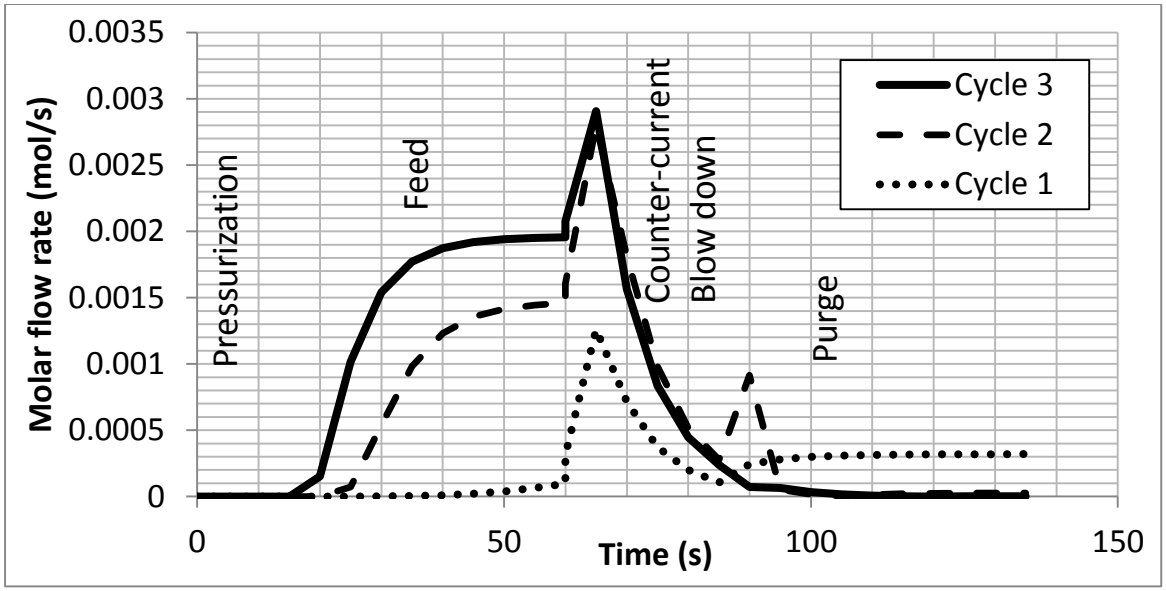

Figure 7.4: Molar flow rate curve of PSA on Mg-MOF-74 for run 2

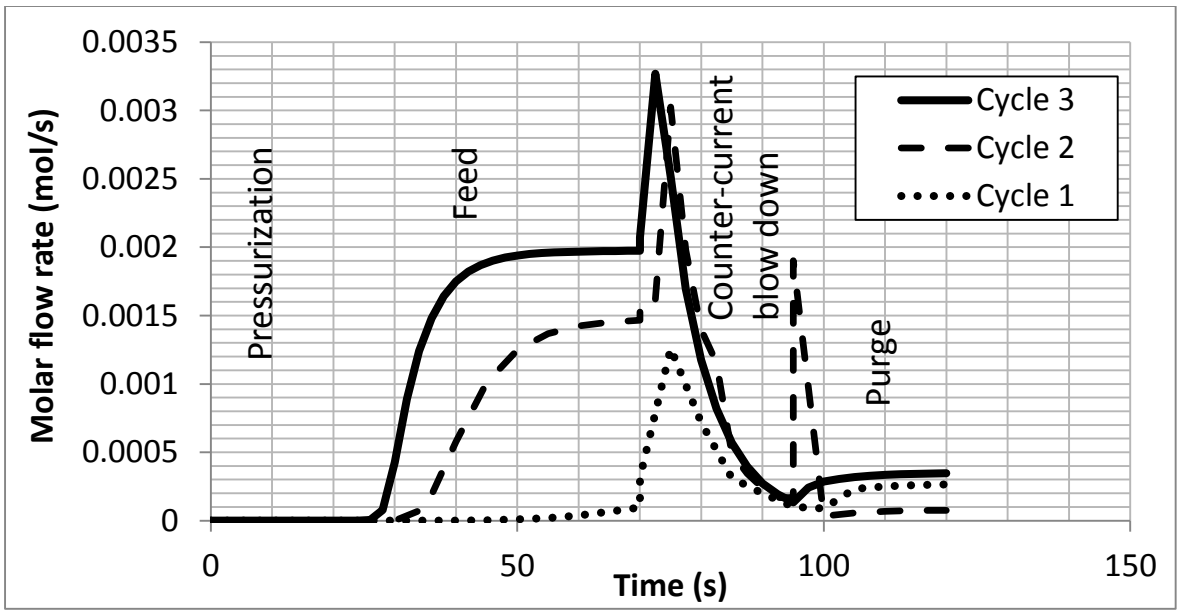

Figure 7.5: Molar flow rate curve of PSA on Mg-MOF-74 for run 3

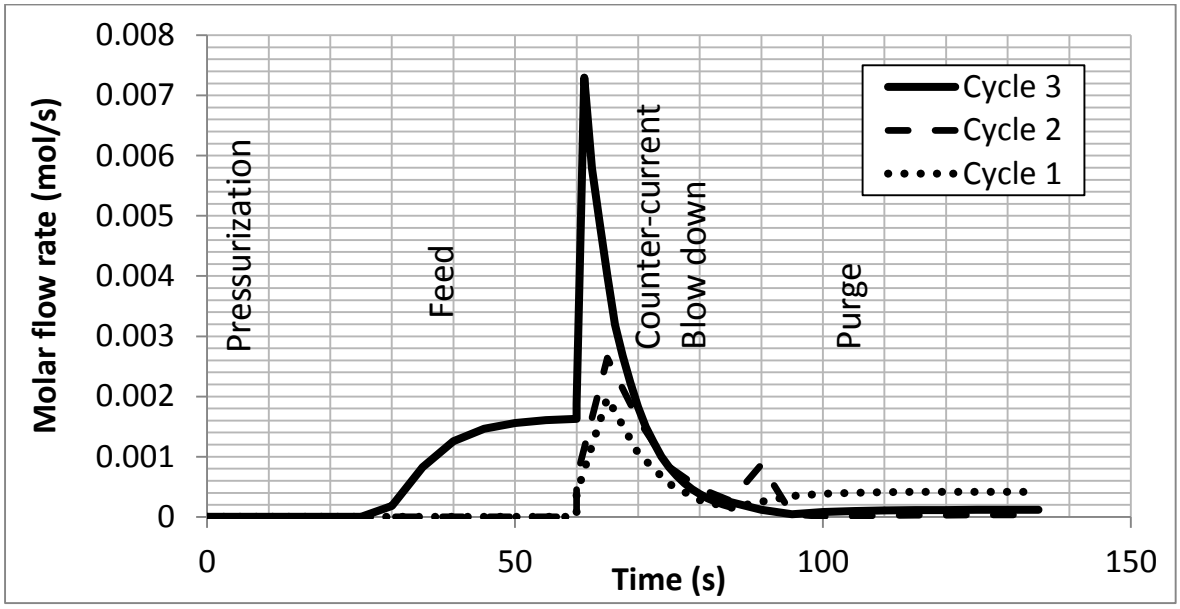

Figure 7.6: Molar flow rate curve of PSA on Mg-MOF-74 for run 4

7.2.2 PSA behaviour of Mg-MOF-74 with heat regenerator (HR-PSA)

After initial simulations, heat regeneration system in form of a packed sand bed was added to the typical adsorption system in order to store the heat given off during pressurization and adsorption steps and dissipate it during blow down and purging steps. For this set of simulations (figures 7.7-7.10), it was assumed that the PSA system exchanged heat with a packed bed of quartz rather than with the ambient. Figures 7.7-7.10 show the curve for molar flow rates at bed exit for a 1-bed, four step HR-PSA for binary gas mixture on Mg-MOF-74; for the removal of CO_2 from a standard gas mixture of 15% CO_2 wt N_2. These figures show four different PSA runs for the same flow conditions used for the PSA (tables 4.3&4.10). Each figure portrays the number of cycles simulated for each run for CO_2 sequestration. From the plots, it can be deduced that the selectivity of Mg-MOF-74 was greatly improved due to heat regeneration. This may be due to the increase in amount of heat supplied during the adsorption process. For subsequent cycles after the first cycle, the packed sand bed creates a form of thermal resistance for the adsorption system thereby trapping the heat given off by

the system, increasing the temperature within the system and improving the selectivity of the system in accordance with existing research [131],[133]. The plots also show that it takes mostly two cycles for Mg-MOF-74 to capture of purity up to at least 99% from the feed stream. The break through time for CO_2 in the described mixture decreased with increase in temperature and increase in number of cycles. At a feed gas temperature of 28^{o}C, Mg-MOF-74 exhibited lesser selectivity and required more number cycles for CO_2 separation from flue gas. The roll-up behaviour of CO_2 is due to the initial increase in concentration of CO_2 during the desorption step caused by the addition of the desorbed gases to the gaseous stream.

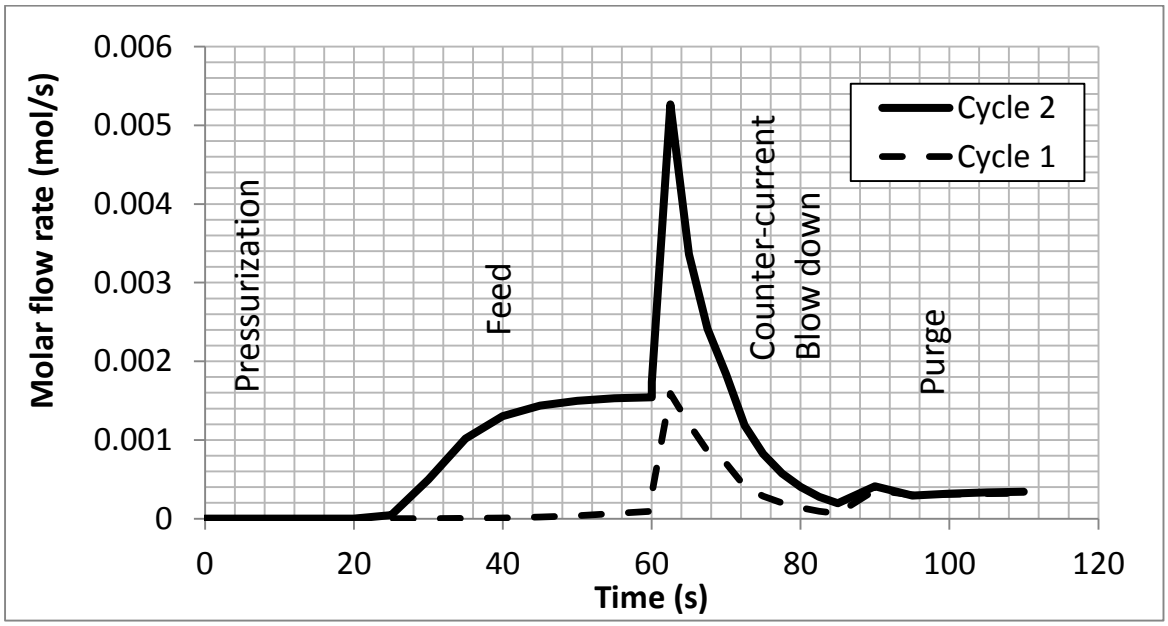

Figure 7.7: Molar flow rate curve of HR-PSA on Mg-MOF-74 for run 1

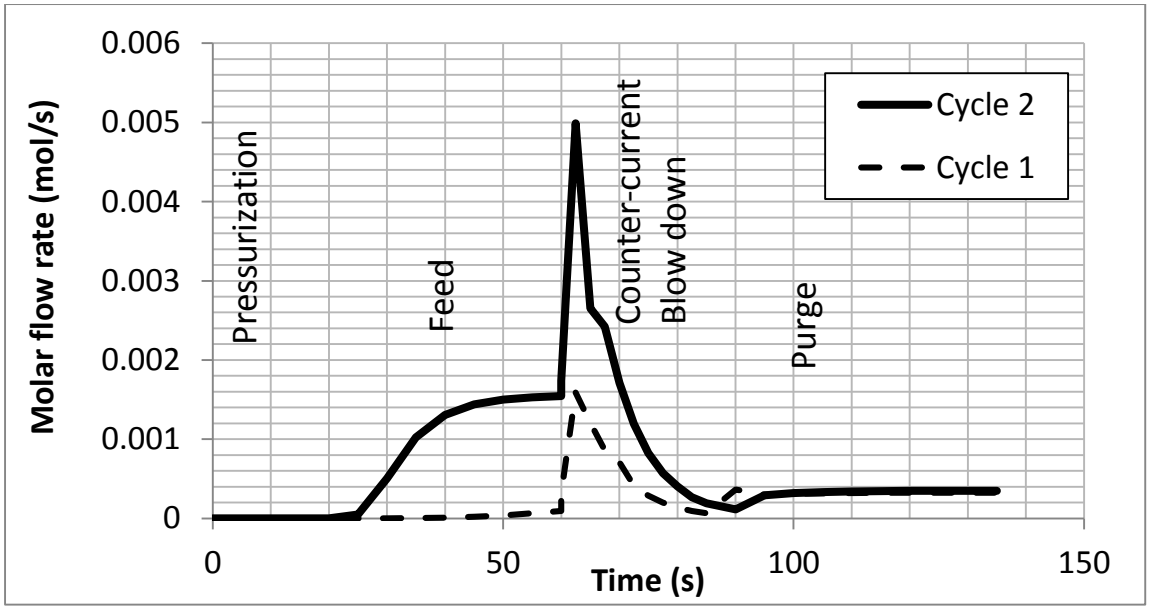

Figure 7.8: Molar flow rate curve of HR-PSA on Mg-MOF-74 for run 2

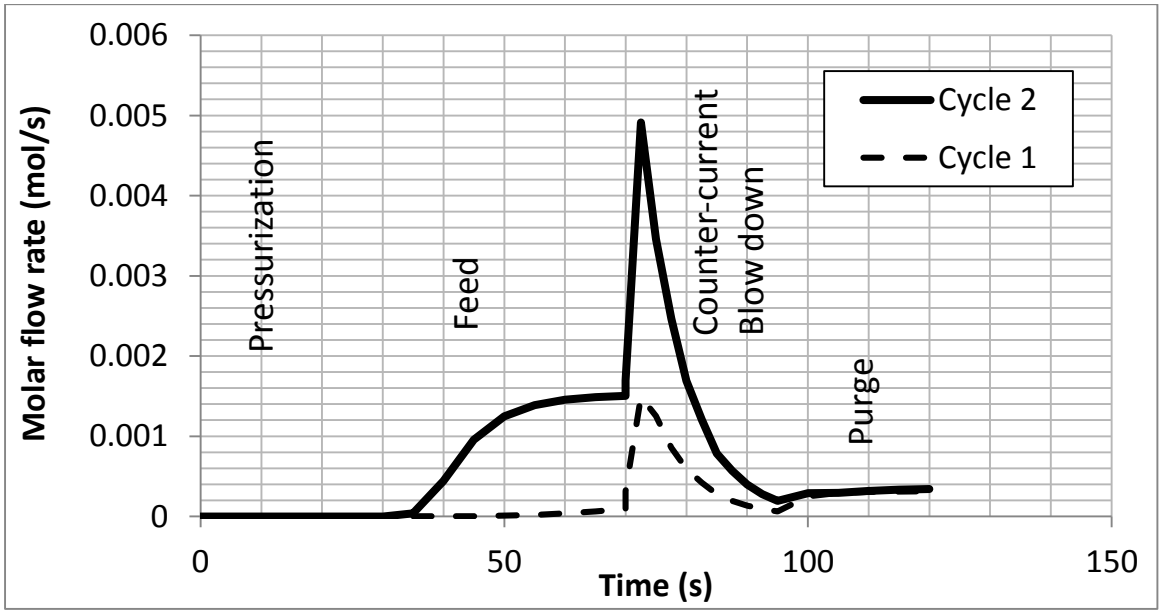

Figure 7.9: Molar flow rate curve of HR-PSA on Mg-MOF-74 for run 3

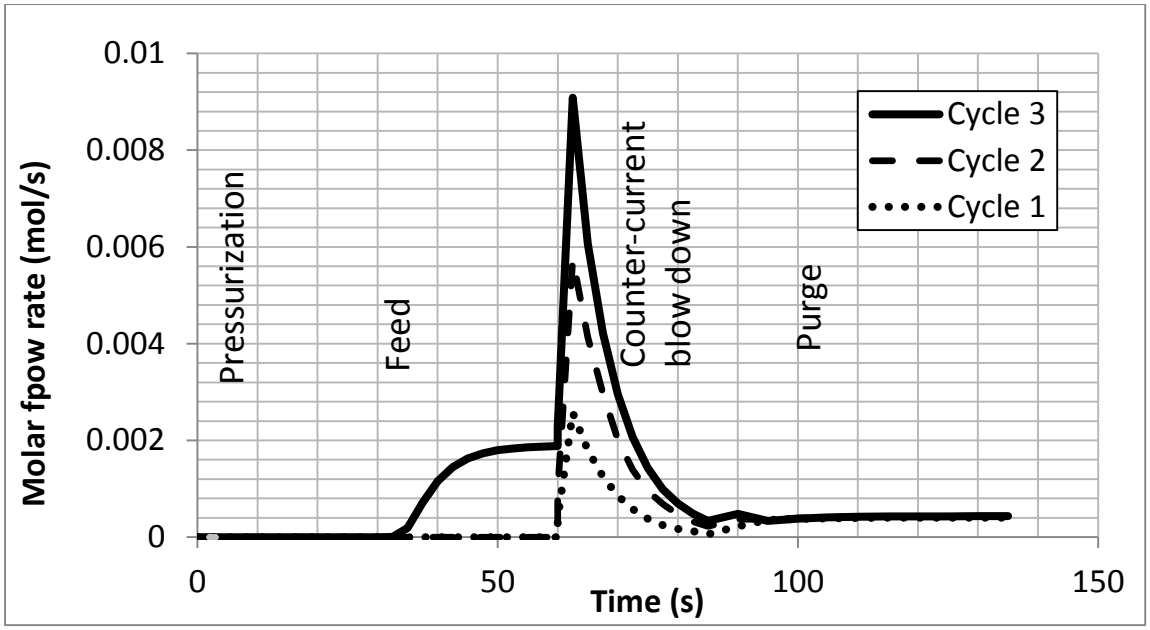

Figure 7.10: Molar flow rate curve of HR-PSA on Mg-MOF-74 for run 4

Figures 7.11-7.14 and table 7.1 shows a comparison of PSA process without heat regenerator and PSA process with heat regenerator (HR-PSA). For better comparison, the last cycles of each run of the PSA and the HR-PSA have been plotted together (figures 7.11-7.14). The performance parameters for the two processes have also been evaluated as shown in table 7.1. From the plots, it can be seen that the amount of CO_2 adsorbed during the feed process is higher for the PSA without heat regenerator this may be due to the heat stored in the sand bed which gives molecules of CO_2 more energy thereby reducing their adsorption onto the surface of the adsorbent. However, in blow down and purge steps, the heat released to bed enhances the desorption process bringing about removal of more CO_2 and better purity of product. This is better illustrated with the climb in peak of the curve for the HR-PSA and the molar flow rate of CO_2 during the purge step. This also enhances durability of the bed for use for higher number of adsorption-desorption cycles.

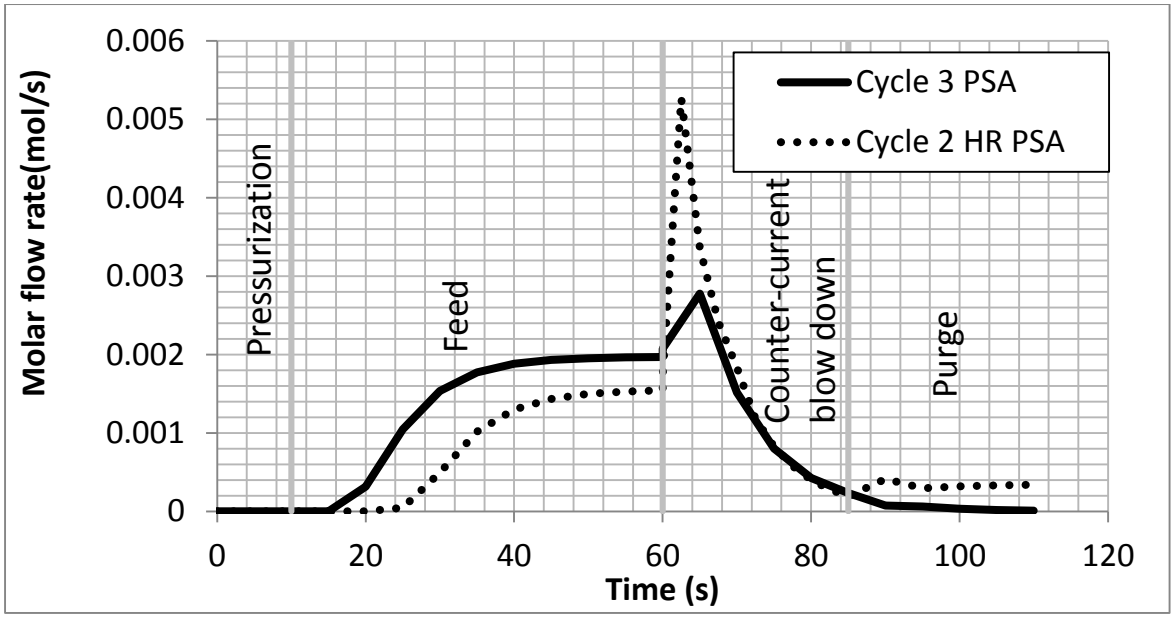

Figure 7.11: Molar flow rate curve for the last cycles of PSA and HR-PSA on Mg-MOF-74 for run 1

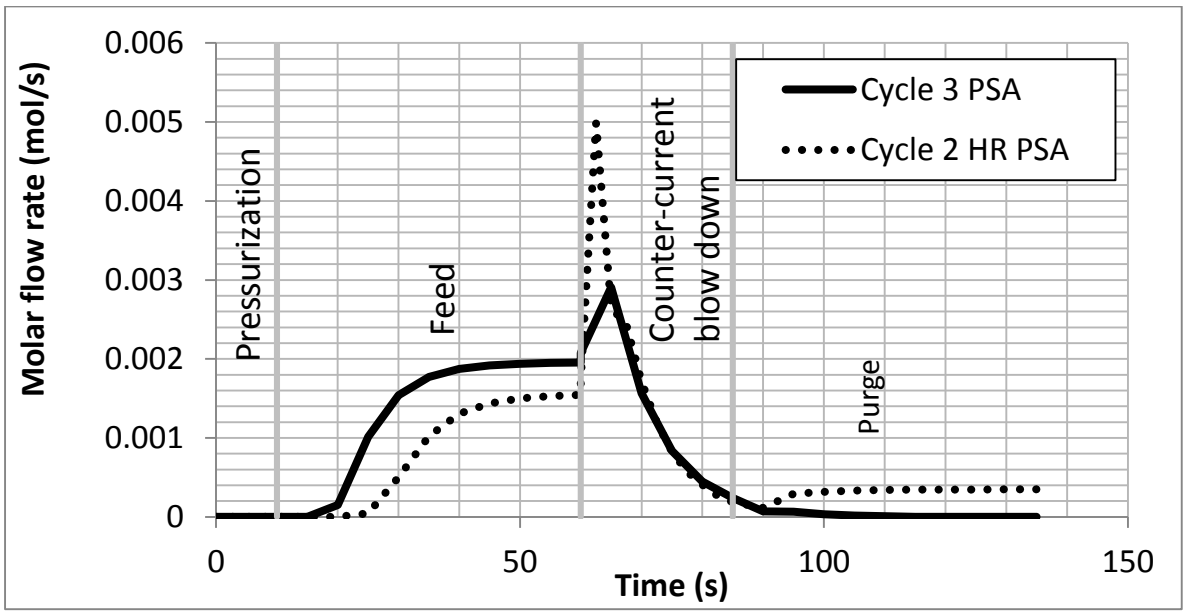

Figure 7.12: Molar flow rate curve for the last cycles of PSA and HR-PSA on Mg-MOF-74 for run 2

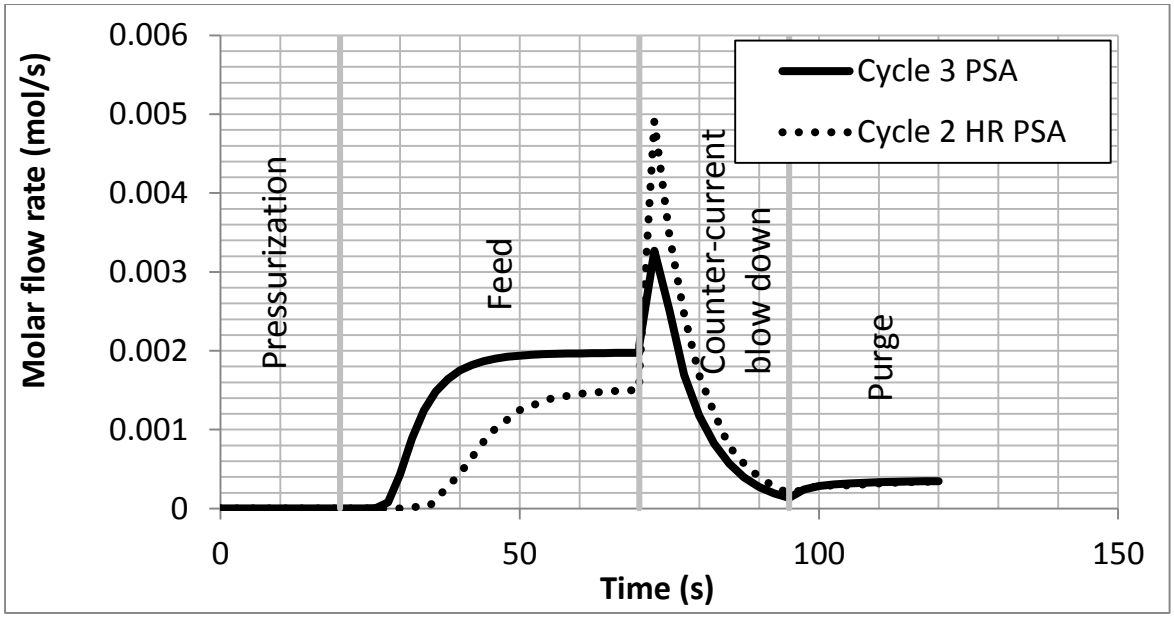

Figure 7.13: Molar flow rate curve for the last cycles of PSA and HR-PSA on Mg-MOF-74 for run 3

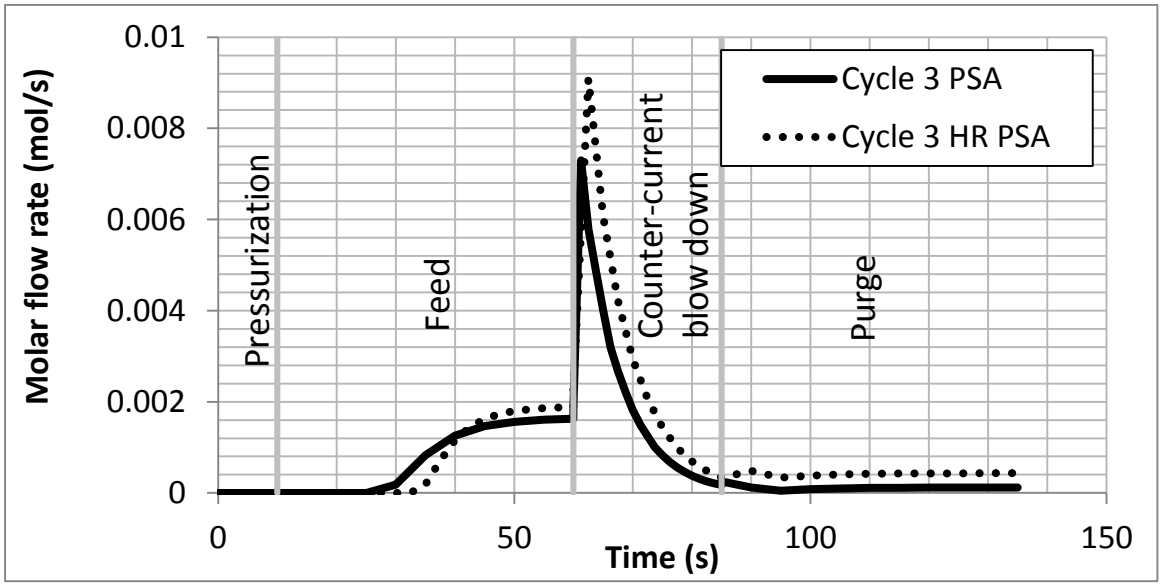

Figure 7.14: Molar flow rate curve for the last cycles of PSA and HR-PSA on Mg-MOF-74 for run 4

Table 7.1 portrays the performance parameters for Mg-MOF-74 for PSA with and without heat regenerator for simulated runs. From the table, it can be seen that CO_2 recovery increases with increase in the duration of purge and pressurization. CO_2 recovery also

increases with decrease in feed gas temperature; however, purity reduces with decrease in temperature. These are true for cases of PSA and HR PSA. As expected, the more the purge duration, the lesser the residual CO_2 in the bed hence the higher the CO_2 recovery. The heat generated however has more effect on the amount of recovered CO_2 than the duration of pressurization. Looking at run 3 for both cases of PSA with and without heat regeneration, it can be seen that the amount of CO_2 recovered for run 3 without heat regeneration is higher than run 2 but the amount of CO_2 recovered for PSA with heat regeneration is lower than run 2. This might be because the amount of heat generated during the prolonged pressurization step reduces the amount of CO_2 adsorbed during the feed step much more than it helps to recover it in the blow down and purge steps. This reduction in CO_2 recovery is substituted with an increase in the purity of the recovered CO_2. It can also be seen that PSA process with heat regeneration achieves equivalent of the amount of CO_2 sequestration in lesser number of cycles compared to the PSA without heat regeneration system.

Table 7.1: Performance parameter for CO_2 recovery from flue gas using PSA process with and without heat regenerator for Mg-MOF-74

PSA	Run	Feed Temp (K)	t_{press} (s)	t_{feed} (s)	t_{blow} (s)	t_{purge} (s)	Purity of CO_2 (%)	Recovery of CO_2 (%)	Cycle
Without heat regenerator	1	373	10	50	25	25	98.23	29.30	3
	2	373	10	50	25	50	98.30	30.50	3
	3	373	20	50	25	25	98.60	32.70	3
	4	301	10	50	25	50	99.04	56.14	3
With heat regenerator	1	373	10	50	25	25	99.20	52.70	2
	2	373	10	50	25	50	99.23	54.71	2
	3	373	20	50	25	25	98.92	52.70	2
	4	301	10	50	25	50	99.65	69.50	3

7.2.3 PSA behaviour of Mg-MOF-74 with constant feed concentration

The simulated pressure curve and total amount of CO_2 adsorbed in bed exit for run 1 are as shown in figures 7.15 and 7.16 respectively. For these cycles, the feed gas concentration for each cycle was maintained as 15% CO_2 and 85% N_2 and experimental condition of run 1 was employed to simulate 25 PSA cycles. From the curve, it can be seen that the adsorption capacity of Mg-MOF-74 reduced with increase in the number of cycles. For a bed size of 0.2m x 0.02mØ, feed gas temperature of 373K and pressure swing between 0.1 bar and 1.3 bar, the amount of CO_2 adsorbed on Mg-MOF-74 reduced drastically from about 0.66g to about 0.24g during the ninth cycle, after which the rate of deterioration of the material reduced. Between the ninth and twenty fifth cycles, the rate of deterioration of the material slowed down as the material achieved cyclic steady state. The amount CO_2 adsorbed in the twentieth cycle is about 0.22g.

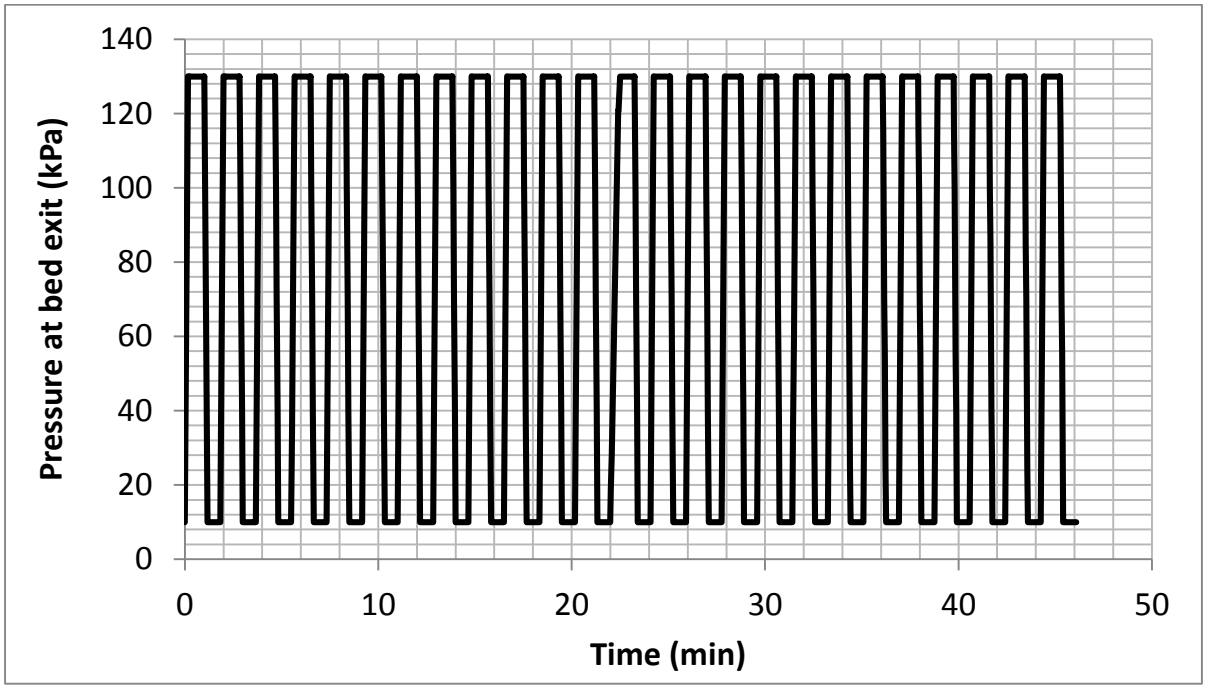

Figure 7.15: Pressure curve at bed exit for 25 cycles of four-step PSA of CO_2 on Mg-MOF-74 from gas mixture of 15%CO_2, 85%N_2 at 373K for run 1.

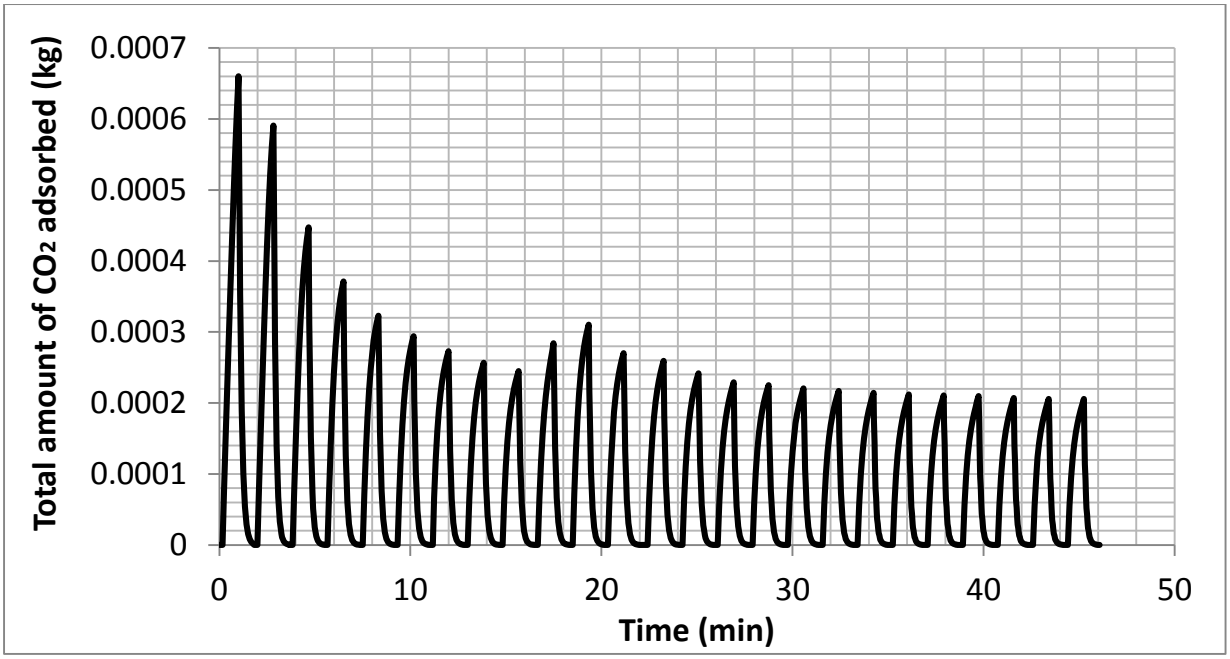

Figure 7.16: Total amount of CO_2 adsorbed in bed for 25 cycles of four-step PSA of CO_2 on Mg-MOF-74 from gas mixture of 15%CO_2, 85%N_2 at 373K for run 1.

The simulated pressure curve and total amount of CO_2 adsorbed in bed exit for run2 are as shown in figures 7.17 and 7.18 respectively. For these cycles, the feed gas concentration for each cycle was maintained as 15% CO_2 and 85% N_2 and experimental condition of run 2 was employed to simulate 25 PSA cycles. From the curve, it can be seen that increase in the duration of purge has effect on the adsorption capacity of the bed. For the same bed size and feed temperature as run1, under similar operating condition, increase in the duration of purge from 25s to 50s helped to slow down the rate of bed deterioration during the first nine cycles with about 0.61g, 0.51g, 0.42g and 0.36g of CO_2 adsorbed in the 2^{nd}, 3^{rd} and 4^{th} cycles respectively as compared to 0.58g, 0.45g, 0.36g and 0.32g adsorbed in similar cycles of run 1 respectively. About 0.26g of CO_2 adsorbed during the ninth cycle, after which the rate of deterioration of the material reduced. The material achieved cyclic steady state after about 15 cycles with the amount CO_2 adsorbed in the fifteenth cycle being about 0.24g.

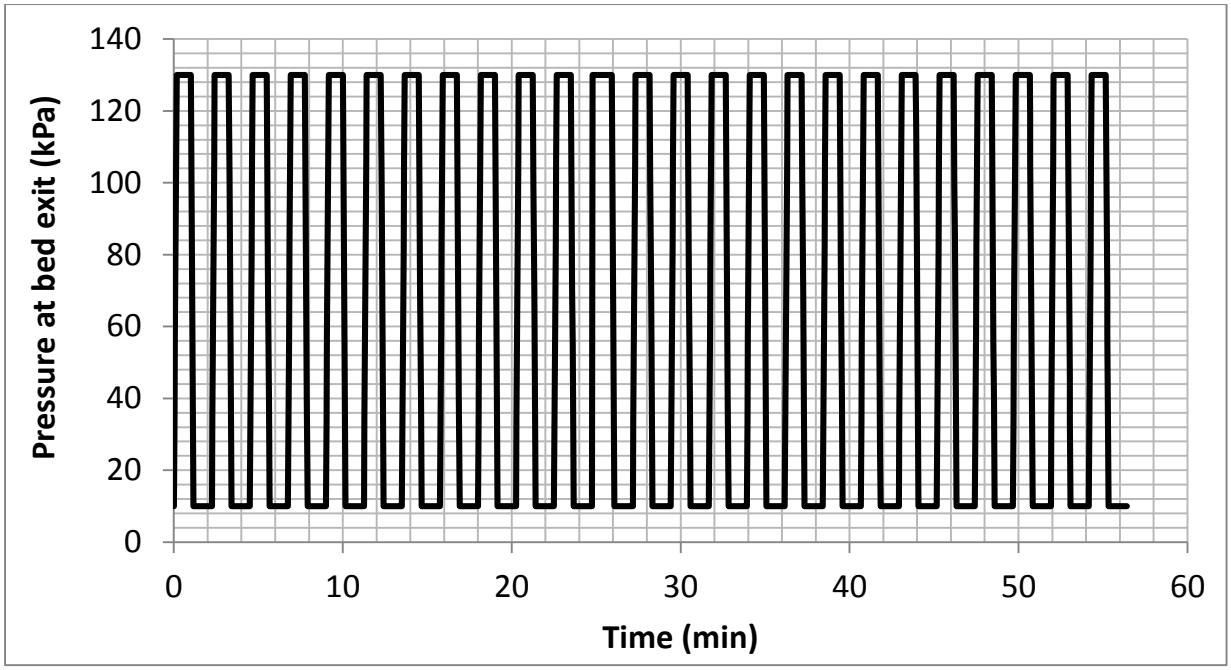

Figure 7.17: Pressure curve at bed exit for 25 cycles of four-step PSA of CO_2 on Mg-MOF-74 from gas mixture of 15%CO_2, 85%N_2 at 373K for run 2.

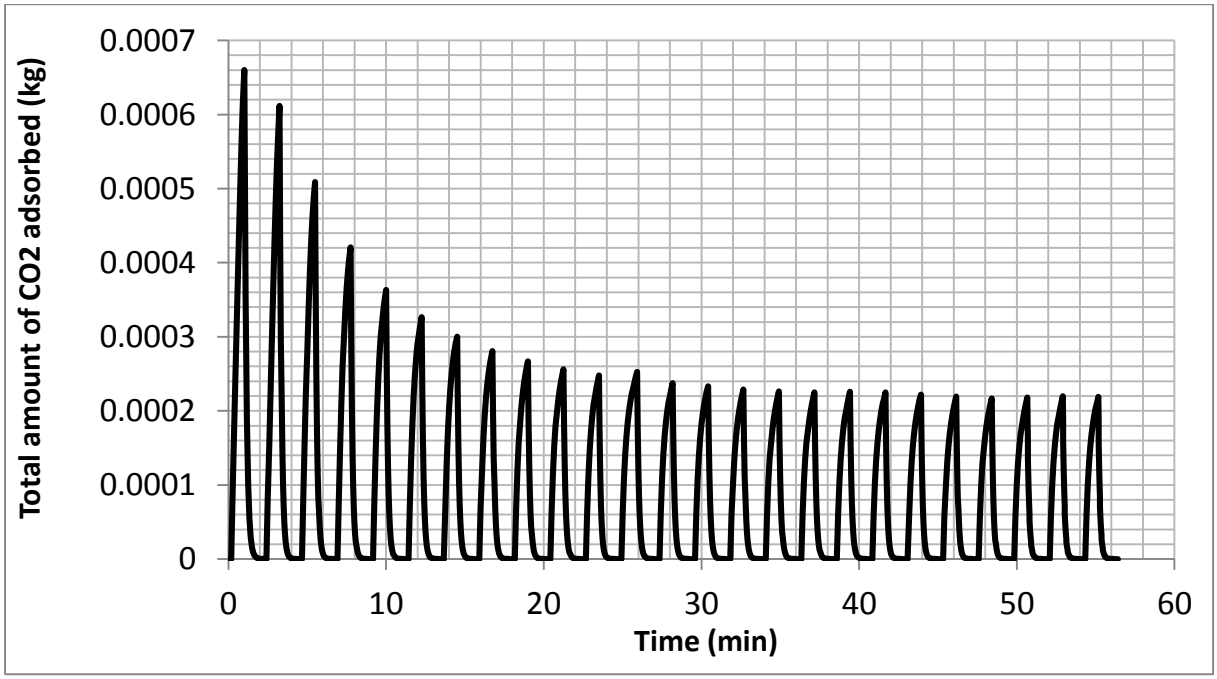

Figure 7.18: Total amount of CO_2 adsorbed in bed for 25 cycles of four-step PSA of CO_2 on Mg-MOF-74 from gas mixture of 15%CO_2, 85%N_2 at 373K for run 2.

CHAPTER 8

CONCLUSIONS AND RECOMMENDATIONS

In this thesis work, fixed bed adsorption of carbon dioxide on Mg-MOF-74, MOF-5, MOF-177 and Activated Carbon have been studied. The breakthrough behaviours of CO_2 on Mg-MOF-74 and Activated Carbon have been studied. Furthermore, CO_2 storage capacities of MOF-5, MOF-177 and Activated Carbon have been evaluated. Finally, the PSA behaviour of Mg-MOF-74 has been evaluated and the following conclusions and recommendations have been made:

8.1 Conclusions

For break through behaviour:

i. The breakthrough time and amount of CO_2 adsorbed at equilibrium decrease with temperature.

ii. The capacity of Mg-MOF-74 for carbon dioxide capture is far greater than that of activated carbon (about 10 times greater).

iii. For the removal of CO_2 from flue gas using Mg-MOF-74, lower temperature is recommended because it has longer breakthrough time [168] hence, a reduction in frequency of regeneration needed for reuse of material, lower amount of energy requirement for regeneration and consequently lesser operation cost.

iv. The temperature behaviour of the solid and gaseous phases for adiabatic adsorption systems are very similar, hence, equilibrium temperature for solid and gaseous phases can be assumed under adiabatic condition.

v. Pressure drop within adsorption column for an adiabatic system as described can be held constant.

It has also been shown that for CO_2 storage process:

vi. The amount of CO_2 stored in MOF-5 and MOF-177 at equilibrium increases pressure and bed size, however, it decreases with the increase in temperature.

vii. Increase in bed diameter has much greater effect on the amount of CO_2 stored compared to increase in bed length.

viii. Adsorption equilibrium constant decreases with the increase in pressure.

ix. The capacity of MOF-5 and MOF-177 for carbon dioxide storage is comparatively high with about 7.4g (MOF-5) in 50minutes and 11.3g (MOF-177) in 30minutes of stored CO_2 in bed size of 0.171m x 0.022m at feed gas temperature of 28^oC and pressure of 50bar.

x. The simulated Activated Carbon material also shows remarkable adsorptive storage capacity for CO_2 with about 13g of CO_2 stored in bed size of 0.171m x 0.022m in 50minutes at feed gas temperature of 28^oC and pressure of 50 bars.

xi. It has also been re-affirmed that temperature behaviours of the solid and gaseous phases for non-adiabatic adsorptive storage systems are very similar, hence, equilibrium temperature for solid and gaseous phases can be assumed under non-adiabatic condition. However, the behaviour of the column wall temperature is different.

xii. To avoid oscillation due to high pressure surge while filling at high pressure, the initial bed pressure can be set to the feed gas pressure as this shows no significant difference in the mass adsorbed for both cases.

xiii. Based on the gotten results, single site Langmuir isotherm model adequately describes the adsorption behaviour of CO_2 in MOF-5 and MOF-177.

Finally, it has been shown that for PSA process:

xiv. CO_2 recovery increases with increase in the duration of purge and pressurization. Pressure swing CO_2 recovery also increases with decrease in feed gas temperature.

xv. Sequestrated CO_2 purity reduces with decrease in temperature. This is true for cases of PSA and HR PSA.

xvi. The PSA process with heat regeneration is advantageous because it achieves equivalent of amount of CO_2 sequestration in lesser number of cycles compared to PSA without heat regeneration system.

xvii. CO_2 recovery with Mg-MOF-74 is low (far less than 90%) however; it gives high percentage of purity (above 98%) for the captured CO_2.

xviii. For carbon capture from flue gas feed of constant concentration (15% CO_2, 85% N_2), the rate of CO_2 recovery reduces with increase in the number of cycles for which the adsorbent has been used and the amount of CO_2 adsorbed in bed size of 0.2m x 0.02mmØ reduced from about 0.66g to about 0.22g at the end of twenty-five cycles however, the carbon capture capacity of Mg-MOF-74 remain relatively constant after about 19 cycles.

xix. Finally, it has been shown that for carbon capture from feed of constant concentration, the rate of CO_2 recovery reduces with increase in the number of cycles for which the adsorbent has been used, the carbon capture capacity of Mg-MOF-74 remain improves with increase in purged time, finally, the number of cycles to reach cyclic steady state reduced from 19 cycles to 15 cycles when the purge time was increased from 25s to 50s.

8.2 Recommendations

For further studies in the field of adsorptive carbon capture, it is recommended that:

i. Research be conducted on the amount of CO_2 concentration in the atmosphere of industrial cities within Saudi Arabia e.g. Jubail industrial city to further advise on the current status and need for carbon capture within the Kingdom.
ii. Experimental and numerical work be carried out on CO_2 capture and sequestration on typical flue gas sample from industrial areas within Saudi Arabia.
iii. Experimental work be carried out in order to get more data on isotherms and adsorption parameters of some popular potential carbon capture materials e.g. MOFs, zeolites etc. because of the inadequacy of such information in literatures.
iv. Research be conducted on how to improve CO_2 adsorption capacity of MOFs in the presence of water vapour as it is peculiar to real flue gas conditions
v. Research be conducted on how to improve CO_2 separation capacity of MOFs from multi component gas mixtures
vi. Research be conducted on ways to easily extract heat generated during CO_2 adsorption in order to improve adsorption capacities of potential adsorbents.
vii. Research be conducted on cost effective methods of preparation of MOF materials.

NOMENCLATURE

A_b	Area of bed outlet (m^2)
b_j	Equilibrium adsorption constant of component j (Pa^{-1})
$b_{o,j}$	Adsorption constant of component j at infinite dilution (Pa^{-1})
$C_{inlet,j}$	Feed concentration of component j (mol/m^3)
C_j	Gas phase concentration of component j ($mol\ m^3$)
$C_{v,g}$	Specific heat at constant volume for gas mixture ($J\ Kg^{-1}\ K^{-1}$)
$C_{p,g}$	Specific heat at constant pressure for gas mixture ($J\ Kg^{-1}\ K^{-1}$)
C_s	Specific heat capacity of solid adsorbent ($J\ Kg^{-1}\ K^{-1}$)
C_{stor}	Specific heat capacity of heat storage material ($J\ Kg^{-1}\ K^{-1}$)
$C_{p,w}$	Specific heat capacity of adsorption column wall ($J\ Kg^{-1}\ K^{-1}$)
D_{ax}	Axial dispersion coefficient (m^2/s)
d_p	Adsorbent particle diameter (m)
d_{int}	Adsorption bed diameter (m)
F_j	Molar flow rate of component j (mol/s)
$-\Delta H_j$	Enthalpy of component j in gas mixture (kJ/mol)
h_f	Film heat transfer coefficient between the gas and solid adsorbent ($Wm^{-2}K^{-1}$)
h_w	Internal convective heat transfer coefficient between the gas and the column wall ($Wm^{-2}K^{-1}$)
$K_{eq,j}$	Equilibrium adsorption constant of component j (Pa^{-1})
$K_{L,j}$	Overall mass transfer coefficient of component j (s^{-1})
$K_{o,j}$	Adsorption constant of component j at infinite dilution (Pa^{-1})
l	Column wall thickness (m)
n	Polytropic index
P	Total pressure of gas mixture (Pa)
P_j	Partial pressure of component j in gas mixture (Pa)
P_{feed}	Feed pressure (Pa)
Q_F	Feed volumetric flow rate of gas mixture (m^3/s)
$\bar{q}_j$	Average amount of adsorbed of component j (mol/kg)
q^*_j	The amount of component j adsorbed at equilibrium (mol/kg)
$q_{m,j}$	Parameter for amount of component j adsorbed in adsorbent at equilibrium (mol/kg)
t	Time of adsorption / desorption (s)
t_{st}	Stoichiometric time (s)
t_{feed}	Feed time (s)
t_{purge}	Feed time (s)
$t_{blow\ down}$	Blow down time (s)
T_s	Temperature of solid adsorbent (K)
T_w	Temperature of column wall (K)
T_g	Gas mixture temperature (K)
u	Superficial velocity of the gas mixture (m/s)

y_j	Mole fraction of component j in gas mixture

Greek Letters

α_w	The ratio of the internal surface area to the volume of adsorption column wall density (m^{-1})
α_{wl}	The ratio of the algorithm mean surface area of the column shell to the volume of the column wall (m^{-1})
ε	Adsorption bed void fraction
ε_{stor}	Regeneration packed bed void fraction
λ_l	Thermal conductivity of gas of the gas mixture in axial direction ($Wm^{-1}K^{-1}$)
μ_g	Dynamic viscosity of gas mixture (Pa s^{-1})
ρ_g	Gas mixture density (kg/m^3)
ρ_p	Adsorbent particle density (kg/m^3)
ρ_{stor}	Heat storage material density (kg/m^3)
ρ_w	Adsorption column wall density (kg/m^3)

REFERENCES

[1] T. Guardian.com, "antarctic-ship-stranding-delights-climate-change-sceptics @ www.theguardian.com." 2014.

[2] United States Environmental Protection Agency (EPA), 2014.

http://www.epa.gov/climatechange/

[3] D. M. D'Alessandro and T. McDonald, "Toward carbon dioxide capture using nanoporous materials," *Pure Appl. Chem.*, vol. 83, no. 1, pp. 57–66, Nov. 2011.

[4] G. C. and E. Project, "Global Climate & Energy Project An Assessment of Carbon Capture Technology and Research Opportunities," 2005.

[5] E. U. Press, "Environmental_impact_of_aviation @ en.wikipedia.org," *Wikipedia*. 2008.

[6] H. Herzog, Jerry Meldon and Alan Hatton, *"Advanced Post-Combustion*

CO_2 Capture," Clean Air Task Force, 2009.
http://www.catf.us/resources/publications/view/205

[7] J.-R. Li, Y. Ma, M. C. McCarthy, J. Sculley, J. Yu, H.-K. Jeong, P. B. Balbuena, and H.-C. Zhou, "Carbon dioxide capture-related gas adsorption and separation in metal-organic frameworks," *Coord. Chem. Rev.*, vol. 255, no. 15–16, pp. 1791–1823, Aug. 2011.

[8] Wikipedia,2013 "Adsorption @ en.wikipedia.org." 2013.

[9] P. Broutin, H. Kvamsdal, C. La, P. Van Os, and L. Robinson, "OCTAVIUS: A FP7 Project Demonstrating CO_2 Capture Technologies," *Energy Procedia*, vol. 00, 2013.

[10] K. Stéphenne, "Start-Up of World ' s First Commercial Post-Combustion Coal Fired CCS Project : Contribution of Shell Cansolv to SaskPower Boundary Dam ICCS Project," *Energy Procedia*, vol. 00, p. 000, 2013.

[11] T. C. Drage, C. E. Snape, L. a. Stevens, J. Wood, J. Wang, A. I. Cooper, R. Dawson, X. Guo, C. Satterley, and R. Irons, "Materials challenges for the development of solid sorbents for post-combustion carbon capture," *J. Mater. Chem.*, vol. 22, no. 7, p. 2815, 2012.

[12] D. G. Chapel and C. L. Mariz, "Recovery of CO_2 from Flue Gases : Commercial Trends Recovery of CO_2 from Flue Gases : Commercial Trends," Saskatoon, Saskatchewan, Canada, 1999.

[13] M. Songolzadeh, M. T. Ravanchi, and M. Soleimani, "Carbon Dioxide Capture and Storage : A General Review on Adsorbents," *World Acad. Sci. Eng. Technol.*, pp. 225–232, 2012.

[14] C.-H. Yu, "A Review of CO_2 Capture by Absorption and Adsorption," *Aerosol Air Qual. Res.*, pp. 745–769, 2012.

[15] A. V. Rayer, A. Henni, and P. Tontiwachwuthikul, "High pressure physical solubility of carbon dioxide (CO_2) in mixed polyethylene glycol dimethyl ethers (Genosorb 1753)," *Can. J. Chem. Eng.*, vol. 90, no. 3, pp. 576–583, Jun. 2012.

[16] A. A. Olajire, "CO_2 capture and separation technologies for end-of-pipe applications – A review," *Energy*, vol. 35, no. 6, pp. 2610–2628, Jun. 2010.

[17] S. Gondal, N. Asif, H. F. Svendsen, and H. Knuutila, "Kinetics of the absorption of carbon dioxide into aqueous hydroxides of lithium, sodium and potassium and blends of hydroxides and carbonates," *Chem. Eng. Sci.*, vol. 123, pp. 487–499, Feb. 2015.

[18] A. A. Khan, G. N. Halder, and a. K. Saha, "Carbon dioxide capture characteristics from flue gas using aqueous 2-amino-2-methyl-1-propanol (AMP) and monoethanolamine (MEA) solutions in packed bed absorption and regeneration columns," *Int. J. Greenh. Gas Control*, vol. 32, pp. 15–23, Jan. 2015.

[19] N. Ramachandran, A. Aboudheir, R. Idem, and P. Tontiwachwuthikul, "Kinetics of the Absorption of CO_2 into Mixed Aqueous Loaded Solutions of Monoethanolamine and Methyldiethanolamine," *Ind. Eng. Chem. Res.*, vol. 45, no. 8, pp. 2608–2616, Apr. 2006.

[20] S. T. and A. M. S. M.K. Wong, Ghulam Murshid, M.A. Bustam, "Solubility of Carbon Dioxide in in Piperazine-activated methyldiethamolamine and 2-Amine-2-Methyl-1-Propanol," *J. Appl. Sci.*, vol. 14, no. 22, pp. 3114–3117, 2014.

[21] S. A. Freeman, R. Dugas, D. H. Van Wagener, T. Nguyen, and G. T. Rochelle, "Carbon dioxide capture with concentrated, aqueous piperazine," *Int. J. Greenh. Gas Control*, vol. 4, no. 2, pp. 119–124, Mar. 2010.

[22] G. S. Hwang, H. M. Stowe, E. Paek, and D. Manogaran, "Reaction mechanisms of aqueous monoethanolamine with carbon dioxide: a combined quantum chemical and molecular dynamics study.," *Phys. Chem. Chem. Phys.*, vol. 17, no. 2, pp. 831–839, Jan. 2015.

[23] A. Sanna, F. Vega, B. Navarrete, and M. M. Maroto-Valer, "Accelerated MEA Degradation Study in Hybrid CO_2 Capture Systems," *Energy Procedia*, vol. 63, no. 0, pp. 745–749, 2014.

[24] H. Zhai and E. S. Rubin, "Systems Analysis of Ionic Liquids for Post-combustion CO_2 Capture at Coal-fired Power Plants," *Energy Procedia*, vol. 00, p. 000, 2014.

[25] A. S. Kovvali and K. K. Sirkar, "Carbon Dioxide Separation with Novel Solvents as Liquid Membranes," *Ind. Eng. Chem. Res.*, vol. 41, no. 973, pp. 2287–2295, 2002.

[26] T. Supap, R. Idem, P. Tontiwachwuthikul, and C. Saiwan, "Investigation of degradation inhibitors on CO_2 capture process," *Energy Procedia*, vol. 4, pp. 583–590, 2011.

[27] F. A. Tobiesen and H. F. Svendsen, "Study of a Modified Amine-Based Regeneration Unit," *Ind. Eng. Chem. Res.*, vol. 45, no. 8, pp. 2489–2496, Apr. 2006.

[28] M. Wang, a. Lawal, P. Stephenson, J. Sidders, and C. Ramshaw, "Post-combustion CO_2 capture with chemical absorption: A state-of-the-art review," *Chem. Eng. Res. Des.*, vol. 89, no. 9, pp. 1609–1624, Sep. 2011.

[29] X. Wu, Y. Yu, Z. Qin, and Z. Zhang, "The Advances of Post-combustion CO_2 Capture with Chemical Solvents: Review and Guidelines," *Energy Procedia*, vol. 63, pp. 1339–1346, 2014.

[30] L.-L. Zhang, J.-X. Wang, Y. Xiang, X.-F. Zeng, and J.-F. Chen, "Absorption of Carbon Dioxide with Ionic Liquid in a Rotating Packed Bed Contactor: Mass Transfer Study," *Ind. Eng. Chem. Res.*, vol. 50, no. 11, pp. 6957–6964, Jun. 2011.

[31] J.-L. Kang, Z.-J. Luo, J.-L. Liu, K. Sun, D. S.-H. Wong, S.-S. Jang, C.-S. Tan, and J.-F. Shen, "Experiment and Modeling Studies on Absorption of CO2 by Dilute Ammonia in Rotating Packed Bed," *Energy Procedia*, vol. 63, pp. 1308–1313, 2014.

[32] C.-H. Yu and C.-S. Tan, "CO2 Capture by Aqueous Solution Containing Mixed Alkanolamines and Diethylene Glycol in a Rotating Packed Bed," *Energy Procedia*, vol. 63, pp. 758–764, 2014.

[33] T. K. Carlisle, J. E. Bara, A. L. Lafrate, D. L. Gin, and R. D. Noble, "Main-chain imidazolium polymer membranes for CO_2 separations: An initial study of a new ionic liquid-inspired platform," *J. Memb. Sci.*, vol. 359, no. 1–2, pp. 37–43, Sep. 2010.

[34] S. Shishatskiy, J. R. Pauls, S. P. Nunes, and K.-V. Peinemann, "Quaternary ammonium membrane materials for CO_2 separation," *J. Memb. Sci.*, vol. 359, no. 1–2, pp. 44–53, Sep. 2010.

[35] S. Wang and X. Han, "Application of Polymeric Membrane in CO_2 Capture from Post Combustion," *Adv. Chem. Eng. Sci.*, vol. 2012, no. July, pp. 336–341, 2012.

[36] A. Darmawan, J. Motuzas, S. Smart, A. Julbe, and J. C. Diniz Da Costa, "Binary iron cobalt oxide silica membrane for gas separation," *J. Memb. Sci.*, vol. 474, pp. 32–38, Jan. 2015.

[37] Y. C. Hudiono, T. K. Carlisle, J. E. Bara, Y. Zhang, D. L. Gin, and R. D. Noble, "A three-component mixed-matrix membrane with enhanced CO_2 separation properties based on zeolites and ionic liquid materials," *J. Memb. Sci.*, vol. 350, no. 1–2, pp. 117–123, Mar. 2010.

[38] N. Du, H. B. Park, M. M. Dal-Cin, and M. D. Guiver, "Advances in high permeability polymeric membrane materials for CO_2 separations," *Energy Environ. Sci.*, vol. 5, no. 6, p. 7306, 2012.

[39] M. Li, X. Jiang, and G. He, “Application of membrane separation technology in postcombustion carbon dioxide capture process,” *Front. Chem. Sci. Eng.*, vol. 8, no. 2, pp. 233–239, Jan. 2014.

[40] E. Favre, “Carbon dioxide recovery from post-combustion processes: Can gas permeation membranes compete with absorption?,” *J. Memb. Sci.*, vol. 294, no. 1–2, pp. 50–59, May 2007.

[41] L. Zhao, E. Riensche, L. Blum, and D. Stolten, “How gas separation membrane competes with chemical absorption in postcombustion capture,” *Energy Procedia*, vol. 4, pp. 629–636, 2011.

[42] T. C. Merkel, H. Lin, X. Wei, and R. Baker, “Power plant post-combustion carbon dioxide capture: An opportunity for membranes,” *J. Memb. Sci.*, vol. 359, no. 1–2, pp. 126–139, Sep. 2010.

[43] A. Brunetti, F. Scura, G. Barbieri, and E. Drioli, “Membrane technologies for CO_2 separation,” *J. Memb. Sci.*, vol. 359, no. 1–2, pp. 115–125, Sep. 2010.

[44] X. Zhang, X. He, and T. Gundersen, “Post-combustion Carbon Capture with a Gas Separation Membrane: Parametric Study, Capture Cost, and Exergy Analysis,” *Energy & Fuels*, vol. 27, no. 8, pp. 4137–4149, Aug. 2013.

[45] R. Bounaceur, N. Lape, D. Roizard, C. Vallieres, and E. Favre, “Membrane processes for post-combustion carbon dioxide capture: A parametric study,” *Energy*, vol. 31, no. 14, pp. 2556–2570, Nov. 2006.

[46] M. Cecopierigomez, J. Palaciosalquisira, and J. Dominguez, “On the limits of gas separation in CO_2/CH_4, N_2/CH_4 and CO_2/N_2 binary mixtures using polyimide membranes,” *J. Memb. Sci.*, vol. 293, no. 1–2, pp. 53–65, Apr. 2007.

[47] S. R. Reijerkerk, A. Arun, R. J. Gaymans, K. Nijmeijer, and M. Wessling, “Tuning of mass transport properties of multi-block copolymers for CO_2 capture applications,” *J. Memb. Sci.*, vol. 359, no. 1–2, pp. 54–63, Sep. 2010.

[48] L. M. Robeson, “The upper bound revisited,” *J. Memb. Sci.*, vol. 320, no. 1–2, pp. 390–400, Jul. 2008.

[49] N. Bryan, E. Lasseuguette, M. van Dalen, N. Permogorov, A. Amieiro, S. Brandani, and M.-C. Ferrari, “Development of Mixed Matrix Membranes Containing Zeolites for Post-combustion Carbon Capture.,” *Energy Procedia*, vol. 63, pp. 160–166, 2014.

[50] H. B. Park, C. H. Jung, Y. M. Lee, A. J. Hill, and S. J. Pas, “Polymers with Cavity Tuned for Fast Selective Transport of Small Molecules and Ions,” *Science (80-.).*, vol. 318, no. October, pp. 254–259, 2007.

[51] H. B. Park, S. H. Han, C. H. Jung, Y. M. Lee, and A. J. Hill, “Thermally rearranged (TR) polymer membranes for CO2 separation,” *J. Memb. Sci.*, vol. 359, no. 1–2, pp. 11–24, Sep. 2010.

[52] J. I. Choi, C. H. Jung, S. H. Han, H. B. Park, and Y. M. Lee, "Thermally rearranged (TR) poly(benzoxazole-co-pyrrolone) membranes tuned for high gas permeability and selectivity," *J. Memb. Sci.*, vol. 349, no. 1–2, pp. 358–368, Mar. 2010.

[53] A. M. Salih, C. Yi, H. Peng, B. Yang, L. Yin, and W. Wang, "Interfacially polymerized polyetheramine thin film composite membranes with PDMS inter-layer for CO_2 separation," *J. Memb. Sci.*, vol. 472, pp. 110–118, Dec. 2014.

[54] D. Wu, Y. Huang, S. Yu, D. Lawless, and X. Feng, "Thin film composite nanofiltration membranes assembled layer-by-layer via interfacial polymerization from polyethylenimine and trimesoyl chloride," *J. Memb. Sci.*, vol. 472, pp. 141–153, Dec. 2014.

[55] H. Maghsoudi and M. Soltanieh, "Simultaneous separation of H_2S and CO_2 from CH_4 by a high silica CHA-type zeolite membrane," *J. Memb. Sci.*, vol. 470, pp. 159–165, Nov. 2014.

[56] X. He, T.-J. Kim, and M.-B. Hägg, "Hybrid fixed-site-carrier membranes for CO_2 removal from high pressure natural gas: Membrane optimization and process condition investigation," *J. Memb. Sci.*, vol. 470, pp. 266–274, Nov. 2014.

[57] L. Zhao, E. Riensche, L. Blum, and D. Stolten, "Multi-stage gas separation membrane processes used in post-combustion capture: Energetic and economic analyses," *J. Memb. Sci.*, vol. 359, no. 1–2, pp. 160–172, Sep. 2010.

[58] C. P. Cabello, G. Berlier, G. Magnacca, P. Rumori, and G. T. Palomino, "Enhanced CO_2 adsorption capacity of amine-functionalized MIL-100(Cr) metal–organic frameworks," *CrystEngComm*, vol. 17, no. 2, pp. 430–437, Sep. 2014.

[59] D. Y. C. Leung, G. Caramanna, and M. M. Maroto-Valer, "An overview of current status of carbon dioxide capture and storage technologies," *Renew. Sustain. Energy Rev.*, vol. 39, pp. 426–443, Nov. 2014.

[60] T. Nakamura, "Recovery and Sequestration of CO_2 from Stationary Combustion Systems by Photosynthesis of Microalgae Quarterly Technical Progress Report # 9 Reporting Period Start Date : 1 October 2002 Reporting Period End Date : 31 December 2002 Prepared by National En," 2003.

[61] M. K. Lam, K. T. Lee, and A. R. Mohamed, "Current status and challenges on microalgae-based carbon capture," *Int. J. Greenh. Gas Control*, vol. 10, pp. 456–469, Sep. 2012.

[62] J. C. M. Pires, M. C. M. Alvim-Ferraz, F. G. Martins, and M. Simões, "Carbon dioxide capture from flue gases using microalgae: Engineering aspects and biorefinery concept," *Renew. Sustain. Energy Rev.*, vol. 16, no. 5, pp. 3043–3053, Jun. 2012.

[63] Y. Shen, "Carbon dioxide bio-fixation and wastewater treatment via algae photochemical synthesis for biofuels production," *R. Soc. Chem. Adv.*, vol. 4, no. 91, pp. 49672–49722, Sep. 2014.

[64] J.-R. Li, J. Sculley, and H.-C. Zhou, "Metal-organic frameworks for separations.," *Chem. Rev.*, vol. 112, no. 2, pp. 869–932, Feb. 2012.

[65] S. Kumar and S. K. Saxena, "A comparative study of CO_2 sorption properties for different oxides," *Mater. Renew. Sustain. Energy*, vol. 3, no. 3, p. 30, May 2014.

[66] M. Songolzadeh, M. T. Ravanchi, and M. Soleimani, "Carbon Dioxide Capture and Storage : A General Review on Adsorbents," *World Acad. Sci. Technol.*, vol. 6, pp. 213–220, 2012.

[67] S. Ma, J. M. Simmons, D. Yuan, J.-R. Li, W. Weng, D.-J. Liu, and H.-C. Zhou, "A nanotubular metal-organic framework with permanent porosity: structure analysis and gas sorption studies.," *Chem. Commun. (Camb).*, vol. 1, no. 27, pp. 4049–51, Jul. 2009.

[68] F. J. Uribe-romo, C. B. Knobler, M. O. Keeffe, and O. M. Yaghi, "Synthesis, Structure and Carbon Dioxide Capture Properties of Zeolitic Imidazolate Frameworks," *Acc. Chem. Res.*, vol. 43, no. 1, 2010.

[69] H. Liu, B. Liu, L.-C. Lin, G. Chen, Y. Wu, J. Wang, X. Gao, Y. Lv, Y. Pan, X. Zhang, X. Zhang, L. Yang, C. Sun, B. Smit, and W. Wang, "A hybrid absorption-adsorption method to efficiently capture carbon.," *Nat. Commun.*, vol. 5, p. 5147, Jan. 2014.

[70] T. Düren, "How does the pore morphology influence the adsorption performance of metal-organic frameworks ? A molecular simulation study of methane and ethane adsorption in Zn-MOFs," in *International Zeolite Conference*, 2007, vol. i, pp. 2042–2047.

[71] CCDC, "SupportSolution @ www.ccdc.cam.ac.uk.", Dec. 2014.

[72] R. J. Kuppler, D. J. Timmons, Q.-R. Fang, J.-R. Li, T. a. Makal, M. D. Young, D. Yuan, D. Zhao, W. Zhuang, and H.-C. Zhou, "Potential applications of metal-organic frameworks," *Coord. Chem. Rev.*, vol. 253, no. 23–24, pp. 3042–3066, Dec. 2009.

[73] H. Lu, "Interfacial Synthesis of Metal-organic Frameworks," McMaster University, 2012.

[74] A. Carné-Sánchez, I. Imaz, M. Cano-Sarabia, and D. Maspoch, "A spray-drying strategy for synthesis of nanoscale metal-organic frameworks and their assembly into hollow superstructures.," *Nat. Chem.*, vol. 5, no. 3, pp. 203–11, Mar. 2013.

[75] N. Campagnol, T. Van Assche, T. Boudewijns, J. Denayer, K. Binnemans, D. De Vos, and J. Fransaer, "High pressure, high temperature electrochemical synthesis of metal–organic frameworks: films of MIL-100 (Fe) and HKUST-1 in different morphologies," *J. Mater. Chem. A*, vol. 1, no. 19, p. 5827, 2013.

[76] M. Li and M. Dinc, "Reductive electrosynthesis of crystalline metal-organic frameworks" *American Chemical Society (MIT Open Access Articles)*, 2014.

[77] U. D. of Energy, pp. 1 - 5, 2007.

[78] P. Monika, "High Throughput assisted Investigation on Lanthanide (III) Tetrakisphosphonates," Ludwig-Maximilans-Universitat Munchen, 2009.

[79] C.-M. Lu, J. Liu, K. Xiao, and A. T. Harris, "Microwave enhanced synthesis of MOF-5 and its CO_2 capture ability at moderate temperatures across multiple capture and release cycles," *Chem. Eng. J.*, vol. 156, no. 2, pp. 465–470, Jan. 2010.

[80] O. V Kharissova, B. I. Kharisov, and U. O. Méndez, "Microwave-assisted Synthesis of Coordination and Organometallic Compounds," *INTECH*, 2009.

[81] D. Plaines, D. Levan, S. Brandani, R. Snurr, A. Matzger, and A. Arbor, "Carbon Dioxide Removal from Flue Gas Using Microporous Metal Organic Frameworks Final Technical Report, April 2007.

[82] D. Zhao, D. Yuan, A. Yakovenko, and H.-C. Zhou, "A NbO-type metal-organic framework derived from a polyyne-coupled di-isophthalate linker formed in situ.," *Chem. Commun. (Camb).*, vol. 46, no. 23, pp. 4196–8, Jun. 2010.

[83] L.-H. Xie and M. P. Suh, "Flexible metal-organic framework with hydrophobic pores.," *Chemistry*, vol. 17, no. 49, pp. 13653–6, Dec. 2011.

[84] D. Yuan, D. Zhao, and H.-C. Zhou, "Pressure-responsive curvature change of a 'rigid' geodesic ligand in a (3,24)-connected mesoporous metal-organic framework.," *Inorg. Chem.*, vol. 50, no. 21, pp. 10528–30, Nov. 2011.

[85] F.-X. Coudert, "The osmotic framework adsorbed solution theory: predicting mixture coadsorption in flexible nanoporous materials.," *Phys. Chem. Chem. Phys.*, vol. 12, no. 36, pp. 10904–13, Sep. 2010.

[86] D. Yuan, R. B. Getman, Z. Wei, R. Q. Snurr, and H.-C. Zhou, "Stepwise adsorption in a mesoporous metal-organic framework: experimental and computational analysis.," *Chem. Commun. (Camb).*, vol. 48, no. 27, pp. 3297–9, Apr. 2012.

[87] D. Zhao, D. Yuan, R. Krishna, J. M. van Baten, and H.-C. Zhou, "Thermosensitive gating effect and selective gas adsorption in a porous coordination nanocage.," *Chem. Commun. (Camb).*, vol. 46, no. 39, pp. 7352–4, Oct. 2010.

[88] C. Mellot-draznieks, A. H. Fuchs, and A. Boutin, "Prediction of Breathing and Gate-Opening Transitions Upon Binary Mixture Adsorption in Metal - Organic Frameworks Franc," *JACS Commun.*, pp. 11329–11331, 2009.

[89] J. Nakhla, "metal-organic-frameworks @ www.sigmaaldrich.com." Aldrich Chem files, 2009.

[90] K. Leus, "The Development of Vanadium and Titanium Containing Metal Organic Frameworks for Applications in Adsorption and Heterogeneous Catalysis Karen Leus Department of Inorganic and Physical Chemistry," UNIVERSITEIT GANET, 2012.

[91] N. A. Khan, Z. Hasan, and S. H. Jhung, "Adsorptive removal of hazardous materials using metal-organic frameworks (MOFs): a review.," *J. Hazard. Mater.*, vol. 244–245, pp. 444–56, Jan. 2013.

[92] J. A. Hurd, "18100901 @ www.rsc.org." Chemistry World, 2009.

[93] K. W. Dawson, "Modification of Proton Conducting Metal-Organic Frameworks for Improved Performance in Fuel Cell Application.," University of Calgary, 2013.

[94] L. E. Kreno, K. Leong, O. K. Farha, M. Allendorf, R. P. Van Duyne, and J. T. Hupp, "Metal-organic framework materials as chemical sensors.," *Chem. Rev.*, vol. 112, no. 2, pp. 1105–25, Feb. 2012.

[95] S. N. Partha Mahata, "4456 @ journal.library.iisc.ernet.in." 2014.

[96] C. P. Canlas, J. Lu, N. A. Ray, N. A. Grosso-giordano, S. Lee, J. W. Elam, R. E. Winans, R. P. Van Duyne, P. C. Stair, and J. M. Notestein, "Shape-selective sieving layers on an oxide catalyst surface," *Nat. Chem.*, vol. 4, no. October, 2012.

[97] R. C. Huxford, J. Della Rocca, and W. Lin, "Metal-Organic Framework as potential drug carrier," *Natl. Inst. Heal.*, vol. 14, no. 2, pp. 262–268, 2011.

[98] M. Technologies, "emerging-applications @ www.moftechnologies.com." MOF Technologies, 2014.

[99] P. D. C. Dietzel, V. Besikiotis, and R. Blom, "Application of metal–organic frameworks with coordinatively unsaturated metal sites in storage and separation of methane and carbon dioxide," *J. Mater. Chem.*, vol. 19, no. 39, p. 7362, 2009.

[100] T. Grant Glover, G. W. Peterson, B. J. Schindler, D. Britt, and O. Yaghi, "MOF-74 building unit has a direct impact on toxic gas adsorption," *Chem. Eng. Sci.*, vol. 66, no. 2, pp. 163–170, Jan. 2011.

[101] Z. Bao, L. Yu, Q. Ren, X. Lu, and S. Deng, "Adsorption of CO_2 and CH_4 on a magnesium-based metal organic framework.," *J. Colloid Interface Sci.*, vol. 353, no. 2, pp. 549–56, Jan. 2011.

[102] D. Britt, H. Furukawa, B. Wang, T. G. Glover, and O. M. Yaghi, "Highly efficient separation of carbon dioxide by a metal-organic framework replete with open metal sites.," *Proc. Natl. Acad. Sci. U. S. A.*, vol. 106, no. 49, pp. 20637–40, Dec. 2009.

[103] D.-A. Yang, H.-Y. Cho, J. Kim, S.-T. Yang, and W.-S. Ahn, "CO_2 capture and conversion using Mg-MOF-74 prepared by a sonochemical method," *Energy Environ. Sci.*, vol. 5, no. 4, p. 6465, 2012.

[104] D. Britt, D. Tranchemontagne, and O. M. Yaghi, "Metal-organic frameworks with high capacity and selectivity for harmful gases," *PNAS*, vol. 199, 2008.

[105] D. J. Tranchemontagne, J. R. Hunt, and O. M. Yaghi, “Room temperature synthesis of metal-organic frameworks: MOF-5, MOF-74, MOF-177, MOF-199, and IRMOF-0,” *Tetrahedron*, vol. 64, no. 36, pp. 8553–8557, Sep. 2008.

[106] A. R. Millward and O. M. Yaghi, “Metal-organic frameworks with exceptionally high capacity for storage of carbon dioxide at room temperature.,” *J. Am. Chem. Soc.*, vol. 127, no. 51, pp. 17998–9, Dec. 2005.

[107] Z. Zhao, Z. Li, and Y. S. Lin, “Adsorption and Diffusion of Carbon Dioxide on Metal - Organic Framework (MOF-5),” *Ind. Eng. Chem. Res.*, vol. 48, pp. 10015–10020, 2009.

[108] D. Saha and Z. Bao, “Adsorption of CO_2, CH_4, N_2O and N_2 on MOF-5 , MOF-177 , and Zeolite 5A,” *Environ. Sci. Technol.*, vol. 44, no. 5, pp. 1820–1826, 2010.

[109] J. Y. Jung, F. Karadas, S. Zulfiqar, E. Deniz, S. Aparicio, M. Atilhan, C. T. Yavuz, and S. M. Han, “Limitations and high pressure behavior of MOF-5 for CO_2 capture.,” *Phys. Chem. Chem. Phys.*, vol. 15, no. 34, pp. 14319–27, Sep. 2013.

[110] J. A. Mason, K. Sumida, Z. R. Herm, R. Krishna, and J. R. Long, “Evaluating metal–organic frameworks for post-combustion carbon dioxide capture via temperature swing adsorption,” *Energy Environ. Sci.*, vol. 4, no. 8, p. 3030, 2011.

[111] H. Furukawa, M. a. Miller, and O. M. Yaghi, “Independent verification of the saturation hydrogen uptake in MOF-177 and establishment of a benchmark for hydrogen adsorption in metal–organic frameworks,” *J. Mater. Chem.*, vol. 17, no. 30, p. 3197, 2007.

[112] G. W. Peterson, G. Wagner, and C. J. Karwacki, “ECBC-TR-659 Evaluation of mof-74, mof-177, and zif-8 for the removal of toxic industrial chemicals,” 2008.

[113] S. Xiang, Y. He, Z. Zhang, H. Wu, W. Zhou, R. Krishna, and B. Chen, “Microporous metal-organic framework with potential for carbon dioxide capture at ambient conditions.,” *Nat. Commun.*, vol. 3, p. 954, Jan. 2012.

[114] R. F. Bruinsma, P. G. De Gennes, J. B. Freund, and D. Levine, “A route to high surface area , porosity and inclusion of large molecules in crystals,” *Nature*, vol. 427, no. February, pp. 523–527, 2004.

[115] M. T. Ho, G. W. Allinson, and D. E. Wiley, “Reducing the Cost of CO_2 Capture from Flue Gases Using Pressure Swing Adsorption,” *Indutrial Eng. Chem. Res.*, vol. 47, no. 14, pp. 4883–4890, 2008.

[116] T. L. P. Dantas, F. M. T. Luna, I. J. S. Jr, A. E. B. Torres, D. C. S. De Azevedo, A. E. Rodrigues, and R. F. P. M. Moreira, “Modeling of the fixed-bed adsorption of carbon dioxide and a carbon dioxide- nitrogen mixture on zeolite 13X,” *Brazilian J. Chem. Eng.*, vol. 28, no. 03, pp. 533–544, 2011.

[117] T. L. P. Dantas, F. M. T. Luna, I. J. Silva, D. C. S. de Azevedo, C. a. Grande, A. E. Rodrigues, and R. F. P. M. Moreira, “Carbon dioxide–nitrogen separation

through adsorption on activated carbon in a fixed bed," *Chem. Eng. J.*, vol. 169, no. 1–3, pp. 11–19, May 2011.

[118] S. Mohsen, "Mathematical Modeling of Single and Multi-Component Adsorption Fixed Beds to Rigorously Predict the Mass Transfer Zone and Breakthrough Curves," *Iran. J. Chem. Chem. Eng.*, vol. 28, no. 3, pp. 25–44, 2009.

[119] M. S. Shafeeyan, W. M. A. Wan Daud, and A. Shamiri, "A review of mathematical modeling of fixed-bed columns for carbon dioxide adsorption," *Chem. Eng. Res. Des.*, no. August, Aug. 2013.

[120] M.-B. Kim, Y.-S. Bae, D.-K. Choi, and C.-H. Lee, "Kinetic Separation of Landfill Gas by a Two-Bed Pressure Swing Adsorption Process Packed with Carbon Molecular Sieve: Nonisothermal Operation," *Ind. Eng. Chem. Res.*, vol. 45, no. 14, pp. 5050–5058, Jul. 2006.

[121] M. Clausse, J. Bonjour, and F. Meunier, "Adsorption of gas mixtures in TSA adsorbers under various heat removal conditions," *Chem. Eng. Sci.*, vol. 59, no. 17, pp. 3657–3670, Sep. 2004.

[122] C.-T. Chou and C.-Y. Chen, "Carbon dioxide recovery by vacuum swing adsorption," *Sep. Purif. Technol.*, vol. 39, no. 1–2, pp. 51–65, Oct. 2004.

[123] R. P. P. L. Ribeiro, C. A. Grande, and A. E. Rodrigues, "Activated carbon honeycomb monolith – Zeolite 13X hybrid system to capture CO2 from flue gases employing Electric Swing Adsorption," *Chem. Eng. Sci.*, vol. 104, pp. 304–318, Dec. 2013.

[125] CRC for greenhouse gas technologies, "capture images", 2015.

http://www.co2crc.com.au/imagelibrary3/capture.php.

[126] C. A. Grande, "Advances in Pressure Swing Adsorption for Gas Separation," *ISRN Chem. Eng.*, vol. 2012, pp. 1–13, 2012.

[127] Charles W. Skarstrom, "Methods and apparatus for fractionating gas mixture by adsorption," U.S. patent 2, 944, 627, 1960627.

[128] J. Yang, M. Park, J. Chang, S. Ko, and C. Lee, "EFFECTS OF PRESSURE DROP IN A PSA PROCESS," *Korean J. Chem. Eng.*, vol. 15, no. 2, pp. 211–216, 1998.

[129] J. S. Ehsan and M. Masoud, "Pilot-Scale Experiments for Nitrogen Separation from Air by Pressure Swing Adsorption," *South African J. Chem. Eng.*, vol. 19, no. 2, pp. 42–56, 2014.

[130] Osaks Gas chemicals: "Gas separation by Pressure Swing Adsorption (PSA)",

2013. www.jechem.co.jp.

[131] T. L. P. Dantas and A. E. Rodrigues, “Separation of Carbon Dioxide from Flue Gas Using Adsorption on Porous Solids,” in *Greenhouse Gases - Capturing, Utilization and Reduction*, 2011.

[132] W. D. Marsh, F. S. Pramuk, R. C. Hoke, and C.W. Skarstrom “Pressure equalization depressurising in heatless adsorption,” U.S. patent no. 3, 142, 547, 1964.

[132] C. A. Grande, S. Cavenati, and A. E. Rodrigues, “Pressure swing adsorption for carbon dioxide sequestration,” in *2nd Conference on Chemical Engineering and 4th Mercosur Congress on Process Systems Engineering2*, 2005, pp. 1–10.

[134] R. Ramachandran, L. H. Dao, and B. Brooks, “Method of producing unsaturated hydrocarbons and separating the same from saturated hydrocarbons,” U.S. patent 5, 365, 011, 1994.

[135] A. J. Xu, D. L. Rarig, T. A. Cook, K. K. Hsu, M. Schoonover, and R. Agrawal, “Pressure swing adsorption process with reduced pressure equalization time,” US patent 6, 565, 628, 2003.

[136] J. F. Nastaj, B. Ambrożek, and J. Rudnicka, “Simulation studies of a vacuum and temperature swing adsorption process for the removal of VOC from waste air streams,” *Int. Commun. Heat Mass Transf.*, vol. 33, no. 1, pp. 80–86, Jan. 2006.

[137] P. Guerin de Montgareuil and D. Domine, “Process for separating a binary gaseous mixture by adsorption,” US patent 3, 155, 468, 1964.

[138] C. Chou and W.-C. Huang, “Simulation of a Four-Bed Pressure Swing Adsorption Process for Oxygen Enrichment,” *Ind. Eng. Chem. Res.*, vol. 33, no. 5, pp. 1250–1258, May 1994.

[139] A. Agarwal, L. T. Biegler, and S. E. Zitney, “Simulation and Optimization of Pressure Swing Adsorption Systems using Reduced-Order Modeling,” 2010.

[140] P. Biswas, S. Agrawal, and S. Sinha, “Modeling and Simulation for Pressure Swing Adsorption System for Hydrogen Purification,” *Chem. Biochem. Eng.*, vol. 24, no. 4, pp. 409–414, 2010.

[141] M. Mofarahi and E. J. Shokroo, “Comparison of two pressure swing adsorption processes for,” *Pet. Coal*, vol. 55, no. 3, pp. 216–225, 2013.

[142] S. Nilchan, C. C. Pantelides, and U. Kingdom, “On the Optimisation of Periodic Adsorption Processes,” *Adsorption*, vol. 147, pp. 113–147, 1998.

[143] H. Khajuria, “and Control of Pressure Swing Harish Khajuria,” Imperial College London, 2011.

[144] D. Ko, R. Siriwardane, and L. T. Biegler, “Optimization of Pressure Swing Adsorption and Fractionated Vacuum Pressure Swing Adsorption Processes for CO2

Sequestration," in *AIChE Annual Meeting, Austin Convention Center*, 2004, no. November.

[145] D. M. Ruthven, *Principles of adsorption and adsorption processes.pdf*, 10th ed. New Brunswick, Fredericton: Wiley & Sons, 1984.

[146] K. Y. Foo and B. H. Hameed, "Insights into the modeling of adsorption isotherm systems," *Chem. Eng. J.*, vol. 156, no. 1, pp. 2–10, Jan. 2010.

[147] S. Farooq and D. M. Ruthven, "Heat effects on adsorption column dynamics. Comparison of 1-dimensional and 2-dimensional models.," *Ind. Eng. Chem. Res.*, vol. 29, no. 6, pp. 1076–1084, 1990.

[148] A. Mostamand and M. Mofarahi, "Simulation of a Single Bed Pressure Swing Adsorption for Producing Nitrogen," in *International Conference for Chemical, Biological and environmental proceedings*, 2011, pp. 362–366.

[149] J. W. Carter, "The Simultaneous Adsorption of Carbon Dioxide and Water Vapour by Fixed beds of Molecular Seives," *Chem. Eng. Sci.*, vol. 29, no. 2, pp. 267–273, 1974.

[150] R. Kumar, "Adsorption column blowdown: adiabatic equilibrium model for bulk binary gas mixtures," *Ind. Eng. Chem. Res.*, vol. 28, no. 11, pp. 1677–1683, Nov. 1989.

[151] K. S. H. & W. K. Lee, "The Adsorption and Desorption Breakthrough Behavior of Carbon Dioxide on Activated Carbon. Effect of Total Pressure and Pressure-Dependent Mass Transfer Coefficients.," *Sep. Purif. Technol.*, vol. 29, no. 14, pp. 1857–1891, 1994.

[152] K. Y. E. S. Hwang, J. A. E. H. O. Jun, and W. O. N. K. Lee, "Fixed-bed adsorption for bulk component," *Chem. Eng. Sci.*, vol. 50, no. 5, 1995.

[153] D. Diagne, M. Gotob, and T. Hiroseb, "Numerical Analysis of a Dual Refluxed PSA Process During Simultaneous Removal and Concentration of Carbon Dioxide Dilute Gas from Air," *J. Chem. Technol. Biotechnol.*, vol. 65, pp. 29–38, 1996.

[154] Y. Ding and E. Alpay, "Equilibria and kinetics of CO_2 adsorption on hydrotalcite adsorbent," *Chem. Eng. Sci.*, vol. 55, no. 17, pp. 3461–3474, Sep. 2000.

[155] S. U. Y. Takamura, S. Narita, J Aoik, S. Hironaka, "Evaluation of Double bed Pressure Swing Adsorption for CO_2 recovery from boiler gas exhaust," *Elsevier Sep. Purif. Tachnology*, vol. 24, pp. 519–528, 2001.

[156] W.-K. Choi, T.-I. Kwon, Y.-K. Yeo, H. Lee, H. K. Song, and B.-K. Na, "Optimal operation of the pressure swing adsorption (PSA) process for CO_2 recovery," *Korean J. Chem. Eng.*, vol. 20, no. 4, pp. 617–623, Jul. 2003.

[157] S. Cavenati, C. A. Grande, and A. E. Rodrigues, "Adsorption Equilibrium of Methane, Carbon Dioxide, and Nitrogen on Zeolite 13X at High Pressures," *J. Chem. Eng. Data*, vol. 49, no. 4, pp. 1095–1101, Jul. 2004.

[158] S. Cavenati, C. A. Grande, and A. E. Rodrigues, "Upgrade of Methane from Landfill Gas by Pressure Swing Adsorption," *Energy & Fuels*, vol. 19, no. 6, pp. 2545–2555, Nov. 2005.

[159] S. Cavenati, C. A. Grande, and A. E. Rodrigues, "Separation of mixtures by layered pressure swing adsorption for upgrade of natural gas," *Chem. Eng. Sci.*, vol. 61, no. 12, pp. 3893–3906, Jun. 2006.

[160] G. L. C. and A. E. R. R.F.P.M. Moreira, J.L. Soares, "Adsorption of CO2 on Hydrotalcite-like Compounds in a Fixed Bed.," *Sep. Sci. Technol.*, vol. 41, no. 2, pp. 341–357, 2006.

[161] J. A. Delgado, M. A. Uguina, J. L. Sotelo, and B. Ruíz, "Fixed-bed adsorption of carbon dioxide–helium, nitrogen–helium and carbon dioxide–nitrogen mixtures onto silicalite pellets," *Sep. Purif. Technol.*, vol. 49, no. 1, pp. 91–100, Apr. 2006.

[162] J. A. Delgado, M. A. Uguina, J. L. Sotelo, B. Ruíz, and M. Rosário, "Separation of carbon dioxide/methane mixtures by adsorption on a basic resin," *Adsorption*, vol. 13, no. 3–4, pp. 373–383, Sep. 2007.

[163] T. L. P. Dantas, S. M. Amorim, F. M. T. Luna, I. J. Silva, D. C. S. de Azevedo, A. E. Rodrigues, and R. F. P. M. Moreira, "Adsorption of Carbon Dioxide onto Activated Carbon and Nitrogen-Enriched Activated Carbon: Surface Changes, Equilibrium, and Modeling of Fixed-Bed Adsorption," *Sep. Sci. Technol.*, vol. 45, no. 1, pp. 73–84, Dec. 2009.

[164] A. Agarwal, "Advanced Strategies for Optimal Design and Operation of Pressure Swing Adsorption Processes," 2010.

[165] N. Casas, J. Schell, R. Pini, and M. Mazzotti, "Fixed bed adsorption of CO_2/H_2 mixtures on activated carbon: experiments and modeling," *Adsorption*, vol. 18, no. 2, pp. 143–161, Jun. 2012.

[166] V. P. Mulgundmath, R. A. Jones, F. H. Tezel, and J. Thibault, "Fixed bed adsorption for the removal of carbon dioxide from nitrogen: Breakthrough behaviour and modelling for heat and mass transfer," *Sep. Purif. Technol.*, vol. 85, pp. 17–27, Feb. 2012.

[167] N. Casas, J. Schell, R. Blom, and M. Mazzotti, "MOF and UiO-67/MCM-41 adsorbents for pre-combustion CO_2 capture by PSA: Breakthrough experiments and process design," *Sep. Purif. Technol.*, vol. 112, pp. 34–48, Jul. 2013.

[168] R. Sabouni, *Carbon Dioxide Adsorption by Metal-organic Frameworks (Synthesis, Testing and Modelling)", University of Western Ontario - Electronic Thesis and Dissertation Repository.* Paper 1472, 2013.
http://ir.lib.uwo.ca/etd/1472

[169] S. Krishnamurthy and V. R. Rao, “Separations : materials , devices and processes CO_2 Capture from Dry Flue Gas by Vacuum Swing Adsorption : A Pilot Plant Study,” *AIChE J. (Separations Mater. devices Process.*, vol. 60, no. 5, 2014.

[170] P. Biswas, S. Agrawal, and S. Sinha, “Modeling and Simulation for Pressure Swing Adsorption System for Hydrogen Purification,” *Chem. Biochem. Eng.*, vol. 24, no. 4, pp. 409–414, 2010.

[171] J. Xiao, M. Hu, P. Bénard, and R. Chahine, “Simulation of hydrogen storage tank packed with metal-organic framework,” *Int. J. Hydrogen Energy*, vol. 38, no. 29, pp. 13000–13010, Sep. 2013.

[172] J. Xiao, L. Tong, C. Deng, P. Bénard, and R. Chahine, “Simulation of heat and mass transfer in activated carbon tank for hydrogen storage,” *Int. J. Hydrogen Energy*, vol. 35, no. 15, pp. 8106–8116, Aug. 2010.

[173] G. Hermosillalara, G. Momen, P. Marty, B. Leneindre, and K. Hassouni, “Hydrogen storage by adsorption on activated carbon: Investigation of the thermal effects during the charging process,” *Int. J. Hydrogen Energy*, vol. 32, no. 10–11, pp. 1542–1553, Jul. 2007.

[174] D. Britt, H. Furukawa, B. Wang, T. G. Glover, and O. M. Yaghi, “Supporting Appendix for Highly efficient separation of carbon dioxide by a metal-organic framework replete with open metal sites Table of Contents.”

[175] Z. Bao, L. Yu, Q. Ren, X. Lu, and S. Deng, “Adsorption of CO_2 and CH_4 on a magnesium-based metal organic framework.,” *J. Colloid Interface Sci.*, vol. 353, no. 2, pp. 549–56, Jan. 2011.

[176] D. Liu, J. J. Purewal, J. Yang, a. Sudik, S. Maurer, U. Mueller, J. Ni, and D. J. Siegel, “MOF-5 composites exhibiting improved thermal conductivity,” *Int. J. Hydrogen Energy*, vol. 37, no. 7, pp. 6109–6117, Apr. 2012.

[177] B. Mu and K. S. Walton, “Thermal Analysis and Heat Capacity Study of Metal À Organic Frameworks,” *J. Phys. Chem.*, vol. 10, no. 115, pp. 22748 – 22754, 2011.

[178] T. L. P. Dantas, F. M. T. Luna, I. J. S. Jr, A. E. B. Torres, D. C. S. De Azevedo, A. E. Rodrigues, and R. F. P. M. Moreira, “Modeling of the fixed-bed adsorption of carbon dioxide and a carbon dioxide- nitrogen mixture on zeolite 13X,” *Brazillian J. Chem. Eng.*, vol. 28, no. 03, pp. 533–544, 2011.

[179] G. Li, P. Xiao, D. Xu, and P. a. Webley, “Dual mode roll-up effect in multicomponent non-isothermal adsorption processes with multilayered bed packing,” *Chem. Eng. Sci.*, vol. 66, no. 9, pp. 1825–1834, May 2011.

[180] X. Wu, Z. Bao, B. Yuan, J. Wang, Y. Sun, H. Luo, and S. Deng, “Microwave synthesis and characterization of MOF-74 (M=Ni, Mg) for gas separation,” *Microporous Mesoporous Mater.*, vol. 180, pp. 114–122, Nov. 2013.

[181] I. Park and K. S. Knaebel, “Adsorption breakthrough behavior: Unusual effects and possible causes,” *AIChE J.*, vol. 38, no. 5, pp. 660–670, May 1992.

[182] J. A. Mason, K. Sumida, Z. R. Herm, R. Krishna, and J. R. Long, “Evaluating metal–organic frameworks for post-combustion carbon dioxide capture via temperature swing adsorption,” *Energy Environ. Sci.*, vol. 4, no. 8, p. 3030, 2011.

VITAE

Name	:	Bamidele, Olufemi Eyitope
Address	:	No 6, Oboroke Street, Agba-Dam Estate, 240222, Ilorin, Kwara State, Nigeria.
Date of Birth	:	21-12-1986
Nationality	:	Nigerian
Contact Address	:	King Fahd university of Petroleum & Minerals Dhahran-31261, Kingdom of Saudi Arabia
Email	:	bamidelephil@yahoo.com

Education :

Master of Science (M.S.) May 2015

Mechanical Engineering Department,

King Fahd University of Petroleum & Minerals, Dhahran,

Saudi Arabia.

Bachelor of Technology (B. Tech) December 2009

Mechanical Engineering Department,

Ladoke Akintola University of Technology, Ogbomoso,

Oyo State, Nigeria.

Paper Submissions :

- Bamidele Olufemi Eyitope and Rached Ben-Mansour, "Simulation of Adsorptive Storage of CO_2 in Fixed Bed of MOF-177". Chinese Journal of Chemical Engineering, 2015. (In review)

- R. Ben-Mansour and O. E. Bamidele, M. A. Habib, A. M. P. Peedikakkal, "Simulation of CO_2 adsorption-separation from a N_2/CO_2 gas mixture in a Fixed Bed Mg–MOF-74 Column". International Journal of Global Warming, 2015. (Accepted)

- R. Ben-Mansour, Mohammed A. Antar and Bamidele Olufemi Eyitope, “Simulation of Adsorptive Storage of CO_2 in Fixed Bed of MOF-5”. Journal of Energy resources Technology, 2015. (In review)

- R. Ben-Mansour, M. A. Habib, O. E. Bamidele, M. basha, N. Qasem, A. Peedikakkal, T. Laoui, and M. Ali, “Carbon Capture by Adsorption: Materials, Experimental Investigation and Numerical Modelling and Simulations – A Review”. Carbon Management Journal, 2015. (In review)

- Rached Ben-Mansour and Bamidele Olufemi Eyitope, “Evaluation of Mg-MOF-74 for Post-Combustion Carbon Capture and Sequestration through Pressure Swing Adsorption”. (Under review) 2015. (In view)